

Synthesis, characterisation and performance of calcium phosphate bone graft substitutes

By Zeeshan A. Sheikh



Faculty of Dentistry
McGill University
Montreal, Quebec, Canada

A thesis submitted to McGill University in partial fulfillment of the requirements for
the degree of Doctor of Philosophy

© Zeeshan A. Sheikh 2014

Dedicated to my loving wife, Varda.

“No man succeeds without a good woman behind him. Wife or mother, if it is both, he is twice blessed indeed.”

Harold Macmillan

Abstract

Synthetic bone graft substitutes are frequently used to fill defects with significant bone loss to prevent fibrous tissue ingrowth and loss of function. Bone grafts are often used to augment deficient alveolar ridges allowing placement of dental implants subsequent to prior bone loss. Although autografts, allografts and xenografts have been used and researched extensively, they have inherent limitations. To overcome these, synthetic alternatives, such as calcium phosphate cement-based biomaterials are being developed. Brushite and monetite are acidic calcium phosphates having similar chemical composition. However, their *in vivo* behavior differs in terms of resorption and bone response. Although brushite and monetite have been shown to resorb faster *in vivo* than hydroxyapatite (HA), a significant reduction in the rate of resorption occurs following phase conversion of brushite to insoluble HA.

As such differences between bone grafts are attributed to material composition even though physical properties such as surface area and porosity invariably differ. This thesis focuses on determining the factors and mechanisms that makes these chemically similar materials behave differently *in vivo*. We produced brushite cement grafts and converted them to two types of monetite by using wet (autoclaving) and dry heat (under vacuum) dehydration which resulted in materials with differing physicochemical properties. These grafts were then aged *in vitro* using bovine serum and phosphate buffered saline (PBS) solutions, implanted subcutaneously, in femoral condyles and onlay grafted on calvaria. The dissolution, resorption and bone formation potential of these dicalcium phosphate cement grafts was assessed and compared. Also, we developed a new alkali ion (sodium and potassium) substituted calcium phosphate cement, reinforced with silica and set using phytic acid. The set cement blocks were aged in PBS solutions and their *in vitro* dissolution and degradation along with other physico-chemical properties was assessed.

Results presented in this Ph.D thesis discuss and shed light on the fundamental yet not understood questions regarding the relative contributions from chemico- vs physico-biomaterial properties in graft resorption and bone regeneration. This will allow in future the preparation of improved calcium phosphate-based bone substitute grafts with potential to achieve higher clinical efficiency.

Re'sume'

Les substituts synthétiques de greffe osseuse sont fréquemment utilisés pour remplir les déficiences avec perte osseuse significative, ceci afin d'empêcher la croissance à l'intérieur de tissu fibreux et la perte de fonction. Les greffes osseuses sont souvent utilisées pour augmenter les crêtes alvéolaires déficientes en permettant le placement d'implants dentaires avant la perte osseuse. Bien que les autogreffes, allogreffes et xélogreffes ont été utilisées et étudiées de façon intensive, elles présentent des limites inhérentes. Pour surmonter cela, des alternatives synthétiques tels que les biomatériaux à base de ciment de phosphate de calcium ont été développées. La brushite et la monétite sont des phosphates de calcium acides à composition chimique similaire. Toutefois, leurs comportements *in vivo* diffèrent en terme de résorption et réponse osseuse. Bien qu'il ait été démontré que la brushite et la monétite résorbent plus rapidement que l'hydroxyapatite (HA) *in vivo*, une réduction significative du taux de résorption se produit après la conversion de phase de la brushite en l'insoluble HA.

En soi, les différences entre les greffons osseux sont attribuées à la composition du matériau même si les propriétés physiques telles que la surface spécifique et la porosité diffèrent invariablement. Cette thèse vise à déterminer les facteurs et les mécanismes qui font que ces matériaux bien que chimiquement similaires se comportent différemment *in vivo*. Nous avons produit des greffes de ciment de type brushite et les avons converties en deux types de monétite en utilisant la déshydratation soit humide (autoclave) soit sèche (sous vide) afin de produire des matériaux ayant des propriétés physico-chimiques différentes. Ces greffes ont ensuite subi un vieillissement *in vitro* dans du sérum bovin ou dans une solution saline tamponnée au phosphate (PBS) et *in vivo*, avec des implantations en sous-cutanée ou alors dans les condyles fémoraux et finalement en greffant sur le dessus de la calotte crânienne. Le potentiel de la dissolution, de la résorption et de la formation osseuse de ces greffes à base de ciment de

phosphate dicalcique a été évalué et comparé. En outre, nous avons développé un nouveau ciment de phosphate de calcium substitué par un ion alcalin (sodium et potassium), renforcé par la silice et pris à l'aide d'acide phytique. Les blocs de ciment durcis ont été vieillis dans les solutions de PBS et leur dissolution et dégradation *in vitro* ainsi que d'autres propriétés physico-chimiques ont été évaluées.

Les résultats présentés dans cette thèse de doctorat répondent aux questions fondamentales mais pas encore comprises, concernant les contributions relatives des propriétés chimiques versus physique des biomatériaux durant la résorption et la régénération osseuse. Cela permettra dans le futur de préparer des substituts améliorés de greffe osseuse à base de phosphate de calcium avec un potentiel d'atteindre une efficacité clinique supérieure.

Acknowledgements

First and foremost I would like to thank and appreciate my supervisor Prof. Jake Barralet who has guided and supported my academic development throughout my Ph.D at McGill. It has been an honor to be mentored by a professor of his calibre.

My thanks also extends to Dr. Faleh Tamimi for providing me with the surgical training required for the *in vivo* projects for my Ph.D.

My sincerest thanks to Dr. Uwe Gbureck for inviting me to Wuerzburg, Germany, to work as an overseas research student under his supervision.

Thanks to my group members, past and present, both at Strathcona Anatomy and Dentistry Building and at the Montreal General Hospital, who supported and helped me along the way, particularly Mrs. Yu Ling Zhang for her assistance during and after all the surgical procedures.

I would like to thank the staff especially Mrs. Marie-Eve and Ms. Julie Browning at the Montreal General Hospital, for their help in organising surgeries and assistance during the CT-scanning procedures.

I would like to thank Mrs. Line Mongeon for sharing her expertise with me and help in obtaining the electron beam analysis data shown in this thesis.

My parents Mr. Azam Sheikh and Mrs. Naureen Azam Sheikh who have supported me throughout my life, in every way possible, and I am eternally grateful to them for encouraging my pursuits and endeavours.

My loving sisters, Mrs. Navin Imtiaz and Dr. Amber Sheikh and who have always taken care of me and shown unconditional love.

My loving aunt Mrs. Jameela Wajid and my late uncle Dr. M. A. Wajid who have always been a source of inspiration to me.

My respected and dearest father and mother in-law Mr. & Mrs. Syed Sarfraz Ali for their love and encouragement.

Last and by no means the least, I give my heartfelt gratitude and love to my wife, Varda, for her steadfast support and love.

Author contributions & statements of originality

This thesis is composed of four manuscripts prepared for publication by the candidate as the primary author. A brief summary of the work and a statement of the involvement and contribution of the candidate and the co-authors are provided below for each of the manuscripts.

1. *In vitro* degradation and *in vivo* resorption of dicalcium phosphate cement based grafts.

Zeeshan Sheikh, Yu Ling Zhang, Faleh Tamimi, Liam Grover and Jake Barralet.

All experiments were designed by the candidate who also wrote the manuscript and performed all of the experimental work except for the surgical procedures (performed by YZ) and the pore size distribution data that was provided by LG. FT provided surgical trainings and guidance for the *in vivo* experiments. FT and JB corrected the manuscript. All authors reviewed the manuscript.

Originality: All content is new and original. This is the first time there has been an attempt to create an *in vitro* degradation model which can correlate with the subcutaneous *in vivo* resorption of dicalcium phosphate grafts.

2. Monetite grafts prepared by wet and dry dehydration of brushite bioceramics: An orthotopic implantation study.

Zeeshan Sheikh, Yu Ling Zhang, Fred Gao, Faleh Tamimi, and Jake Barralet.

All experiments were designed and performed by the candidate. YZ assisted in the surgical and explant processing procedures. FG developed the customized micro-CT analysis model. Trainings and guidance for surgical procedures was provided by FT. The manuscript was written by the candidate and corrected by JB and FT.

Originality: This is the first report which compares graft resorption and bone response to two types of monetite materials prepared by varying processing conditions and compares them with brushite grafts after orthotopic implantation.

3. Vertical bone augmentation: A comparison between monetite onlay grafts prepared by wet and dry heat conversion of brushite.

Zeeshan Sheikh, Yu Ling Zhang, Justin Drager, Mohamed-nur Abdallah, Faleh Tamimi, and Jake Barralet.

All experiments were designed and performed by the candidate. YZ assisted in the surgical and explant processing procedures. JD developed the customized micro-CT analysis model. MA provided the 3D modelled images presented in the manuscript. Trainings and guidance for surgical procedures was provided by FT. The manuscript was written by the candidate and corrected by JB and FT. All authors reviewed the manuscript.

Originality: This is the first report which presents and compares graft resorption and bone infiltration data from onlay grafting procedures using conventional autoclave prepared monetite grafts and dry heat prepared monetite grafts.

4. Development of alkali ions substituted-silica reinforced calcium phosphate cement, set with phytic acid.

Zeeshan Sheikh, Martha Geffers, Jake Barralet, and Uwe Gbureck.

All the experimental work was carried out by the candidate except for the preparation of the alkali ions substituted calcium phosphate cement powders by MG. The manuscript was written by the candidate and corrected by JB and UG. All authors reviewed the manuscript.

Originality: This study reports and introduces the development of alkali ions substituted calcium phosphate cements reinforced with silica and set by different concentrations of phytic acid.

Table of contents

Abstract.....	5
Resume.....	7
Acknowledgements.....	9
Author contributions and statements of originality.....	11
List of figures.....	22
List of tables.....	31

Chapter 1. General introduction..... 33

Chapter 2. Literature review..... 35

2.1 Introduction.....	35
2.2 Bone.....	35
2.2.1 Bone composition.....	35
2.2.1.1 Bone cells.....	36
2.2.1.2 Bone matrix.....	39
2.2.1.3 Bone minerals.....	41
2.2.2 Bone development.....	41
2.2.2.1 Intramembranous ossification.....	41
2.2.2.2 Intracartilagenous ossification.....	43
2.2.3 Bone types according to morphology.....	43
2.2.3.1 Cortical bone.....	43
2.2.3.2 Trabecular bone.....	45
2.2.4 Bone types according to collagen pattern in osteoid.....	46
2.2.4.1 Woven bone.....	46
2.2.4.2 Lamellar bone.....	47
2.2.5 Bone types according to shape.....	47
2.2.5.1 Flat bones.....	47
2.2.5.2 Long bones.....	47
2.2.5.3 Short bones.....	48

2.2.5.4	Sesamoid bones.....	48
2.2.5.5	Irregular bones.....	49
2.3	Bone modelling and repair.....	49
2.4	Bone grafting.....	51
2.5	Bone replacement graft materials.....	52
2.5.1	Autografts.....	54
2.5.2	Allografts.....	56
2.5.2.1	Fresh or frozen iliac cancellous bone and marrow grafts.....	56
2.5.2.2	Mineralized freeze-dried bone allografts (FDBA).....	56
2.5.2.3	Demineralized freeze-dried bone allografts (DFDBA).....	57
2.5.3	Xenografts.....	58
2.5.3.1	Bovine-derived xenografts.....	58
2.5.3.2	Calcium carbonate xenografts.....	59
2.5.4	Alloplasts.....	59
2.5.4.1	Polymers.....	60
2.5.4.2	Bioactive glasses.....	61
2.5.4.3	Ceramics.....	61
2.5.4.4	Calcium phosphates.....	62
2.6	Introduction to dicalcium phosphate dihydrate (DCPD) cements.....	64
2.6.1	Cement composition.....	64
2.6.1.1	Alkaline calcium sources.....	65
2.6.1.2	Acidic phosphate sources.....	65
2.6.1.3	Additives.....	66
2.6.2	Cement setting reaction.....	67
2.6.2.1	Effect of additives and other factors on setting reaction.....	68
2.6.3	Monetite preparation.....	69

2.6.3.1	Hydrothermal and dry thermal methods.....	69
2.6.3.2	Low pH during cement setting.....	70
2.6.3.3	Limiting free water during cement setting.....	70
2.6.3.4	Altering cement reaction with additives.....	70
2.6.4	Mechanical properties.....	71
2.6.5	Dissolution and resorption.....	72
2.6.6	Bone formation.....	73
2.6.7	Applications.....	75
2.6.7.1	Orthopaedics.....	75
2.6.7.2	Craniofacial repair and augmentation.....	76
2.6.7.3	Bioactive molecular delivery.....	78
2.6.7.4	Biosensors.....	79

Chapter 3. Characterisation techniques..... 80

3.1	X-ray diffraction (XRD).....	80
3.1.1	Theory.....	80
3.1.2	Instrumentation & measurement.....	81
3.2	Scanning electron microscopy (SEM).....	82
3.2.1	Theory.....	82
3.2.2	Instrumentation.....	83
3.3	Energy dispersive X-ray spectroscopy (EDX).....	88
3.3.1	Theory.....	88
3.3.2	Instrumentation & measurement.....	88
3.4	Brunauer–Emmett–Teller (BET) method.....	88
3.4.1	Theory.....	89
3.4.2	Measurement.....	89
3.5	Helium pycnometry.....	89
3.5.1	Theory.....	89
3.5.2	Instrumentation & measurement.....	90
3.6	Mercury intrusive porosimetry.....	90
3.6.1	Theory.....	90

3.6.2 Instrumentation & measurement.....	91
3.7 Digital radiography.....	91
3.7.1 Instrumentation & image formation.....	92
3.8 Computed tomography.....	92
3.8.1 Principle and scanning.....	92

Chapter 4. Surgical models and procedures..... 94

4.1 Factors to be considered in choosing a model.....	94
4.1.1 Model relevance.....	94
4.1.2 Bone healing and remodelling features.....	95
4.1.3 Anatomical and morphological features.....	95
4.1.4 Gender of the animals.....	96
4.1.5 Species used for the models.....	96
4.2 Animal models currently used for bone replacement material evaluation.....	98
4.2.1 Heterotopic implantation.....	98
4.2.2 Orthotopic implantation.....	98
4.2.3 Cranial surgery.....	99
4.2.4 Maxillo-facial surgery.....	99
4.2.4.1 Filling defects.....	99
4.2.4.2 Segmental bone defects.....	99
4.2.4.3 Onlay grafting.....	100
4.2.5 Orthopaedic surgery.....	101
4.2.5.1 Filling defects.....	101
4.2.5.2 Segmental bone defects.....	101
4.2.6 Spinal surgery.....	102
4.2.6.1 Vertebroplasty.....	102
4.2.6.2 Spinal fusions.....	102
4.3 Surgical methodology employed during Ph.D experiments.....	103
4.3.1 Subcutaneous implantation procedure.....	103
4.3.2 Orthotopic implantation procedure.....	104

4.3.3 Onlay grafting procedure..... 106

Chapter 5. *In vitro* degradation and *in vivo* resorption of dicalcium phosphate cement based grafts..... 109

5.1 Preface..... 109

5.2 Abstract..... 110

5.3 Introduction..... 112

5.4 Results..... 114

5.5 Discussion..... 118

5.5.1 In vitro dissolution & *in vivo* resorption..... 118

5.5.2 Disintegration..... 120

5.5.3 Physical properties..... 121

5.6 Conclusion.... 122

5.7 Acknowledgements..... 122

5.8 Experimental..... 123

5.8.1 Method and materials..... 123

5.8.1.1 Synthesis..... 123

5.8.1.2 Characterisation..... 124

5.8.1.2 In vitro ageing..... 125

5.8.1.3 Animal study..... 125

5.8.1.4 Statistical analysis..... 126

5.9 Tables & figures..... 127

5.10 Supplementary figures..... 135

Chapter 6. Monetite grafts prepared by wet and dry dehydration of brushite bioceramics: An orthotopic implantation study..... 142

6.1 Preface..... 142

6.2 Abstract..... 143

6.3 Introduction..... 145

6.4 Results..... 147

6.4.1 Physicochemical analyses of grafts prepared..... 147

6.4.2 In vivo study.....	148
6.5 Discussion.....	151
6.5.1 Physicochemical characteristics of the bioceramics.....	151
6.5.2 In vivo.....	152
6.6 Conclusion.....	155
6.7 Acknowledgements.....	156
6.8 Experimental.....	157
6.8.1 Method and materials.....	157
6.8.1.1 Synthesis.....	157
6.8.1.2 Characterisation of grafts prepared.....	157
6.8.1.3 In vivo study.....	159
6.8.1.4 Statistical analysis.....	160
6.9 Tables & figures.....	161
6.10 Supplementary figures.....	167

Chapter 7. Vertical bone augmentation: A comparison between monetite onlay grafts prepared by wet and dry heat conversion of brushite..... 168

7.1 Preface.....	168
7.2 Abstract.....	169
7.3 Introduction.....	171
7.4 Results.....	173
7.4.1 Physicochemical properties of the prepared disc grafts.....	173
7.4.2 In vivo study.....	173
7.4.2.1 Surgical and clinical observations.....	173
7.4.2.2 Histological observations.....	174
7.4.2.3 SEM and XRD analysis.....	175
7.4.2.4 Histomorphometrical analysis.....	175
7.4.2.4.1 Vertical bone height gained.....	175
7.4.2.4.2 Bone augmented within onlay grafts.....	176

7.4.2.4.3 Onlay graft resorption.....	177
7.5 Discussion.....	178
7.5.1 Physicochemical properties of the prepared disc grafts.....	178
7.5.2 Vertical bone height gained.....	178
7.5.3 Bone augmented within onlay grafts.....	180
7.5.4 Onlay graft resorption.....	181
7.6 Conclusion.....	182
7.7 Acknowledgements.....	182
7.8 Experimental.....	183
7.8.1 Method and materials.....	183
7.8.1.1 Synthesis.....	183
7.8.1.2 Characterisation of the prepared discs.....	183
7.8.1.3 Surgical procedure.....	185
7.8.1.4 Histomorphometric analysis.....	185
7.8.1.5 Scanning electron microscopy and micro-computed tomography.....	186
7.8.1.6 Statistical analysis.....	187
7.9 Tables & figures.....	188
7.10 Supplementary figures.....	195

Chapter 8. Development of alkali ions substituted-silica reinforced calcium phosphate cement, set with phytic acid..... 196

8.1 Preface.....	196
8.2 Abstract.....	197
8.3 Introduction.....	199
8.4 Results and discussion	201
8.4.1 Compressive strength	201
8.4.2 Porosity	202
8.4.3 In vitro dissolution and mass loss	203
8.4.4 Scanning electron microscopic imaging	203

8.4.5 X-Ray diffraction	203
8.4.6 Density and specific surface area	204
8.5 Conclusion.....	205
8.6 Acknowledgements.....	205
8.7 Experimental.....	206
8.7.1 Synthesis	206
8.7.2 Characterisation	206
8.7.3 In vitro ageing	207
8.7.4 Statistical analysis	208
8.8 Tables & figures.....	209

Chapter 9. Final discussion and conclusions..... 215

Chapter 10. Bibliography..... 217

Chapter 11. Additional co-authored research articles published by the candidate during Ph.D studies..... 275

List of Figures

- 2.2.1.1.1** Interaction of stromal and hematopoietic cells leading to the formation of an osteocyte..... 38
- 2.2.1.1.2** A diagrammatic representation of the interaction of stromal and hematopoietic cells forming osteoclasts and osteoblasts..... 39
- 2.2.2.1.1** A diagrammatic representation of the microscopic structure of bone..... 42
- 2.2.3.1.1** A long bone (femur) showing various types of bone tissue according to morphology..... 44
- 2.2.3.2.1** An inverted X-ray image of Long bone (femur) showing: 2 green arrows -Trabecular bone, 1 blue arrow – Cortical bone, and 1 red arrow – marrow cavity..... 45
- 2.2.3.2.2** Micro-Computed Tomographic images of cross sections of A: cortical bone, and B: cancellous bone..... 46
- 2.2.5.2.1** Bone according to varying shapes. (Adapted from: Queen Mary, University of London handout notes)..... 48
- 3.1.1.1** Representation of (a) destructive and (b) constructive Interference based on Bragg condition being not satisfied and satisfied..... 81
- 3.2.2.1** Schematic representation of the parts of a scanning electron microscope..... 84

- 3.2.2.2** The cosine distribution of Backscatter electrons..... 85
- 3.2.2.3** Schematic representation of a solid state detector for BSE imaging..... 86
- 3.2.2.4** Schematic representation of Everhart-Thornley detector..... 87
- 4.3.1.1** Subcutaneous implantation: surgical steps..... 104
- 4.3.2.1** Orthotopic implantation: surgical steps..... 105
- 4.3.3.1** Onlay grafting surgical steps..... 107
- 5.9.1** Pore size distribution of (a) 3:1 P/L ratio brushite, autoclaved monetite and dry heat monetite grafts, and (b) 1:1 P/L ratio brushite, autoclaved monetite and dry heat monetite grafts..... 128
- 5.9.2** Photographs of the retrieved brushite, dry heat monetite and autoclaved monetite grafts after 4 weeks of implantation (a,b,c) and after 12 weeks (d,e,f) [yellow dotted lines denote 6 x 12 mm initial dimensions of the grafts]. Radiographs showing brushite (right) and autoclaved monetite (left), (g) upon implantation, (h) after 4 weeks, and (i) after 12 weeks *in vivo*..... 129
- 5.9.3** X-ray diffraction patterns indicating the initial and post ageing in PBS phase composition of brushite, autoclaved and dry heat monetite grafts. Grafts initially consisted of phase pure DCPD (*). The dry heat and autoclaved monetite grafts show the conversion from DCPD to DCPA (†). After ageing in PBS for 60 days the brushite shows conversion from DCPD to OCP (O) and HA (X)

and remnants of DCPD. The dry heat and autoclaved monetite grafts do not show any phase change upon ageing in PBS for 60 days..... 130

5.9.4 X-ray diffraction patterns showing phase composition before and post implantation of: a. Brushite graft cylinders. The grafts initially consisted of phase pure DCPD (*). After 12 weeks of subcutaneous implantation, the analysis of the grafts revealed the presence of a mixture of OCP (O), HA (X) and remnants of DCPD. b. Autoclaved and dry heat monetite grafts. Analysis of both monetite grafts confirmed conversion from DCPD to DCPA (†) before implantation. The autoclaved and dry heat monetite grafts did not show any phase change upon implantation for 12 weeks..... 131

5.9.5 SEM images of brushite (a, b, c, d), autoclaved monetite (e, f, g, h) and dry heat monetite (i, j, k, h) grafts before and after immersion in PBS, serum, and subcutaneous implantation in rats on Days 0, 60, and 84 respectively (Scale bars represent 5µm)..... 132

5.9.6 Mass loss of grafts *in vitro* for up to 60 days; (a) 3:1 P/L ratio brushite and monetite grafts in PBS, (b) 3:1 P/L ratio brushite and monetite grafts in serum, (c) 1:1 P/L ratio brushite and monetite grafts in PBS, and (d) 1:1 P/L ratio brushite and monetite grafts in serum..... 133

5.9.7 Comparison between mass loss of all bioceramic graft implanted subcutaneously..... 134

5.10.1 Effect of *in vitro* ageing on relative porosity of, (a) 3:1 P/L ratio

grafts in PBS; (b) 3:1 P/L ratio grafts in serum; (c) 1:1 P/L ratio grafts in PBS; and (d) 1:1 P/L ratio grafts in serum. (Grey-brushite, Blue- autoclaved monetite, and Red-dry heat monetite)..... 135

5.10.2 Effect of subcutaneous implantation on relative porosity of, (a) 3:1 P/L ratio grafts, and (b) 1:1 P/L ratio grafts. (Grey-brushite, Blue- autoclaved monetite, and Red-dry heat monetite)..... 136

5.10.3 Effect of *in vitro* ageing on specific surface area (SSA) of, (a) 3:1 P/L ratio grafts in PBS; (b) 3:1 P/L ratio grafts in serum; (c) 1:1 P/L ratio grafts in PBS; and (d) 1:1 P/L ratio grafts in serum. (Grey-brushite, Blue- autoclaved monetite, and Red-dry heat monetite)..... 137

5.10.4 Effect of subcutaneous implantation on specific surface area (SSA) of, (a) 3:1 P/L ratio grafts, and (b) 1:1 P/L ratio grafts. (Grey-brushite, Blue- autoclaved monetite, and Red-dry heat monetite)..... 138

5.10.5 Effect of *in vitro* ageing on density of, (a) 3:1 P/L ratio grafts in PBS; (b) 3:1 P/L ratio grafts in serum; (c) 1:1 P/L ratio grafts in PBS; and (d) 1:1 P/L ratio grafts in serum. (Grey-brushite, Blue- autoclaved monetite, and Red-dry heat monetite)..... 139

5.10.6 Effect of subcutaneous implantation on density of, (a) 3:1 P/L ratio grafts, and (b) 1:1 P/L ratio grafts. (Grey-brushite, Blue- autoclaved monetite, and Red- dry heat monetite)..... 140

5.10.7 Effect of powder to liquid ratio on the compressive strength and relative porosity of cements. (B: brushite, H-M: dry heat

monetite and AC-M: autoclaved monetite)..... 141

- 6.9.1** SEM images of: (a) brushite, (b) autoclaved monetite, and (c) dry heat monetite before implantation. (Scale bars in the images represent 1 μ m)..... 162
- 6.9.2** Digital radiographical assessment of the retrieved femurs with bioceramic grafts after 4 and 12 weeks of implantation (dotted areas represent original graft dimensions of 3 x 4 mm)..... 163
- 6.9.3** Histological sections (H&E stain) of brushite (a & b), autoclaved monetite (c & d), and dry heat monetite (e & f) after 4 and 12 weeks of implantation (dotted areas represents original graft diameter of 3 mm)..... 164
- 6.9.4** BSE-SEM images of brushite (a & b), autoclaved monetite (c & d), and dry heat monetite (e & f) after 4 and 12 weeks of implantation..... 165
- 6.9.5** X-ray diffraction patterns obtained from core of: (a) brushite grafts before and after 4 and 12 weeks *in vivo*, (b) Autoclaved monetite grafts before and after 4 and 12 weeks *in vivo*, and (c) Dry heat grafts before and after 4 and 12 weeks *in vivo*. (*) represents brushite, (X) represents HA, and (†) represents monetite peaks..... 165
- 6.9.6** (a) BSE-SEM image showing brushite cement core surrounded by a dark zone of material and new bone (NB) at the graft perimeter after 12 weeks of implantation (scale bar represents 1 mm). (b) The XRD point analysis of the darkened zone revealed phase conversion of brushite to hydroxyapatite

(X represents peaks of HA)..... 166

- 6.10.1** Post implantation radiographs (inverted) to confirm position of bioceramics in bone..... 167
- 6.10.2** BSE-SEM images of (a) autoclaved monetite and (b) dry heat monetite after 4 weeks of implantation showing the resorbing cement grafts surrounded by new formed bone (NB)..... 167
- 7.9.1** (A) Retraction of tissues after incision, (B) Disc onlay graft being fixed onto the calvaria, (C) Screw stabilized monetite grafts, (D) Appearance of retrieved grafts after 12 weeks of onlay grafting, (E) Computed tomographic 3D image of grafts immediately after implantation, (F) Computed tomographic 3D image of grafts after 12 weeks of implantation, (G) Resin embedded bone blocks with autoclaved monetite graft after sectioning, (H) Resin embedded bone blocks with dry heat monetite graft after sectioning, (I) μ -CT slice of autoclaved monetite graft before implantation, (J) μ -CT slice of autoclaved monetite graft after 12 weeks of implantation, (K) 3D-modelling of autoclaved monetite graft before implantation, (L) 3D-modelling of autoclaved monetite graft after 12 weeks of implantation, (M) μ -CT slice of dry heat monetite graft before implantation, (N) μ -CT slice of dry heat monetite graft after 12 weeks of implantation, (O) 3D-modelling of dry heat monetite graft before implantation, and (P) 3D-modelling of dry heat monetite graft after 12 weeks of implantation. (Single arrow represents autoclaved monetite grafts and double arrows represent dry heat monetite grafts in the images)..... 189

- 7.9.2** Histological micrographs of a coronal section from the bone explant sites stained with H&E of: (A) autoclaved monetite onlay graft (1 arrow) after 12 weeks, (B) Dry heat monetite onlay graft (2 arrows) after 12 weeks, (C) Higher magnification image of the area marked in image A, (D) Higher magnification image of the area marked in image B. The sections show remaining monetite block material (*), bone augmented free of unresorbed graft material (+), and the original bone calvarium (X). (Scale bars in images A & B represents 2 mm and in images C & D represents 0.5 mm)..... 190
- 7.9.3** BSE-SEM images of: (A) autoclaved monetite graft after 12 weeks, (B) dry heat monetite graft after 12 weeks, (C) higher magnification image of the area marked in image A, (D) higher magnification image of the area marked in image B. The images show remaining monetite graft material (*), bone augmented (+), and the original bone calvarium (X). (Scale bars in the images A & B represents 2 mm and in images C & D represents 0.5 mm)..... 191
- 7.9.4** BSE-SEM images of disc grafts prepared: (A) autoclaved monetite, and (B) dry heat monetite. (Scale bars in the images represent 0.5 μm). X-ray diffraction patterns obtained before and after implantation from: (C) autoclaved monetite grafts, and (D) dry heat monetite grafts. [(†) represents monetite and (x) represents HA peaks]..... 192
- 7.9.5** (A) Relative bone height gained along the mediolateral axis of the grafts. The measurements represent percentage of bone height (mean plus standard deviation) gained between the original calvarial surface and the superior surface of the

monetite grafts. (B) The percentage of bone tissue within the grafts' augmented area. (C) Mapping of average bone height augmented with autoclaved monetite grafts. (D) Mapping of average bone height augmented with dry heat monetite grafts..... 193

7.9.6 (A) Graft and bone block histological section divided into 16 smaller areas (1x1mm each), using a 4x4 grid for histomorphological measurements. (B) The percentage of remaining graft area after 12 weeks of onlay grafting. (C) Histomorphological measurements showing percentage of bone volume present in the areas delimited by the grids. (D) 3D-model of autoclaved monetite onlay graft from above (top image) and surface in contact with calvarial bone (bottom image) constructed after 12 weeks of implantation. Lateral area shows more bone augmented than the medial area. (E) 3D-model of dry heat monetite onlay graft from above (top image) and surface in contact with calvarial bone (bottom image) constructed after 12 weeks of implantation. The lateral most area shows more bone than the medial area, but less in comparison to the autoclaved monetite graft..... 194

7.10.1 (A) 3D image of grafts immediately after implantation. (B) 3D image of grafts after 4 weeks of implantation. (C) Appearance of retrieved grafts after 12 weeks of onlay grafting. (D) 3D image obtained by removing the calvarial surface to visualize the graft and screw from underneath after 4 weeks of implantation. (Single arrows in the images represent autoclaved monetite grafts prepared with a P/L ratio of 1)..... 195

- 8.9.1** Photograph of cement blocks prepared for *in vitro* experiments..... 209
- 8.9.2** Effect of *in vitro* ageing on the mechanical properties of cement blocks..... 210
- 8.9.3** Effect of *in vitro* ageing on total porosity of cement blocks set with 20, 30, 40 and 50% concentrated phytic acid..... 210
- 8.9.4** Comparison between mass loss of all cement blocks aged in PBS solutions..... 211
- 8.9.5** SEM images of cements set with varying concentrations of phytic acid respectively after *in vitro* ageing at day 0 (a, b, c, d), day 7 (e, f, g, h) and day 60 (i, j, k, h) (Scale bars represent 5 μ m)..... 212
- 8.9.4** X-ray diffraction patterns showing phase composition before and after ageing of:
- a. Cement set with 20% phytic acid.
 - b. Cement set with 30% phytic acid.
 - c. Cement set with 40% phytic acid.
 - d. Cement set with 50% phytic acid.
- (●) represents $\text{Ca}_2\text{KNa}(\text{PO}_4)_2$, and (▼) represents SiO_2 peaks..... 213
- 8.9.6** Effect of *in vitro* ageing on density of cement blocks set with 20, 30, 40 and 50% concentrated phytic acid..... 214
- 8.9.7** Effect of *in vitro* ageing on specific surface area of cement blocks set with 20, 30, 40 and 50% concentrated phytic acid..... 214

List of Tables

- 2.2.1.1.1 Various cell types that play a role in bone formation and resorption..... 37
- 2.5.1 Requirements of bone grafts for successful bone tissue replacement..... 53
- 2.5.2 Different types of bone replacement graft tissues and materials..... 54
- 2.5.1.1 Merits and demerits of using autogenous bone grafts (autografts)..... 55
- 2.5.2.3.1 Autografts versus Allografts..... 58
- 2.5.4.4.1 List of existing calcium phosphate compounds..... 63
- 5.9.1 Summary of physicochemical properties of brushite, autoclaved and dry heat monetite..... 127
- 5.9.2 Summary of the total percentage of mass loss of brushite and monetite cements after *in vitro* ageing in PBS and bovine serum and after subcutaneous implantation..... 127
- 5.9.3 Summary of changes in calcium-to-phosphorous ratio of brushite and monetite grafts after ageing in PBS, serum, and subcutaneous implantation..... 127
- 6.9.1 Characterisation of prepared brushite and monetite bioceramics..... 161
- 6.9.2 Histomorphometric analysis of the implanted bioceramic grafts..... 162

7.9.1 Characterisation of prepared monetite disc grafts..... 188

8.9.1 Characterisation of cements set with phytic acid..... 209

Chapter 1: General Introduction

Although bone has the potential to repair itself following injury, disease, surgical removal and tissue loss following trauma; placement of bone grafts is frequently indicated to prevent fibrous tissue in-growth, facilitate repair and to maintain mechanical function. Bone grafting is a common surgical procedure which is performed in approximately 10% of all orthopaedic reconstruction cases (1). More than 2.2 million bone grafting procedures are carried out annually worldwide in order to repair orthopaedic, dental, congenital and neurosurgical defects (2, 3).

The most frequently used bone graft material is autologous bone which is commonly harvested from ribs and the iliac crest (1, 4, 5). Currently, autologous bone grafting is considered to be the gold standard as autografts have suitable biological compatibility (6-8). However, donor site morbidity and the limited amounts which can be obtained have a restricting effect on their use and have stimulated research towards exploring suitable alternatives (9-11).

Ideally, bone substitutes should demonstrate good local and systemic compatibility, undergo bioresorption and have the capability to be substituted by the regenerating bone (10, 12). Recent studies have shown that synthetic grafts prepared from acidic calcium phosphates, brushite and monetite, resorb faster *in vivo* than hydroxyapatite (HA) (13-16). Although both materials have similar chemical composition, their *in vivo* behaviour differs. Monetite, unlike brushite, does not reprecipitate as HA *in vivo*, and recent animal studies have demonstrated its good osteoconductive and osteoinductive properties (14, 17, 18).

Biomaterial-bone tissue interactions are interpreted in terms of material chemistry even though physical properties are not controlled. As such the differences between bone grafts are attributed to material composition even though surface

area and porosity invariably differ. These potentially are the key factors that affect the *in vivo* response and behavior and require investigation. The primary objectives of this research were to:

- Investigate and assess the dissolution, degradation and resorption of dicalcium phosphate bone grafts in an *in vitro* ageing model and after subcutaneous implantation.
- Investigate the ability of dicalcium phosphate grafts to be resorbed and replaced by newly forming bone after implantation in orthotopic sites.
- Assess the ability of dicalcium phosphate onlay grafts to achieve vertical bone augmentation.
- Develop an alkali ion substituted calcium phosphate cement set with a strong chelating agent and evaluate the physico-chemical properties before and after *in vitro* ageing.

This thesis comprises of four manuscripts that report experiments which target these objectives providing a new insight to how altering the physico-chemical properties of calcium phosphate cements affects graft resorption and bone response towards them.

The work was performed by the author between September 2010 and March 2014 in the laboratory and hospital surgical facilities and under the supervision of Dr. Jake Barralet at the Faculty of Dentistry, McGill University.

Chapter 2: Literature review

2.1 Introduction

This literature review will provide an overview of the development, architectural structure and constituents of bone tissue. The processes of bone repair and regeneration will be briefly discussed leading to the introduction of bone grafting as a technique used in dental and orthopaedic surgery. Various bone grafting materials (natural and synthetic) will be reviewed followed by an introduction to calcium phosphate cements being used as biomaterials. A greater emphasis will be on discussing dicalcium phosphate cements namely: brushite and monetite.

2.2 Bone

Evolutionary process has led to the existence of the complex, multiphasic, anisotropic and heterogeneous microstructure of bone. It is a highly specialized tissue forming a supporting framework of the body, characterised by its hardness, stiffness and the intrinsic ability to regenerate and repair itself (19, 20). It provides protection to vital organs, acts as a mineral reservoir for growth factors and cytokines, plays a role in calcium homeostasis, provides space to enclose marrow, and helps in muscle based movements (21). Bone is not inert but in fact is a dynamically metabolized connective tissue (22). It continuously undergoes a remodelling process in order to adapt to the changing biomechanical forces, as well as to replace damaged and old bone with newer tissue maintaining bone strength (23).

2.2.1 Bone composition

Bone is a composite material comprised of specific cells, collagen, mucopolysaccharides, non-collagenous proteins, and minerals. The dry weight of bone comprises (24):

- Inorganic component (~70%), consisting mainly of hydroxyapatite (HA) (~99%).
- Organic component (~30%), having Type I collagen (~90%) and non-collagenous structural proteins (~10%) .

The following subsections will discuss the origin and role of the variety of cell types, matrix components and minerals in formation and maintenance of bone.

2.2.1.1 Bone cells

There are three cell types that play a vital role in the development and maintenance of bone tissue throughout the life of an individual. These cell types will briefly be discussed in this section.

- **Osteoblasts:** The precursor mesenchymal (osteoprogenitor) or stromal stem cell for osteoblasts is pluripotent and can also differentiate into marrow support cells and/or adipose cells, and possibly also into muscle cells, fibroblasts, or cartilage cells (25). Osteoblasts are formed and reside in the periosteum and bone marrow. These cells produce bone by the synthesis of matrix and its subsequent mineralization. Osteoblasts are mononucleated cells, and their shape varies from flat to plump, reflecting the level of cellular activity and maturity. They have a cuboidal shape during periods of high activity but become flat and line the bone surface at end of the matrix synthesis cycle (22). These cells line up along the bone forming surfaces and are responsible for deposition of bone matrix and regulation of osteoclasts (bone resorbing cells) (26). Osteoblasts possess receptors for estrogen and parathyroid hormones and have a high content of alkaline phosphatase, an organic phosphate-splitting enzyme. A variety of growth factors, hormones and physical stimuli act mainly through osteoblasts to bring about their effects on bone (27).

Table 2.2.1.1.1: Various cell types that play a role in bone formation and resorption.

Cell type	Source	Location	Functions
Osteoblasts	Mesenchymal stem cells	Bone surface (periosteal and endosteal)	Bone formation
Osteocytes	Osteoblasts trapped within bone	In bone	Sensing mechanical strain; transport of calcium and phosphate
Lining cells (periosteal, endosteal)	Osteoblasts	Periosteal and endosteal surfaces of bone	Regulate movement of calcium and phosphate into and out of bone
Osteoclasts	Hematopoietic stem cells	Bone surface (periosteal and endosteal)	Bone resorption

- Osteocytes:** These are terminally differentiated osteoblasts which get trapped in the matrix secreted by them. These cells are the most numerous in bone and possess the ability to communicate with not only each other but also with surrounding matrix through extensions of their plasma membrane (syncytial network of filopodial cellular processes) (27). Once osteocytes stop secreting osteoid they act as mechanosensors, instructing osteoclasts and osteoblasts to resorb and form bone respectively (28), hence ensuring a highly-coordinated and controlled remodelling process (29).

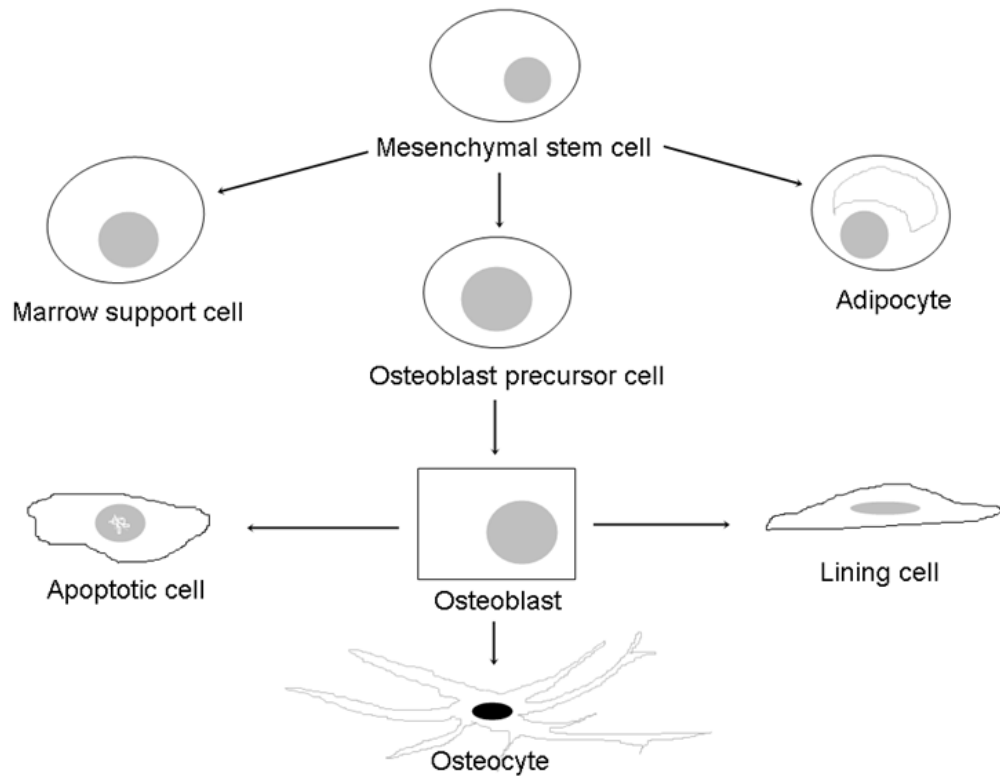


Figure 2.2.1.1.1: Interaction of stromal and hematopoietic cells leading to the formation of the osteocyte.

- Osteoclasts:** These are multinucleated giant cells responsible for the resorption of bone tissue. Activated osteoclasts are derived from the mononuclear precursor cells of monocyte-macrophage lineage (30). Active osteoclasts come in contact with calcified bone surface and exist within Howship's lacunae which are eroded pits created by their own resorptive activity (31). A feature that distinguishes osteoclasts from other cells is the presence of multiple nuclei and their relatively large size. In addition to multiple nuclei, osteoclasts also contain tubular and non-tubular lysosomes, vacuoles, numerous mitochondria, endoplasmic reticulum and well a developed Golgi apparatus (31, 32). The presence of these structures indicates the high activity of osteoclasts in energy production and protein synthesis, especially the production of lysosome enzyme (22).

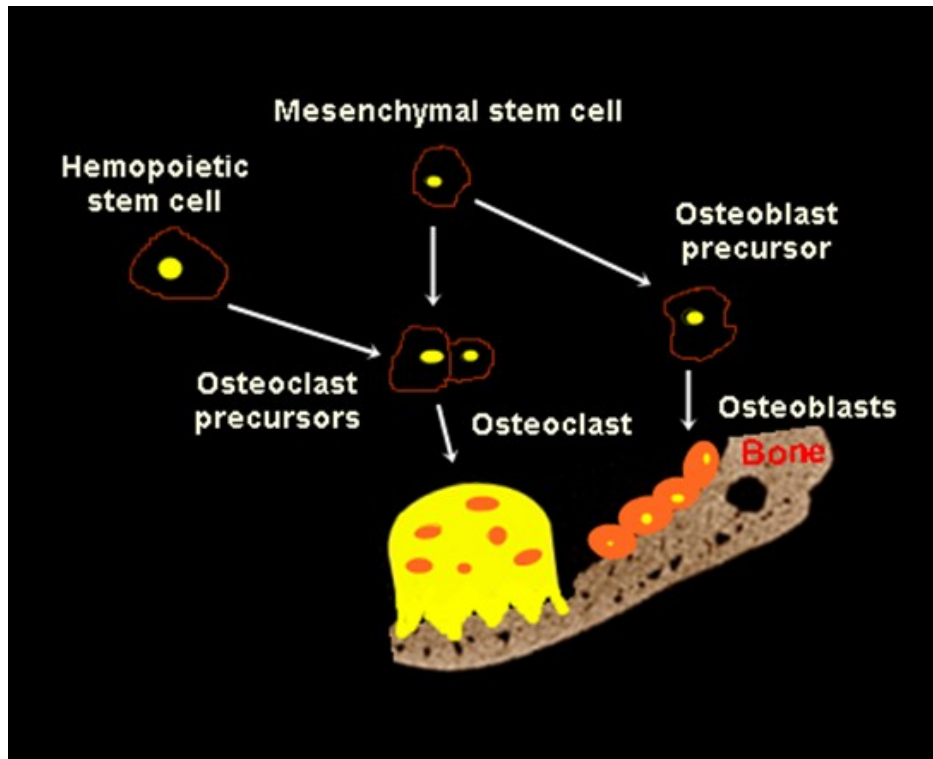


Figure 2.2.1.1.2: A diagrammatic representation of the interaction of stromal and hematopoietic cells forming osteoclasts and osteoblasts.

2.2.1.2 Bone matrix

Matrix by definition is an environment or a substance in which something develops. Bone matrix is the intercellular substance of bone which consists of collagenous fibers, ground substance (non-cellular component), mucopolysaccharides and non-collagenous proteins (33). Newly formed bone matrix does not mineralize immediately and this non-calcified matrix is known as osteoid, which exists under the regulation of osteoblasts (34). The quantity of osteoid is dependant and directly proportional to the bone forming activity of osteoblasts. A brief discussion about the components that make up the bone matrix follows:

- **Collagen:** Collagen is a fibrous protein that is assembled into fibrils that form fibers and bundles. The bonds present between collagen molecules provide stability and mechanical strength to bone. Collagen Type I constitutes ~90% of the organic matrix of bone, with little amounts of Type III, V, and FACIT (Fibril-Associated Collagens and Interrupted Triple Helices) collagens (35). FACIT are non-fibrillar collagens that are important for the organization and stability of extracellular matrices. Osteoblasts are responsible for the synthesis and deposition of precursors of collagen Type I in a parallel fashion or in concentric layers to produce mature (lamellar) bone (discussed later) (36).

- **Mucopolysaccharides:** This term is given to any group of polysaccharides which contain an amino sugar and uronic acid; a constituent of mucoproteins and glycoproteins. Mucopolysaccharides were previously known as Glycosaminoglycans (GAGs). The most predominant mucopolysaccharides include hyaluronic acid, dermatan sulfate, heparin, chondroitin sulfate, keratan sulfate, and heparin sulfate (37). These are highly negatively charged molecules located primarily on the surface of cells or in the extracellular matrix (ECM). Due to their high viscosity and low compressibility, these molecules are ideal for acting as a lubricating fluid in joint capsules (37). At the same time, their rigidity renders structural integrity to cells and provides passageways between cells, allowing for cell migration (37).

- **Non-collagenous proteins:** Osteoblasts are responsible for the synthesis and secretion of non-collagenous proteins, such as osteocalcin (most abundant non-collagenous protein in bone matrix), bone sialoprotein, osteopontin, osteonectin, glycosylated proteins with and without potential cell-attachment activities, proteoglycans (decorin and biglycan), and γ -carboxylated (Gla) proteins (38, 39). Alkaline phosphatase is the main glycosylated protein present in bone which is thought to be responsible for the mineralization of bone (40).

2.2.1.3 Bone minerals

The main mineral component of bone is crystalline HA having a chemical formula of $\text{Ca}_{10}(\text{PO}_4)_6(\text{OH})_2$. This accounts for approximately 25% by volume and 69% by weight the mass of adult bone (41, 42). HA is formed through several stages of maturation of amorphous calcium phosphate into small plates and rods. The crystals which form bone structure are deposited along the collagen fibrils and are located in spaces around the collagen molecules (43). Inorganic ions of these crystals like calcium and phosphorous are derived from blood plasma (44). The integral strength and hardness that is required for bone to serve the mechanical functions of the skeleton are a result of the mineral part of the bone composite.

2.2.2 Bone development

Intramembranous and intracartilaginous ossifications are the two essential processes during the development of mammalian skeletal tissue.

2.2.2.1 Intramembranous ossification

This is characterised by the laying down of bone into a primitive connective tissue (mesenchyme). This takes place by the formation of an ossification center, followed by calcification leading to the formation of trabeculae and eventually development of periosteum around the forming bone tissue (45). The process of intramembranous ossification is the direct mineralization of highly vascular connective tissue and it starts at certain points known as the centers of ossification (46). At these centers, the MSCs multiply and condense around a profuse capillary network. Among these proliferating cells and vessels is the amorphous ground substance with a fine network of collagen fibers (47). The MSCs differentiate and convert to osteoblasts and deposit osteoid in the center of the aggregated cell mass. At this point osteoid becomes mineralized and this creates the nidus which contains mineralized osteoid (entrapping osteoblasts to form the osteocytes) that is lined by active osteoblasts (45). The nidus which starts as a collection of MSCs becomes a rudimentary bone tissue and the

process of entrapment of osteoblasts continues as trabeculae thicken and vascular spaces become progressively narrower (19, 46). This process also occurs during the healing process of fractures (particularly compound fractures) treated by open reduction and stabilized by metal plates and screws (48, 49). Some examples of bones formed by intramembranous ossification are the skull, clavicle, maxilla, and mandible.

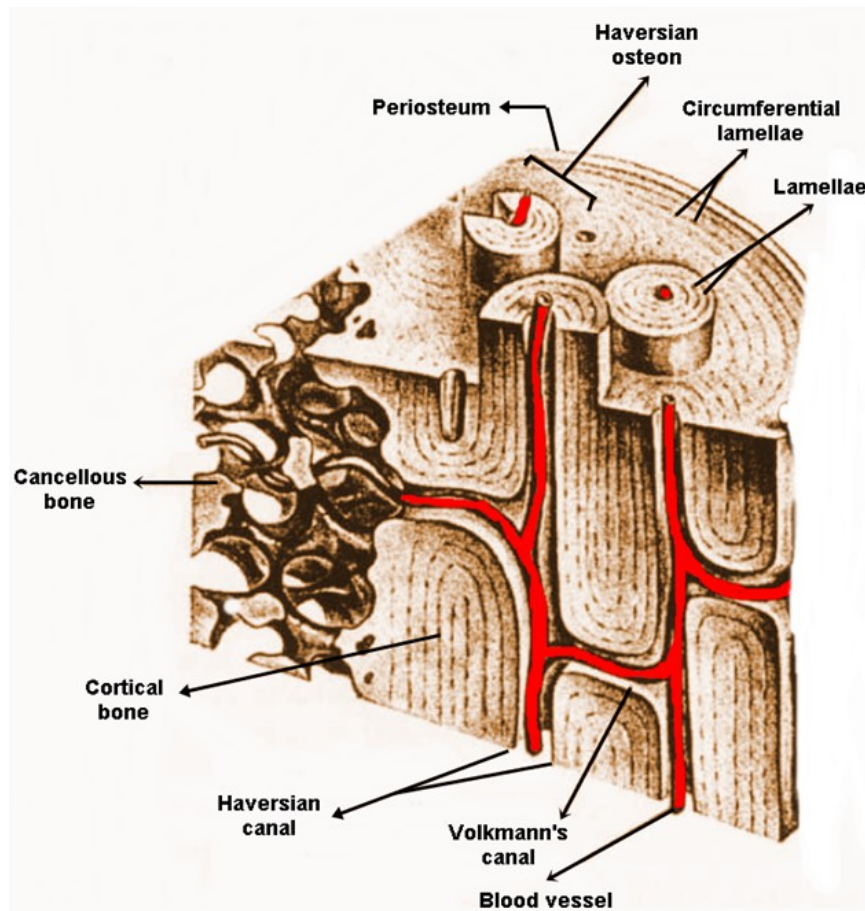


Figure 2.2.2.1.1: A diagrammatic representation of the microscopic structure of bone.

2.2.2.2 Intracartilaginous ossification

In this process, there is a cartilage model which acts as a precursor for bone formation. Intracartilaginous ossification requires an initial hyaline cartilage and is initiated at points which are called primary ossification centers, which mostly appear during fetal development (46). Secondary ossification occurs after birth and is responsible for the formation of epiphyses of long bones and the extremities of flat and irregular bones (50). The diaphysis and epiphysis are separated by a growing zone of cartilage (the epiphyseal plate). Upon reaching the age of maturity (~18-25 years, with variation between males and females), all of the cartilage is replaced by bone and the diaphysis and both epiphyses are fused together termed as epiphyseal closure (51). Intracartilaginous ossification takes place via following stages (46):

- Development of cartilage.
- Growth of cartilage.
- Development of the primary ossification center.
- Development of the secondary ossification center.

Intracartilaginous ossification is the most dominant process which occurs during fracture healing when treated by cast immobilization (43). Some bones which form by cartilaginous ossification are the humerus, radius, tibia, and femur.

2.2.3 Bone types according to morphology

Bone can be divided into two cortical and trabecular types based on morphology.

2.2.3.1 Cortical bone

The cortical or compact bone is the dense and solid component of bone surrounding marrow space and the cancellous bone. Cortical bone is characterised by having an outer periosteal surface and an inner endosteal surface (52). The periosteum is a fibrous connective tissue sheath that contains nerve fibers, blood vessels, osteoblast, and osteoclasts. Periosteum nourishes,

protects, aids in bone formation, and also plays a vital role in fracture repair and appositional growth (53). The endosteum is the membranous structure covering the inner surface of cortical bone (also cancellous) and the canals present which contains blood vessels. Cortical bone consists of cylindrical structures known as osteons or Haversian systems, with a diameter of $\sim 200 \mu\text{m}$ formed by cylindrical lamellae surrounding the Haversian canal (52). The boundary between the osteon and the surrounding bone is commonly known as cement line. Cortical bone has $\sim 5\text{-}10\%$ porosity with varying pore sizes (33). The largest pore sizes ($\sim 50 \mu\text{m}$ diameter), are formed by the Haversian canals (aligned with the long axis of the bone) and Volkmann's canals (transverse canals connecting Haversian canals) with capillaries and nerves (54). Other porosities are associated with lacunae (cavities connected through small canals known as canaliculi) and with space between collagen and HA ($\sim 10 \text{ nm}$) (55).

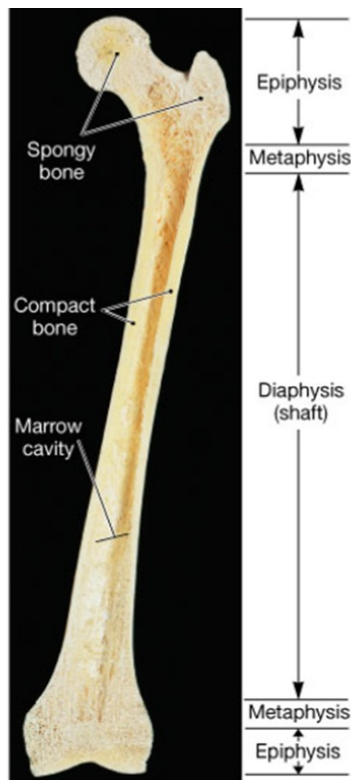


Figure 2.2.3.1.1: A long bone (femur) showing various types of bone tissue according to morphology. (Adapted from: Queen Mary, University of London handout notes).

2.2.3.2 Trabecular bone

Cancellous bone, also known as trabecular or spongy bone is composed of a honeycomb-like network of trabecular plates and rods interspersed in the bone marrow compartment. Cancellous bone has ~50-95 % porosity, usually found in cuboidal bones, flat bones and at ends of long bones (55). The bone matrix of cancellous bone has variable patterns of struts and plates called trabeculae, with a thickness of about 200 μm (56). These pores present are interconnected and filled with marrow tissue (composed of blood vessels, nerves, and cells whose main function is production of blood cells). The cancellous endosteum covers the inner surface of all cancellous bone.

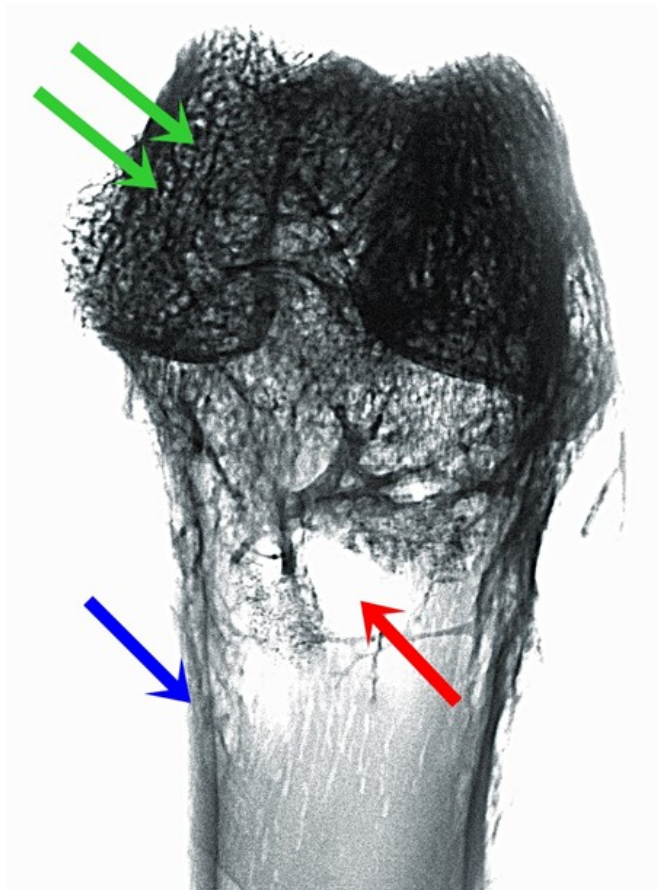


Figure 2.2.3.2.1: An inverted X-ray image of Long bone (femur) showing: 2 green arrows – Trabecular bone, 1 blue arrow – Cortical bone, and 1 red arrow – Marrow cavity.

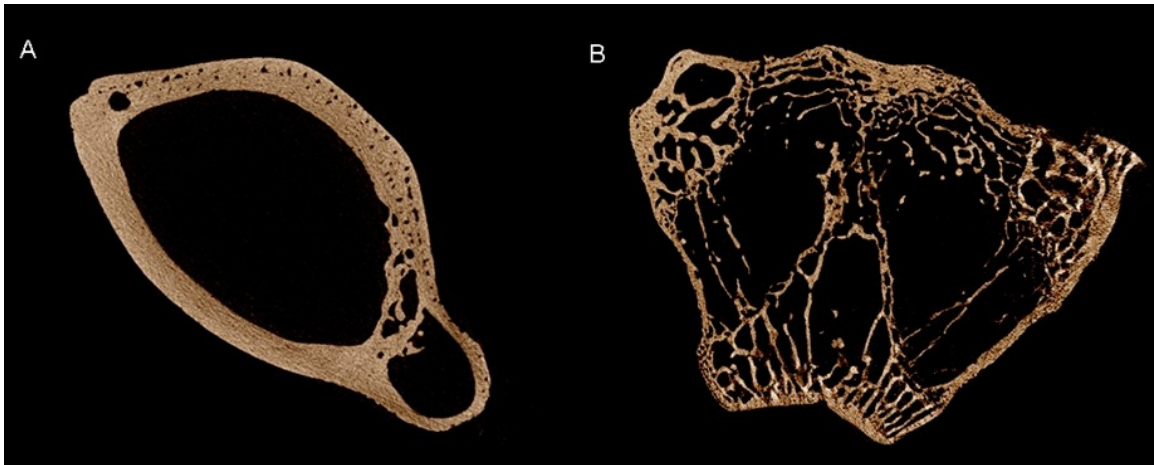


Figure 2.2.3.2.2: Micro-computed tomographic images of cross sections of A: cortical bone, and B: cancellous bone.

2.2.4 Bone types according to collagen pattern in osteoid

According to collagen patterns observed in the osteoid tissue, bone tissue can be divided into the woven and the lamellar types.

2.2.4.1 Woven bone

Woven bone is characterised by the haphazard laying down of collagen fibers and crystals, with absence of any organized pattern (57). It is produced when osteoblasts produce osteoid rapidly, which usually occurs during the initial phases of bone formation in the fetus; hence, the skeletal embryo consists entirely of woven bone (52). This woven bone is ultimately replaced by the process of bone remodeling that deposits more lamellar bone (19). Normally, there is no woven bone in the human skeleton after 4 or 5 years post birth but it reappears during the initial stages of healing process after suffering bone fracture (19, 55). Woven bone may also be seen in conditions that cause a high bone turnover such as, osteitis fibrosa cystica, hyperparathyroidism, and Paget's disease (52).

2.2.4.2 Lamellar bone

This type of bone is characterised by having a regular parallel alignment of collagen into sheets (lamellae) (52). Lamellar bone, as a result of the alternating orientations of collagen fibrils, has increased mechanical strength. In a healthy mature adult human, virtually all bone tissue is of lamellar type unless there is damage and the healing process takes place resulting in woven bone formation (53). Lamellar bone formation is a slower process in comparison with the less organized woven counterpart (58).

2.2.5 Bone types according to shape

Bones can be classified according to various shapes.

2.2.5.1 Flat bones

Flat bones are generally curved and thin with two parallel layers of cortical bones sandwiching a layer of cancellous bone. Flat bones include the skull, scapulae, mandible, ribs and the sternum.

2.2.5.2 Long bones

The long bones are composed of a hollow shaft (diaphysis), flared, cone-shaped metaphysis below the growth plates, and a rounded epiphyses above the growth plates (52). The diaphysis is primarily composed of dense compact bone, whereas the metaphysis and epiphysis are composed of cancellous (spongy) meshwork of bone surrounded by a very thin compact bone. Long bones include the clavicles, radii, humeri, metacarpals, femurs, tibiae, ulnae, fibulae, metatarsals and phalanges.

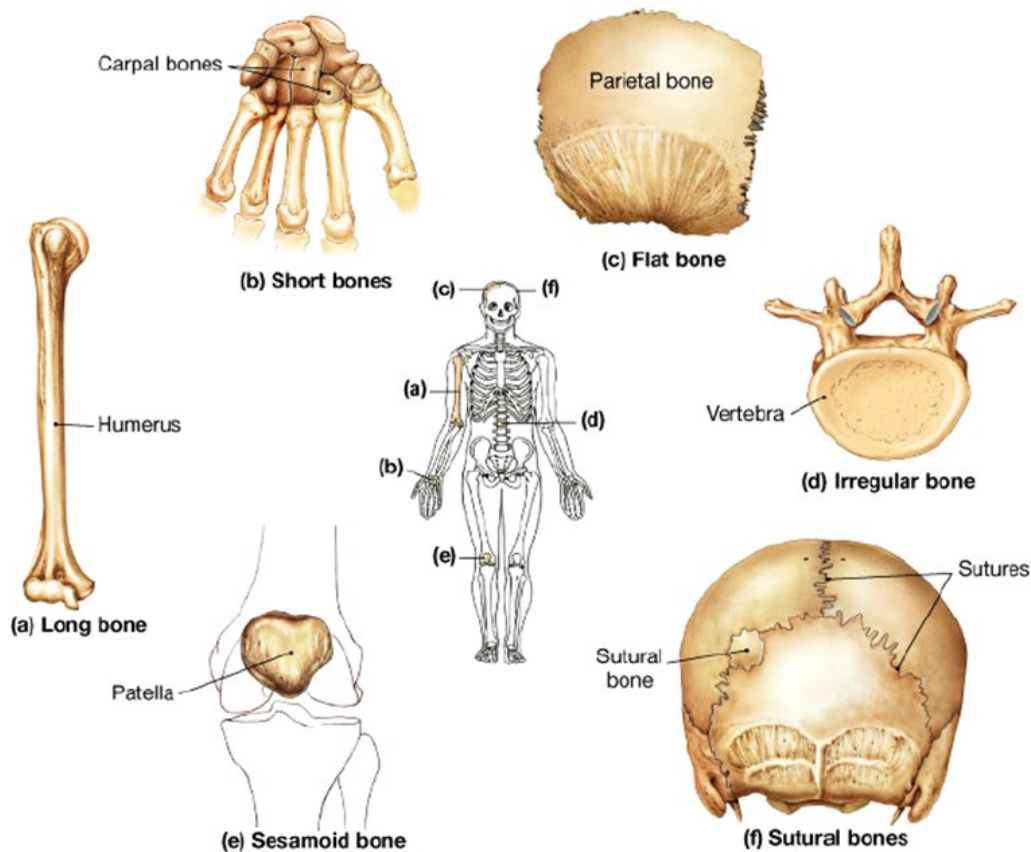


Figure 2.2.5.2.1: Bone according to varying shapes. (Adapted from: Queen Mary, University of London handout notes).

2.2.5.3 Short bones

Short bones are roughly cubical in shape and only have a very thin layer of compact bone surrounding a cancellous interior (59). These include the tarsals, carpals, and the bones of ankles and wrists.

2.2.5.4 Sesamoid bones

Sesamoid bones are bones embedded within the tendons. They act to hold the tendon further away from the joint which increases the angle of the tendon leading to increased leverage of the muscle. Patella and pisiform are examples of sesamoid bones.

2.2.5.5 Irregular bones

These are bones which do not conform to a particular shape. They consist of thin layers of compact bone surrounding a spongy interior. Their irregular shape is thought to be caused by their many centers of ossification or due to the presence of bony sinuses within them (60). Irregular bones include the vertebrae, coccyx, sacrum, ethmoid, sphenoid and the hyoid bone.

2.3 Bone remodelling and repair

Physiological bone remodelling is a process by which bone is maintained by removal from and addition to the skeleton. It is a lifelong continuous process of removal of portions of old bone to be replaced with newly synthesized proteinaceous matrix, and its subsequent mineralization (61-63). It is a balance to maintain bone mass and can provide minute-to-minute exchanges of minerals from bone matrix. Bone remodelling is essential in maintenance of bone strength and mineral homeostasis by responding to functional demands (64). Remodelling not only regulates the reshaping and replacement of bone during growth and fracture healing, but is also responsible for healing bone micro-damage which occurs through normal activity (24, 63). The bone remodelling cycle involves a series of highly regulated steps that depend on the interaction of osteoblasts and osteoclasts, coupled via paracrine cell signalling (65). Bone remodelling process can be subdivided into six phases (64):

- Quiescence
- Activation
- Resorption
- Reversal
- Formation
- Mineralization

The quiescent phase is a state of bone at rest prior to the activation phase that involves the stimulation of bone surface through retraction of bone lining cells (29, 66, 67). The recruitment of mononuclear monocyte-macrophage osteoclast precursors from the blood, results in the interaction of osteoclast and osteoblast precursor cells. This results in differentiation, migration, and fusion of the osteoclasts, which attach to mineralized bone surface and initiate resorption (68). In the resorptive phase osteoclasts begin to dissolve the mineral matrix and cleave the osteoid matrix resulting in formation of resorption pits (66). Osteoclast-mediated resorption takes two to four weeks during each remodeling cycle. In the reversal phase, bone resorption transitions to bone formation and preosteoblasts are recruited to begin new bone formation (68). During the formation phase osteoclasts detach from the bone surface and are replaced by cells of osteoblast lineage which initiate bone formation. The differentiated osteoblasts synthesize the osteoid matrix which fills the resorbed cavity (54). The osteoblasts continue to produce bone and ultimately stop and transform to quiescent lining cells that cover the newly formed bone surface connecting the osteocytes in bone matrix through a network of canaliculi (66, 68). The mineralization phase is characterised by the precipitation of HA in the osteoid matrix. This begins by ~30 days after deposition of osteoid, ending at ~90 days in trabecular and at ~130 days in cortical bone (66, 69). The quiescent (or the rest phase) commences again after this mineralization phase is completed and the cycle starts again (63, 70).

Bone structure undergoes fractures or develops defects due to excessive stresses (e.g. micro-fractures) or because of trauma which can lead to larger defects. Fracture repair involves the following three phases (71, 72):

- Inflammation
- Repair
- Remodelling

Following injury, inflammation takes place immediately peaking after about 48 h and resolving by 1 week following the injury (73). Inflammation serves to provide stabilization of the fracture via protection due to pain (limits movement) and hydrostatic pressure due to swelling at the injury site (53). Also, a hematoma is formed between the ends of the fracture during the inflammatory phase of repair (74). The reparative phase begins within a few days of the injury and lasts several weeks. The formation of callus occurs which stabilizes the fracture through lateral support. Early into the phase, callus is a mixture of fibrous connective tissue, cartilage, blood vessels, woven bone and osteoid (72). With time, ossification occurs and the callus calcifies connecting the two fracture ends (53, 74). The woven bone which is formed by this process is replaced with lamellar bone and the resorption of excess callus takes place in the remodelling phase (72). This remodelling process is very similar to that occurring in normal, uninjured bone tissue but occurs at an accelerated rate for some time until stability is achieved comparable to prior to injury (53, 74).

2.4 Bone grafting

Bone grafting is required in conditions of significant skeletal bone defects and is frequently used to prevent fibrous tissue in-growth and to maintain mechanical function. The treatment of fractures and other defects provide a great challenge to orthopaedic and dental surgeons. Apart from the fractures that heal in an uncomplicated manner, 5-10% of patients face problems because of bone defects or impaired fracture healing, sometimes a combination of both (75). Bone grafting is a common surgical procedure which is performed in approximately 10% of orthopaedic reconstruction cases (32). It has been estimated that around 2.2 million surgical grafting procedures are performed annually (2, 3).

Bone grafts serves as a structural framework that ideally leads to bone formation within defects (72). After implantation, hard and soft tissue host bed surrounding the graft must be viable and have adequate blood supply for the graft material to

be resorbed and infiltrated by new bone (43, 76, 77). In the weeks following implantation, new blood vessels, interstitial cells and woven bone (by new osteoblasts) are produced by the host bed (23, 76). These tissues embedded within the graft create the graft-woven bone complex. Bone formation in grafting procedures involves one or more of the following mechanisms:

- Osteogenesis: New bone formation by osteoblasts (76).
- Osteoinduction: The ability of a material to induce the differentiation of osteoblasts from the surrounding tissue at the graft host site, resulting in new bone formation and growth (78, 79).
- Osteoconduction: The ability of graft material to support the growth of bone over its surface (7, 43, 80).

From a periodontal viewpoint, an ideal bone replacement graft should also be able to induce osteogenesis, cementogenesis and formation of periodontal ligament (PDL) (11, 81).

2.5 Bone replacement graft materials

Bone replacement grafts can generally be divided into natural and synthetic grafts according to their origin. The natural sources of these grafts can be human and/or animal tissues. Bone substitutes should ideally demonstrate good localized and systemic compatibility and have the capability to be substituted by the regenerating bone and to completely fill any defect (12). To achieve these objectives it is of prime importance that the implant demonstrates osteoconductive and osteoinductive properties comparable to those of the natural bone (52). Most bone replacement grafts are osteoconductive, relatively inert filling materials; integrate with new bone without providing much histological evidence of extensive regeneration (1, 3, 12). These osteoconductive graft materials provide a scaffold allowing bone deposition and in-growth. Although osteointegration, which is the ability to bind to surrounding bone, is not directly

responsible for bone formation, is a desirable property that aids in the incorporation of graft material at host site (1, 82). The most important aspect for the success of a bone graft is to be completely resorbed and remodelled, allowing the graft to not interfere with physiologic bone adaptation (63).

Table 2.5.1: Requirements of bone grafts for successful bone tissue replacement.

Characteristics	Comments
Biocompatibility	Should not provoke any graft rejection (immune response) and inflammation.
Bioactivity	Stimulate osteoconduction, osteoinduction and create biochemical bonding with host tissue (osseointegration).
Biodegradability	Act as a temporary scaffold to be replaced with new bone formation at adequate pace (match degradation rate with bone formation rate).
Degradation modality	Surface and/or bulk erosion/biodegradation.
Osteoconductivity	Have intrinsic potential to support in-growing capillary network, perivascular mesenchymal tissues and the osteoprogenitor cells from the host.
Porosity within graft structure	To provide sufficient revascularization leading to adequate nutrition and oxygen supply. Also to maximize surface area for protein adsorption, cellular adhesion and extra cellular matrix secretion.
Three dimensional architecture	For support to the cellular in-growth and deep penetrative transport of nutrition and oxygen.
Vascular support	Channels for blood vessels ensuring adequate blood supply to maintain healthy bone growth
Ease of manipulation	Should be easy to handle during surgical procedures.
Sufficient mechanical strength	Adequate structural integrity to bear the in vivo stresses during bone formation phase.
Sterilization compatible	Biologic and physico-chemical and mechanical properties should not be compromised.
Cost-effectiveness	Clinically affordable.

Table 2.5.1.1: Merits and demerits of using autogenous bone grafts.

Advantages of autografts	Disadvantages of autografts
Biocompatible	Additional surgery to harvest bone and extensive hospitalization
High osteogenic potential	Increase in operative time and cost
Osteoconductive	Post-operative pain and increased blood loss
Osteoinductive	Increased risk of fracture (donor site)
Adequate mechanical strength providing structural support	Dead bone is at potential risk for infection to set in
Easier incorporation into host site (none or minimal immune response)	High variability in quality of harvested bone tissue
Availability in cortical and cancellous forms	Limited amount of graft tissue can be harvested

Autografts can be cancellous or cortical in nature or a combination of both. Owing to their sponge like architecture, cancellous grafts have the ability to revascularize sooner than cortical grafts (83). This revascularization begins around the fifth day post transplantation (89). Prior to the revascularization, cellular survival in the graft tissues is heavily dependent upon the plasma diffusion for providing adequate nutrition and waste product removal. Osteocytes residing in their lacunae have been shown to survive if they are within 0.3 mm of the perfusion surface (90). In comparison, cortical autografts undergo considerable osteoclast mediated resorption before osteoblastic bone formation can commence (91). Cortical grafts show initial high strength which diminishes overtime before increasing again (81). Dynamic loading has been shown to be a critical factor for the preservation of bone mass after implantation and on a cellular level for the modulation of osteoclastic and osteoblastic processes (92, 93). After several weeks to 6 months post implantation, cortical autografts have been shown to be 40-50% weaker than normal bone (89). Conversely, cancellous autografts are weak initially after implantation because of their porous

architecture. Over a period of time they continue to gain strength and mechanical loading is imperative for achieving adequate dimensional stability and strength (84).

2.5.2 Allografts

Allografts are bone grafts harvested from other individuals of same species. There has been great interest in allografts due to their abundance in supply and also because they match closely match human bone in elemental constitution and architecture (84, 94). Though allografts undergo various treatments prior to use, risk of disease transmission is still a possibility (95-97). Despite these risks, the recognition of distinct advantages associated with allografts has resulted in the widespread use of bone grafting procedures with them (93, 98). Allografts are mostly prepared as fresh, frozen, freeze-dried, mineralized and demineralized, and each of these are available as cortical chips, cortical granules, cortical wedges or cancellous powdered grafts (84).

2.5.2.1 Fresh or frozen iliac cancellous bone and marrow grafts

Fresh or frozen iliac cancellous bone and marrow tissues possess the highest osteoconductive and osteoinductive potential among all the available allografts (10). The risk of disease transmission, antigenicity and extensive cross-matching and treatment required has rendered the use of frozen iliac allografts unacceptable in modern orthopaedic and dental surgery (99, 100).

2.5.2.2 Mineralized freeze-dried bone allografts (FDBA)

There has been an extensive use of FDBA in treatment of periodontal defects (101, 102). This can be attributed to evidence that the health risks associated with fresh frozen bone are markedly reduced (100), and also due to the successful results of grafting procedures with them (103). It is assumed that the process of freeze drying affects immune recognition in the host by distorting the three dimensional presentation of human leukocyte antigens on the surface of

these allografts (100, 104). Cortical FDBA does not appear to elicit an immune response in non-human primates (105). The use of cortical FDBA is recommended over their cancellous counterparts because there is more bone matrix present and a higher inductive potential and also because the cortical bone is less antigenic (83). FDBA is considered osteoconductive (83) and studies have shown that mixing these with autografts enhances the osteogenic potential (103, 106).

2.5.2.3 Demineralized freeze-dried bone allografts (DFDBA)

Research has indicated that the removal of mineral component from grafts allows greater expression of osteoinductive proteins (98, 107). This is because the minerals present, blocks the effect of factors stimulating bone growth sequestered in bone matrix including bone morphogenetic proteins (BMPs) (107, 108). Animal studies have shown that DFDBA has osteogenic potential (106, 109, 110). However, Unlike FDBA, the addition of autograft materials to DFDBA does not increase the osteogenic potential to a significant degree (111, 112). The bioactivity of DFDBA has been shown to be age dependent, with grafts harvested from the younger individuals having higher osteogenic potential in comparison to grafts procured from older individuals (19, 113). DFDBA is used frequently for maxillofacial and periodontal grafting procedures. In maxillary sinus augmentation procedures, DFDBA showed 29% new bone formation while autogenous grafts showed 40% in comparison (5). It has also been observed that DFDBA particles situated near pre-existing bone were enclosed by new bone, whereas particles located near the center of the graft showed no signs of remineralization or new bone formation (5, 114).

Table 2.5.2.3.1: Autografts versus Allografts.

Bone grafts	Structural strength	Osteogenesis	Osteoconduction	Osteoinduction
<u>Autografts</u>				
-Cortical	3	2	2	2
-Cancellous	0	3	3	3
<u>Allografts</u>				
-Cortical				
Frozen	3	1	0	0
Freeze-dried	1	1	0	0
-Cancellous				
Frozen	0	2	1	0
Freeze-dried	0	2	1	0

Scores: 0 (none), 1 (moderate), 2 (good) and 3 (excellent)

2.5.3 Xenografts

These are graft materials that are harvested from non-human species. Currently, there are two kinds of xenografts commercially available for bone replacement therapy and regenerative applications; bovine bone and natural coral (23, 114). Both sources provide bone grafts that are biocompatible and structurally similar to human bone, however, their processing techniques are quite different. Xenografts are osteoconductive in nature and are readily available for clinical use (114, 115).

2.5.3.1 Bovine-derived xenografts

Commercially available bovine bone is processed to yield natural bone mineral without the organic component. Inorganic bone derived from bovine origin is the HA skeleton that retains the microporous and macroporous structure of cancellous and cortical bone (116), following low-heat and chemical extraction of the organic component. A given advantage of these grafts is the improved osteoconductive potential compared with synthetically derived materials. Bovine-

derived HA bone replacement grafts increase the available surface area that can act as an osteoconductive scaffold owing to their higher level of porosity and have a mineral content that is comparable to human bone facilitating integration with host bone (115). Previously, bovine xenografts have failed due to graft rejection (117), probably because of chemical detergent extraction techniques which left residual proteins (118). Xenografts of bovine origin carry a theoretical risk of disease transmission (bovine spongiform encephalopathy). Although evidence suggests that the risk is negligible, concerns still exist (119, 120). Bovine-derived bone grafts have successfully been used for the treatment of intrabony defects and also in ridge augmentation procedures (115, 121).

2.5.3.2 Calcium carbonate xenografts

Coralline calcium carbonate is obtained from natural coral, genus *porites*, and is composed primarily of aragonite (>98% CaCO₃). It has a pore size of 100 to 200 µm which is quite similar to that seen in cancellous bone (122). The relative high porosity of ~45% provides a large surface area for graft resorption and replacement by new bone (123). Unlike HA, calcium carbonate is resorbable *in vivo* and can also be derived from the same coral by heat conversion. Calcium carbonate does not require surface transformation to carbonate like other grafts in order to induce bone formation; hence it can potentially initiate new bone deposition rapidly (122). Coralline calcium carbonate has also shown to have high levels of osteoconductivity because it does not undergo fibrous encapsulation (124). Coralline calcium carbonate have demonstrated a gain in PDL clinical attachment, reduction of probing depths and greater defect fill in periodontal applications (125-127).

2.5.4 Alloplasts

Alloplastic bone grafts are synthetic materials that have been manufactured and investigated extensively for clinical use. Alloplasts include synthetic polymers, bioactive glasses, glass-ionomers and ceramics. The major advantage of using

alloplastic materials are: their unlimited availability, no risk of disease transmission and the absence of antigenic response from host towards them (128). Alloplasts can be manufactured in various forms and with varying physico-chemical properties. They can be made available in both resorbable and non-resorbable forms and can be customized with varying levels of porosity and pore sizes (129).

2.5.4.1 Polymers

Polymers can be classified based on their origin: natural or synthetic. Natural polymers that have been utilized in the fabrication of bone grafts include polysaccharides (e.g., alginate, argose, chitosan and hyaluronic acid) and polypeptides (e.g., gelatin and collagen) (130). Natural polymers possess low mechanical properties and variable or negligible rates of degradation, hence their use is limited as bone grafting materials. However, natural polymers play an important role in composite graft production by serving as polymeric shell capsule which incorporate allograft particles (131). Synthetic polymers (e.g., poly-glycolic acid, poly-lactic acid and poly-anhydride) provide a platform for regulating and controlling the biomechanical properties of scaffolds and also serve as drug delivery carriers in tissue engineering applications (132).

HTRTM Synthetic Bone (Bioplant, Norwalk, CT) is a biocompatible microporous composite made up of poly-methylmethacrylate, poly-hydroxyethylmethacrylate, and calcium hydroxide. The acronym HTR stands for 'Hard Tissue Replacement' and acceptable clinical results have been achieved in treatment of intrabony and furcation defects with its use (123, 133). Histologically, new bone growth has been observed on the particles of this material (134, 135). This material has hydrophilicity that enhances clotting, and the negative particle charges on the surface allows adherence to bone. Clinically acceptable defect fill and resolution has been achieved and supports the use of HTRTM as a biocompatible alloplastic bone substitute (136, 137).

2.5.4.2 Bioactive glasses

Bioactive glasses were invented for use as bone substitutes more than 3 decades ago. The designation “bioactive” is in relation to their ability to bond to bone and soft tissues and enhance bone-tissue formation. This is attributed to their inherent similarity with the architecture of host bone. Bioactive glasses are non-porous and consist of silicon dioxide (SiO_2), calcium oxide (CaO), phosphorous pentoxide (P_2O_5), and sodium oxide (Na_2O) (138, 139). The solubility of these grafts is directly dependent upon the proportion of sodium oxide found in the formulation. By alteration in the concentrations of sodium oxide and calcium oxide, glasses with different properties can be produced (140, 141). Bioactive glasses are essentially non-resorbable bone graft materials and when exposed to tissue fluids, these bioactive glass particles are encompassed in a double layer composed of silica gel and a calcium-phosphorous rich (apatite) layer. The calcium-phosphorous rich layer attracts, promotes and concentrates the adsorption of proteins which are utilised by osteoblasts to form a mineralized extracellular matrix (142, 143). It is thought that these bioactive properties guide and promote osteoconduction and osteogenesis (58, 126, 143), allowing the rapid bone formation that is subsequently observed (140, 144).

2.5.4.3 Ceramics

Ceramics are inorganic, non-metallic materials. Bioceramics have been in use in orthopaedics and dentistry since the 1980s (145, 146). Ceramics or bioceramics (owing to their biological use) are alloplastic materials comprising mainly of calcium phosphate or sulfates. They have been used as load bearing surfaces for joint replacements and as dental implants for tooth replacement (147). Ceramics are strong under compression but weak in tension (146). They are brittle solids and can easily undergo catastrophic failure upon crack initiation (148, 149). This inherent weakness of bioceramics has limited their use to non-load bearing applications in orthopaedic surgery (146). In subsequent sections we will discuss in detail calcium phosphates as a class of bioceramics used for bone replacement and repair applications in dentistry and orthopaedics.

2.5.4.4 Calcium phosphates

Calcium phosphates are a group of minerals that contain calcium ions (Ca^{2+}) in combination with orthophosphates (PO_4^{3-}). There are a number of calcium phosphate compounds that exist (**Table 2.5.4.4.1**). Some compounds precipitate at room temperature in aqueous systems whereas other compounds are obtained by thermal decomposition or thermal synthesis. A subdivision can be made between calcium phosphate ceramics and calcium phosphate cements. For calcium phosphate ceramics the thermal treatment known as sintering is often used to change powders to granules or monoliths (150). This process removes volatile chemicals and increases the crystal size, often resulting in a porous solid material (151). Calcium phosphate cements comprise of powder or a mixture of powders which, upon mixing with water or an aqueous solution, react forming a precipitate of crystals and set solid by the entanglement of crystals (152).

Calcium phosphates are used for a variety of orthopaedic and dental applications. The two most commonly used synthetic graft materials are tricalcium phosphate (TCP) and hydroxyapatite (HA) (150). TCP is often used clinically as a porous form. TCP has two crystallographic forms, β -tricalcium phosphate (β -TCP) and α -tricalcium phosphate (α -TCP) (16). The most common type is β -TCP and it is used as a filler that is partially resorbable allowing bone formation and replacement (153-155). Over the years TCP has gained clinical acceptance as a bone filler material. However, when a direct comparison is made, the allogenic grafts outperform TCP in terms of resorption and bone formation (156). There is evidence that TCP granules undergo fibrous tissue encapsulation and do not stimulate bone growth sufficiently for bone replacement applications (157, 158).

Table 2.5.4.4.1: List of existing calcium phosphate compounds.

Compound name	Chemical formula	Symbol	Ca/P ionic ratio	Mineral
Monocalcium phosphate monohydrate	$\text{Ca}(\text{H}_2\text{PO}_4)_2 \cdot \text{H}_2\text{O}$	MCPM	0.5	-
Monocalcium phosphate anhydrous	$\text{Ca}(\text{H}_2\text{PO}_4)_2$	MCPA	0.5	-
Dicalcium phosphate dihydrate	$\text{CaHPO}_4 \cdot 2\text{H}_2\text{O}$	DCPD	1.0	Brushite
Dicalcium phosphate anhydrous	CaHPO_4	DCPA	1.0	Monetite
Octacalcium phosphate	$\text{Ca}_8(\text{HPO}_4)_2(\text{PO}_4)_4 \cdot 5\text{H}_2\text{O}$	OCP	1.33	-
α -Tricalcium phosphate	$\alpha\text{-Ca}_3(\text{PO}_4)_2$	α -TCP	1.5	-
β -Tricalcium phosphate	$\beta\text{-Ca}_3(\text{PO}_4)_2$	B-TCP	1.5	-
Amorphous calcium phosphate	$\text{Ca}_x\text{H}_y(\text{PO}_4)_z \cdot n\text{H}_2\text{O}$, $n \approx 3\text{-}4.5$; 15-20% H_2O	ACP	1.2-2.2	-
Precipitated hydroxyapatite	$\text{Ca}_{8-x}(\text{HPO}_4)_x(\text{PO}_4)_{6-x}(\text{OH})_{2-x}$	PHA	1.33-1.67	-
Calcium-deficient hydroxyapatite	$\text{Ca}_{10-x}(\text{HPO}_4)_x(\text{PO}_4)_{6-x}(\text{OH})_{2-x}^f$ ($0 < x < 1$)	CDHA	1.5-1.67	-
Hydroxyapatite	$\text{Ca}_{10}(\text{PO}_4)_6(\text{OH})_2$	HA	1.67	Hydroxyapatite
Oxyapatite	$\text{Ca}_{10}(\text{PO}_4)_6\text{O}$	OXA	1.67	-
Fluorapatite	$\text{Ca}_{10}(\text{PO}_4)_6\text{F}_2$	FA	1.67	-
Tetracalcium phosphate	$\text{Ca}_2(\text{PO}_4)_2\text{O}$	TTCP	2.0	Hilgenstockite

Synthetic HA has been marketed for use in variety of forms: porous non-resorbable, solid non-resorbable, and resorbable (porous). The resorbability of HA is dependent upon the temperature at which it is processed. When prepared at high temperatures, the HA produced is dense and has non-resorbable crystals (159). Dense HA is osteoconductive and acts primarily as a biocompatible filler material. It has been shown that HA when used in conjugation with periodontal flap debridement results in greater defect fill in comparison to flap debridement

alone in active treatment of intrabony periodontal defects (160, 161). Resorbable HA, which is particulate and porous, processed at low temperatures is a non-sintered (not fired) precipitate with particles measuring 300 to 400 μm in size. It is believed that this non-sintered HA acts as a mineral reservoir inducing bone formation via osteoconductive mechanisms (162). This HA has slow resorption rate, yet it acts as a scaffold for bone replacement (163) [111]. In summary; HA is non-osteogenic, neither conclusively osteoinductive, but rather functions as an osteoconductive graft material which performs as a scaffold for in-growth and deposition of new bone.

2.6 Introduction to dicalcium phosphate dihydrate (DCPD) cements

Dicalcium phosphate dihydrate (DCPD) cements were first prepared in 1989 by Mirtchi and Lemaître who mixed a powder consisting of an acidic calcium phosphate (monocalcium phosphate monohydrate) and a basic calcium phosphate (β -TCP) with water (164). The result of this mixture was a mouldable paste that solidified over time forming set DCPD also known as brushite (mineral name) (165). Brushite cements are biocompatible and possess a unique advantage over HA cement, which is the ability to be resorbed under physiological conditions due to higher solubility. This original formula of brushite cement resulted in a material that was weak in terms of mechanical properties ($\sim 1\text{MPa}$ compressive strength) and set quickly ($\sim 30\text{s}$) not allowing adequate working time for *in vivo* applications. Since then, research has been conducted to improve mechanical properties and optimize the setting time of these cements.

2.6.1 Cement composition

The main constituents of dicalcium phosphate (DCP) cements are an alkaline calcium source, an acidic phosphate source and water. Additives are often used to increase cement setting time, increase mechanical properties and improve handling. Different compositions of brushite cements have been formulated and evaluated (166).

2.6.1.1 Alkaline calcium source

Since brushite has calcium to phosphate (Ca/P) ratio of 1, calcium phosphate compounds with higher Ca/P ratios can be used as alkaline calcium source in brushite cements. The most common basic calcium source in brushite cements is TCP which has Ca/P ratio of 1.5. TCP has two crystallographic forms: (1) β -TCP, and (2) α -TCP. Both of these minerals can and have been used to prepare DCP cements, but since β -TCP has lower energy requirements for its production, it is most frequently used (167-169).

Other alkaline calcium sources can be used such as calcium oxide (170) and calcium hydroxide, both of which are very alkaline (171). Tetracalcium phosphate (TTCP) has calcium to phosphate ratio of 2. This ratio is ideal for DCP cements but its preparation is rather complex and since it confers no benefit, its use in DCP cement preparation has been very limited (172). HA has Ca/P ratio of 1.67, and its ions can be easily substituted (173-175). Nano-crystalline HA (nHA) has also been used to prepare DCP cements (172).

2.6.1.2 Acidic phosphate sources

Acidic phosphate ions are needed to prepare DCP cements. The simplest source is phosphoric acid which is inexpensive and has been used in many cement preparations (167, 169, 172). Acidic calcium phosphates can also be used in the preparation of DCP cements but only if they have Ca/P ratio lower than 1. The only calcium phosphates with this ratio are monocalcium phosphate monohydrate (MCPM) and monocalcium phosphate anhydrous (MCPA) (170, 176). Both of these calcium phosphates have been used to prepare DCP cements. Cements containing MCPM are easier to handle because the presence of a water molecule in MCPM facilitates the setting reaction of by donating one of the two water molecules required to form each unit of dihydrate.

2.6.1.3 Additives

In addition to the alkaline and acidic calcium and phosphate sources respectively other additives can be added to alter or improve the properties of the set DCP cements. Some of the additives that have been added to cement formulations include pyrophosphates, sulphate ions, carboxylates and polymeric materials. Pyrophosphates are natural inhibitors of mineralization and when added to DCP cement formulae, regulate cement setting reaction. Calcium pyrophosphate (164), sodium pyrophosphate (177-179) and pyrophosphoric acid (180) are some of the pyrophosphate salts that have also been used as additives.

Sulfate ions interact with calcium phosphates and substitute for phosphate ions; hence they can be used to modify the setting reaction of DCP cements (178). Calcium sulfate dihydrate and calcium sulfate hemihydrate can be added to the cement powder phase (164, 181), or those such as sulfuric acid to the cement liquid phase (177, 179).

Carboxylates and carboxylic acids such as sodium citrate (178) and citric acid (182) have been used and evaluated as retardants in DCP cements. Other α -hydroxyl acids such as tartaric acid (183) and glycolic acid (176) have also been assessed. Acetic and oxalic acid have also been studied as additives in DCP cements (176, 184).

Polymeric materials can be added to brushite to improve the mechanical properties and injectibility of the cements. Studies have tested the effect of collagen and other hydrophobic polymers added to reinforce DCP cements (185, 186). Type I collagen can be added to cement by dissolving it in an acidic cement liquid phase (187). Other hydrophobic polymers, such as poly(lactic acid-co-glycolic acid), are added as fibers or dissolved in organic solvents after the cement has already set (187, 188). Polymeric materials can also be combined with DCP cements by adding small amounts of cement powder into a polymeric matrix. The cement acts as filler that reinforces the polymeric matrix in these materials (189). For improving the injectibility of cement pastes, hydrophilic

polymers hydrogels such as xanthan gum, hydroxypropyl methylcellulose, polyacrylic acid, silica gel, hyaluronic acid, albumin and fibrinogen can be dissolved in small quantities in the cement liquid phase (189-193).

Metallic ions such as strontium and magnesium can be added by mixing the cement powder with a salt containing metallic ion (194, 195). Another way of adding metallic ions can also be added by doping the cement precursors with the different ions. This can be done by preparing the alkaline calcium source from calcium and metal ion salts mixture instead of pure calcium and phosphate precursors. In this way zinc and silicon ions have been doped into β -TCP (196, 197), strontium ions into α -TCP and β -TCP (168, 197, 198) and magnesium ions into α -TCP, β -TCP and nHA (175, 199, 200).

2.6.2 Cement setting reaction

The brushite cement setting reaction consists of:

- (1) The dissolution of cement powder in a solvent;
- (2) The formation of a super-saturated solution;
- (3) Nucleation within the solution;
- (4) Crystal growth and interlocking of crystals forming a hardened material (16).

Cements prepared with β -TCP/MCPM powder mixtures begin their setting reaction by the dissolution of MCPM, which is accompanied by a rapid decrease in pH (201, 202). This low pH (<4) is required for the setting of brushite (or monetite if lower than 2). Low pH during setting is due to the presence of acidic phosphate source used. If the cement has excess MCPM in comparison with β -TCP then the pH remains low even after the setting reaction is complete. However, if the cement has excess β -TCP the cement pH settles at 5 (201). Final setting of the cement is usually confirmed by the use of Gilmore or Vicat needles (176, 182). The cement is considered to be set when the needles do not create a visible indentation on the surface.

2.6.2.1 Effect of additives and other factors on setting reaction

Additives present in brushite cements have the potential to modify the setting reaction by affecting the dissolution of DCP powders and precipitation of brushite crystals. Sulfate, citrate and pyrophosphate ions present in the setting cement have been shown to inhibit brushite precipitation (202). Citrate ions have been shown to interact with β -TCP particles in the β -TCP/MCPM systems, limiting their dissolution (183). The effect of sulfate ions present in the cement systems is concentration dependent. They delay cement setting reaction when used at low concentrations but at high concentrations result in the formation of calcium sulfate dihydrate crystals that act as nuclei for the crystallization of brushite thus accelerating the setting reaction. Sodium sulfate, sulfuric acid, gentamicin sulfate, the polysaccharide C4S, calcium sulfate dihydrate and calcium sulfate hemihydrate are some sources of sulfate ions that have been utilised to prolong the cement setting time (164, 178, 179, 181, 203, 204).

Pyrophosphate compounds such as sodium pyrophosphate, calcium pyrophosphate and pyrophosphoric acid have also been used to delay setting time of brushite cements (180, 202, 205). Organic acids bind with calcium ions enabling them to interact with growing brushite crystals and inhibit cement setting. α -Hydroxyl carboxylic acids such as tartaric, citric and glycolic acid show an inhibitory effect on brushite cement setting. In comparison, carboxylic acids with no hydroxyl groups, such as oxalic acid and acetic acid, have no inhibitory effect on brushite crystal growth and may even reduce the cement setting time (176, 184).

The presence of strontium ions in strontium-doped β -TCP and in α -TCP shows evidence of prolonging the setting time of cements (168, 197, 206). On the other hand, the addition of strontium chloride results in a decrease in setting time of brushite cements (183). The addition of magnesium ions prolongs the cement setting time due to the strong inhibitory effect they have on brushite crystals (184,

199). Brushite cements with silicon-substituted β -TCP have increased setting times when compared with cements that do not have silica (196).

During cement mixing the amount of water available is an important factor regulating the setting reaction. Cements mixed with a lower powder to ratio tend to have longer setting times (164). Limiting the water available for the setting reaction by using higher powder to liquid ratio results in the acceleration of setting time of cements by causing a faster precipitation of brushite crystals (190, 203).

2.6.3 Monetite preparation

Brushite can be utilised as a precursor to the anhydrous form of DCP cements, which is DCPA (also known as monetite). Heating pre-set brushite cements can result in conversion of brushite to monetite (14). Monetite can also be precipitated by modifying the precipitation conditions of brushite cements in order to favour DCPA crystallization. Under appropriate conditions DCP cement can react to form monetite. This occurs when the cements are prepared in water-deficient environments, with very low pH or in the presence of metallic ions (strontium) that disrupt brushite crystals favouring monetite formation.

2.6.3.1 Hydrothermal and dry thermal methods

Brushite cements that have already been set can be dehydrated into monetite through heating above 60 °C (167, 180). Thermal dehydration alone can result in cracking and shrinkage of the monetite material formed. Studies have shown that if pre-set brushite cements are autoclaved, sufficient moisture is maintained during the dehydration process, and shrinkage can be avoided accompanied by internal pore size increase (14, 207, 208).

2.6.3.2 Low pH during cement setting

Monetite can form with low pH (equal or lower than 2) during cement setting. Solutions of calcium nitrate mixed with sodium dihydrogen phosphate and urea can precipitate as monetite at low pH (209). Monetite can also form when calcium nitrate is reacted with concentrated phosphoric acid solutions (210). Monetite can also be formed when β -TCP powder is mixed with excess MCPM (167, 202) or with 1.5 M citric acid (211). Calcium hydroxide can also be mixed with phosphoric acid and sodium hydrogen carbonate to form crystalline monetite (171). Monetite can also be prepared by dipping pre-set macro-porous α -TCP cements in phosphoric acid (212).

2.6.3.3 Limiting the free water during cement setting

When brushite cements are set at extremely low concentrations of water they can partially react to form monetite instead of brushite (213). Also the precipitation of DCP in solutions rich in alcohol groups, and with less water content (ethanol or glycerol) favors monetite formation instead of brushite. It has also been seen that cements which are dried soon after initial mixing, or DCP cement powders stored under partially humid conditions, react to form monetite instead of brushite (169, 213).

2.6.3.4 Altering cement reaction with additives

DCP cement powders containing strontium-doped β -TCP react to form monetite instead of brushite. The slow introduction of large strontium ions into brushite crystal lattice destabilizes it, favoring the formation of monetite (198). Cements loaded with gentamycin sulfate also have shown to form monetite upon setting (214). Cements with high silicate content, such as the phosphoric acid/wollastonite system react to form a mixture of brushite, monetite and dicalcium phosphate monohydrate (214, 215).

2.6.4 Mechanical properties

According to the standards set for testing bone cements by the American Society for Testing and Materials (ISO 5833, 2002), cements should be allowed to set for at least 24 h prior to being cured under either dry conditions (room temperature and humidity) (203) or physiological conditions (37 °C and 100% humidity) (216). Data relevant to clinical applications is best obtained when cement samples are stored under physiological conditions. Usually two types of mechanical assessments are performed on DCP cements, tensile strength and compressive strength tests. Tensile strength is difficult to measure in brittle materials (217) and compressive strength measurements in brushite and monetite cements are performed on cylindrical samples with an aspect ratio of 2 until fracture occurs. The compression modulus of DCP cements is 10% higher than the tensile modulus (218). The compressive and tensile strengths of DCP cements are inversely correlated to the total porosity present (179, 216). Hence, by decreasing the porosity present it is possible to increase the mechanical strength. This can be done by better compaction of the setting cement (182). One can theoretically produce near zero porosity cements by optimizing the powder to liquid ratio, adjusting the particle size of the cement powders and by inhibiting crystal growth (by using setting retardants) which increases the cement compaction aided by crystal size decrease (216).

The extent of cement setting plays an important role in the mechanical properties of cements. Introduction of additives, such as acetic acid that accelerate the setting reaction of DCP cements have a negative impact on the mechanical properties (176). Whereas, cement setting retardants such as pyrophosphates, sulfates, carboxylic acids, and addition of ions like magnesium, strontium, silicon and zirconia improve the mechanical strength (170). However, these additives have to be present in optimal concentration to have the beneficial effects. Optimization of P/L ratio, cement particle size and cement retardant concentration (800 mM citric acid in the cement liquid phase) can result in a wet compressive strength of 52 MPa for hand mixed brushite cements (216). There

have also been attempts to freeze cements during mixing process which results in a 4-fold increase in compressive strength (219). The formation of ice crystals during the freezing process is thought to help arrange growing brushite crystals upon precipitation.

In order to increase the tensile strength of brushite cements many studies have been aimed at the combination of DCP cements with polymeric materials. Addition of Type I collagen to TTCP/MCPM cements has shown an increase in the compressive strength from 17 to 22 MPa (186). In addition, after ageing these cements in simulated body fluid (SBF) the compressive strength increases to 31 MPa due to the HA crystals precipitating on the collagen fibers resulting in material reinforcement (186). By adding hydrophobic polymers, such as polyglycolic acid resorbable suture fibers in proper arrangement in the cement matrix the tensile strength can be increased up to 7 times than the original strengths recorded (188).

2.6.5 Dissolution and resorption

Studies have demonstrated that DCP cements resorb to a greater extent when compared with HA cements (220, 221). Following implantation, during the first week simple dissolution and cellular activity seems to be the main factors causing resorption of brushite cements (177, 222, 223). Cellular activity seems to dominate the resorption process (224). Out of the cellular components, *in vivo* observations have shown that early resorption of DCP cements is modulated by macrophage and not as much by osteoclasts (223, 225). Osteoclasts penetrate DCP cements at an early stage post implantation and demineralize them to a certain extent (226). Brushite cements *in vivo* show a linear degradation rate of 0.25mm per week (44), which is faster than the bone regeneration capacity (227). This results in a small gap at the bone material interface initially (227). This gap is later filled as the newly forming bone catches up due to the conversion of brushite into less soluble apatite (205). When this conversion to

apatite takes place there is almost no dissolution of the cement and the resorption is solely dependent upon osteoclast activity instead of macrophage mediated phagocytosis (224, 225).

In vitro analysis has demonstrated that the mass loss noted for cements incubated can occur due to disintegration and fragmentation of the grafts rather than dissolution (228). When DCP cement grafts are incubated under physiological conditions they exhibit a decrease in mass, an increase in total percentage porosity and deterioration in mechanical properties (229). DCP cement physico-chemical properties, the properties of surrounding medium, the fluid exchange rate and adsorption of serum proteins also affect initial resorption (184, 228). *In vitro* ageing regimens have shown that brushite cements are stable and do not convert to apatite when stored in distilled water or under alkaline conditions (167, 230). Addition of certain organic molecules such as citrate ions can result in the reduction in the interfacial energy barrier between the brushite solution and HA solution and allow conversion of brushite to apatite (230).

Monetite bioceramics that are obtained by hydrothermal conversion of brushite cements show greater resorption than their original brushite precursors *in vivo* (18, 207). The mechanism for monetite resorption is similar to that of brushite with passive dissolution and cellular activity being the main factors (224). So, the reason for monetite showing greater resorption is due to their non-conversion to apatite after implantation (18, 231).

2.6.6 Bone formation

Brushite and monetite based bioceramics have been prepared and tested by *in vitro* and *in vivo* experiments. Both have been used for bone regeneration applications in different physical forms such as pre-set casted blocks (16, 232, 233), injectable pastes (13, 82, 157, 220, 223, 233, 234), granules (14, 15, 235) and 3D printed blocks (17, 231, 236). *In vitro* experiments on brushite cements

loaded with zinc and strontium have shown an increased alkaline phosphatase activity, collagen type I secretion and fiber deposition in the extracellular matrix (197). Cell cultures performed on magnesium-doped brushite cements have demonstrated increased cell differentiation and proliferation (199). Polymeric additives, such as collagen have been shown to improve cell adhesion to brushite (185), while xanthan results in greater formation of fibrous tissue and less bone hence has a negative biological effect (191). The surfaces of brushite and monetite grafts have been shown to stimulate osteoblasts activity *in vitro* (237).

Brushite and monetite have been utilised for regeneration of bone at various surgical sites in animal models, including bone defects at the distal femoral condyle, metaphysis and epiphyses (191, 220, 234, 238, 239), in the tibial condyle (234), and the calvaria (223, 235), as well as for bone augmentation in the craniofacial area (13, 231). Brushite and monetite cement based grafts have shown the potential to be osteoconductive (14, 17, 18, 225, 235), and upon intramuscular implantation (236) they have also shown signs of osteoinduction. The amount of bone formation is dependent on the site of implantation and the vascular supply. Increased blood supply enhances cement resorption and replacement by new bone (225). Both brushite and monetite have been used on their own or combined with other materials such as β -TCP (44) and bioglass granules (240, 241). In these mixtures the cement provides mechanical stability to the granules and fast resorption, while the granules resorb at a slower pace acting as bone anchors that stimulate the formation of mature bone (157).

The fast resorption rate of brushite cements *in vivo* (20 $\mu\text{m}/\text{day}$), results in a physical gap between the cement and newly formed bone during the first weeks following implantation (16). This might be the reason for osteoblast differentiation occurring *in vivo* at some distance from the graft surface. Later, when brushite converts to HA, new bone is formed in direct contact with the cement margins, resulting in osteointegration of the cement (82, 234). DCP cements show greater

resorption *in vivo* and this frees up space for new bone to form and hence the amount of bone regenerated is usually higher than that obtained with non-resorbable materials (15, 158, 220).

Bone formation has also been stimulated by the release of growth factors from the DCP biomaterials (239, 242). Vascular endothelial growth factor (VEGF), receptor activator of nuclear factor ligand (RANKL) and platelet-derived growth factor (PDGF) are some of the growth factors that have been evaluated. PDGF-loaded brushite–chitosan scaffolds demonstrated a significantly increased bone formation (239). RANKL is a growth factor that encourages osteoclast differentiation which in turn increases DCP biodegradation. Resorption of brushite is imperative for the creation of space required for newly forming bone (242).

2.6.7 Applications

DCP cements have been tested *in vitro* and *in vivo* for a variety of orthopaedic and dental clinical applications. They have also been evaluated for other biotechnological uses, such as drug delivery, biosensor productions and cancer therapy.

2.6.7.1 Orthopaedics

Treatment with casts of bone defects in the proximity of joints (metaphyseal defects) is not always successful, especially in older patients. Treatment with angle stable plating systems can result in bone defects which require autologous bone grafting that cause morbidity of the donor site (243). DCP cements have been evaluated in both animals and humans to treat metaphyseal defects (222, 243). Animal studies have demonstrated their potential in the treatment of fractures in tibia (222), clinical studies have shown a success rate of 76% in distal radial metaphysic fractures and 89% in tibial plateau fracture reconstruction (243).

Injectable brushite cements have also been evaluated as filling material to repair vertebrae that have been damaged due to osteoporosis. Cadaver studies have shown that brushite cement has the ability to increase the bone mineral density by up to 20–50% of osteoporotic vertebrae (244). Osteosynthesis screw fixation is challenging in patients with poor bone quality, especially those suffering from osteoporosis. It is imperative to have a stable and securely fixed osteosynthesis screw for the treatment of complicated fractures to be successful. Poly(methyl methacrylate) (PMMA) cement is non-resorbable *in vivo*, has an exothermic setting reaction and its monomer is cytotoxic. Resorbable brushite cements have been tested as a solution to these problems. *In vitro* assessment of the force required to remove an osteosynthesis screw from bone has revealed a 3-fold increase in the pull-out force when using brushite cements (245).

The potential of brushite cements to be used for anchoring ligaments to bone by the creation of an optimal mechanical interface has also been evaluated (246). 3D printing techniques have been used for preparing brushite and monetite brackets for bone–ligament–bone replacement. The *in vitro* testing has revealed a wet compressive strength similar to hand-made brackets (247). Anterior cruciate ligament (ACL) reconstruction in rabbits has also been carried out with brushite cements used to anchor the bone–tendon interface demonstrating a reduction in the number of intra-tunnel mechanical failures and also improvement in the bone-tendon interface strength (248). Preparation of bone ligament sinews have also been evaluated by connecting cast brushite ceramic anchors to fibroblasts embedded fibrin gels (249).

2.6.7.2 Craniofacial repair and augmentation

DCP cements have been tested for vertical bone augmentation and bone defect healing in oral and maxillofacial surgery. Brushite has been evaluated for these procedures as injectable cements and as pre-set cement granules (13, 235). Brushite cements for minimally invasive craniofacial vertical bone augmentation have been tested in animals by injecting cement under the periosteum and

allowing it to set on the bone surface (13). Clinical studies have shown that injectable brushite cements are capable of regenerating bone in buccal dehiscence defects, atrophic areas and maxillary sinuses (250). However, the limited *in vivo* resorption of brushite cements results in incomplete vertical bone growth in the treated site (13). Animal models have demonstrated the efficacy of brushite cement granules towards promotion of craniofacial vertical bone augmentation in animal models (235). *In vivo* studies have revealed a greater amount of vertical bone growth obtained with brushite granules was higher than with commercially available xenografts (HA) (14). Craniotomy defects have been treated with brushite cements in several animal models. The implanted cements showed a certain amount of resorption and bone formation but considerable fibrous tissue formation was observed (223). Brushite cements have also been used clinically in attempt to prevent temporal depression in cases of parietal craniotomies. The results were not ideal as complete resorption and replacement by bone did not occur (251).

3D printed monetite onlay blocks have also been tested for vertical bone augmentation and in the form of granules for bone defect healing with promising results (14, 15, 17). Monetite blocks for synthetic onlay bone grafting have shown to achieve vertical augmentation of bone sufficiently to allow dental implant placement (17, 231). Monetite granules have also shown to promote bone healing in dental alveolar sockets (post teeth extraction) in humans (15), and of craniofacial defect in animals (14). When the clinical performance of monetite granules is compared with commercial bovine HA, the monetite granules show greater resorption and bone formation in the alveolar ridge sockets (15). Monetite granules have also demonstrated bone regeneration in craniotomy defects when placed in rabbit calvarial defects with promising resorption profiles (14). In an experimental study, 3D printed monetite grafts have shown the ability to provide accurate patient-specific craniofacial implants for bone defects in cadavers (252).

2.6.7.3 Bioactive delivery

In order to improve the biological properties of brushite cements various bioactive molecules have been added; these include antibiotics, metallic ions and growth factors. These can be added by dissolving them into the cement liquid phase or by immersing the set cements in a solution containing the drug (253, 254). Chlorhexidine-loaded cements can be used for dental applications (255). Ciprofloxacin is often prescribed for the treatment of bone infections. However, when added to brushite cements, due to having low water solubility, the release of the drug is very slow and incomplete (216).

At very low concentrations, copper ions are known to possess angiogenic properties. 3D printed brushite cements loaded with copper sulfate have been seen to induce angiogenesis (256). For the release of growth factors *in vivo*, such as VEGF and PDGF, brushite cement matrices have been used (239). These growth factors stimulate angiogenesis and bone growth and by their release the bone formation capacity of the scaffolds was considerably enhanced (239). In an attempt to enhance biodegradation of brushite cements they have been coated with RANKL. This lead to an increase in the *in vitro* osteoclast activity on brushite cements (242). BMP2 is a bone growth factor has great potential for use in bone tissue engineering owing to its osteoinductive properties. 3D printed brushite cements have been evaluated by adding BMP2 to them (257). VEGF which is an angiogenic growth factor has also been added to the 3D printed grafts (236).

2.6.7.4 Biosensors

Biosensors are electronic devices which have the ability to detect and quantify small amounts of specific molecules in solutions or gasses. Most of the biosensors are used to monitor enzymatic reactions on highly sensitive electrodes. Brushite cements have the ability to conduct electricity through a mechanism known as proton conduction. They also have the ability to adsorb proteins and these properties of brushite cements make them suitable

candidates for use as biosensors. Brushite-based biosensors have been used for the detection of glucose using the enzyme glucose oxidase (258) and also for phenol detection by combining the cement with the enzyme tyrosinase (259).

Chapter 3: Characterisation techniques

This chapter discusses the main characterisation techniques used by the candidate for the completion of experiments for this thesis.

3.1 X-ray diffraction (XRD)

X-ray diffraction is used to ascertain the spacing between crystallographic planes, and from this the crystal phases present in a sample are analysed. It provides a non-destructive analysis and identification of the ultrastructural crystallography of a material. The measurement of constructive and destructive interferences of the X-rays as a function of diffraction angle and wavelength is the basis of this technique.

3.1.1 Theory

X-rays are known to be scattered elastically from regularly spaced atoms (lattices) in crystals. If these elastic waves are in phase they interact constructively and increase the intensity of the scattered radiation (constructive interference). However, if they are out of phase they interact destructively which results in a decrease in intensity (destructive interference). In order for constructive interference to occur the path length difference of the diffracted X-ray beams must be an integer multiple of the wavelength. The path length difference is determined by the spacing between atoms in a lattice (d), and the sine function of the angle formed between the incident angle and the scattering angle (2θ). This is mathematically explained by what is known as the Bragg's law which is defined as:

$$n\lambda = 2d\sin\theta \quad [3.1]$$

In this equation n is an integer (other than zero), λ being the wavelength of the incident X-rays, d is the spacing between the planes of crystal lattice and 2θ is the angle between the incident and diffracted X-ray beams.

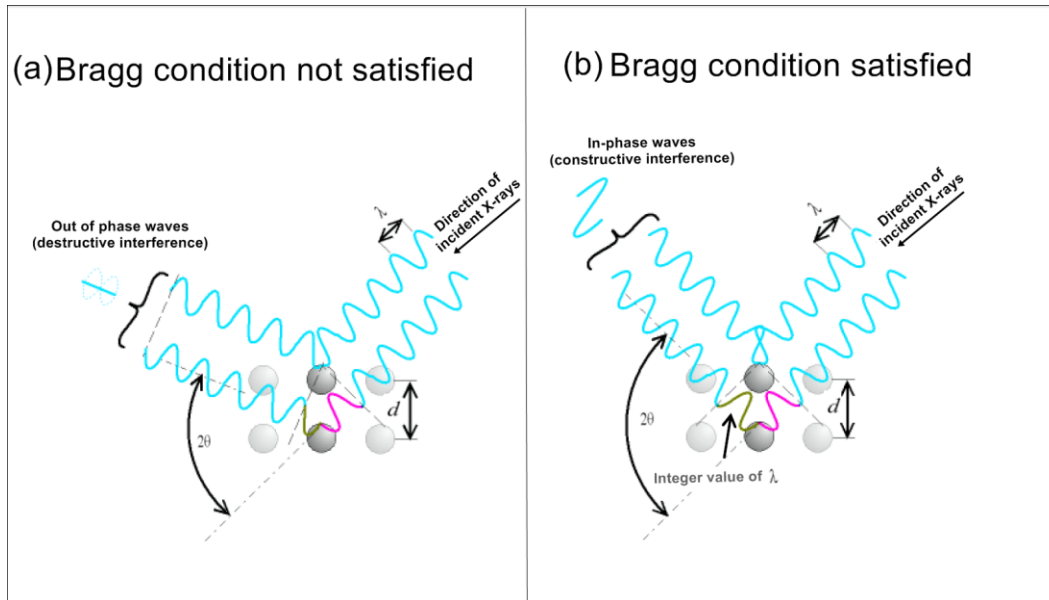


Figure 3.1.1.1: Representation of (a) destructive and (b) constructive interference based on Bragg condition being not satisfied and satisfied.

3.1.2 Instrumentation & measurement

An X-ray diffractometer is fitted with a source of usually copper-K α X-rays, a sample goniometer, a detector for the diffracted X-rays, a data recording system, and devices for displaying and printing the spectra obtained. It is usually possible for the source and the detector to be moved and rotated around the sample in order to select different diffraction angles. Diffracted X-rays are collected on a charge-coupled device (CDD). The obtained diffraction pattern is then utilised to determine spacing of the crystal plane, crystal orientation, crystal size, and crystal phase identification with a database that has reference spectra of known materials.

In order to obtain a diffraction pattern with an extremely sharp peak that matches exactly with that predicted by Bragg's law, we would need a perfect crystal of infinite size that is measured using a perfect diffractometer. This is practically not

possible and the diffraction patterns and peak profiles obtained are dependent on a variety of factors. Imperfections in the instrumentation (mostly in the X-ray source and physical geometry of diffractometer) result in aberrations (peak shift and broadening). Peak broadening from the sample may arise if there are imperfections in the crystal structure and dimensions (which cause strain in the lattice). Peak broadening may also be observed when crystallite size is greatly reduced. It was Scherrer first who described the relationship between crystallite size and the x-ray diffraction peak width, which is the full width (in 2θ) at half the maximum intensity of the peak being observed (260). This can be used to calculate the crystallite size after subtracting the effects caused by lattice strain and instrumental conditions and errors (261).

$$B_{crystallite} = k\lambda/L\cos \theta \quad [3.2]$$

Where λ is the wavelength of the x-rays, L is the “average” crystallite size measure (perpendicular to the specimen surface), θ is the Bragg angle, and k is a constant (mostly assumed to be =1).

3.2 Scanning electron microscopy (SEM)

This is a form of electron beam analysis that is very useful to image the microscale and nanoscale features of materials. A high energy beam of electrons are used as a source for illumination of the sample for imaging. The popularity of the SEM is due its capability to obtain three-dimensional images of the surfaces of a very wide range of materials.

3.2.1 Theory

The SEM permits the observation and characterisation of materials on a nanometer to micrometer scale due to the use of electrons to form an image. Unlike the optical microscope that forms an image from light reflected from a sample surface, the use of electrons in SEM results in different resolution levels

due to the difference in wavelengths of these radiation sources. The electrons have a much shorter wavelength than light photons, and hence are capable of generating higher-resolution information. The enhanced resolution in SEM allows for higher magnification without the loss of detail. The wavelength of electrons is less than 0.5 Å, which theoretically allows the maximum magnification of SEMs to be beyond 800,000X. Another feature of the SEM imaging is the greater depth of field (distance between nearest and farthest object in an image that can appear sharp) provided by using electrons having shorter wavelengths.

3.2.2 Instrumentation

The SEM instrumentation can be divided into four subsystems. Their components and the functions are:

(I) The illuminating/imaging system: This system includes an electron gun and several magnetic lenses that produce a collimated beam of electrons which is focused onto the specimen. The electron gun can be subdivided into (1) a filament (cathode) or electron source, which generates electrons; (2) an aperture shield held at slightly negative potential relative to the filament; and (3) an *anode* held at very high positive potential with respect to the filament. Together these components function as an electrostatic lens. The electrons are produced by passing a current through the filament and heating it and then accelerated by the potential difference between the anode and filament. The common electron sources that are employed in SEMs are the tungsten hairpin filament, Schottky field emitters, lanthanum hexaboride, thermal field emitters and cold field emitters. The difference in potential between the filament and the anode determines the accelerating voltage (262).

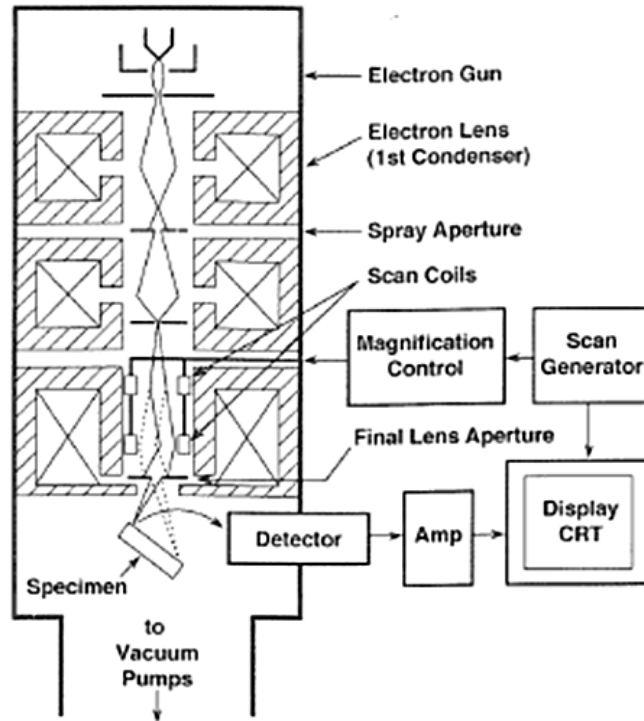


Figure 3.2.2.1: Schematic representation of the parts of a scanning electron microscope (61).

Electromagnetic lenses are responsible for the diameter of the electron beam, focus and magnification of the image. Focus is achieved by varying the current passing through the final lens (objective lens) and thus changing the focal length. Stigmators are weak lenses which exert a magnetic field that correct the aberration known as astigmatism. An aperture intercepts electrons which are not part of the imaging beam and prevents stray electrons from striking the specimen, thereby reducing the background noise in the image. The resolution, depth of field, and image clarity are enhanced with the use of smaller apertures. Larger apertures may be preferred when conducting an X-ray analysis, where a more intense electron beam probe is required (263).

(II) The information system: This includes the data signals released from the sample after the electron beam strikes it and the associated detectors for these corresponding signals.

The various signals that are created are:

- Backscattered electrons (BSE)
- Secondary electrons (SE1, SE2, SE3)
- Characteristic X rays
- Bremsstrahlung X rays
- Auger electrons
- Cathodoluminescence

We will limit our discussion to backscattered (BSE) and secondary electrons and their respective detectors as they were used by the candidate for completion of experiments presented in this thesis.

The BSEs are electrons which undergo elastic collisions with a high angle of scattering and negligible loss of energy. The number of BSEs produced depends upon the atomic number of the material. The higher the atomic numbers, the more the BSEs are produced due to the higher probability of elastic scattering.

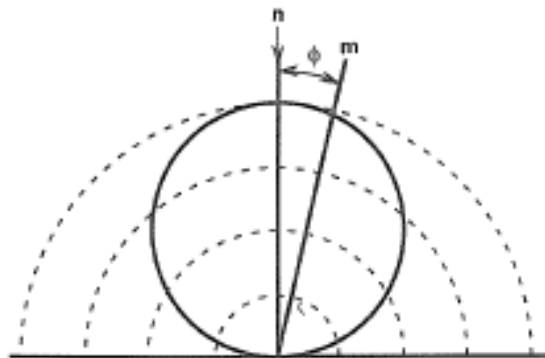


Figure 3.2.2.2: The cosine distribution of Backscatter electrons (61).

The solid state detector is the most common type of detector employed for BSE imaging. The detector consists of a silicon wafer coated by a layer of gold. The solid state detector functions upon the principle of electron-hole pair production by pushing an electron into the conduction band. The BSEs strikes the detector and results in the production of a hole in the valence band and the electron-hole pair recombination is prevented by the external bias. The current produced by this process is utilized to create an image on the screen.

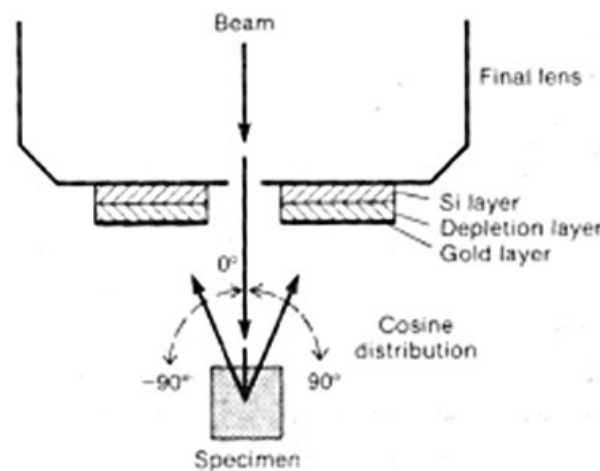


Figure 3.2.2.3: Schematic representation of a solid state detector for BSE imaging (262).

The SEs are produced via inelastic collisions of the beam electrons with the specimen's outer valence electrons of the atoms. These SEs usually have low energy (less than 50eV) and hence can only escape from shallow depth in the sample surface.

The Everhart-Thornley type of detector is commonly and widely used for collection of the SEs in the SEM. The detector has a Faraday cage that is biased with positive voltage which attracts the SEs. The SEs are accelerated (10kV to

12kV) towards the scintillator and upon striking produces light photons which are passed through the photomultiplier tube which works on the principle of total internal reflection. This part of the detector converts the photons to electrons again and multiplies them before they are passed on to the amplifier and used to create a signal forming the image (61).

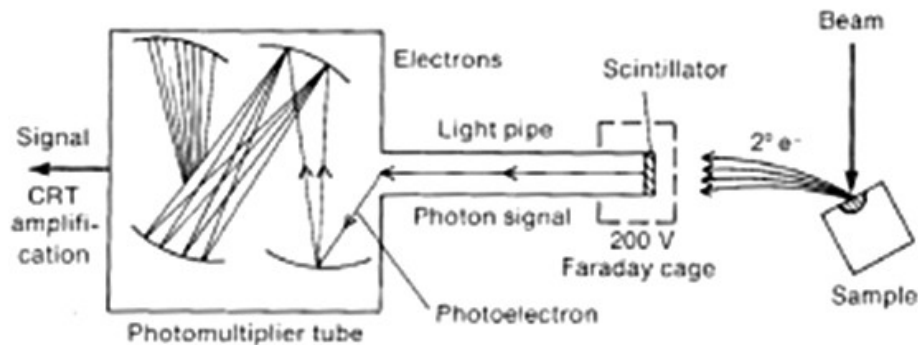


Figure 3.2.2.4: Schematic representation of Everhart-Thornley detector (262).

(III) The display system: SEM images are displayed on the screen of a cathode-ray tube (CRT).

(IV) The Vacuum system: The SEM column and specimen chamber are required to operate under high vacuum (10^{-4} Torr or more). Without high vacuum the residual gas molecules result in the scattering of the electron beam, and electrons start travelling at different velocities, giving rise to chromatic aberration which limits the resolution. Hence, the SEM is equipped with pumps that operate continuously to maintain high vacuum. Turbomolecular pumps are preferred over diffusion pumps because they minimize contamination and achieve a very high level of vacuum (262).

3.3 Energy dispersive X-ray spectroscopy (EDX)

This is a non-destructive technique for the chemical analysis and characterisation of a material.

3.3.1 Theory

This technique works on the principle that a surface being irradiated with a beam of electrons (usually penetrate 0.5–10 μm into the specimen) emit characteristic X-rays (264). These characteristic X-rays generated are due to inelastic scattering (loss of energy) and can be collected to determine the quantitative elemental composition of a material.

3.3.2 Instrumentation & measurement

The characteristic X-rays emitted are collected by the EDX unit that is fitted to the SEM. A highly penetrating electron beam of ~ 1 mm in diameter is required to emit these X-rays which are generated beneath the sample surface. Due to this reason the resolution is highly limited. The information collected by the EDX detector can be obtained as an overall spectrum of a selected area of the sample or as an elemental map whereby colors are assigned to each element and pixels of these colors are assigned as a map in two dimensions in relation to the position of the electron beam where they are detected.

3.4 Brunauer–Emmett–Teller (BET) method

Specific surface area (SSA) is a measure of the total surface area per unit of mass, bulk volume or cross-sectional area of solid materials. SSA can be calculated geometrically from particle size distribution and making assumptions about the particle shape. However, this method of SSA measurement does not take into consideration the surface associated with the surface texture of particles. SSA can be more accurately measured by gas adsorption using the BET method which commonly utilizes nitrogen physisorption that has the advantage of measuring and taking into account the texture of the particle

surface. BET method is also used to determine pore size distribution and estimate primary particle size (265, 266).

3.4.1 Theory

BET method is an extension of the Langmuir theory, for monolayer molecular adsorption, to multilayer adsorption. BET theory was developed by Brunauer, Emmett and Teller (BET) in 1938 is based on adsorption of gas on a surface with the amount of gas adsorbed at a given pressure allows calculation of the surface area. The hypothesis for the BET theory is that gas molecules physically adsorb on a solid infinitely in layers; there is no interaction between each adsorbed layer; and the Langmuir theory can be applied to each layer is adsorbed (266).

3.4.2 Measurement

The SSA is measured by the adsorption and desorption of nitrogen gas on the surface of a material (usually particulate) of known mass in a chamber of known volume. The minimum surface required for accurate measurement is 1 m² and the results obtained are dependent upon the amount of gas adsorbed. The measured amount of gas adsorbed is relative to the relationship between the surface area and the resistance to gas-flow of porous powders. Particles in the micron size range have a specific surface areas less than 10 m²/g range whereas nano-sized particles have higher specific surface areas (265, 266).

3.5 Helium pycnometry

Gas pycnometers are devices that are used to calculate the true density of porous and non-porous solid materials and particulate matter.

3.5.1 Theory

Helium pycnometry is a method to calculate the true density of solids by employing a method of gas displacement and the volume-pressure relationship known as the Boyle's Law. Although pycnometers are known as density

measuring devices they in fact measure volume only. Density of the material is calculated as the ratio of mass to volume (267, 268).

3.5.2 Instrumentation & measurement

The helium pycnometer consists of two chambers, one to hold the sample (with a removable air-tight lid) and a second chamber of fixed, known internal volume which is known as the reference volume. The pycnometer additionally has a valve to allow helium under pressure to one of the chambers. There is also a pressure measuring device known as transducer connected to the first chamber and a tube with a valve connecting the two chambers. The volume measured in a gas pycnometer is the amount of three-dimensional space which the helium cannot gain access to. Helium is used due to the small size of its molecules but also because it is inert. A disadvantage of this technique is that the closed pores, which do not communicate with the surface of the materials, are included in the measured volume (267-269).

3.6 Mercury intrusive porosimetry

Porosity affects adsorption, density, mechanical properties and it is of acute importance to be able to measure it. Mercury intrusive porosimetry is an extremely useful technique for the determination of the range of pore sizes present in the materials being investigated. Mercury porosimetry provides information regarding the pore size distribution, the total porosity present, the skeletal and apparent density and also the specific surface area of the sample. Porosity present in a material affects its physical properties and subsequently its performance in its application (270, 271).

3.6.1 Theory

The non-wetting property of mercury along with its high surface tension allows it to be utilized for evaluating pore spaces. When mercury is placed along a pore opening, the surface tension of mercury acts along the line of contact with the

opening equal in length to the perimeter of the opening a creating a force that resists the entry of mercury into to the pore. An external pressure being applied forces the mercury inside the pore. By measuring the volume of mercury that intrudes the pore space with each pressure change the volume of pores can be calculated (270-272).

3.6.2 Instrumentation & measurement

The intrusion of mercury into the pore space is measured by a mercury penetrometer. This penetrometer is made of glass and is very sensitive having the ability to measure mercury volume changes under 0.1 μL . The stem of this glass penetrometer is a capillary that functions as a mercury reservoir for the analytical volume of mercury. The glass acts as an insulator and the mercury is a conductor. The stem is placed against a metal which also acts as a conductor thus these two conductors separated by the middle glass insulator acts as a coaxial capacitor. As pressure forces mercury out of the capillary into the sample the volume of mercury within the capillary decreases and so does the resistance. This decrease in resistance is directly proportional to the amount of volume intruding the material (pore space) with each pressure change. A limitation of mercury intrusive porosimetry is that it does not take into account closed pores as there is no way for the mercury to access closed spaces within a material. Hence the pore size measurements are somewhat arbitrary (270, 272, 273).

3.7 Digital radiography

Digital radiography is an advanced form of X-ray imaging, where digital sensors are used for collecting X-rays for image formation instead of traditional photographic film. Time efficiency by not requiring chemical processing and the ability to digitally transfer and obtain images with high quality and sharpness are the advantages of using digital radiography (274, 275). Also lower levels of radiation can be used to produce an image in comparison to conventional radiography (276).

3.7.1 Instrumentation & image formation

The X-ray source is the same as used in conventional radiography although the voltage and current required is greatly reduced. Digital radiography uses a digital image capture device instead of radiographic film. This allows immediate image previewing ability. There are two types of digital image capture devices available for use: flat panel detectors (FPDs) and high-density line-scan solid state detectors. The FPDs can be indirect in which a silicon detector is coupled with a scintillator and converts X-rays to light (277). The light is converted to a digital output signal. The digital signal is then sent to a computer for display. Whereas, the direct FPDs convert X-ray photons directly to charge. A high-density detector is composed of a barium fluorobromide doped with caesium bromide phosphor. The phosphor detector records the X-ray energy during exposure and is scanned by a laser diode to excite the stored energy which is released, captured and displayed as a digital image (276, 278).

3.8 Computed tomography (CT)

Tomography is obtaining cross-sections from a set of external measurements of a spatially variable function. Computed tomography (CT) is conventionally performed using X-rays and is based on the difference in radiation absorption by different materials (279). CT uses computer processed X-rays to produce tomographic images of specific areas of the scanned object. CT can be used to analyse bone samples and graft materials implanted (280). Analysis can be used to reveal information regarding total volume, bone volume and tissue volume ratio and total porosity (open and closed). By doing comparison between a CT scan of a graft before implantation and after it is also possible to quantify the total volume of resorption (280, 281).

3.8.1 Principle & scanning

Computed tomography is based on the principle of X-rays traversing an object along a straight line. The attenuated signals from various directions are recorded

providing the individual slices for the reconstruction algorithms that are used to convert the projections. The three dimensional image of the inside of a specimen is generated from a series of two dimensional radiographic images by utilising digital geometric processing (282). The radiographic images are taken around a single axis of rotation before the reconstruction of all the slices which can be analysed (281). Data for slices is generated by using an X-ray source that is rotated around the object. The X-ray sensors are positioned on the opposite side from the X-ray source. The continuous rotation (degree of rotation decided by the operator) of the object to be imaged is carried out slowly and smoothly (281). The time required for scanning an object is dependent on the resolution and number of scans required (for averaging each frame) selected by the operator (279, 282).

Chapter 4: Surgical models and procedures

Bone repair and regeneration processes give rise to a highly complex *in vivo* environment with a variety of mechanisms that remain largely unknown nor controlled. Since bone repair involves a combination of many factors and interactions it is not well suited towards *in vitro* modelling, computational modelling, or tissue culture alone (28). The *in vivo* animal studies can evaluate the bioresorption, osteoconduction and osteoinduction capacity of the test grafts in orthotopic and ectopic sites with and without loading.

4.1 Factors to be considered in choosing a model

Biomaterials have to be tested in animal models before being used in human trials as animal testing is a midway step between *in vitro* studies and human clinical applications. For studying bone repair and regeneration choosing a suitable animal model is imperative in order to obtain results which have relevance to human systems (28). The animal species and the site of implantation chosen depends on the research question that is being asked. Several factors are of major importance which may modulate the final choice of the model used.

4.1.1 Model relevance

A model is only relevant if the experimental conditions and the effects generated are linked. For the evaluation of *in vivo* biocompatibility, biodegradation, osseointegration, osteoconductivity, osteogenic and osteoinductive potential, simple tests such as implantation in ectopic (subcutaneous or intramuscular) and orthotopic (femoral condyle and calvaria) sites of animals are employed (283). The main use of bone replacement materials in orthopaedic surgery is bone loss replacement or augmentation (283). The most commonly designs for such evaluations are surgically induced bone defects also known as critical size defect that progress to non-union if not replaced with graft materials. Critical sized defects were first described by Schmitz as “the smallest intraosseous wound that

does not heal by bone formation during the life time of the animal” (31). Hollinger further defined it as “a defect which has less than 10% of bony regeneration occurring within the lifetime of the animal” (32).

4.1.2 Bone healing and remodelling features

Bone healing and remodelling in the animals being used for the study depend on a variety of variables such as the species or age of the animal, bone blood supply and mechanical loading after implantation. Bone repair capacity is higher in rodents and rabbits than in other species (32). The type of bone remodelling and rate of formation also differ between species. Large animals such as dogs, cats, rabbits, pigs and non-human primates show Haversian type remodelling in cortical bone, whereas rodents do not (34). The rate of bone remodelling in rabbits is twice as fast in dogs and three times as fast when compared with humans (36). Younger animals have higher bone repair and regeneration capacity compared with older animals. For this reason the magnitude of a critical size defect is therefore inversely related to the age of the animal being used (37). Local blood flow is also critical when assessing the bone healing procedures as it has been observed that increased blood supply promotes heterotopic osteoinduction by rhBMP-2 (38). Skeletal loading or lack of it post implantation can greatly affect results as unloading in weight bearing bones decreases osteoblast count, bone mass, bone formation rate, bone maturation and mechanical strength (39).

4.1.3 Anatomical and morphological features

The feasibility of performing surgical procedures in preclinical tests is dependent upon specific anatomic features such as the shape and size of the animal bones. Rodents and rabbits have small-sized bones and thin fragile cortices, hence requiring delicate surgical techniques and custom made smaller implants for bone fixation (41, 42). Dogs, sheep, cats and pigs have larger bones, hence allowing the use of conventional surgical techniques and implants designed for human clinical use (42). The types of bone tissue in which the bone replacement

materials will be tested are selected based on the intended future applications of the materials. Trabecular bone (metaphyseal extremities) or cortical bone (diaphysis) are preferred if the graft materials are to be used for filling defects in long bones (41). Membranous bone (calvaria) is selected for testing if the materials are to be used in cranioplasties (41).

4.1.4 Gender of the animals

Bone healing and regeneration procedures are usually performed in male animals because hormonal cycles can have a significant effect on bone turnover (43). However, bone loss models developed by ovariectomy of rats and mice to mimic human osteoporosis are also used (53). Preliminary studies have also been carried out using ovariectomised sheep (34) or ferret (47).

4.1.5 Species used for the models

There are a variety of species which are used for orthopaedic research (56, 284). An analysis by Martini et al. (285) revealed that the most common choice were rats (36%), mice (26%), rabbits (13%), dogs (9%), non-human primates (3%), sheep, cats and pigs (~2% each).

There is a variation in the anatomy, biochemistry and biomechanics of normal bone, and the repair processes do not always match with the properties of human bone (56, 61, 70). Rats have lamellar type of bone and show good cancellous but less cortical remodelling. Rats are used for both long bone and calvarial models. They are cost effective to house and female rats can be kept in one cage (56). There are significant differences in composition, quality and density between rat and human bones (56). Mice lack a Haversian canal system (62), but are still chosen due to their ease of handling, low cost, an increasing knowledge of their genetic blueprint and availability of genetic knockout varieties (breeding of animals with specific genes deactivated) (62).

The rabbit is one of the most commonly used animals for musculoskeletal research studies (260). They have larger skeletons in comparison with rats and mice and are easily housed. Another reason for the increased use of rabbits is that they reach skeletal maturity shortly after sexual maturity around 6 months of age (261). However, there are size and number limitations (implant not larger than 2mm in diameter and 6 mm in length and maximum of 6 implants per animal) when accessing implants for orthopaedic and dental applications (284). Rabbit bone remodels quickly (284) and has different microstructure from humans (61). In contrast to the secondary bone structure of mature human bone, rabbits have a vascular longitudinal tissue structure. Vascular canals of osteons run parallel with long axis of the bone, which surround the medullary canal as well as the periosteal surface. The bone between these layers is composed of dense Haversian type bone (264). There is limited literature on the differences between human and rabbit bone composition and density, some similarities are observed in the bone mineral density (BMD) and fracture toughness of mid-diaphyseal rabbit and human bone (61, 262).

Dogs have bone composition, architecture and remodelling similar to humans but have a combination of lamellar and plexiform bone (284, 286). Their biomechanical properties differ and remodelling is highly variable (61, 284, 286). Dogs are expensive to keep and use for animal studies and have additional ethical issues regarding their use. Cats are an uncommon choice and pigs have been used in models for investigating systemic response towards trauma, but rarely for bone healing studies (75, 89). The size of pigs, their short limbs and expensive housing requirements make them an unpopular choice. Sheep have cancellous and cortical bone, but also have a woven bone like plexiform bone and very few Haversian canals (56, 284). Their bones undergo remodelling at a rate similar to humans but there is a difference in composition and fracture stress levels (56, 74, 284).

4.2 Animal models currently used for bone replacement material evaluation

There are a variety of animal models that are used for bone material replacement evaluation for orthopaedics, maxillo-facial and spinal surgery applications. Evaluation of bone replacement materials and implants are performed in animal models prior to preclinical studies are performed to determine whether the materials are to reach the clinical trial stage in humans.

4.2.1 Heterotopic implantation

The gold standard for testing the biocompatibility, osteogenic and osteoinductive potential of bone replacement materials and constructs *in vivo* is intramuscular implantation (in large animals). Biocompatibility and graft resorption can also be assessed by subcutaneous implantation in rats (207). These tests are mostly performed on rabbits and rats due to them being cost effective and also because of their technical simplicity (The bone replacement materials are directly implanted into the recipient bed). They have also been tested on larger species such as sheep (78) and goats (287, 288).

4.2.2 Orthotopic implantation

Orthotopic implantation models allow the assessment of osteoconductivity, osteointegration, osteointegration and biodegradability in a bone environment. Implantation in the rat calvaria is the gold standard model for orthotopic implantation (289). Calvarium undergoes membranous bone formation having poor blood supply and little bone marrow therefore creating a hostile setting for bone healing. When single mid-sagittal circular lesion (8 mm) and bilateral parietal lesions (5 mm) are created in rats: both result in critical size defects and fibrous non-union occurs and bone loss is not replaced (31, 289). Craniotomies are relatively easy to perform, are highly reproducible, have low morbidity rates and granular or paste like materials can be implanted on a large number of animals allowing statistically significant analysis (290, 291).

Orthotopic implantations using bone chamber models (diaphysis of long bones) can be used to test biomaterials in loaded or unloaded environments (283). Bone chambers have been used at the femoral level in rabbits and goats. This model can be used to study differences in scaffold processing, to compare scaffolds loaded with various growth factor concentrations and to assess the effects of loads on bone healing (291).

4.2.3 Cranial surgery

Studies on skull defects have been performed on rabbits, sheep, dogs, minipigs, and non-human primates (31, 290, 292). These lesions are highly reproducible, created easily and demonstrate low morbidity rates (31, 32). Different biomaterials can be compared in the same animal by creating multiple defects to obtain positive and negative control data on the same animal (290).

4.2.4 Maxillo-facial surgery

4.2.4.1 Filling defects

Alveolar bone resorption at tooth extraction sites results in defects and models using dogs have been developed by performing maxillary and mandibular premolar extractions (293). Particulate bone fillers have also been tested for unicortical and bicortical mandibular filling defects in sheep (36), dogs (32) and minipigs (294).

4.2.4.2 Segmental bone defects

Segmental bone resections are performed in oncological maxillofacial surgery and mandibular discontinuity defects in animal models have been created to mimic these resections (31, 32, 295). These models to an extent simulate the adverse clinical settings in which bone replacement usually take place after maxillofacial surgery has been performed. Models have been described in the rabbit, rat, sheep, dog and non-human primates (32, 295). Mandibular bone is very thin in rodents and rabbits and it is preferable to induce mandibular

discontinuity defects in sheep, dogs or non-human primates, where resections are easier to perform (32). Orbital wall defects have been performed in sheep (296) and the reproducibility is greater and morbidity lower of this model when compared with mandibular defects. However, since these defects are created in unstressed bones; this model should be used only to test biomaterials to be used with unloaded bones (296).

4.2.4.3 Onlay grafting

Vertical alveolar bone loss in patients who are partially or completely edentulous makes prosthetic rehabilitation difficult and does not allow for dental implant placement. There are anatomical restrictions based on the maxillary sinus, nasal cavity and the inferior alveolar nerve that limit the height available for implant placement and present surgical challenges. Data obtained from clinical studies support the use of bone grafts to allow placement of dental implants. The most commonly used procedures for this purpose include distraction osteogenesis (297-301), guided bone regeneration (GBR) (302-305) and onlay bone grafting (306-311). Although distraction osteogenesis and GBR can produce greater or equal bone height than onlay grafting, there are more complications associated with this technique (312). Onlay grafting using bone blocks was first introduced clinically in the early 1900s to augment the maxillary and mandibular bone height (313). Onlay grafting involves the extraction a block of autologous bone from a donor site (iliac crest or the mandibular ramus) or a synthetic graft, and fixing with osteosynthesis screws onto the recipient site. Currently there is no satisfactory alloplastic alternative to the conventional autologous bone grafts for maxillofacial bone augmentation applications. Animal studies using onlay bone grafting on rabbit calvaria have shown promising results and limited complications (17, 314, 315). Dog models have also been used to evaluate onlay bone grafting (316, 317).

4.2.5 Orthopaedic surgery

4.2.5.1 Filling defects

Bone fillers are often used to fill defects resulting from bone procurement for grafting procedures, metaphyseal traumas, or surgical removal of tumors (benign or malignant). Bone fillers are used as granules, pastes or preset blocks (318-322). Metaphyseal defects have been induced using animal models in sheep (232), rabbit (323) and in the dog proximal tibia (324). No special immobilization is required for these defects and statistical analysis can be carried out on the histological data obtained due the high reproducibility of these models (232, 323, 324).

4.2.5.2 Segmental bone defects

Segmental long bone defects created 1.5 times the size of the diaphyseal diameter under experimental conditions are beyond the regenerative capacities of bone in skeletally mature dogs and results in non-union when the missing bone is not replaced (325). This is also observed in the case of feline tibia (37). The length of the bone resections at which non-union occurs is species and bone dependent and must therefore be established whenever a new model is developed.

Segmental defects must be kept in a stable biomechanical environment while healing occurs (by plating or intramedullary rods) and this is more difficult in animals than in humans. Femoral (98, 326, 327), tibial (328), radial (329) and ulnar (329) resections performed on dogs have been stabilized using either external fixation methods (328) or bone plating (326, 327). Femoral, tibial, ulnar, and humeral resections have been performed on non-human primates (330-332).

4.2.6 Spinal surgery

Bone replacement materials have two major applications in spinal surgery: 1) as bone filler to maintain or augment the vertebral body volume (vertebroplasty) when bone loss has resulted due to osteoporosis or tumors, 2) in spinal fusion as an augmenting bone healing procedure.

4.2.6.1 Vertebroplasty

In literature, a model of vertebral bone loss has been demonstrated in sheep (263) where a defect was surgically created in the vertebral body (lumbar), filled with coral or with autologous corticocancellous graft or left intact (negative control). The purpose of this model is to develop and research upon materials that can be used in patients suffering from osteoporosis (333, 334).

4.2.6.2 Spinal fusions

Spinal fusion is performed in order to achieve a mechanically optimal solution in a damaged spinal unit, and not just to restore normal anatomy in bone loss situations (335). There are two types of spinal fusion procedures that may be used in combination with each other: interbody fusion and posterolateral fusion (335). Spinal fusion with synthetic bone graft materials or constructs is very challenging since even the use of autologous bone is associated with relatively high failure rates (287). Interbody vertebral fusion procedures have been described in the sheep (336-338), goat (339-342), dog (343, 344), rat (345, 346), rabbit (347), pig (348, 349), and non-human primates (345, 350, 351). These animal models are used to make a cost-effective comparison between different osteoinductive materials and scaffolds (347).

4.3 Surgical methodology employed during PhD experiments

The following sections describe the surgical methodology and techniques employed by the student towards the completion of the animal implantation experiments for the PhD.

4.3.1 Subcutaneous implantation procedure

Male rats for the subcutaneous implantation were received and acclimatized for 72 hours. Prior to the surgical procedure, the surgical area and instruments were prepared. The rats were anesthetized using isoflurane. Aseptic procedures were carried out once the animals shown complete signs of being under anesthesia. The animals were placed on their bellies and their backs shaved and disinfected. A 1 inch mid-scapular incision made in the skin along the length of the animal's back. Using a blunt probe a subcutaneous pocket was created laterally on either side of the incision down the flanks of the animals. The cement cylindrical grafts (6X12 mm) were next introduced through the incision down the flanks on either side. The wound was irrigated with sterile normal saline and closed in layers: the subcutaneous tissue was closed with 3-0 vicryl, and the skin closed with 4-0 monocryl sutures. Then animals received 5-10 mg/kg carprofen analgesic 30 mins prior to surgery and 24 hours post operatively for 3 days. The animals were allowed to recover from the anesthetic and monitored for the next 3 days. After 4 and 12 weeks the animals were sacrificed using carbon dioxide and the grafts retrieved.

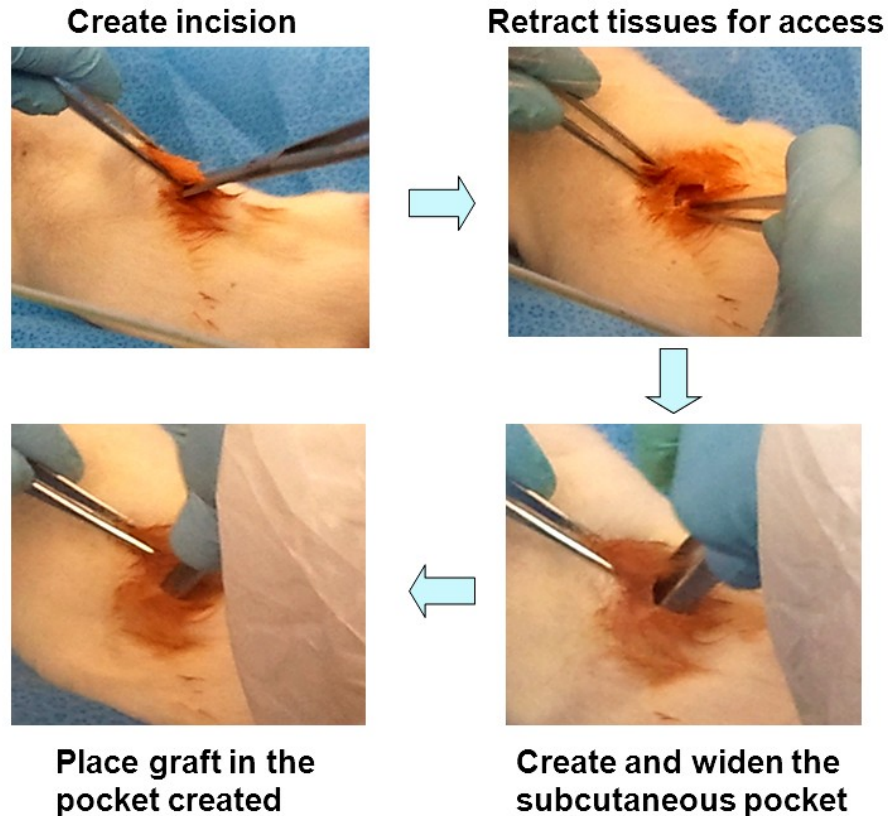


Figure 4.3.1.1: Subcutaneous implantation: surgical steps.

4.3.2 Orthotopic implantation procedure

Male rabbits for orthotopic implantation were received and acclimatized for 14 days before surgical procedure. Prior to starting the procedure, the surgical area and the surgical instruments were sterilized and prepared in order to avoid post operative infections. Anesthesia premedication was induced with I.M. injection of 10 mg/kg of xylazine and 1mg/kg of acepromazine followed by I.M injection of 35-50mg/kg of ketamine. Isoflurane mask was used for anesthesia induction. Following induction, the rabbits were intubated and anesthesia was maintained with isoflurane 2% endotracheal intubation. Aseptic procedures were carried out after the animals showed signs of being fully anaesthetized (lack of response to pinching the toe). The animals were next placed on their back and both their legs shaved and prepared for surgery.

Using a lateral approach to the knee, a two inch incision was made below and above the knee joint through the skin (from points 1 inch above and 1 inch below the joint) to expose the lateral condyle of the femur. Two drill holes (3.2 X 4 mm each) were created below the femoral condylar region to accommodate the cylindrical calcium phosphate grafts (3 X 4 mm). The grafts were next gently tapped into place. The wound was irrigated with sterile normal saline and closed in layers: the fascia and muscle was closed closed with 3-0 vicryl, and the subcutaneous tissue and skin closed with a 3-0 running subcuticular monocryl. The same procedure was repeated on the other leg for each animal.

The entire procedure for each animal lasted approximately 1.5 hours. With this procedure the animals were able fully to walk within 24 hours after the surgery. The rabbits received 0.05 mg/kg buprenorphine 30 minutes prior to the end of surgery and then a post-op regimen of buprenorphine every 8 to 12 hours was administered (0.02-0.05 mg/kg), for a minimum of 72 hours.

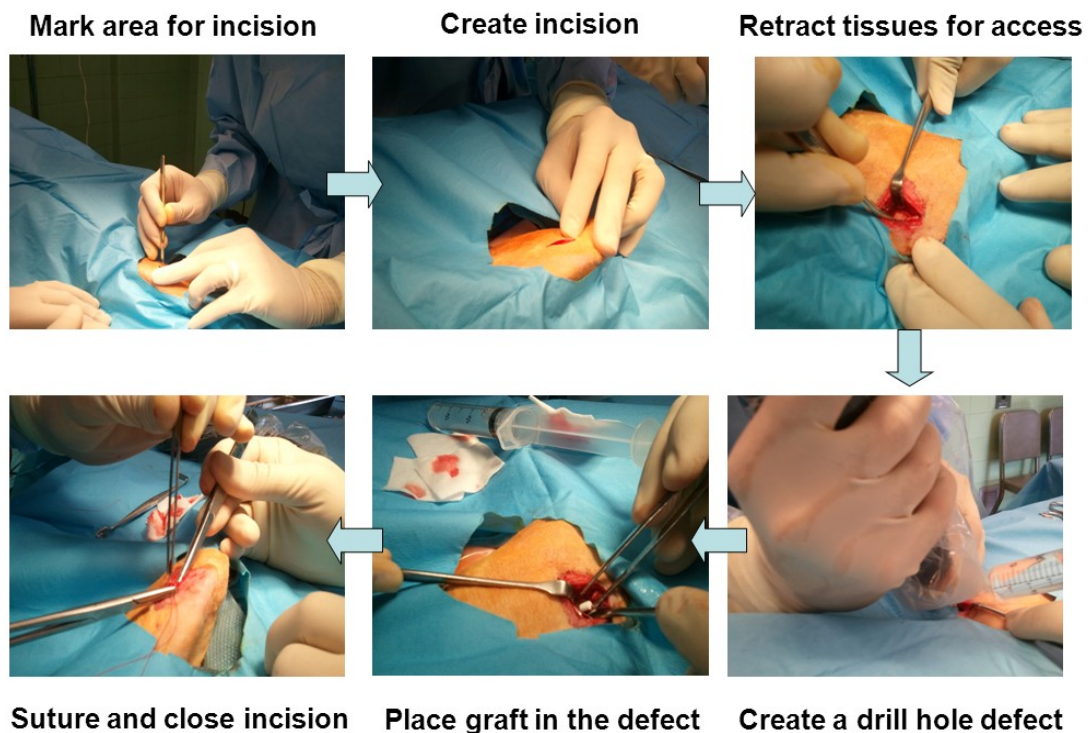


Figure 4.3.2.1: Orthotopic implantation: surgical steps.

The protocol period was 4-12 weeks. Sacrifice was effected after sedation of the animals. Animals were sedated with a subcutaneous injection of buprenorphine 0.2mg/kg and acepromazine 1mg/kg. Once the animals were fully sedated sacrifice would be effected with an intravenous overdose of nembutal. Post mortem, femurs containing the implanted calcium phosphate grafts were retrieved from the animals and processed for μ -CT/histology, XRD, SEM and histomorphometric analysis.

All of the surgical procedures including the post surgical X-ray and live animal CT-scanning was done at the Montreal General Hospital (MGH) Animal Research Facility, in the same room where the surgery was performed, to avoid possible distress to the animals. The digital X-ray images obtained for the femur obtained post sacrifice of the animals was performed at the Center for Bone & Periodontal Disease (McGill University).

4.3.3 Onlay grafting procedure

Male rabbits for onlay grafting were received and acclimatized for 14 days for onlay grafting. Prior to starting the surgical procedure, the surgical area and the surgical instruments were sterilized and prepared in order to avoid post operative infections. Anesthesia premedication was induced with I.M. injection of 10 mg/kg of xylazine and 1mg/kg of acepromazine followed by I.M injection of 35-50mg/kg of ketamine. Isoflurane mask was used for anesthesia induction. Following induction, the rabbits were intubated and anesthesia was maintained with isoflurane 2% endotracheal intubation. Aseptic procedures were carried out after the animals showed signs of being fully anaesthetized (lack of response to pinching the toe). The animals were next placed in sternal recumbency, the head shaved and the cutaneous surface disinfected with povidone iodine solution, and the animal was covered with a sterile drape.

The calvaria bone was exposed through a skin incision approximately 4 cm in length over the linea media. A pair of tweezers were used to lift the skin before the periosteum was also incised in the same place. A periosteal elevator was used for separating the periosteum from the bone surface. Two holes (1.4 mm diameter) were drilled in the parietal bone using a trephine on a slow-speed electric handpiece by applying 0.9% physiologic saline irrigation. The drill holes were made on each side of the median sagittal suture without crossing it. The bioceramic implant discs (9.5 mm diameter by 3 mm thickness) were stabilized by utilising stainless steel screw (1.5 mm screw diameter and 5 mm screw length) on either side. The wound was irrigated with sterile normal saline and closed in layers: the fascia was closed with 3-0 vicryl, and the skin closed with a 3-0 running subcuticular monocryl.

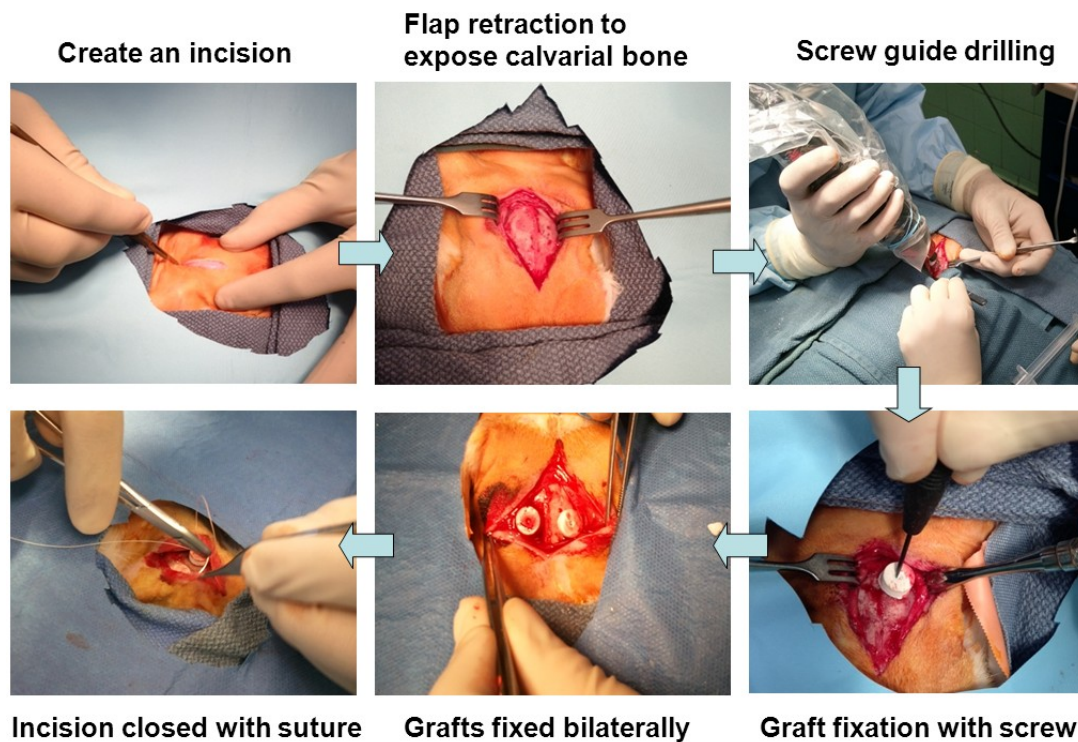


Figure 4.3.3.1: Onlay grafting: surgical steps.

The entire procedure for each animal lasted approximately 1 hour. This procedure necessitated no cutting of musculature or major disruption of blood supply. Similar procedure has been used previously for calvaria implantation studies (17, 158). With this procedure the animals were able fully to walk within 24 hours after the surgery. The rabbits received 0.05 mg/kg buprenorphine 30 minutes prior to the end of surgery and then a post-op regimen of buprenorphine every 8 to 12 hours was administered (0.02-0.05 mg/kg), for a minimum of 72 hours.

The protocol period was 12 weeks. Sacrifice was effected after sedation of the animals. Animals were sedated with a subcutaneous injection of buprenorphine 0.2 mg/kg and acepromazine 1mg/kg. Once the animals were fully sedated sacrifice would be effected with an intravenous overdose of nembutal. Post mortem, bone blocks containing the stainless steel screw stabilized bioceramic discs were retrieved from the animal's calvaria and processed for μ -CT/histology, XRD, SEM and histomorphometric analysis.

All of the surgical procedures including the post surgical X-ray and live animal CT-scanning was done at the Montreal General Hospital (MGH) Animal Research Facility, in the same room where the surgery was performed, in order to avoid possible distress to the animals.

Chapter 5: *In vitro* degradation and *in vivo* resorption of dicalcium phosphate cement based grafts.

5.1 Preface

Dicalcium phosphate cements setting to form brushite and monetite are of great interest as bone replacement substitutes for orthopaedic and dental applications. The clinical success of these materials depends upon the rate and extent of *in vivo* resorption. This chapter details experiments performed to gain an insight into the effect of physicochemical properties of brushite and monetite cements on the *in vitro* dissolution/degradation and *in vivo* resorption processes. Bovine serum and phosphate buffered saline (PBS) was chosen for the *in vitro* comparison after ageing between bioceramics produced with differing levels of porosity, density and specific surface areas. In oral maxillofacial applications, bone substitute materials are often in direct contact with soft tissues and hence a subcutaneous rat model was employed for *in vivo* testing comparing resorption in a soft tissue environment between the implanted bioceramics.

***In vitro* degradation and *in vivo* resorption of dicalcium phosphate cement based grafts**

Zeeshan Sheikh¹, Yu Ling Zhang¹, Liam Grover², Faleh Tamimi¹, Jake Barralet^{1,3}

¹Faculty of Dentistry, 3640 McGill University, Montreal, Quebec, H3A 0C7, Canada

²School of Chemical Engineering, University of Birmingham, Edgbaston, Birmingham, B15 2TT, UK

³Division of Orthopaedics, Department of Surgery, Faculty of Medicine, McGill University, Montreal, Quebec, Canada.

5.2 Abstract

Dicalcium phosphates (DCP) are acidic calcium phosphates used in orthopaedic and dental bone repair and regeneration applications. There are two types of DCPs: dihydrated (brushite) and unhydrated (monetite). After implantation, brushite converts to HA which resorbs very slowly and negligibly, limiting the success of bone replacement procedures. This conversion is not observed after implantation in monetite cements and results in greater resorption. However, the mechanisms of resorption and degradation remain largely unknown. This study was designed to investigate the effect of: porosity, surface area and hydration on *in vivo* resorption and *in vitro* degradation of DCP. Brushite and two types of monetite cement based grafts (produced by wet and dry thermal conversion) were aged in PBS, bovine serum solutions and implanted subcutaneously in rats. Here we show that for high porosity grafts, solubility and surface area does not play a significant role towards *in vitro* mass loss with disintegration and fragmentation being the main factors dictating mass loss. For grafts having lower porosity, solubility plays a more crucial role in mass loss during *in vitro* ageing and *in vivo* resorption. Also, *in vitro* serum inhibits the formation of HA in

brushite. However, when aged in PBS, brushite undergoes phase conversion to a mixture of octacalcium phosphate (OCP) and HA. This phase conversion is not observed for monetite when aged (PBS or serum) or implanted subcutaneously. The results obtained provide a greater understanding of the degradation and resorption process of DCP based grafts, allowing us to prepare bone replacement materials with greater clinical efficacy.

5.3 Introduction

Dicalcium phosphates (DCP) are acidic calcium phosphates of great interest for orthopaedic and dental applications. Brushite cements set via a dissolution/precipitation process at low pH (<6) (145, 151). One of the methods by which brushite cements can be prepared is by mixing an acidic calcium phosphate such as monocalcium phosphate monohydrate (MCPM) and a basic calcium phosphate like beta tricalcium phosphate (β -TCP) with water. This method results in a mouldable paste that sets into a solid cementitious material composed mainly of dicalcium phosphate dihydrate (DCPD) (164, 165, 352). Brushite cements can also be utilized as precursors to the anhydrous form of dicalcium phosphate (DCPA), also known as monetite. Brushite crystals when heated above 60°C start to dehydrate into monetite (167), and if moisture is maintained during the heating process (as in autoclaving) then bulk shrinkage is prevented and an increase in the internal pore size is observed (208). This conversion into monetite can also be carried out by dry heating preset brushite cements (16). These wet and dry heat conversions of brushite to monetite results in two materials that are chemically very similar yet differ with respect to physical properties (total porosity, pore size distribution, density and surface area) (16, 18).

The success of bone replacement procedures is limited by the low or negligible resorption rates associated with the use of calcium phosphate cements (145). A significant reduction in the rate of resorption is frequently reported due to the phase conversion of brushite to HA (225, 353). It has been observed that monetite does not re-precipitate into HA *in vivo*, and recent research demonstrates its good osteoconductive and osteoinductive properties (14-18, 231).

Studies investigating behaviour of brushite cements after implantation or immersion in aqueous media have reported resorption, disintegration or long-term stability (44, 177, 232). Brushite cements have been shown to exhibit a

decrease in mass, an increase in porosity, and a deterioration in mechanical properties upon *in vitro* incubation (229). It has been reported that the inherent cement properties (i.e. cement porosity), as well as the properties of surrounding medium and the rate of fluid exchange affects initial brushite resorption (228). Disintegration and fragmentation of cement matrix rather than simple dissolution can also contribute to mass loss during brushite incubation *in vitro* (228).

Brushite cements experience an initial linear degradation rate of 0.25 mm per week once implanted *in vivo* (44). After implantation, during initial few weeks brushite cements appear to resorb by disintegration, simple dissolution and cellular activity (macrophages and osteoclasts) (177, 222, 223). It has also been observed that serum can adsorb onto cement surface altering the interfacial properties promoting brushite resorption *in vivo* and *in vitro* (228). The resorption mechanism of monetite is similar to that observed for brushite cement grafts, in that it is mainly mediated by cellular activity and simple dissolution (224). Recent studies have shown that monetite grafts produced by autoclaving of preset brushite cements appear to resorb more in comparison to the original brushite grafts (18, 207).

In this study, brushite cement grafts were prepared and monetite grafts obtained from them via wet heat and dry heat conversion. The *in vitro* and *in vivo* behaviour of these grafts was investigated by ageing in PBS and bovine serum solutions and also after subcutaneous implantations in rats. We attempted to discern the effect of DCP hydration, porosity and surface area on *in vitro* and *in vivo* degradation and resorption.

5.4 Results

The powder to liquid (P/L) ratio employed to prepare brushite and monetite grafts had a marked influence on their compressive strengths. The compressive strength approximately doubled when the P/L ratio for brushite grafts was increased from 1 to 3 g/ml (**Table 5.9.1**). An approximate three-fold increase and a four-fold increase was observed when the P/L ratio was increased from 1 to 3 for the dry heat and autoclave converted monetite grafts respectively (**Table 5.9.1**). The increase in compressive strength of brushite grafts when the P/L ratio was increased from 1 to 3 was associated with a reduction in the relative porosity from ~65% to ~36%. Similar effects of reduction in relative porosity with increase in the P/L ratio were observed for the dry heat monetite and autoclaved monetite grafts.

Mercury porosimetry of the grafts prepared with a P/L mixing ratio of 3 prior to immersion in PBS, serum and subcutaneous implantation showed that the diameter of the majority of pores were between ~500 nm and ~600 nm for brushite, ~800 nm to ~1 μm for autoclaved monetite, and ~700nm to ~1 μm for the dry heat monetite (**Figure 5.9.1 a**). The results for the 1:1 P/L ratio grafts revealed bimodal pore diameter distribution with modal values of ~4 μm and ~9 μm for brushite, ~5 μm to ~8 μm for autoclaved monetite, and ~3 μm to ~8 μm for the dry heat monetite (**Figure 5.9.1 b**).

Upon visual inspection and mass loss quantification of the retrieved grafts (prepared with P/L ratio of 3) from rats, brushite explants after 4 weeks of implantation showed slightly less resorption (~6%) (**Figure 5.9.2 a**) in comparison to the dry heat (~9%) (**Figure 5.9.2 b**) and autoclaved (~12%) (**Figure 5.9.2 c**) monetite explants. Similar observations were made for the brushite (~17%) (**Figure 5.9.2 d**), dry heat monetite (~25%) (**Figure 5.9.2 e**), and autoclaved monetite (~30%) (**Figure 5.9. 2 f**) grafts retrieved after 12 weeks. The radiographs obtained from the animals after implantation of the grafts (**Figure 5.9.2 g**), after 4 weeks (**Figure 5.9.2 h**), and after 12 weeks (**Figure**

5.9.2 i) also demonstrated the visual difference in the extent of resorption between brushite and the monetite grafts *in vivo*.

X-ray powder diffraction (XRD) and phase analysis confirmed that the prepared bioceramic grafts were brushite, and that the autoclaving and dry heating processes resulted in conversion of brushite to monetite (**Figures 5.9.3 and 5.9.4**). The brushite grafts aged in PBS showed phase conversion from brushite to a mixture of octacalcium phosphate (OCP) and HA after 60 days (**Figure 5.9.3**). The brushite grafts aged in serum did not show phase change at any time point (data not shown). Similar results were obtained for the brushite grafts after 4 weeks of implantation with no phase change observed. A mixture of OCP and HA peaks were seen in the XRD patterns of the surface of brushite at 12 weeks *in vivo* (**Figure 5.9.4**). The monetite cement grafts (autoclaved and dry heated), aged *in vitro*, and implanted subcutaneously, did not show any phase change or conversion to apatite when characterised (**Figures 5.9.3 and 5.9.4**).

SEM micrographs of the prepared brushite grafts showed blade like crystals in the ~5 μm size range (**Figure 5.9.5 a**). When aged in PBS, the brushite grafts showed blade or needle like crystal growth of OCP (**Figure 5.9.5 b**). When the same brushite grafts were aged in serum, smaller crystals were observed with the size being less than 2-3 μm (**Figure 5.9.5 c**). Subcutaneously implanted brushite grafts showed similar blade like crystal morphology of OCP (**Figure 5.9.5 d**). These microstructural observations were consistent irrespective of P/L ratio used to prepare the bioceramics. The primary crystal morphology of the autoclaved monetite grafts when prepared showed crystals mostly in the ~2-4 μm size range (**Figure 5.9.5 e**). After ageing in serum, the microstructure of autoclaved monetite grafts changed to ~1 μm in size (**Figure 5.9.5 g**). Autoclaved monetite grafts aged in PBS solution and implanted subcutaneously also showed small sized crystals (**Figures 5.9.5 f and h**). The dry heat monetite grafts prepared for the ageing experiments and implantations had mostly extremely small crystals with size smaller than 1 μm (**Figure 5.9.5 i**). After ageing

in PBS, we observed similar crystal morphology with the original grafts yet the crystal size had become smaller (**Figure 5.9.5 j**). It was interesting to note the appearance of the dry heat graft microstructure after ageing in serum as the original brushite crystal morphology seemed to have been maintained but they had transformed into porous assemblies of nanocrystals (**Figure 5.9.5 k**). After subcutaneous implantation the dry heat monetite grafts showed an appearance which was a mixture of that seen in the PBS aged samples (smaller crystals) and the subcutaneously implanted samples (porous blocks) (**Figure 5.9.5 k**). No blade like crystals of OCP were observed in any of the monetite grafts after being in PBS, serum or *in vivo* for any given time period.

Elemental analysis of the bioceramics revealed that brushite and both the autoclaved and dry heat monetite grafts had a similar calcium-to-phosphate (Ca/P) ratio, slightly higher than 1.0 (**Table 5.9.3**). However when the samples were aged in PBS and implanted subcutaneously it was observed that the Ca/P ratio for brushite grafts increased, matching closely to the Ca/P ratio expected for OCP (1.33). This increase was not observed for the grafts aged in serum. The autoclaved and dry heat monetite grafts did not show significant changes in the Ca/P ratio after being aged in PBS or implanted (**Table 5.9.3**).

All grafts aged in serum showed a greater loss of mass over 60 days when compared to ageing in PBS ($p < 0.05$) (**Table 5.9.2 and Figure 5.9.6**). Brushite grafts prepared with P/L ratio of 3 after 26 days of ageing in PBS started to lose more mass daily and this trend continued till about day 56 (**Figure 5.9.6 a**). After day 56, the brushite seemed to have stopped losing mass (**Figure 5.9.6 a**). When this was compared with the results from the *in vitro* ageing in serum for the 3:1 P/L ratio grafts, we observed that brushite lost mass continuously till day 60 (**Figure 5.9.6 b**). When the 1:1 P/L ratio grafts were aged in PBS and serum, they lost similar amount of mass (~10%) during the first 10 days (**Figures 5.9.6 c and d**). However after the first 10 days, the grafts aged in serum continued to lose more mass daily over the next 50 days. The 1:1 P/L ratio grafts being more

porous than their 3:1 P/L ratio counterparts demonstrated a quicker rate of disintegration (**Figures 5.9.6 c and d**). In comparison, the 3:1 P/L ratio grafts underwent less fragmentation and maintained physical integrity better. The difference in the mechanical properties of these grafts also matches with this observation, since 3:1 P/L ratio grafts had higher compressive strength when compared with the 1:1 P/L ratio grafts (**Table 5.9.1**). The 3:1 P/L ratio grafts aged in PBS showed minimal mass loss for the first 26 days (~2.5%). Autoclaved monetite grafts continued to lose mass at a similar rate for the next 34 days and at the end lost ~4.5% of its starting mass. Autoclaved monetite demonstrated the greatest amount of *in vivo* resorption ($p < 0.05$) followed by dry heat monetite grafts, while the least amount of resorption was shown by brushite grafts for the similar P/L ratios employed (**Table 5.9.2 and Figure 5.9.7**).

5.5 Discussion

5.5.1 *In vitro* dissolution & *in vivo* resorption

Passive dissolution, fragmentation, cellular activity (macrophage and osteoclast mediated) and phase conversion are the key mechanisms that determine the rate and amount of mass loss from brushite cements during *in vitro* incubation and *in vivo* implantation (183, 228, 354). Dissolution occurs when brushite is placed in an environment that is under saturated in calcium and phosphate ions and proceeds according to the following equation:



The process of dissolution stops once the solubility limit has been reached (228, 229, 355). Brushite dissolution supersaturates the environment with respect to HA, ultimately resulting in HA precipitation. Brushite conversion to HA occurs via two steps; dissolution and precipitation (356) and proceeds according to the following equation:



Once the cement was immersed, the process of brushite dissolution could begin immediately since PBS used in our study contained no calcium ions. This would be expected to increase the calcium and phosphate ion concentration, slowing the rate of cement dissolution. By removing the dissolution products on a daily basis a relatively higher rate of dissolution was maintained, analogous to the *in vivo* process of fluid turn over.

Phase conversion to OCP and HA along with limited mass loss observed for brushite grafts aged in PBS match with the results obtained from same grafts after subcutaneous implantation. It is already known that the Ca/P ratio of OCP and HA are 1.33 and 1.67 respectively (16, 18). The Ca/P ratio noted for the PBS

aged and subcutaneously implanted brushite grafts was between these two values indicating a mixed phase content of the remaining cement. In a previous study, brushite cement set by mixing β -TCP with orthophosphoric acid showed the presence of HA after 14 days of immersion in PBS resulting in reduction in the rate at which mass was lost from the cement (228). It has been reported that formation of HA in brushite cement can occur as early as 72 h after initial immersion in PBS, reaching complete conversion within 19 days of ageing (357). In our *in vitro* and *in vivo* experiments this early conversion of brushite grafts was not observed. The late conversion of brushite phase to a mixture of OCP and HA observed in our study can be attributed to the *in vitro* media refreshment performed daily and fluid turnover *in vivo* after subcutaneous implantation.

The presence of calcium in serum (~50-90%) reduces solubility of brushite to between ~2% and 4% of that in the absence of calcium (201). However, we did not observe this reduction in solubility when the grafts were aged in bovine serum. Conversion of brushite cements to HA has been observed *in vivo* (232, 357), and therefore this could be expected after ageing in serum. As there was no HA detected at any time point investigated it appeared that serum constituents inhibited apatite formation. Several studies have reported that proteins depending on their types and levels can either inhibit or encourage the formation of HA or its precursor (OCP) in calcium phosphates (18, 358). It has been observed that the proteins present in serum can adsorb onto cement surfaces, altering the interfacial properties of the crystals (184), favoring *in vitro* resorption. It has already been demonstrated *in vitro* previously that albumin retards the transformation of brushite to HA (356, 359). Since serum contains all of the proteins and ionic constituents that are present *in vivo*, other factors such as enzymes or cellular activity may be responsible for HA formation in brushite cements after implantation. These observations are also supported by the results from our *in vivo* study which demonstrated phase conversion of brushite to OCP & HA after subcutaneous implantation.

The results from our study showed that monetite grafts although having lower solubility than brushite cements (16), still resorbed faster *in vivo*. This was also observed in other recent studies (207). The mechanism of *in vivo* resorption of monetite cements is similar to that of brushite, with cellular activity accounting for most of the resorption with passive dissolution being less crucial (224). The possible reason for the monetite grafts showing greater resorption *in vivo* could be the greater total porosity present than brushite. Another reason could be the presence of higher levels of macroporosity in monetite in comparison with brushite cements. It has been reported that materials with macroporosity can be invaded by resorbing cells and show an increase in the rate and amount of resorption (360).

5.5.2 Disintegration

It was observed that a large proportion of mass lost in PBS and serum for cement grafts prepared with P/L ratio of 1 could be attributed to disintegration of the cements due to their highly porous and mechanically weak structure rather than dissolution. This mass loss due to disintegration has also been noted in other *in vitro* (228) and also *in vivo* (357) studies. The fragmentation of high porosity grafts was observed with serum solutions collected every day having murky appearance. As a consequence, higher porosity brushite grafts lost mass throughout the experiment at a constant rate. The greater mass loss of the 1:1 P/L ratio brushite and monetite cements when compared with the 3:1 P/L ratio cements aged in serum and PBS is thought to be due to higher relative porosity of the 1:1 P/L ratio grafts. The differences in weight loss observed for the less porous 3:1 P/L ratio brushite and monetite cements could be attributed to the difference in the solubility constants and not so much dependent upon fragmentation or disintegration of the cement matrix.

5.5.3 Physical properties

The relationship between porosity and strength is inversely logarithmic (179, 216); thus the effect of increase in relative porosity resulted in the loss of compressive strength observed (**Figure 5.10.7**). Relative porosity, crystal morphology, degree of conversion, homogeneity of the cement matrix, compaction of the setting cement and critical flaw size are a number of factors which may influence cement strength (166, 182, 361, 362). The highest wet compressive strength value measured for our prepared cement grafts was for the brushite cylinders prepared with P/L ratio of 3 being ~16 MPa. This when compared with the highest compressive strength of ~52 MPa reported in literature for hand mixed brushite cements (216); is significantly lower. The reduction in compressive strength observed after ageing was likely to have been caused by dissolution of the brushite cement resulting in the increase in the relative porosity *in vitro* and *in vivo*. Mirtchi *et al.* have reported a similar reduction in compressive strength in brushite cements formed from β -TCP and MCPM following ageing in water (363). A significant reduction in the compressive strength was also noted upon the conversion of brushite grafts to monetite by autoclaving. This detrimental effect can be attributed to the increase in the relative porosity observed after autoclaving. Interestingly, the brushite grafts converted to monetite by dry heating demonstrated a much higher compressive strength in comparison to their autoclaved counterparts and did not exhibit as great a loss of compressive strength after ageing and implantation. We believe that the dry heating process under vacuum not only converts brushite to monetite but also the crystals get aggregated as observed in the SEM micrographs. This aggregation and interlocking of monetite crystals is probably the reason for the higher compressive strength recorded.

The density of the brushite grafts was higher than what is expected from phase pure brushite (2.27 g/cm^3) (16). This was possibly due to the presence of small amounts of dense β -TCP (3.14 g/cm^3) in the brushite cement grafts. The monetite grafts prepared by the two different conversion methods had lower

density than the pure form of monetite (2.92 g/cm^3) (16), indicating some trace amounts of brushite cement may have remained unconverted. The increase in the SSA observed after conversion of brushite to monetite was due to the autoclaving process resulting in smaller sized monetite crystals and an increase in total porosity percentage. The brushite cement grafts converted to monetite by dry heating under vacuum demonstrated a greater increase in the SSA and this was observed via SEM imaging which showed decreased crystal size in comparison with the autoclaved monetite crystals.

5.6 Conclusion

This study shows that serum inhibits the formation of HA in brushite cement. Monetite cements produced by autoclaving and dry heating methods do not demonstrate any phase conversion when aged in PBS or serum. While surface area does not play a significant role, disintegration and fragmentation of grafts seems to be the main factors which dictate mass loss in high porosity bioceramics. For cements having lower porosity, solubility plays a more crucial role towards mass loss during *in vitro* ageing and *in vivo* resorption. It appears that it is not only the material composition that dictates cement behavior *in vitro* and *in vivo*, but is a combination of various physical and chemical characteristics. Cement removal from implant site is a complex phenomenon and dependent on a variety of physiologic processes other than simple dissolution. The results obtained from this study lays down the ground work for further investigation to obtain a better understanding of the degradation processes and hence achieving the possibility of graft preparation with higher clinical efficacy.

5.7 Acknowledgements

The authors acknowledge financial support from RSBO, Quebec Government MDEIE Catalonia-Quebec grant.

5.8 Experimental

5.8.1 Method and materials

5.8.1.1 Synthesis

Brushite cement grafts were prepared with a mixture of β -TCP (Merck) and commercially available monocalcium phosphate hydrate (MCPM) (ABCR, GmbH & Co.KG) using a ratio of 1.2 to 1 respectively. In order to investigate the effect of powder to liquid (P/L) ratio on physical properties and degradation, brushite and monetite cements were produced at P/L mixing ratio of 3 and 1 g/ml. The powders were hand ground with a pestle and mortar and cement pastes prepared by mixing the powder with appropriate amount of distilled water on a glass slab for 20 s. Once all of the powder was combined with the liquid, the cement paste was kneaded for a further 30 s. The manipulated cement slurry was cast into a polytetrafluoroethylene (PTFE) split mould forming hardened cement cylinders \varnothing (~12 x 6 mm). The cylinders were allowed to set for 24 h at $37^{\circ}\text{C} \pm 1^{\circ}\text{C}$ in a vacuum desiccator to form hard brushite. At the end of the incubation period, the samples were removed from the mould and weighed until constant mass was reached. Five different batches of thirty cylinders each were produced to obtain a total of one hundred and fifty cylinders with 3 and 1 P/L ratios. Even though the sample homogeneity was very high (either within a batch or between batches), the sample assignment was randomized.

Monetite cement grafts ($n=70$ in total) were synthesized by conversion of the preset brushite cement cylinders utilizing two different methods: thermal and hydrothermal conversion. For thermal conversion, the brushite cylinders ($n=35$) were dry heated at 250°C for 30 minutes under vacuum (80 mTorr). Hydrothermal transformation was performed with the brushite cylinders ($n=35$) being autoclaved at sterilizing conditions (120°C , 100% humidity and 15 psi, for 30 minutes).

5.8.1.2 Characterisation

The phase purity of the prepared brushite and the monetite grafts was confirmed using X-ray diffraction (XRD). XRD data was collected (Bruker Discover D8 diffractometer) with Ni filtered CuK α radiation ($\lambda = 1.54\text{\AA}$) with a two dimensional VANTEC area detector at 40 kV and 40 mA. A step size of 0.02° was used to measure from 10 to 50° 2θ over 3 frames with a count time of 300 s per frame. The phase composition was compared and confirmed with the International Centre for Diffraction Data reference patterns for brushite (PDF Ref. 09-0077) and monetite (PDF Ref. 09-0080), JCPDS 2010 database.

The compressive strength of all prepared grafts was measured before and after *in vitro* ageing and subcutaneous implantation. Before testing, geometrical measurements of the graft cylinders were made in triplicate and the samples weighed. Samples were mounted on the testing machine (5544, Instron) so that the long axes of the cement cylinders were perpendicular to the lower anvil. A compressive force was then applied to the upper surface of the cylinders at a constant crosshead displacement rate of 1 mm/min until failure occurred. The applied load was measured using a 100 N load cell (5544, Instron). Mean compressive strength was determined from the average of 10 measurements.

After testing in compression, cement fragments were retrieved, weighed and dried in a vacuum desiccator at a temperature of 37°C . The fragments were then ground to powder using a pestle and mortar. The true density of the powdered grafts was determined using a helium pycnometer (Accupyc 1330, Micromeritics). The volume of each sample was measured 10 times following 10 purges of the measurement chamber with helium. The relative porosity (bulk porosity) of the cements was calculated from apparent and true density measurements. The specific surface area (SSA) of cements was determined by using the Brunauer–Emmett–Teller (BET) method with helium adsorption–desorption (Tristar3000, Micromeritics).

Bioceramic microstructure was observed using scanning electron microscopy (Hitachi S-4700 FE-SEM; Tokyo, Japan), at an accelerating voltage of 2 kV. Elemental composition of the bioceramics was assessed with energy dispersive X-ray (EDX) analysis using Oxford detector and INCA software (Oxford Instruments, Abingdon, UK). The pore size distribution of the prepared brushite and monetite cement grafts prior to *in vitro* and *in vivo* experiments was measured by using mercury intrusion porosimetry (9420, Micromeritics, Bedfordshire, UK).

5.8.1.2 In vitro ageing

After initial characterisation was complete, the graft cylinders were stored at $37 \pm 1^\circ\text{C}$ and $\sim 100\%$ relative humidity for 24 h. Brushite and the autoclaved and dry heat monetite grafts ($n=3$) were immersed in PBS solutions, and also in bovine serum containing sodium azide (Sigma-Aldrich) at a concentration of 0.1%. The graft cylinders were aged at a liquid to cement volume ratio (LCVR) of 60 as used by Grover et al. (228) for 7, 30 and 60 days at $37 \pm 1^\circ\text{C}$. Dynamic ageing protocols were achieved by refreshing the liquid every 24 h throughout the experiment to remove any dissolution products. To quantify the amount of mass loss over time, the graft cylinders were removed daily from the ageing medium and weighed. After periods of 7, 30 and 60 days of ageing, the grafts were removed from the solutions and tested in compression and characterised for changes in phase composition, SSA, density and porosity.

5.8.1.3 Animal study

The surgical protocol for animal testing for research was approved by the McGill University Ethical Committee (Animal use protocol # 6020). For evaluation of bio-resorption and changes in the physicochemical properties *in vivo*, the prepared calcium phosphate grafts were implanted subcutaneously in rats ($n=6$). 36 male Wistar rats (35-40 days old, 126-150 g weight) were purchased from Charles River Laboratories, Montreal, Quebec, Canada. Briefly, two subcutaneous pockets on either side in the flanks of the animals were accessed via a mid-

scapular surgical incision. The implants were placed (unfixed) into the pocket. It was ensured using blunt dissection that the subcutaneous pocket is made and that the graft does not rest directly beneath the incision, as this could have potentially interfered with wound healing. After placement of grafts in their respective pockets, the incision was closed using resorbable monocryl sutures. After 4 and 12 weeks of implantation, animals were sacrificed and implants retrieved. Digital radiographs were obtained using Kubtec[®] XPERT80 X-ray system (KUB Technologies Inc. Milford, CT) employing a voltage of 90 kV and a tube current of 1.0 μ a. The retrieved grafts were tested in compression, characterised for changes in phase structure, SSA, density, porosity and mass loss.

5.8.1.4 Statistical analysis

Data are presented as the mean plus or minus the standard deviation. Statistical analysis was performed using the statistical software IBM[®]SPSS[®] (v. 19, IBM SPSS Inc., Chicago, IL). Statistical significance ($p < 0.05$) between groups was determined by non-parametric analysis with *Wilcoxon sign rank test*. Statistical significance was set at a value of $p < 0.05$.

5.9 Tables & Figures

Table 5.9.1: Summary of physicochemical properties of brushite, autoclaved and dry heat monetite cement grafts.

Graft type and P/L ratio	Porosity (%)	S.S.A (m ² /g)	Density (g/cm ³)	Compressive strength (MPa)
3:1 Brushite	36 ± 2	0.62 ± 0.21	2.42 ± 0.06	16.6 ± 1.0
3:1 AC monetite	53 ± 2	1.66 ± 0.09	2.87 ± 0.02	8.1 ± 1.3
3:1 DH monetite	45 ± 3	20.05 ± 1.14	2.85 ± 0.05	15.0 ± 1.6
1:1 Brushite	65 ± 2	0.89 ± 0.12	2.45 ± 0.04	8.4 ± 1.1
1:1 AC monetite	60 ± 3	1.12 ± 0.13	2.89 ± 0.04	2.4 ± 0.8
1:1 DH monetite	60 ± 2	19.36 ± 1.77	2.83 ± 0.09	5.3 ± 0.6

AC- Autoclaved

DH- Dry heat

S.S.A - Specific surface area

Table 5.9.2: Summary of the total percentage of mass loss of brushite and monetite cements after *in vitro* ageing in PBS and bovine serum and after subcutaneous implantation.

Biomaterial (P/L ratio)	PBS 60 days (mass loss %)	Serum 60 days (mass loss %)	Subcutaneous 84 days (mass loss %)
3:1 Brushite	13 ± 1.0	16 ± 1.0	17 ± 2.0
3:1 Dry heat monetite	10 ± 1.5	12.5 ± 1.0	25 ± 2.5
3:1 Autoclaved monetite	4.5 ± 0.5	7.0 ± 0.5	30 ± 2.0
1:1 Brushite	26 ± 2.0	42.5 ± 2.0	29 ± 3.0
1:1 Dry heat monetite	29 ± 1.5	37 ± 2.0	39 ± 2.0
1:1 Autoclaved monetite	33 ± 1.5	47 ± 1.5	48 ± 4.5

Table 5.9.3: Summary of changes in calcium-to-phosphorous ratio of brushite and monetite grafts after ageing in PBS, serum, and subcutaneous implantation.

Biomaterial	Before experiments	PBS (60 days)	Serum (60 days)	Subcutaneous (84 days)
3:1 Brushite	1.10 ± 0.08	1.42 ± 0.08*	1.10 ± 0.11	1.44 ± 0.13*
1:1 Brushite	1.04 ± 0.11	1.38 ± 0.07*	1.15 ± 0.07	1.42 ± 0.08*
3:1 Autoclaved monetite	1.17 ± 0.06	1.13 ± 0.06	1.14 ± 0.09	1.16 ± 0.06
1:1 Autoclaved monetite	1.15 ± 0.10	1.18 ± 0.08	1.12 ± 0.11	1.15 ± 0.14
3:1 Dry heat monetite	1.13 ± 0.07	1.11 ± 0.12	1.11 ± 0.12	1.13 ± 0.09
1:1 Dry heat monetite	1.06 ± 0.12	1.15 ± 0.10	1.14 ± 0.05	1.12 ± 0.11

(*) signifies the statistical significance of increase in Ca/P ratio from start of experiments

(P < 0.05)

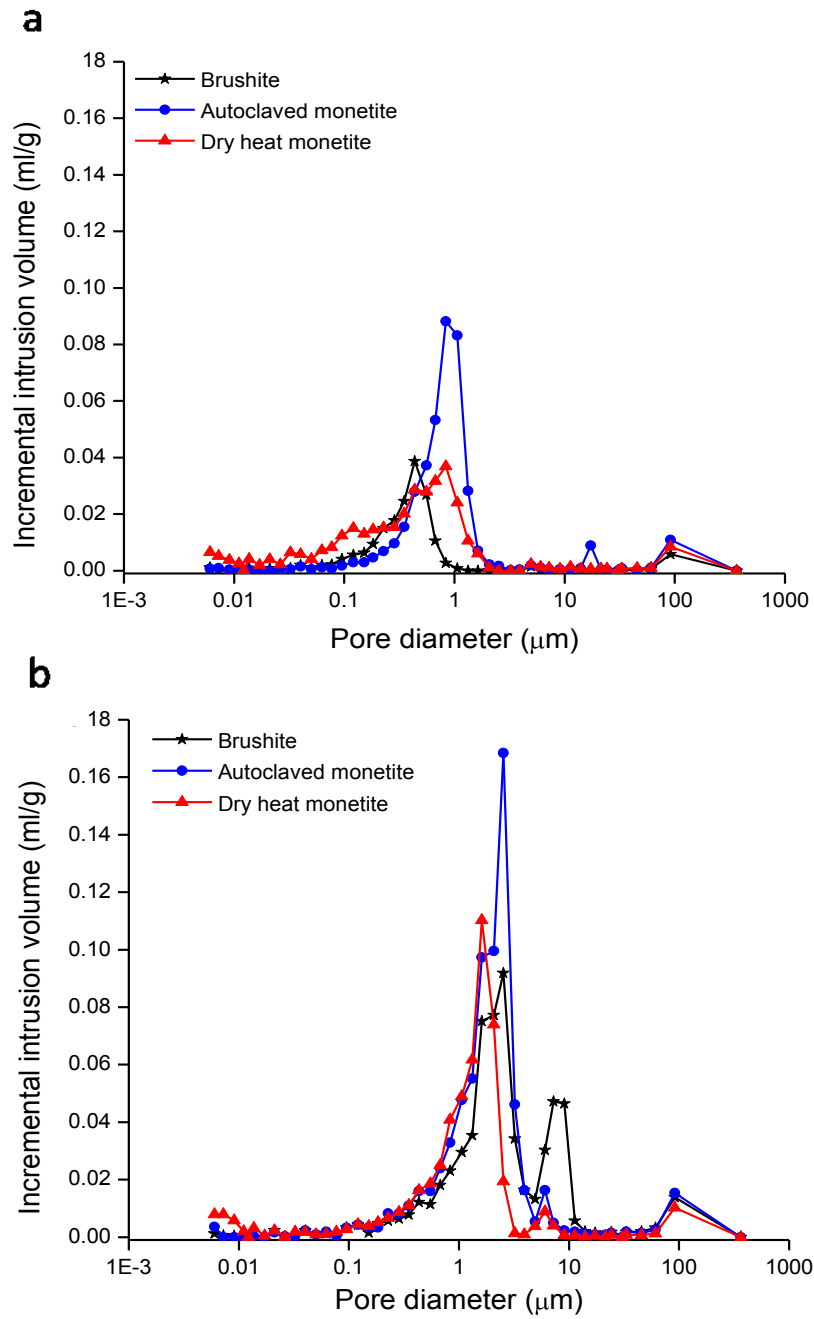


Figure 5.9.1: Pore size distribution of **(a)** 3:1 P/L ratio brushite, autoclaved monetite and dry heat monetite grafts, and **(b)** 1:1 P/L ratio brushite, autoclaved monetite and dry heat monetite grafts.

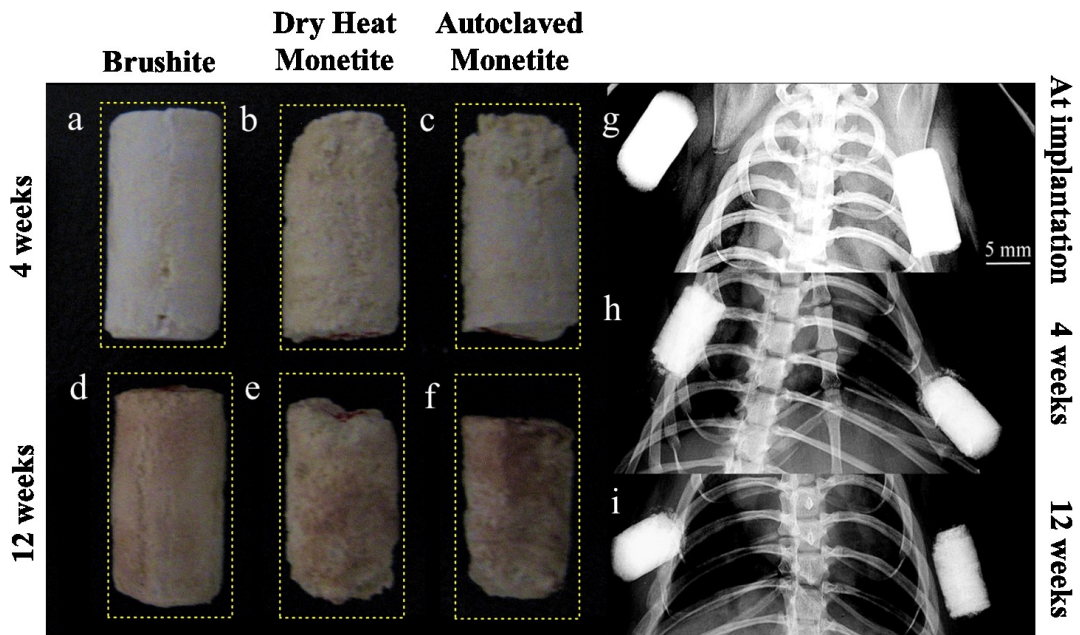


Figure 5.9.2: Photographs of the retrieved brushite, dry heat monetite and autoclaved monetite grafts after 4 weeks of implantation (**a,b,c**) and after 12 weeks (**d,e,f**) [yellow dotted lines denote 6 x 12mm initial dimensions of the grafts]. Radiographs showing brushite (right) and autoclaved monetite (left), (**g**) upon implantation, (**h**) after 4 weeks, and (**i**) after 12 weeks *in vivo*.

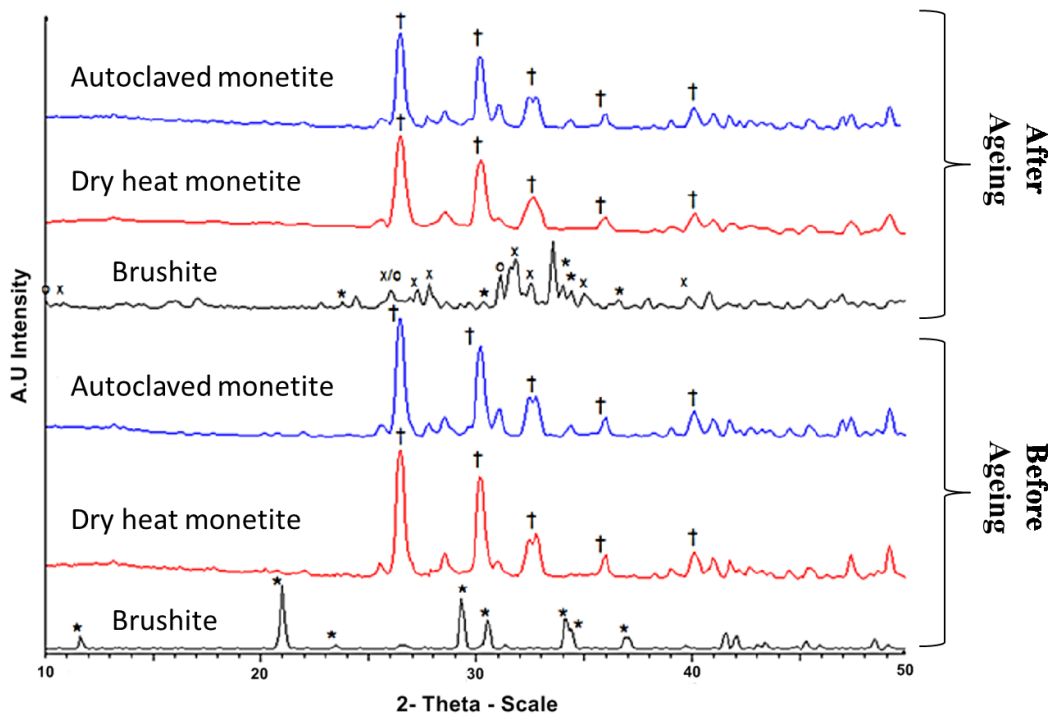


Figure 5.9.3: X-ray diffraction patterns indicating the initial and post ageing in PBS phase composition of brushite, autoclaved and dry heat monetite grafts. Grafts initially consisted of phase pure DCPD (*). The dry heat and autoclaved monetite grafts show the conversion from DCPD to DCPA (†). After ageing in PBS for 60 days the brushite shows conversion from DCPD to OCP (O) and HA (X) and remnants of DCPD. The dry heat and autoclaved monetite grafts do not show any phase change upon ageing in PBS for 60 days.

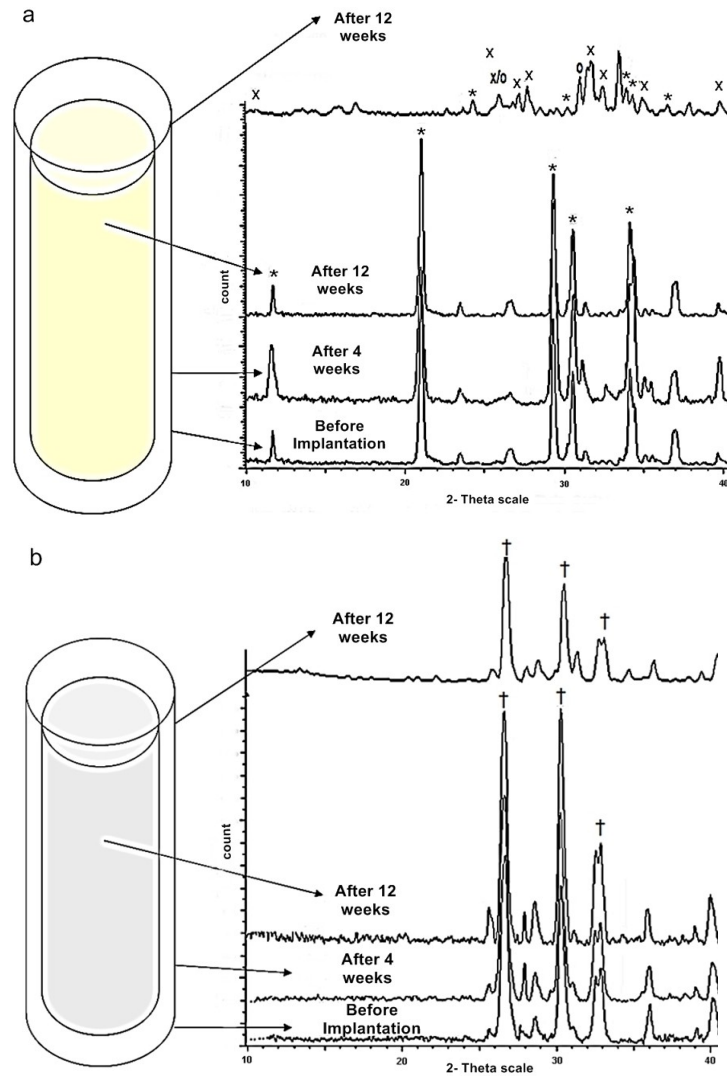


Figure 5.9.4: X-ray diffraction patterns showing phase composition before and post implantation of:

a. Brushite graft cylinders. The grafts initially consisted of phase pure DCPD (*). After 12 weeks of subcutaneous implantation, the analysis of the grafts revealed the presence of a mixture of OCP (O), HA (X) and remnants of DCPD.

b. Autoclaved and dry heat monetite grafts. Analysis of both monetite grafts confirmed conversion from DCPD to DCPA (†) before implantation. The autoclaved and dry heat monetite grafts did not show any phase change upon implantation for 12 weeks.

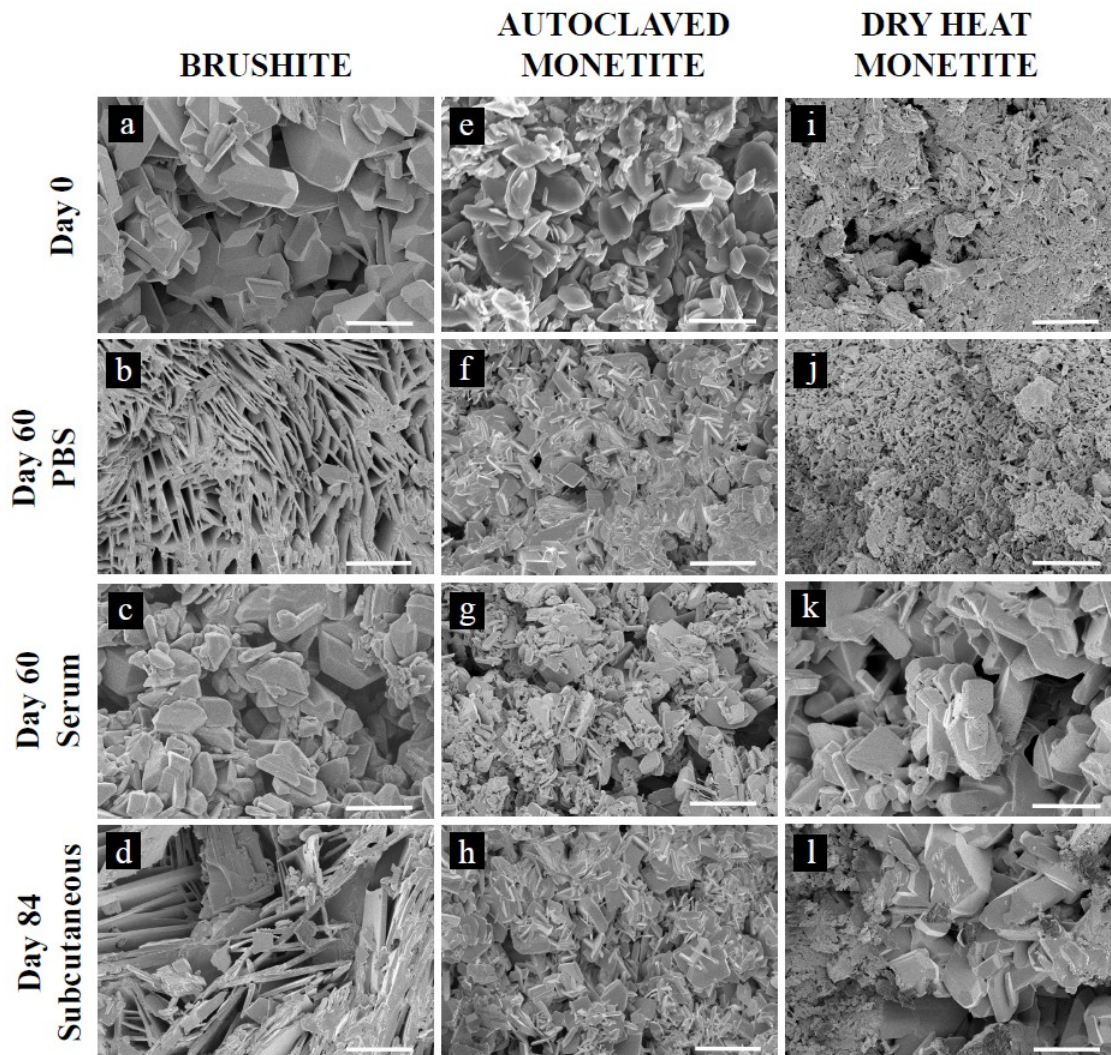


Figure 5.9.5: SEM images of brushite (a, b, c, d), autoclaved monetite (e, f, g, h) and dry heat monetite (i, j, k, h) grafts before and after immersion in PBS, serum, and subcutaneous implantation in rats on Days 0, 60, and 84 respectively (Scale bars represent 5 μ m).

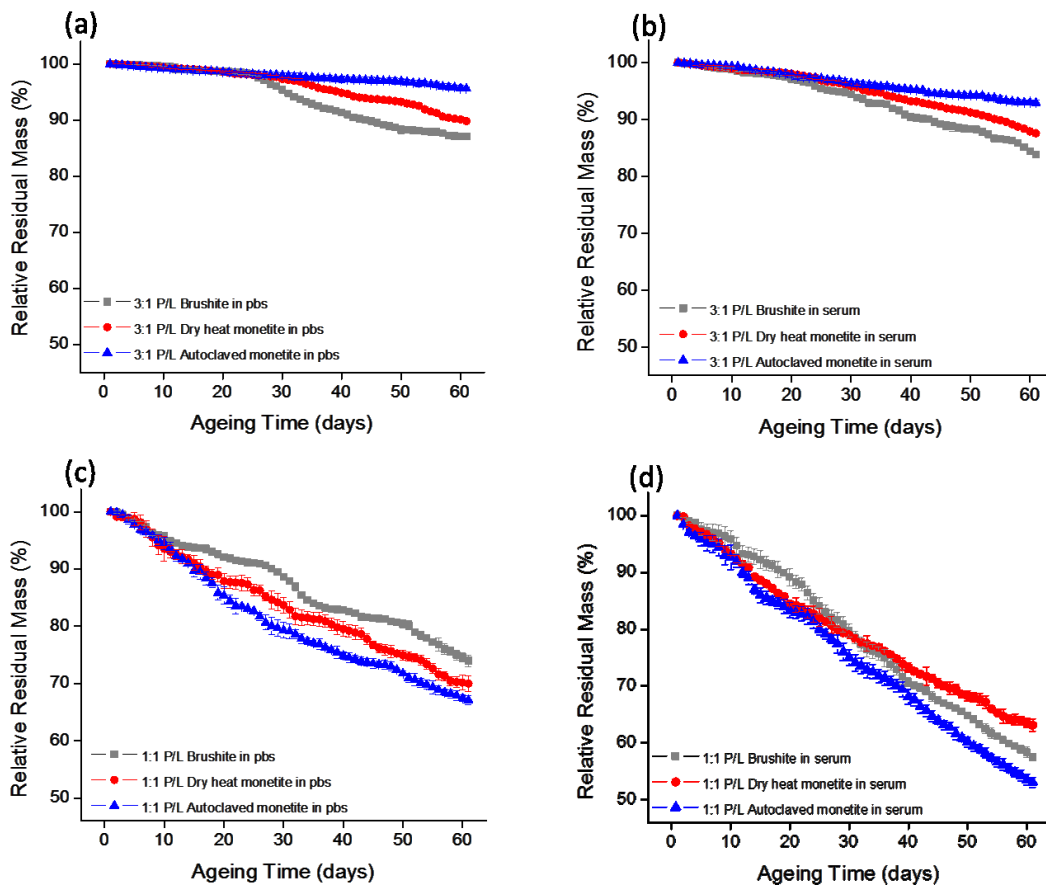


Figure 5.9.6: Mass loss of grafts *in vitro* for up to 60 days; **(a)** 3:1 P/L ratio brushite and monetite grafts in PBS, **(b)** 3:1 P/L ratio brushite and monetite grafts in serum, **(c)** 1:1 P/L ratio brushite and monetite grafts in PBS, and **(d)** 1:1 P/L ratio brushite and monetite grafts in serum.

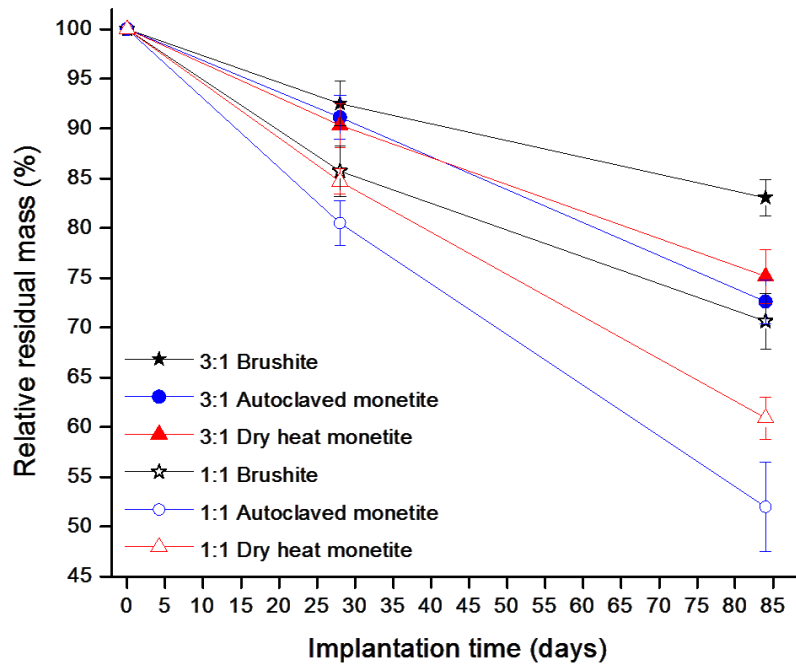


Figure 5.9.7: Comparison between mass loss of all bioceramic grafts implanted subcutaneously.

5.10 Supplementary figures

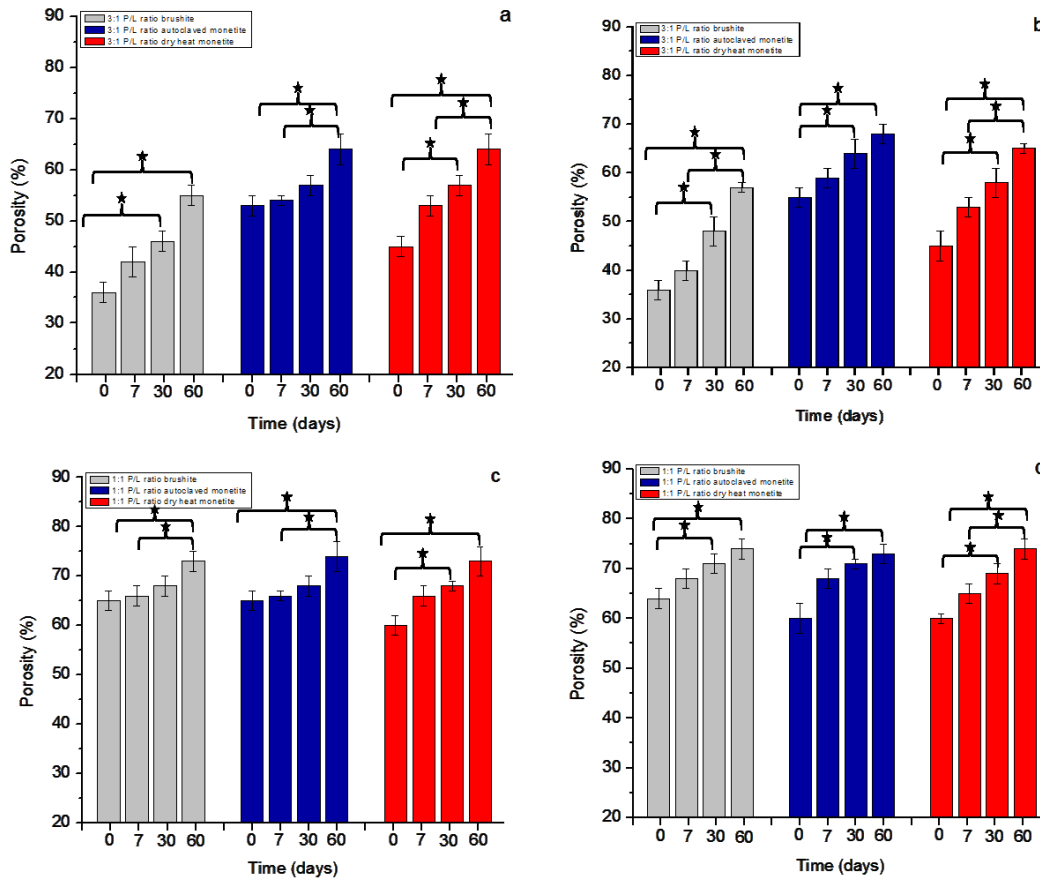


Figure 5.10.1: Effect of *in vitro* ageing on relative porosity of, **(a)** 3:1 P/L ratio grafts in PBS; **(b)** 3:1 P/L ratio grafts in serum; **(c)** 1:1 P/L ratio grafts in PBS; and **(d)** 1:1 P/L ratio grafts in serum. (Grey-brushite, Blue-autoclaved monetite, and Red-dry heat monetite).

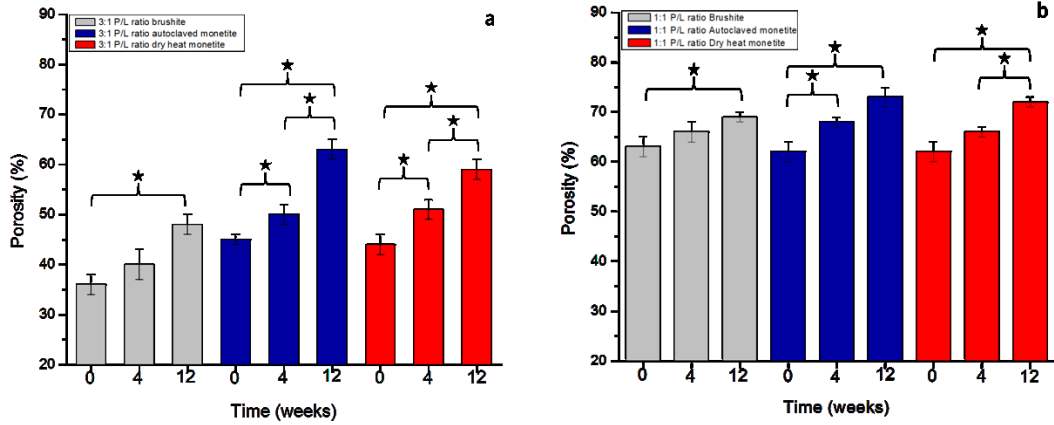


Figure 5.10.2: Effect of subcutaneous implantation on relative porosity of, (a) 3:1 P/L ratio grafts, and (b) 1:1 P/L ratio grafts. (Grey-brushite, Blue-autoclaved monetite, and Red-dry heat monetite).

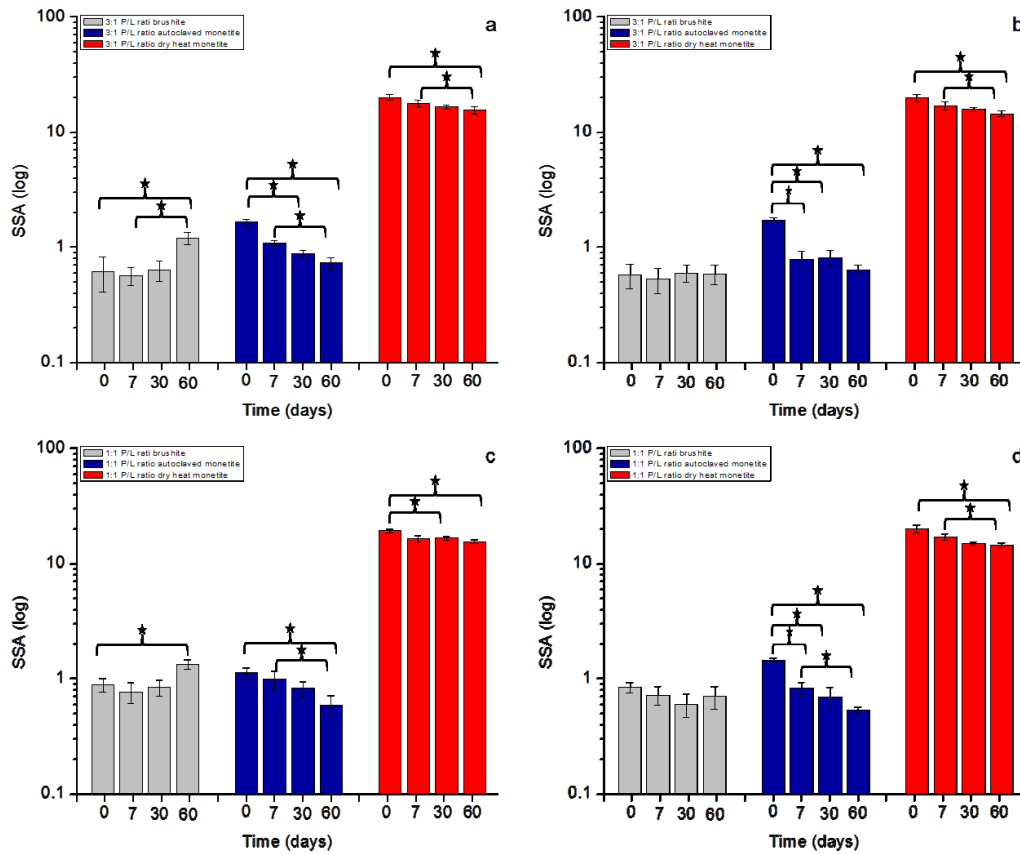


Figure 5.10.3: Effect of *in vitro* ageing on specific surface area (SSA) of, **(a)** 3:1 P/L ratio grafts in PBS; **(b)** 3:1 P/L ratio grafts in serum; **(c)** 1:1 P/L ratio grafts in PBS; and **(d)** 1:1 P/L ratio grafts in serum. (Grey-brushite, Blue- autoclaved monetite, and Red-dry heat monetite).

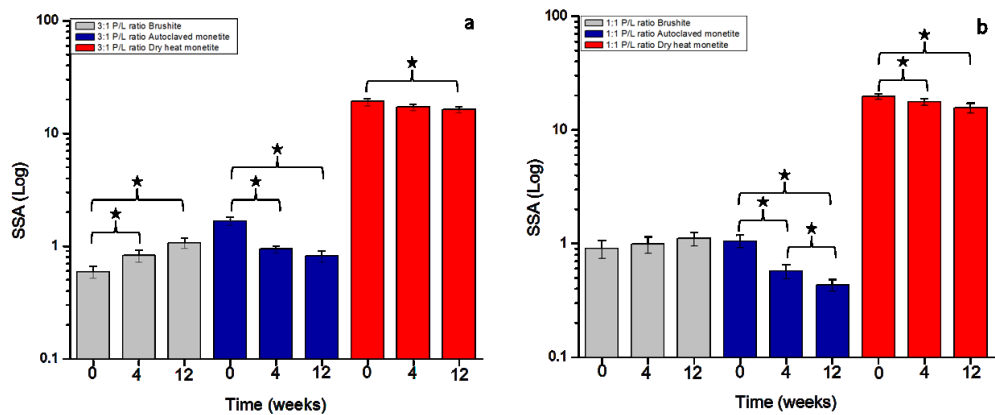


Figure 5.10.4: Effect of subcutaneous implantation on specific surface area (SSA) of, **(a)** 3:1 P/L ratio grafts, and **(b)** 1:1 P/L ratio grafts. (Grey-brushite, Blue- autoclaved monetite, and Red-dry heat monetite).

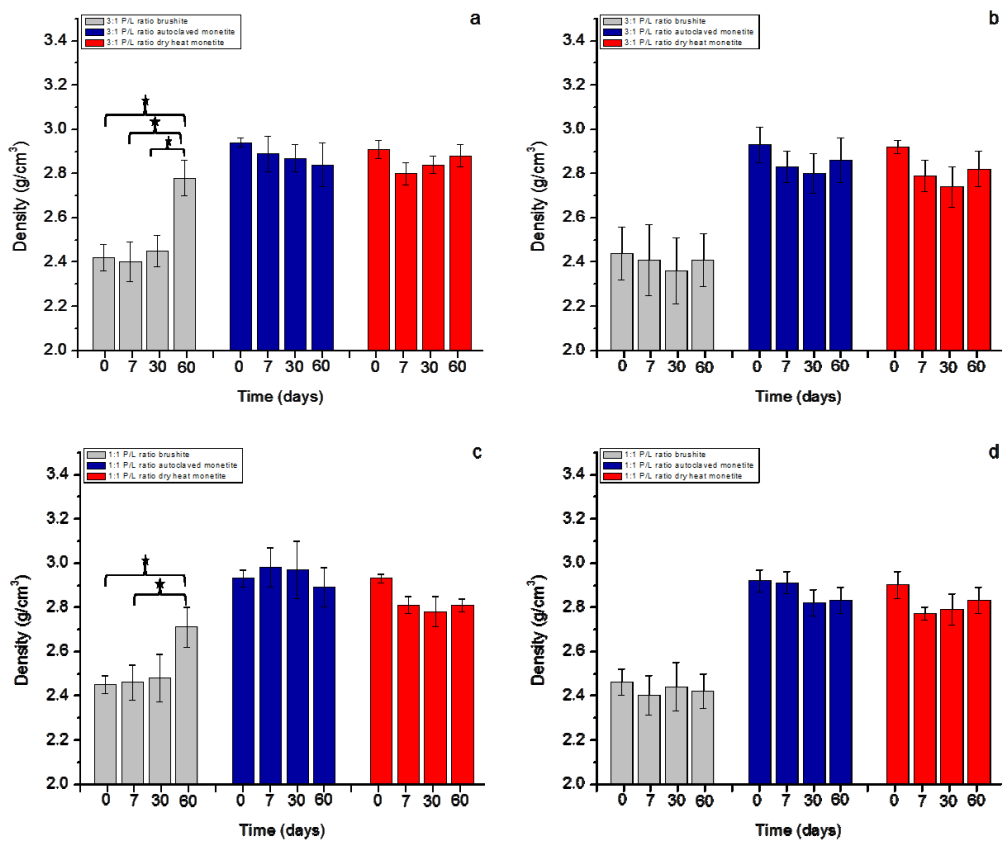


Figure 5.10.5: Effect of *in vitro* ageing on density of, (a) 3:1 P/L ratio grafts in PBS; (b) 3:1 P/L ratio grafts in serum; (c) 1:1 P/L ratio grafts in PBS; and (d) 1:1 P/L ratio grafts in serum. (Grey-brushite, Blue-autoclaved monetite, and Red-dry heat monetite).

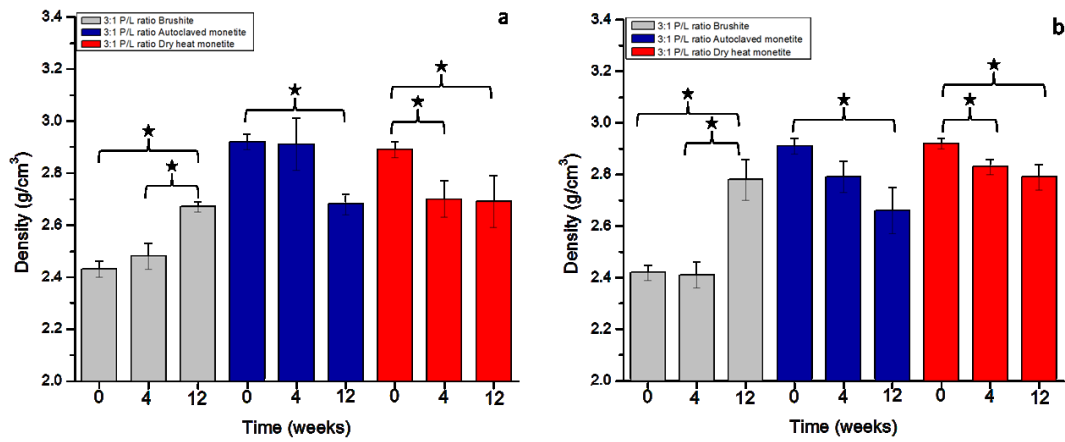


Figure 5.10.6: Effect of subcutaneous implantation on density of, **(a)** 3:1 P/L ratio grafts, and **(b)** 1:1 P/L ratio grafts. (Grey-brushite, Blue-autoclaved monetite, and Red- dry heat monetite).

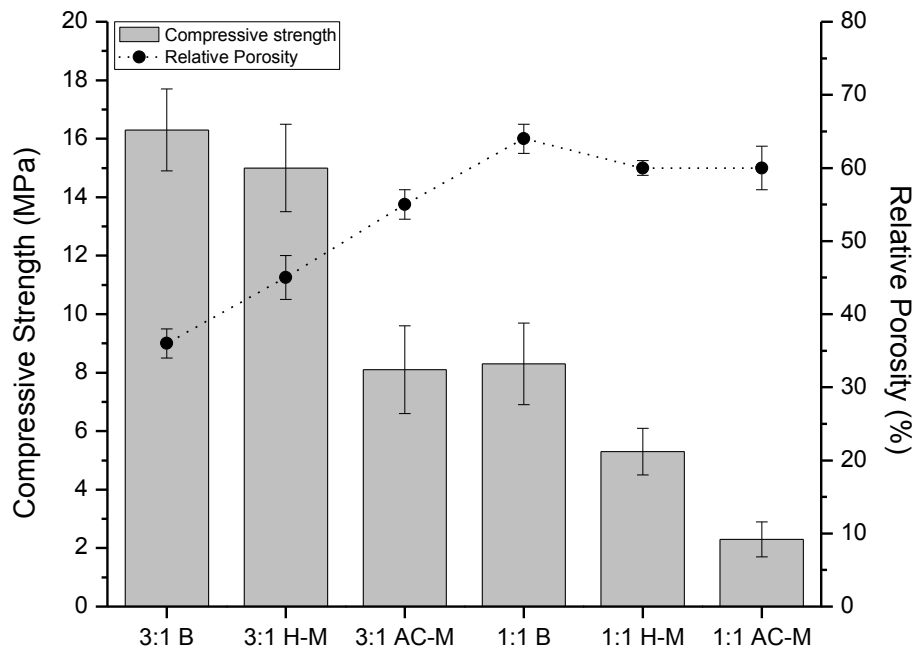


Figure 5.10.7: Effect of powder to liquid ratio on the compressive strength and relative porosity of cements. (B: brushite, H-M: dry heat monetite and AC-M: autoclaved monetite).

Chapter 6: Monetite grafts prepared by wet and dry dehydration of brushite bioceramics: An orthotopic implantation study.

6.1 Preface

In the previous chapter, the effect of physical properties of prepared bioceramic grafts on *in vitro* dissolution/degradation and subcutaneous resorption was investigated. As a direct continuation of this work, the higher P/L ratio (3) bioceramics were assessed for resorption and bone formation response after orthotopic implantation. The reason for excluding the lower P/L ratio (1) bioceramics from this study was due to their tendency to fragment and having extremely poor mechanical properties rendering them clinically unusable for dental or orthopaedic applications. The *in vivo* model used in the preceding chapter revealed information regarding resorption of dicalcium phosphate bioceramics in a soft tissue enclosed environment. However, that model has inherent limitations such as the absence of osteoclasts which play a crucial role in graft resorption once implanted within bone. This chapter focuses on revealing information regarding the differences between brushite and two types of monetite grafts in terms of resorption. Also discussed is the new bone formation within and around the implanted bioceramics. The chapter compares three implanted graft materials (brushite, autoclaved monetite and dry heat monetite) and discusses their *in vivo* behaviour and bone response towards them in relation to the physicochemical differences between them.

Monetite grafts prepared by wet and dry dehydration of brushite bioceramics: An orthotopic implantation study

Zeeshan Sheikh¹, Yu Ling Zhang¹, Chan Gao^{2,3}, Faleh Tamimi¹,
Jake Barralet^{1,3}

¹Faculty of Dentistry, McGill University, Montreal. Quebec, Canada.

²Experimental Medicine, McGill University, Montreal, Quebec, Canada.

³Division of Orthopaedics, Department of Surgery, Faculty of Medicine, McGill University, Montreal, Quebec, Canada.

6.2 Abstract

Dicalcium phosphate cements (brushite and monetite) are resorbable biomaterials with osteoconductive potential in bone repair and regeneration applications. Brushite can be converted to monetite by heat treatment resulting in various additional changes in the physicochemical properties. However, since most commonly conversion is performed during sterilisation (wet heating), it is uncertain whether heating brushite under dry conditions affects resorption and bone formation favourably. This study was designed to produce monetite grafts by autoclaving and dry heating to be compared with brushite bioceramics in an orthotopic pre-clinical implantation model for 12 weeks. This is the first study that reports complete resorption of calcium phosphate cement based grafts. We observed that the monetite grafts had higher porosity, density and specific surface area than their brushite precursors. Results from *in vivo* experiments revealed that the higher levels of total porosity and macroporosity of the autoclaved monetite grafts appeared to have resulted in greater new bone formation than the higher specific surface area of the dry heat monetite grafts. Both type of monetite bioceramics resorbed faster than brushite grafts and more

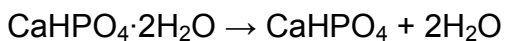
bone formation was noted. The implanted brushite grafts underwent phase conversion to form insoluble hydroxyapatite limiting bioresorption. However, this was not observed in monetite grafts and they continued to resorb *in vivo*. In summary, autoclaving and dry heating pre-set brushite cement grafts resulted in biomaterials which were completely resorbable with improved properties for bone repair and regeneration procedures.

6.3 Introduction

Bone substitutes are frequently used in dental and orthopaedic surgery (75, 146, 250). Currently, autologous bone grafting is considered to be the best option due to having high biological acceptability after implantation (7, 9, 364). However, disadvantages such as limited availability, donor site morbidity and increased procedural cost (9, 10, 365, 366) give rise to reservations over its use and have lead towards research to find more suitable substitutes.

Calcium phosphate biomaterials have similar composition to bone and are of interest as bone substitutes (16). The mineral named brushite (dicalcium phosphate dihydrate, DCPD), has the ability to support new bone generation but with varying amounts of woven bone and fibrovascular tissue (12, 177, 220, 225). Resorption of bone graft substitutes allows simultaneous replacement of the grafts material with newly forming bone. Ideally, the rate of resorption should be the same as the rate of new bone formation, in order to obtain stabilized repair and eventually a fully healed bone defect with no remnants of the graft material (236). The rate of dissolution and resorption is thought to be dependent on the chemical composition and physical characteristics of the calcium phosphate bioceramics (367). Although initially after implantation brushite bioceramics do resorb, they tend to react with the surrounding environment and convert to insoluble HA (16, 202), whereupon resorption slows down. This phase conversion affects the rate of resorption negatively and so ultimately limits their clinical usefulness (18, 222, 368).

Dicalcium phosphate anhydrous can be prepared by either modifying the precipitation conditions of brushite to promote setting as monetite (202, 369-371), or by dehydration of pre-set brushite bioceramics (14, 16). The following equation represents conversion of DCPD to DCPA:



Dehydration of brushite can be carried out under humid or dry conditions which alter the physical properties of produced monetite bioceramics. Dry heating is known to cause shrinkage of the material (16). However, by maintaining humidity, pressure and adequate temperature (by autoclaving which is also used for sterilisation) this can be prevented (208). Monetite prepared by autoclaving has inferior mechanical properties in comparison to their brushite precursor bioceramics (18) but have shown the ability to regenerate bone in animal and human bone defects and to also stimulate vertical bone augmentation (14, 15, 17, 18, 231). These monetite bioceramics have also demonstrated higher volumes of bone regeneration achieved than with hydroxyapatite based graft substitutes (14, 158). Monetite bioceramics prepared by autoclaving resorb *in vivo* at a quicker rate than brushite (18, 207) and do not convert to HA (14, 158).

Within the limit of our knowledge, there has been no direct comparison in literature between autoclaved and dry heat converted monetite grafts with regards to resorption and the ability to regenerate new bone *in vivo*. This study was designed to compare resorption and bone response *in vivo* between brushite grafts and the two types of monetite grafts prepared by autoclaving and dry heat conversion. The study was tested for the hypotheses, that both monetite bioceramics would resorb to a greater extent forming more bone *in vivo* compared to brushite and that there would be a discernable difference between the two monetites.

6.4 Results

6.4.1 Physicochemical analyses of grafts prepared

The density was ~20% higher in autoclaved and dry heat monetite grafts than in brushite grafts (**Table 6.9.1**). SSA was ~3 and ~35 times higher for the autoclaved and dry heat monetite grafts respectively in comparison with brushite grafts (**Table 6.9.1**). Total porosity was ~52% and ~27% higher in autoclaved and dry heat monetite grafts respectively than in the brushite ones. The μ -CT measurements revealed that the brushite and monetite graft types were mostly microporous (brushite ~31.5%, autoclaved monetite ~46.5% and dry heat monetite ~39% of the total graft volume) having limited macroporosity (brushite ~3.6%, autoclaved monetite ~9% and dry heat monetite ~6.5% of the total graft volume) (**Table 6.9.1**). Brushite samples had a compressive strength ~100% and ~11% greater than the autoclaved and dry heat monetite grafts respectively (**Table 6.9.1**).

Elemental analysis of the bioceramics revealed that the brushite and both types of monetite grafts had a similar calcium-to-phosphate ratio, slightly higher than 1.0 (**Table 6.9.1**). This confirmed that the graft composition was mainly of dicalcium phosphate. The small amount of excess calcium indicated that there were traces of unreacted β -TCP in the final composition of the graft cements because the initial composition of the cement reactants was not stoichiometric, and included excess β -TCP.

SEM micrographs of the brushite and autoclaved monetite bioceramics revealed that they were both composed of small crystals (**Figures 6.9.1 a and b**). However, the dry heat monetite crystals were thinner and smaller in size (**Figure 6.9.1 c**) in comparison with brushite and autoclaved monetite crystals. X-ray diffraction patterns obtained before implantation confirmed that the prepared bioceramics were brushite and monetite respectively (**Figures 6.9.5 a, c and d**).

6.4.2 In vivo study

After implantation of grafts in the femoral condylar region of rabbits, digital radiographs were obtained to confirm the positioning of bioceramics in bone (**Figure 6.10.1**). Post sacrifice, femoral bones were retrieved and digital radiographs obtained to visually compare differences between the grafts. The brushite grafts along with autoclaved and dry heat monetite grafts could be seen on radiographs after 4 weeks of implantation (**Figure 6.9.2**). After 12 weeks, brushite grafts could still be observed but the autoclaved and dry heat monetite grafts appeared to have resorbed completely (**Figure 6.9.2**).

After 4 weeks of implantation in rabbits, brushite and both monetite grafts appeared to be integrated in the femur bone and bone formation was observed on the outer surface (**Figures 6.9.3 a, c and e & Figures 6.9.4 a, c and e**). However, brushite grafts showed limited signs of resorption as compared to monetite grafts. A ring of material differing in appearance was seen enveloping the original brushite graft material (**Figure 6.9.4 a**). The monetite grafts, especially autoclaved monetite showed greater resorption and more bone growing inwards from the surface of the grafts (**Figures 6.9.3 c and e**). BSE-SEM images also confirmed that bone infiltration was more pronounced in the monetite grafts than in the brushite ones (**Figures 6.9.4 a, c and e & Figures 6.9.6**). After 12 weeks of implantation, brushite grafts appeared to have resorbed, but the core was surrounded by a material that appeared darker in color upon histological examination (**Figure 6.9.4 b**). This ring surrounding the core could also be observed in the BSE-SEM micrographs (**Figure 6.9.4 b & Figure 6.9.6 a**). For the autoclaved and dry heat monetite grafts, the histological sections and the BSE-SEM images did not show any graft material remaining within the cancellous bone (**Figures 6.9.3 d and f & Figures 6.9.4 d and f**).

Histomorphometric analysis revealed consistent differences between the three types of implanted grafts (**Table 6.9.2**). After 4 weeks of implantation, autoclaved monetite grafts and dry heat monetite grafts showed greater new bone formation

when compared with brushite grafts ($p < 0.05$). The autoclaved monetite grafts demonstrated slightly more new bone formation in comparison to the dry heat counterparts but the difference was not significant ($p > 0.05$). Autoclaved and dry heat monetite grafts also showed greater *in vivo* resorption when compared with brushite grafts after 4 weeks ($p < 0.05$). The autoclaved monetite grafts showed slightly greater resorption than the dry heat monetite grafts after 4 weeks but the results were insignificant ($p > 0.05$). Kruskal-Wallis one-way analysis revealed that the differences between the implanted brushite and the two monetite grafts for resorption and bone formation were statistically significant ($p < 0.05$).

After 12 weeks of implantation, histomorphometry revealed that the monetite grafts showed a tendency towards being more infiltrated with bone ($p < 0.05$) and resorbed more ($p < 0.05$) than the brushite grafts. When comparing the two monetite grafts it was noted that the autoclaved monetite grafts had more new bone formation than its dry heat counterparts, reaching the level of statistical significance ($p < 0.05$). Although autoclaved monetite grafts resorbed slightly more than the dry heat monetites, the difference was not significant ($p > 0.05$). The difference in resorption and bone formation between the three groups of bioceramics was significant ($p < 0.05$). Both autoclaved and dry heat monetite showed similar amounts of resorption with ~6% of the both graft materials remaining after 12 weeks. On average, both monetite graft types appeared to have resorbed 3.3 times more than brushite grafts, whereas bone in-growth within autoclaved monetite was 5 times more and within dry heat monetite 4 times more than in brushite grafts.

X-ray powder diffraction and phase analysis of the brushite grafts embedded in bone after 4 weeks of implantation revealed peaks of HA along with the peaks typical for brushite (**Figure 6.9.5 a**). The analysis from the 12 weeks brushite samples showed phase conversion to a mixture of HA and brushite (**Figure 6.9.5 a**). When point analysis was performed on the darkened ring around brushite, the pattern showed peaks for HA (**Figures 6.9.6 a and b**). The XRD patterns

obtained from the remaining autoclaved and dry heat monetite grafts after 4 weeks in vivo matched with those of monetite before implantation and did not show any phase conversion (**Figure 6.9.5 b & Figure 6.9.5 c**). The XRD analysis after 12 weeks of the area of bone where monetite grafts were originally implanted revealed a pattern matching with that of rabbit cancellous bone showing broad peaks of amorphous HA with absence of monetite peaks (**Figure 6.9.5 b & Figure 6.9.5 c**).

6.5 Discussion

6.5.1 Physicochemical characteristics of the bioceramics

The dehydration of brushite via autoclaving and dry heating resulted in producing monetite bioceramics with similar calcium phosphate content but different physical properties. The conversion of brushite into monetite induced changes in four physical characteristics: density, porosity, surface area and mechanical properties. The autoclaving process provides humidity, heat and pressure to the brushite grafts that results in increase in skeletal density without causing overall shrinkage (208). The dry heating process under vacuum removed water quickly from brushite to also produce monetite with increased density. The density of brushite grafts was higher than pure brushite (2.27 g/cm^3), which indicates the presence of small amounts of denser β -TCP (3.14 g/cm^3) in the grafts (14, 15, 202). The autoclaved and dry heat monetite bioceramics had the similar density to the pure form (2.92 g/cm^3). The slightly less density noted could be due to the presence of unreacted trace amounts of brushite (14, 15, 18, 202). The autoclaving and dry heating of brushite resulted in a 52% and 27% increase in porosity in the monetite bioceramics respectively. The increase in the surface area for autoclaved and dry heat monetite was almost 3 and 35 times more respectively than that of brushite grafts. μ -CT analysis revealed that the autoclaved and dry heat monetite grafts had macroporosity almost 3 and 2 times more than the brushite grafts respectively. Autoclaved monetite grafts also had more open macroporosity and microporosity than the dry heat monetite and brushite grafts. Dehydration of brushite using wet heat has already been shown to increase surface area significantly (18). However, it was interesting to note the greatly increased surface area produced by the dry heating process. We hypothesize that dry heating under vacuum removes water quickly resulting in the aggregation of smaller sized monetite crystals. The compressive strength of the monetite grafts produced by autoclaving was reduced to half of that observed for their brushite precursors. It is already known that increasing cement porosity results in reduction of mechanical properties (16). Since our prepared autoclaved

monetite grafts had both higher total porosity and microporosity, this explains the dramatic reduction in the compressive strength observed in comparison to brushite grafts. On the other hand, dry heat produced monetite grafts had compressive strength comparable with that of brushite grafts. The tightly aggregated monetite crystals were probably responsible for the higher mechanical strength noted. Also, the dry heating process resulted in less increase in total porosity as compared to the autoclaving process leading to higher compressive strength. Therefore, the incorporation of macropores within cement structure has to occur ideally without increasing total porosity to maintain sufficient mechanical strength. This can be achieved by the use of porogens like manitol (372) or by using gelatin powder template, which produces closely packed macroporous cement structures (373). The autoclaving process provides increased surface area and porosity (202, 208), but the limitation is the decrease in the mechanical properties. The results from this study have shown that by dry heating under vacuum we can produce monetite grafts that possess greatly increased surface area, and higher porosity than brushite without severely compromising the original mechanical properties.

6.5.2 In vivo

Brushite and monetite bioceramics have been compared and assessed *in vivo* following subcutaneous (207) and tibial bone (18) implantation. 3D printed brushite and monetite cement blocks have also been evaluated for vertical bone formation in vertebrae (236). However, this is the first *in vivo* study that prepared monetite bioceramics by two different heating methods and provided a direct comparison between them and also with brushite bioceramics.

Results from several other studies (18, 207) have shown monetite bioceramics to resorb at a quicker rate and to a greater extent than their original brushite precursors. However, this is the first time that complete resorption of calcium phosphate graft materials has been reported. The resorption mechanism of brushite and monetite bioceramics is similar with cellular activity being mainly

responsible and, to a lesser extent, by passive dissolution (224). After implantation, during the first weeks brushite resorbs by simple dissolution, disintegration/fragmentation and cellular activity (177, 222, 223, 228). *In vivo* and *in vitro* observations have shown that early resorption of brushite cement is regulated by macrophages (223, 225, 226) and later predominately via osteoclasts (226). The Initial resorption of calcium phosphate bioceramics is affected by the physicochemical properties and the rate of fluid exchange of the surrounding medium (228).

It was observed in this study that after implantation, brushite grafts initially resorbed but then started to convert to less soluble apatite limiting graft resorption. It has also been noted previously that due to this phase transformation, resorption of the remaining cement becomes very slow (205). Previously it has been observed that brushite converts to apatite completely after 24 weeks of implantation in sheep and there is almost no dissolution of the cement (353). Our study confirmed that monetite bioceramics prepared by dry heating brushite under vacuum do not convert to HA *in vivo*. Also this non-conversion following implantation for autoclaved monetite cements was noted in our study and has also previously been observed (231). Monetite cements are known to have lower water solubility than brushite cements (16). This lower solubility of monetite results in release of ions at a slower rate providing adequate time for the removal of ions from the *in vivo* environment before they can reprecipitate into insoluble apatite (14, 158).

The difference in bone response to the implanted bioceramics was revealed by histomorphometry. Previous research has shown that monetite resorbs more than brushite upon subcutaneous implantation (207). This was also confirmed by our study where monetite grafts showed greater resorption than brushite grafts, and this difference was statistically significant. Graft resorption does not always occur parallel to new bone formation, with the implanted material at times being surrounded by fibrovascular tissue (151, 225). This was not observed in our

study as grafts appeared to be surrounded by new bone without any soft tissue. Brushite grafts demonstrated bulk volume reduction with new bone forming at the graft perimeter mostly. In contrast, monetite grafts, especially those prepared by autoclaving demonstrated not only bulk resorption but also resorption patterns that weaved inwards from the graft surface. This resulted in bone growing not only around but also inwards within the monetite bioceramic grafts.

The rate at which new bone formation occurs is dependent upon cement composition, implantation site and physical characteristics of the biomaterials (9, 220, 225, 233). The compositional differences between the grafts in our study were minimal as brushite and monetite grafts are chemically very similar having same Ca/P ratio (16). Differences in results due to implantation site are expected, since vascularity, and thus the appearance of cellular components of resorption process varies with the bone type (9). Areas with higher vascularity, such as cancellous bone of the femoral condyle and metaphysis in the proximal humerus are known to enhance resorption when used as sites for cement implantation (177, 225).

The differences in biological behaviour observed in this study between the two types of monetite grafts and the brushite grafts were heavily dependent on the physical characteristics of the bioceramics. Porosity present in bioceramics is crucial towards resorption and rate of bone growth and integration *in vivo* as macroporosity affects the final volume of generated bone (148). Both autoclaved and dry heat monetite grafts had higher levels of total porosity and macroporosity than the brushite grafts. It has been reported that macroporosity of bioceramics plays a major role in enhancing *in vivo* resorption by invasion of resorbing cells (360). Since brushite and monetite implants are mainly resorbed by cellular activity (224), it seems probable that the higher porosity present in monetite bioceramics resulted in more resorption leading to enhanced new bone growth and higher degree of bone infiltration compared to brushite. Previous studies have also shown that the supplementation of microenvironment with calcium and

phosphate ions due to increased resorption seems to encourage bone regeneration and mineralization (374, 375). The higher levels of porosity and the increased ability of monetite to stimulate bone cells have also been reported recently in *in vitro* experiments (18).

In summary, both the autoclaved and dry heat converted monetite grafts demonstrated improved bioresorption and bone regeneration than their brushite precursors. Also, autoclaved monetite grafts demonstrated greater bone formation than the dry heat monetite grafts. The higher total porosity and macroporosity levels of autoclaved monetite grafts seemed to favour bone formation more than the higher surface area of the dry heat monetite grafts. These differences observed *in vivo* can be attributed to the changes in the material physical characteristics caused by varying the monetite processing conditions.

6.6 Conclusions

Autoclaving and dry heating pre-set brushite bioceramics resulted in their transformation to monetite-based biomaterials with higher porosity, density and specific surface area than their original brushite precursors. It was observed that the dry heat monetite grafts demonstrated much higher surface area and had mechanical properties that were comparable with brushite grafts. Whereas, the autoclaved monetite grafts had significantly reduced mechanical properties. These bioceramics were implanted in a rabbit model, with the aim of comparing materials with different physicochemical properties with regards to resorption and bone response. Upon *in vivo* implantation for 12 weeks, both types of monetite bioceramics demonstrated complete resorption and more bone formation than brushite. The brushite grafts underwent phase conversion to form insoluble HA. No phase conversion was observed for any of the monetite grafts. The autoclaved monetites had significantly greater amount of new bone formation than the dry heat monetite grafts. The increase in surface area observed for the

dry heat grafts did not result in an increase in bone formation in comparison to the autoclave prepared monetite grafts. Our study confirmed that the differences in the physical and chemical characteristics of monetite and brushite grafts had a profound effect on their *in vivo* behaviour and that monetite bioceramics perform much better than their brushite precursors.

6.7 Acknowledgements

The authors acknowledge financial support from RSBO, Quebec Government MDEIE Catalonia-Quebec grant.

6.8 Experimental

6.8.1 Method and materials

6.8.1.1 Synthesis

Brushite cement grafts were prepared with a mixture of β -TCP (Merck) and commercially available monocalcium phosphate hydrate (MCPM) (ABCR, GmbH & Co.KG) using a ratio of 1.2 to 1 respectively. The cements were produced at P/L mixing ratio of 3 g/ml. The powders were hand ground with a pestle and mortar and cement pastes prepared by mixing the powder with appropriate amount of distilled water on a glass slab for 20 s. Once all of the powder was combined with the liquid, the cement paste was kneaded for a further 30 s. The manipulated cement slurry was cast into a polytetrafluoroethylene (PTFE) split mould forming hardened cement cylinders \varnothing (~4 x 3 mm). The cylinders were allowed to set for 24 h at $37^{\circ}\text{C} \pm 1^{\circ}\text{C}$ in a vacuum desiccator to form brushite. At the end of the incubation period, the samples were removed from the mould and weighed until constant mass was reached. Three different batches of fifteen cylinders each were produced to obtain a total of forty five cylinders. Even though the sample homogeneity was very high (either within a batch or between batches), the sample assignment was randomized.

Monetite cement grafts ($n=30$ in total) were synthesized by conversion of the preset brushite cement cylinders utilizing two different methods: dry heat and wet heat conversion. For dry heat conversion, brushite cylinders ($n=15$) were heated at 250°C for 30 minutes under vacuum (80 mTorr). Wet heat transformation was performed with brushite cylinders ($n=15$) being autoclaved at sterilizing conditions (121°C , 100% humidity and 15 psi, for 20 min).

6.8.1.2 Characterisation of grafts prepared

The phase purity of the prepared brushite and monetite grafts was confirmed using X-ray diffraction (XRD). XRD data was collected (Bruker Discover D8 diffractometer) with Ni filtered $\text{CuK}\alpha$ radiation ($\lambda = 1.54\text{\AA}$) with a two dimensional

VANTEC area detector at 40 kV and 40 mA. A step size of 0.02° was used to measure from 10 to 50° 2θ over 3 frames with a count time of 180 s per frame. The phase composition was compared and confirmed with the International Centre for Diffraction Data reference patterns for brushite (PDF Ref. 09-0077) and monetite (PDF Ref. 09-0080), JCPDS 2010 database. The true density of the powdered grafts was determined using a helium pycnometer (Accupyc 1330, Micromeritics). The volume of each sample was measured 10 times following 10 purges of the measurement chamber with helium. The relative porosity (bulk porosity) of the cements was calculated from apparent and true density measurements. Macroporosity of the prepared grafts was calculated by using μ -CT (SkyScan 1172; SkyScan; Kontich, Belgium) set at a resolution of $6.0\ \mu\text{m}$ and $0.5\ \text{mm}$ Al filter. The specific surface area (SSA) of cements was determined by using the Brunauer–Emmett–Teller (BET) method with helium adsorption–desorption (Tristar3000, Micromeritics). The compressive strength of all prepared brushite and monetite grafts was measured. Before testing, geometrical measurements of the graft cylinders were made in triplicate and the samples weighed. Samples were mounted on the testing machine (5544, Instron) so that the long axes of the cement cylinders were perpendicular to the lower anvil. A compressive force was then applied to the upper surface of the cylinders at a constant crosshead displacement rate of $1\ \text{mm/min}$ until failure occurred. The applied load was measured using a $100\ \text{N}$ load cell (5544, Instron). Mean compressive strength was determined from the average of 10 measurements. Electron microscopy was used to examine the microstructure of grafts prepared with scanning electron microscopy (Hitachi S-4700 FE-SEM; Tokyo, Japan) operating at an accelerating voltage of $10\ \text{kV}$ using a secondary electron (SE) detector. Elemental composition (Ca/P ratio) of the bioceramics was assessed with energy dispersive X-ray (EDX) analysis using Oxford detector and INCA software (Oxford Instruments, Abingdon, UK). All the physical-chemical characterization analyses of the grafts were performed in triplicate.

6.8.1.3 In vivo study

An animal study was performed in order to evaluate *in vivo* differences between the three prepared bioceramic grafts upon orthotopic implantation. After obtaining approval from McGill University Health Care Center Ethical Committee, the study was performed on eight male New Zealand rabbits (4-6 months) weighing 3-4 kg each. The animals were anaesthetized, by using a lateral approach to the knee, a two inch incision was made below and above the knee joint through the skin to expose the lateral condyle of the femur. Two drill holes, 4 x 3.1 mm Ø each, were created below the femoral condylar region medially and laterally to accommodate the cylindrical calcium phosphate grafts. The grafts were next gently tapped into place and the surgical site was sutured. The procedure was performed on both legs with each femur receiving two grafts and the animals were left to heal. The placement of brushite and monetite grafts was randomized. Post implantation digital radiographs were obtained using Fidex imaging system (Animage, LLC, Pleasanton, CA, U.S.A) with a voltage of 110 kv and a current of 0.080 µa to confirm the graft location. The animals were sacrificed after 4 and 12 weeks and the femurs were dissected and retrieved for histological analysis.

Once the implant sites were retrieved, radiographs were obtained using Kubtec® XPERT80 digital cabinet X-ray system (KUB Technologies Inc. Milford, CT) employing a voltage of 90 kV and a tube current of 1.0 µa. The femurs were then fixed in 4% formaldehyde for 1 day before being dehydrated in ascending concentrations of ethanol and infiltrated with polymethyl methacrylate histological resin (Technovit® 9100, Heraeus Kulzer, Wehrheim, Germany). After the resin was polymerized, samples were sectioned into histological slides with a diamond saw (SP1600, Leica Microsystems GmbH, Wetzlar, Germany) and dyed with basic fuchsin and methylene blue for histological analysis with optical microscopy. A series of three slides (~20 µm each), cutting through the centre of the cylindrical implants, were prepared for each sample. Histomorphometry analysis of the slides was performed using a Zeiss microscope Axio Imager.M2 (Zeiss® Gottingen, Germany) with a digital AxioCam IC camera (Zeiss®

Göttingen, Germany) and the image software GIMP2 (v2.10). All histomorphometric measurements were calculated as percentage values \pm the standard deviation.

XRD data from sections with grafts embedded within the bones was collected (Bruker Discover D8 diffractometer) with Ni filtered CuK α radiation ($\lambda = 1.54\text{\AA}$) with a two dimensional VANTEC area detector at 40 kV and 40 mA. A step size of 0.02° was used to measure from 10 to 50° 2θ over 3 frames with a count time of 300 s per frame. The resin embedded cut sections were sputter coated with gold–palladium alloy prior to electron beam analysis at high vacuum. Back-scattered electron micrographs (BSE-SEM) were taken using scanning electron microscopy (Hitachi S-4700 FE-SEM; Tokyo, Japan) operating at an accelerating voltage of 30 kV using a back scatter electron (BSE) detector.

6.8.1.4 Statistical analysis

Statistical analysis was performed using IBM[®] SPSS[®] (v. 19, IBM Corp.; New York; USA) statistical software. Mann-Whitney test was used to evaluate head-to-head differences between the implanted bioceramics. Kruskal-Wallis one-way analysis was used to evaluate any differences among the three implanted grafts materials. Statistical significance was set at a value of $p < 0.05$.

6.9 Tables & Figures

Table 6.9.1: Characterization of prepared brushite and monetite bioceramics.

Bioceramic graft type	Physico-chemical characteristics							Compressive strength (MPa)	
	Density (g/cm ³)	SSA (m ² /g)	Ca/P	Total relative porosity (%) ^a	Macroporosity (%) ^b		Microporosity (%) ^b		
Brushite	2.32 ± 0.04	0.58 ± 0.03	1.12 ± 0.14	35.24 ± 2.04	2.52 ± 0.97	1.17 ± 0.31	3.68 ± 1.03	31.56 ± 1.51	15.8 ± 1.5
Monetite AC	2.90 ± 0.02	1.54 ± 0.05	1.17 ± 0.11	55.62 ± 1.28	5.10 ± 1.25	4.11 ± 0.21	9.20 ± 1.20	46.42 ± 1.74	7.9 ± 1.7
Monetite DH	2.88 ± 0.03	19.07 ± 0.04	1.15 ± 0.13	46.08 ± 3.10	3.19 ± 0.15	3.70 ± 0.33	6.93 ± 0.27	39.15 ± 1.30	14.1 ± 1.3

Values are presented as mean ± standard deviation (*n*=5).

AC-autoclaved & DH- dry heat.

Total porosity, macroporosity and microporosity calculated as percentages from total volume of graft material.

^a Calculated from density measurements.

^b Calculated from μ -CT measurements and all pores larger than 11 μ m in diameter were considered macropores.

Table 6.9.2: Histomorphometric analysis of the implanted bioceramic grafts.

Bioceramic graft type	Observation period (weeks)	New bone within graft area (%)	Free space within graft area (%)	Remaining graft material (%)
Brushite	4	7.4 ± 4.2	15.0 ± 4.2	77.0 ± 6.9
	12	11.6 ± 5.5	16.8 ± 7.8	71.5 ± 3.9
Monetite AC	4	27.6 ± 6.4	21.5 ± 4.6	50.4 ± 6.4
	12	58.4 ± 7.5	35.7 ± 3.0	5.9 ± 4.0
Monetite DH	4	21.0 ± 4.7	16.9 ± 4.2	62.3 ± 7.3
	12	47.6 ± 6.6	46.0 ± 9.5	6.4 ± 5.3

Values are presented as mean percentages ± standard deviation ($n=5$).
AC-autoclaved & DH- dry heat.

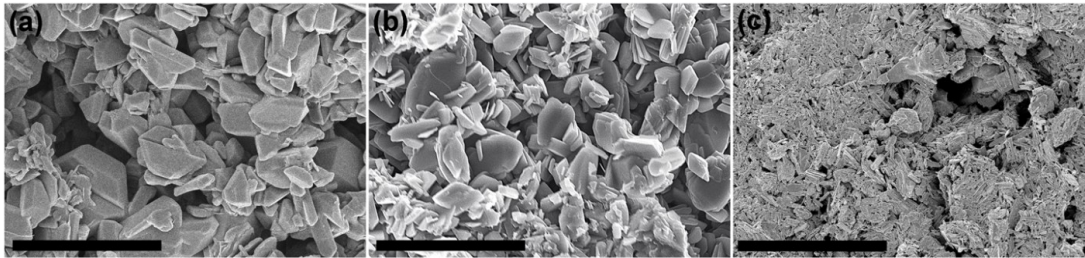


Figure 6.9.1: SEM images of: (a) brushite, (b) autoclaved monetite, and (c) dry heat monetite before implantation. (Scale bars in the images represent 1 μ m).

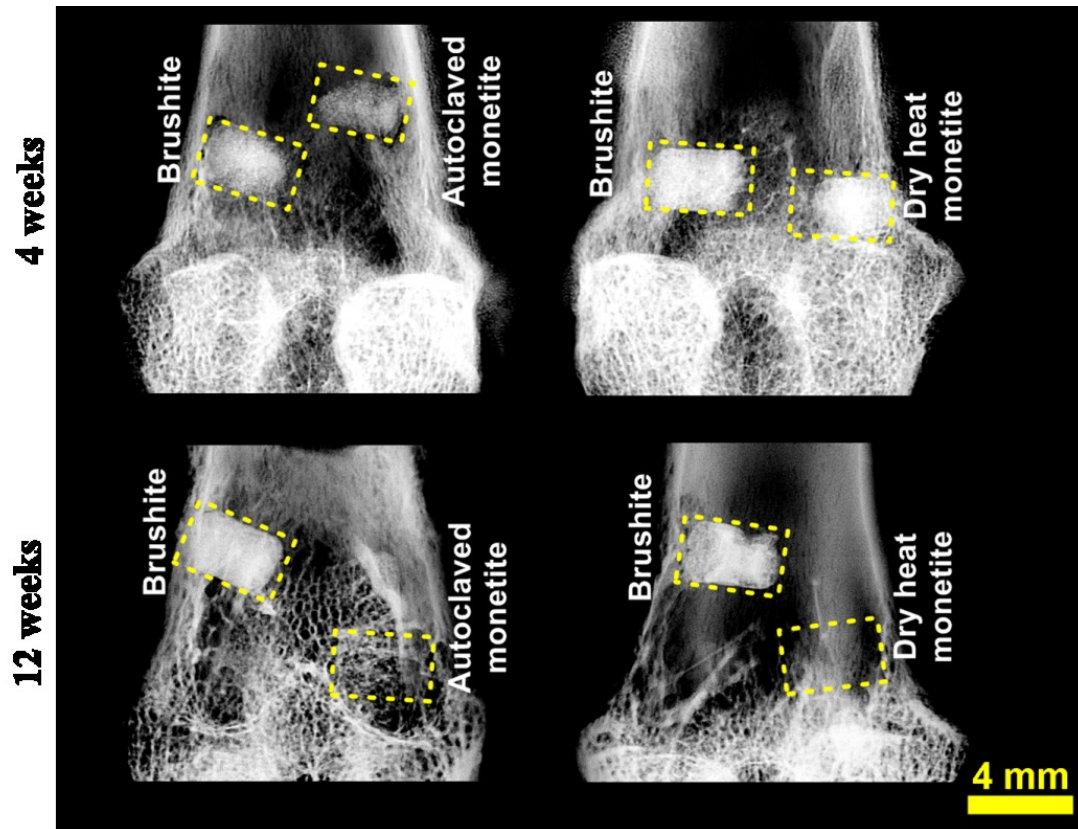


Figure 6.9.2: Digital radiographic assessment of the retrieved femurs with bioceramic grafts after 4 and 12 weeks of implantation (dotted areas represent original graft dimensions of 3 x 4 mm).

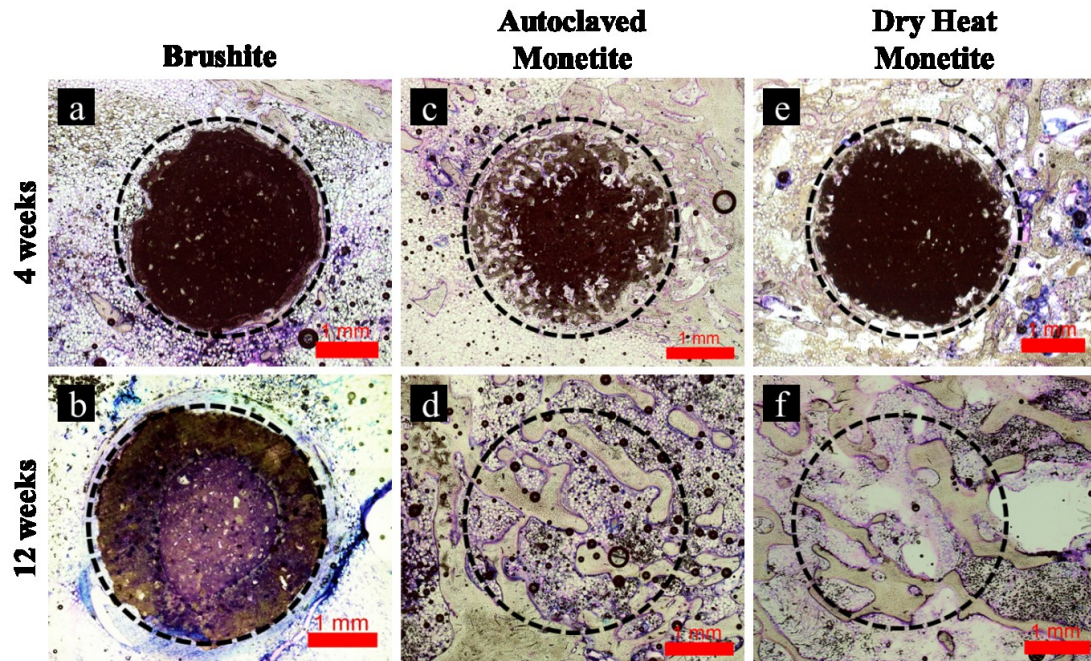


Figure 6.9.3: Histological sections (H&E stain) of brushite (a & b), autoclaved monetite (c & d), and dry heat monetite (e & f) after 4 and 12 weeks of implantation (dotted areas represents original graft diameter of 3 mm).

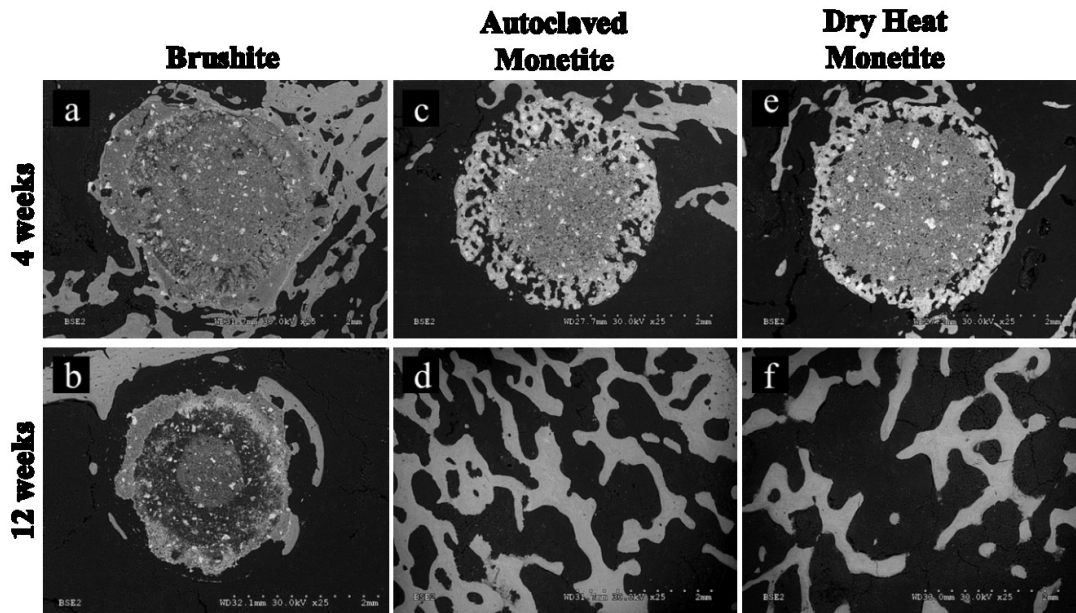


Figure 6.9.4: BSE-SEM images of brushite (a & b), autoclaved monetite (c & d), and dry heat monetite (e & f) after 4 and 12 weeks of implantation.

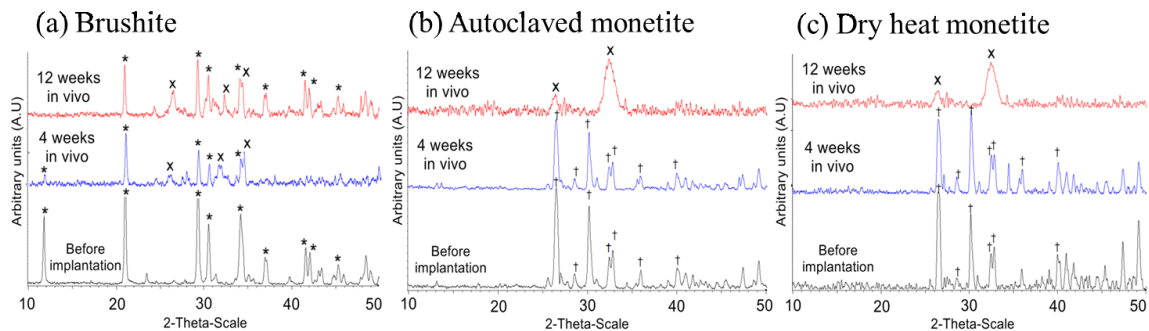


Figure 6.9.5: X-ray diffraction patterns obtained from core of: (a) brushite grafts before and after 4 and 12 weeks *in vivo*, (b) autoclaved monetite grafts before and after 4 and 12 weeks *in vivo*, and (c) dry heat grafts before and after 4 and 12 weeks *in vivo*. (*) represents brushite, (X) represents HA, and (†) represents monetite peaks.

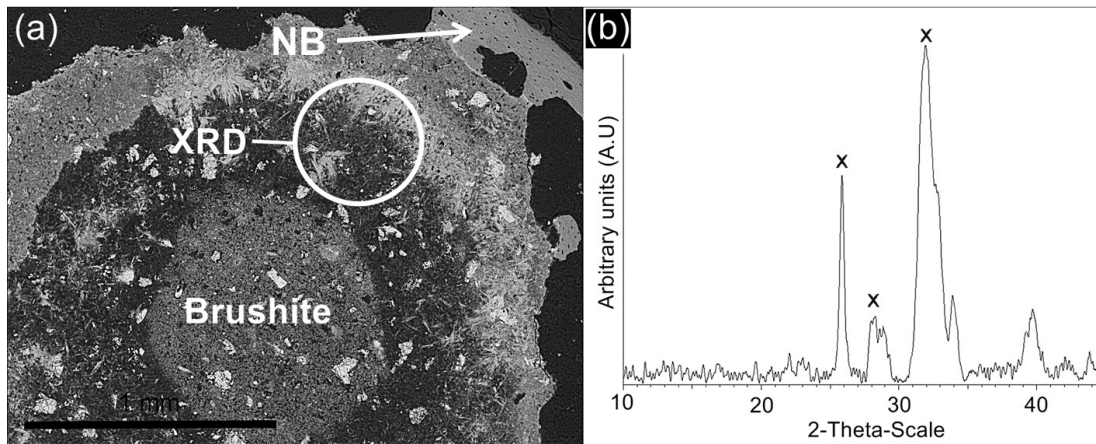


Figure 6.9.6: (a) BSE-SEM image showing brushite cement core surrounded by a dark zone of material and new bone (NB) at the graft perimeter after 12 weeks of implantation (scale bar represents 1 mm).

(b) The XRD point analysis of the darkened zone revealed phase conversion of brushite to hydroxyapatite (X represents peaks of HA).

6.10 Supplementary figures

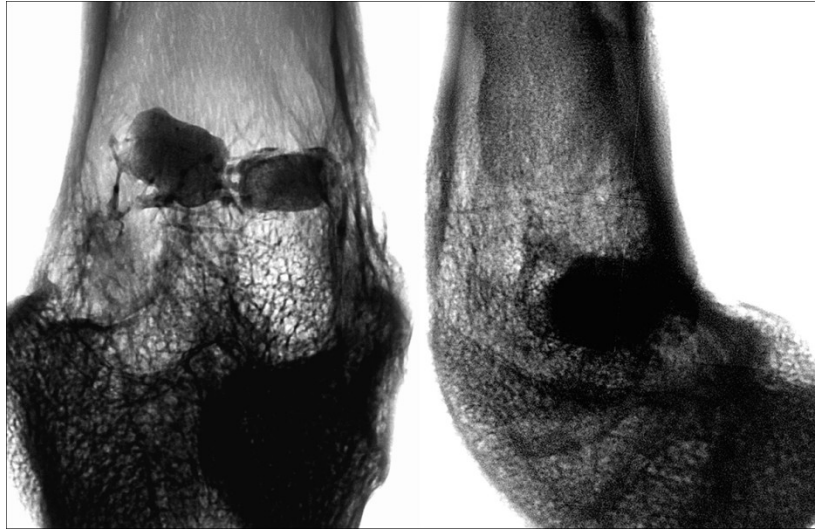


Figure 6.10.1: Post implantation radiographs (inverted) to confirm position of the bioceramics in bone.

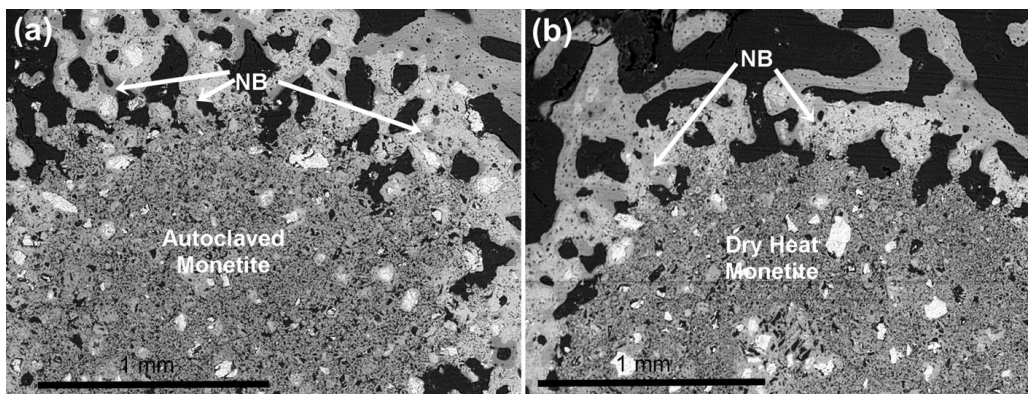


Figure 6.10.2: BSE-SEM images of (a) autoclaved monetite and (b) dry heat monetite after 4 weeks of implantation showing the resorbing cement grafts surrounded by new formed bone (NB).

Chapter 7: Vertical bone augmentation: A comparison between monetite onlay grafts prepared by wet and dry heat conversion of brushite.

7.1 Preface

It was established in the previous chapter that monetite grafts prepared by wet and dry heating of pre-set brushite cements had differing physical properties. The dry heat converted monetite grafts had higher specific surface area and compressive strength but lower levels of porosity (micro and macro-porosity) when compared with their autoclaved counterparts. These monetite cement grafts resorbed to a significantly greater extent and had much higher bone formation in comparison with their original brushite precursors. Also, unlike brushite, the monetite grafts showed no phase conversion to insoluble apatite hence improving their bioresorption. These promising results in an orthotopic implantation model encouraged us to assess monetite cement implants in an onlay grafting calvarial model in rabbits. Bone augmentation of deficient alveolar ridges is frequently required prior to dental implant placement. To assess the ability of monetite bioceramics to be used for vertical bone augmentation, monetite cement discs were prepared by wet and dry heat conversion of brushite and onlay grafted on rabbit calvaria for twelve weeks. This chapter provides a head to head comparison between the performances of two types of monetite grafts in terms of vertical bone height gained, bone volume generated within the augmented area and the total graft resorption achieved.

Vertical bone augmentation: A comparison between monetite onlay grafts prepared by wet and dry heat conversion of brushite

Zeeshan Sheikh¹, Yu Ling Zhang¹, Justin Drager², Mohamed-Nur Abdallah¹, Faleh Tamimi¹, Jake Barralet^{1,2}

¹Faculty of Dentistry, McGill University, Montreal, Quebec, Canada

²Division of Orthopaedics, Department of Surgery, Faculty of Medicine, McGill University, Montreal, Quebec, Canada.

7.2 Abstract

Vertical bone augmentation procedures are frequently carried out to allow successful placement of dental implants in otherwise atrophic ridges. Onlay autografting is one of the most popular and predictable techniques to achieve this, however, there are several complications associated with it and synthetic alternatives are being researched upon. Monetite is a bioresorbable dicalcium phosphate with osteoconductive and osteoinductive potential that has been previously investigated for onlay bone grafting. In this study we produced monetite disc grafts by wet (autoclaving) and dry heating (under vacuum) methods which altered their physical properties such as porosity, surface area and mechanical strength. Histological observations after 12 weeks of implantation on rabbit calvaria revealed higher bone volume (38%) in autoclaved monetite grafts in comparison to the dry heat monetite grafts (26%). The vertical bone height gained was similar for both the autoclaved and dry heat monetite grafts (up to 3.2 mm). However, it was observed that bone height augmented was greater in lateral than the medial areas of both types of monetite grafts. It was also noted that the higher micro and macro-porosity of autoclaved monetite grafts increased the bioresorbability, whereas, the dry heat monetite grafts

having lower porosity but higher surface area resorbed significantly to a lesser extent. This study provides information regarding two types of monetite onlay grafts prepared with different physical properties that could be utilised for clinical vertical bone augmentation applications.

7.3 Introduction

Dental implants are commonly used to replace lost teeth and maintain surrounding bone and other periodontal tissues in good health (376-378). Sufficient bone volume and ridge height is imperative for achieving long-term success of osteointegrated dental implants (302, 376). Trauma and/or pathology such as advanced periodontitis often results in reduction of bone height and quality (302). Partial or completely edentulous patients also present with vertical alveolar bone loss which makes dental implant placement and prosthetic rehabilitation extremely challenging due to anatomical restrictions and surgical difficulties (302, 378).

A variety of graft materials and surgical techniques have been investigated to enable implant placement in severely resorbed alveolar bone (379). Autografts, allografts, xenografts and alloplasts have been tested for vertical ridge augmentation with surgical techniques such as distraction osteogenesis (297, 298, 300, 301, 380-384), guided bone regeneration (GBR) (302-305, 385-387), and onlay block grafting (231, 306-311, 315, 384). It has been observed that although distraction osteogenesis produces greater bone height than GBR and onlay block grafting used alone, it has higher rate of complications associated with it (57, 312). GBR was first used in the early 1900s for the treatment of vertical defects in atrophic jaws (303). Although the results of GBR for vertical bone augmentation are promising, clinical success is limited due to the procedure being highly technique sensitive (302-305, 385-388) and often failing due to wound dehiscence (302, 304, 385, 389-391).

Onlay block grafting is also used to increase the vertical height of the mandible and maxilla and usually requires extraction of an autologous bone block from donor site (mandibular ramus or iliac crest) and its fixation with screws onto the recipient site (313, 392). Autologous onlay grafting appears to have acceptable bone augmentation results but complications are frequently noted at the donor site (309, 392, 393). Also, autologous onlay grafts are associated with rapid

resorption in sites that receive mechanical load and soft tissue tension (309, 394). Hence, research has been focused upon development and investigation of biomaterials that could successfully replace autologous onlay bone grafts (231, 394-396).

Calcium phosphates such as HA and β -TCP have limited capacity to remodel and resorb *in vivo* and therefore are unsuitable for onlay grafting procedures (16, 145, 150). Dicalcium phosphate cements, brushite and monetite, show osteoconductive, osteoinductive and *in vivo* resorption potential (14, 15, 18, 158, 236, 314). They can and have been used with success for vertical bone augmentation (17, 231, 315). However, brushite tends to reprecipitate as insoluble HA *in vivo* that slows resorption and limits replacement by new bone. Monetite has been shown not to convert to HA and demonstrates greater resorption than brushite (14, 18, 207, 236).

The purpose of this study was to develop monetite disc grafts by varying the heating conditions which results in different physical properties and to assess and compare their efficacy in vertical bone augmentation procedures on rabbit calvaria. To achieve this objective, monetite disc grafts prepared by wet and dry heat conversion of brushite were fixed on rabbit calvaria for 12 weeks and later assessed and compared for vertical height gained and bone volume occupied of the total initial graft volume.

7.4 Results

7.4.1 Physicochemical properties of the prepared disc grafts

The density was similar for both the autoclaved and dry heat monetite disc grafts (**Table 7.9.1**). The SSA was ~12 times higher and total porosity ~10% less in dry heat monetite grafts in comparison with autoclaved monetite grafts (**Table 7.9.1**). The μ -CT measurements revealed that both types of monetite grafts were mostly microporous (autoclaved monetite ~44% and dry heat monetite ~38% of the total graft volume). Macroporosity present in the autoclaved monetite grafts was ~12% and ~7% in the dry heat monetite grafts (**Table 7.9.1**). The compressive strength of the dry heat grafts was almost twice greater than that of the autoclaved monetite grafts (**Table 7.9.1**).

BSE-SEM micrographs of the grafts prepared revealed that the dry heat monetite crystals were thinner and much smaller in size (**Figure 7.9.4 B**) in comparison with autoclaved monetite crystals (**Figure 7.9.4 A**). XRD patterns obtained before implantation confirmed that the prepared disc grafts were composed of monetite (**Figures 7.9.4 C and D**). Elemental analysis of the bioceramics revealed that both type of monetite grafts had a similar calcium-to-phosphate ratio, slightly higher than 1.0 (**Table 7.9.1**). This confirmed that the graft composition was mainly of dicalcium phosphate anhydrous.

7.4.2 In vivo study

7.4.2.1 Surgical and clinical observations

No complications were noted during the surgical phase of onlay grafting (**Figures 7.9.1 A, B, C and D**). Healing progressed uneventfully for all surgical sites during the 12 weeks post implantation without any signs of rejection being observed. Animal CT was carried out upon implantation (**Figure 7.9.1 E**) and before sacrifice at 12 weeks (**Figure 7.9.1 F**). Surgical re-entry and animal CT constructed images revealed that the shape of the grafts had been preserved

when compared with at the time of implantation (**Figures 7.9.1 C, D, E and F**). The blocks appeared to be stable and fused to the calvarial bone.

Prior to sectioning and histological examination, the retrieved bone with grafts was scanned using μ -CT. The CT slices acquired for the autoclaved and dry heat monetite grafts after 12 weeks of implantation (**Figure 7.9.1 J** for autoclaved and **Figure 7.9.1 N** for dry heat monetite grafts) showed resorption areas in cement structure when compared with the CT slices from the same grafts before implantation (**Figures 7.9.1 I and M** for autoclaved and dry heat grafts respectively). 3D-modelling of the autoclaved and dry heat monetite grafts before (**Figures 7.9.1 K and O** respectively) and after 12 weeks of onlay grafting (**Figures 7.9.1 L and P** respectively) was performed. Autoclaved monetite grafts had a more porous appearance (**Figure 7.9.1 L**) than the dry heat monetite grafts (**Figure 7.9.1 P**).

7.4.2.2 Histological observations

Upon histological observation, the monetite grafts appeared to be infiltrated with newly formed bone and well integrated with the calvarial bone (**Figure 7.9.2**). There were no histological signs of necrosis, osteolysis or foreign body reaction (**Figures 7.9.2 C and D**). Soft tissue was seen covering both the autoclaved and dry heat monetite grafts and both grafts were partially resorbed and substituted with newly formed bone (**Figure 7.9.2, [+]**). Resorption appeared to be greater in the autoclaved monetite grafts (**Figure 7.9.2 A**) than in dry heat monetite grafts which showed incomplete areas of resorption (**Figure 7.9.3 A**). Resorption and subsequent infiltration with new bone was more pronounced on the lateral side of both type of monetite grafts as well as for areas in close contact with the calvarial bone surface. The medial ends of both types of grafts showed limited resorption.

At higher magnification, the remaining graft material in both type of monetite grafts (**Figures 7.9.2 C and D, [*]**) appeared to be surrounded by surrounded by new bone (**Figures 7.9.2 C and D, [+]**). However, the thickness of the bone

trabeculae growing within the autoclaved monetite grafts appeared to be greater than that in the dry heat monetite grafts.

7.4.2.3 SEM and XRD analysis

The BSE-SEM cross-section micrographs of the implanted monetite grafts revealed a dense porous structure where the material was unresorbed (**Figure 7.9.3**). After 12 weeks the remaining unresorbed autoclaved and dry heat monetite graft material (**Figures 7.9.3 C and D, [*]**) could be easily differentiated from the original calvarial surface and the newly formed bone within the original implant area. The remaining monetite within the newly forming bone (**Figures 7.9.3 C and D, [+]**) appeared lighter grey than the bone tissue (**Figures 7.9.3 C and D**). Isolated sites of new bone formation were observed away from the original bone surface in the autoclaved monetite grafts which indicated good osteoconductive properties (**Figure 7.9.3 C**).

Phase analysis via XRD of the unresorbed area of monetite grafts after 12 weeks matched with patterns before implantation and did not show any phase conversion (**Figure 7.9.4 C and D**). The XRD analysis after 12 weeks of the area of monetite grafts that were infiltrated with bone revealed a pattern with peaks of HA originating from bone and peaks of monetite from remaining graft material (**Figures 7.9.4 C and D**).

7.4.2.4 Histomorphometrical analysis

Histomorphometry revealed information regarding vertical height gained, amount of bone augmented, and graft resorption in the autoclaved and dry heat monetite onlay grafts.

7.4.2.4.1 Vertical bone height gained

The maximum bone height gained in the autoclaved monetite grafts on average was 3.2 ± 0.3 mm in comparison to 2.9 ± 0.4 mm for the dry heat monetite grafts

on the distal side of the implants (**Figure 7.9.5 A**). The height of bone decreased progressively from lateral area to the screw in the middle of both grafts (**Figure 7.9.5 A, C and D**). On the medial side adjacent to the screw, the average height of bone gained for autoclaved and dry heat monetite grafts was 2.1 ± 0.8 mm and 1.9 ± 0.4 mm respectively. The least amount of bone augmented was noted for the most medial area of the onlay grafts (0.7 ± 0.1 mm for autoclaved monetite and 0.4 ± 0.3 for dry heat monetite). Similar to the trend observed for the height gained in the lateral area, the area from the screw to the most medial part of the grafts showed a progressive decrease in bone height gained (**Figure 7.9.5 C and D**). Bone height gained in the distal areas was significantly greater ($p < 0.05$) than height gained in the medial areas of the grafts. Although autoclaved monetite grafts showed slightly greater bone height gained than their dry heat counterparts, the Mann-Whitney test showed that the differences between the autoclaved and dry heat monetite grafts with regards to vertical bone height gained were not statistically significant ($p > 0.05$).

7.4.2.4.2 Bone augmented within onlay grafts

Histomorphometric analysis revealed that the total percentage of new bone tissue measured within the autoclaved monetite grafts' augmented area ($38.2 \pm 7.8\%$) was more than that for the dry heat monetite grafts ($25.7 \pm 6.6\%$) ($p < 0.05$) (**Figure 7.9.5 B**). Histomorphometrical analysis of the specific smaller areas of the cross-sections was carried out by dividing the grafts into lower $\frac{1}{4}$, lower middle $\frac{1}{4}$, upper middle $\frac{1}{4}$ and upper $\frac{1}{4}$ areas. (**Figure 7.9.6 A & Figure 7.6 C**). The analysis revealed that bone growth was heterogeneous within both type of monetite grafts in the lower $\frac{1}{4}$ area. The lower middle $\frac{1}{4}$ area showed a reduction in bone volume from lateral to medial side. Also noted was that from 3 mm onwards to 9.5 mm of the graft, the dry heat monetite grafts had significantly less bone volume than the autoclaved monetite grafts in the lower middle $\frac{1}{4}$ area ($p < 0.05$). In the upper middle $\frac{1}{4}$ section of the grafts, the lateral area (0-1 mm and 2-3 mm) of autoclaved monetite grafts had significantly greater bone volume than the dry heat monetite grafts in the same area ($p < 0.05$). The bone volume

on the medial side of the grafts was greatly reduced in comparison to the lateral side. From 7.5 mm onwards on the medial side, bone volume was negligible for both types of monetite grafts. The upper ¼ of the grafts had ~12% and ~8% bone volume in the lateral most part of autoclaved and dry heat monetite grafts respectively. Apart from this the rest of the area either had negligible or nonexistent bone volume.

7.4.2.4.3 Onlay graft resorption

The percentage of remaining unresorbed monetite onlay grafts ranged between $43.5 \pm 5.9\%$ (in autoclaved grafts) and $61.8 \pm 6.2\%$ (in dry heat grafts) (**Figure 7.9.5 B**). The autoclaved monetite grafts showed significantly greater levels of resorption (~55%) than the dry heat prepared grafts (~38%) ($p < 0.05$).

7.5 Discussion

7.5.1 Physicochemical properties of the prepared disc grafts

The dehydration of brushite using autoclaving and dry heating process resulted in producing monetite bioceramics with similar calcium phosphate content but different physical properties. The conversion of brushite into monetite affected density, porosity, surface area and mechanical properties. The autoclaved and dry heat monetite bioceramics had the similar density to the pure form (2.92 g cm³). The slightly less density noted could be due to the presence of unreacted trace amounts of brushite (14, 15, 18, 202). The greater SSA noted for the dry heat monetite grafts could be attributed to the heating process carried out under vacuum. Dry heating under vacuum resulted in smaller sized monetite crystals and efficient removal of water causing monetite crystal aggregation. Autoclaved monetite grafts had more open macroporosity and microporosity than the dry heat monetite and brushite grafts. Dehydration of brushite using wet heat has already been shown to increase porosity (15, 16, 18). The compressive strength of the monetite grafts produced by autoclaving was reduced to half of that observed for their dry heated counterparts. Since the prepared autoclaved monetite grafts had both higher total porosity and microporosity, this explains the dramatic reduction in compressive strength observed. The tightly aggregated monetite crystals probably resulted in the higher mechanical strength noted. Also, the dry heating process resulted in less increase in total porosity, resulting in better mechanical properties as compared to the autoclaving process. Although the compressive strength of prepared monetite grafts was lower than that of cortical bone, it resembled that of cancellous bone (9.4-25.2 MPa) which is commonly used for maxillofacial bone augmentation procedures receiving masticatory loads (397).

7.5.2 Vertical bone height gained

Both calvaria and mandible originate from intra-membranous type of bone. The parietal bone of adult mammals has low bone marrow content and limited vascular supply and hence resembles an atrophic mandible. Some authors have

suggested that calvaria can be considered a reliable site for testing bone augmentation procedures (31, 398).

Histomorphometric analysis indicated that the bone height gained was slightly higher in the autoclaved monetite grafts than in the dry heat monetite grafts, but the difference was not significant. This suggests that ~10% total porosity and ~4% macroporosity that was greater in the autoclaved monetite onlay grafts than their dry heat counterparts did not produce a statistically significant difference. The maximum gain in vertical bone height was similar in both onlay monetite grafts (~3.2 & ~2.9 mm in autoclaved and dry heat monetite grafts respectively). The bone thickness of calvarium is 2 mm, this when added to the ~3.2 mm of vertical height gained with autoclaved monetite grafts results in a total height of ~5.2 mm. This amount of bone height is sufficient for the placement of short implants (5.0-6.0 mm) (399-402). However, it was observed that in the distal areas of the grafts the bone height gained was higher than in the medial areas. This was consistent for both the autoclaved and dry heat monetite onlay grafts. The anatomical contouring of the rabbit calvarial bone along with differences in blood supply between lateral and medial areas might be responsible for this observation. The posterior branch of the middle meningeal artery that emanates from the maxillary artery supplies the parietal bone. One perfused major branch of the meningeal artery runs laterally, curving towards the sagittal suture on each parietal bone with the arterial blood flow towards the linea media (403). This strongly indicates that the anatomical arrangement of blood vessels in calvaria results in lateral portions of grafts are better irrigated than the medial portions and hence can resorb to a greater extent providing opportunity for bone growth to reach higher levels vertically in comparison to the poorly perfused medial areas.

Prior to the screw fixation of the grafts, periosteum was removed from the midline laterally on either side of linea media. Majority of the outer surface of the craniofacial skeleton is supplied by tiny perforators by the overlying periosteum

(404). It is highly plausible that by the removal of periosteum, the medial areas of grafts were deprived of resorptive and bone forming cellular components to a greater extent in comparison to the lateral areas of grafts closer to the ends of the remaining periosteum distally. Previous studies have suggested that although periosteum covering the calvarial bone has a minor role in osteogenesis, they enhance bone formation in areas in close proximity to it (405, 406). To confirm this, further studies would be required where periosteum is stripped from distal ends towards the medial side or left in contact with the medial side of the grafts to observe if the findings are reversed in terms of vertical bone height gained.

7.5.3 Bone augmented within onlay grafts

Upon histological observation, both types of monetite onlay grafts appeared to be infiltrated by newly formed bone. This has also been observed previously in studies utilising monetite bioceramics for onlay grafting and bone augmentation (15, 17, 314). Dental implants can be successfully placed into regenerated bone having a volume of 30-40% (407, 408). The volume of new bone formed within the remaining graft materials was $38.2 \pm 7.8\%$ and $25.7 \pm 6.6\%$ for the autoclaved and dry heat monetite onlay grafts respectively. This indicates that the volume of bone augmented using autoclaved monetite grafts is likely to be sufficient for placement of titanium dental implants as has been reported in other bone augmentation procedures (15, 409-411). The higher levels of porosity present, especially macroporosity in the autoclaved monetite grafts affected the bone volume augmented. This strongly indicates that the increased porosity results in increased bone volume in the augmented areas of grafts. However, increase in porosity results in a drastic decrease in the mechanical properties of grafts. A recent study by Tamimi *et al.* has reported that their graft designs having groove facing calvarial bone had a higher percentage volume of new bone formation in comparison to the designs facing periosteum (17). This indicated that bone formation might be originating from calvarial bone rather than from periosteum. In our study the periosteum was stripped prior to graft fixation.

In future it would be interesting to perform onlay grafting with periosteum remaining intact to confirm this observation.

Although the dry heat monetite grafts had less bone volume, they had significantly higher mechanical strength (twice than autoclaved monetite grafts). This suggests that by altering the P/L ratio it is possible in future to fabricate dry heat monetite grafts with the ability to generate greater bone at the expense of mechanical strength by increasing total porosity present. The results from this study provide a comparison between a high strength, lower porosity (less bone volume achieved) and low strength, higher porosity (greater bone volume achieved) grafts. However, we also prepared autoclaved monetite grafts with a lower P/L of 1 which had a total porosity of ~62% and compressive strength of ~3 MPa. Upon implantation of these highly porous grafts on rabbit calvaria it was observed that the grafts collapsed within the few weeks leaving the screw without any monetite material and no bone growth (**Figures 7.10.1 A, B,C and D**). So, it has to be taken into consideration that although higher porosity grafts may provide greater bone regeneration, the drastic decrease in mechanical strength associated with this increased porosity may render the grafts unsuitable for clinical use.

7.5.4 Onlay graft resorption

The percentage of remaining monetite material after 12 weeks of onlay grafting was ~43% and ~60% for the autoclaved and dry heat grafts respectively. In previous studies the remaining monetite has been shown to be approximately 43% (17) and 50% (231) when implanted as onlay grafts and 66% (207) when implanted intramuscularly. Since the resorption of monetite is mainly regulated by passive dissolution or by cellular activity (224), the total porosity and especially macroporosity would be expected to greatly influence the total resorption of grafts by providing access to resorptive cellular components (osteoclasts and macrophages). The average total resorption noted for the autoclaved monetite grafts was ~55% in comparison to ~38% for the dry heat monetite grafts. The

multifold greater surface area of the dry heat monetite grafts did not appear to enhance resorption. The higher total porosity and macroporosity levels of the autoclaved monetite grafts can be attributed to the greater resorption and ultimately the enhanced biological behaviour observed in terms of bone volume augmented. This can be explained by the fact that monetite being an osteoconductive material, allows new bone formation throughout its material matrix after resorption by allowing greater infiltration of bone forming cells. In addition, the higher rate of resorption of autoclaved monetite grafts results in a localized concentration of calcium and phosphate ions that can potentially aid in the mineralization and bone formation process (145, 150).

7.6 Conclusion

This study has demonstrated that monetite onlay grafts produced by two different heating methods can be used to achieve vertical bone augmentation as high as ~3.2 mm and can be directly fixed to bone surfaces using screws. Onlay monetite grafts prepared by autoclaving and dry heat conversion of brushite achieved similar levels of vertical bone augmentation. However, the total resorption and the bone volume percentage of the area augmented with autoclaved monetite grafts were significantly greater than their dry heat counterparts. The dry heat monetite grafts had greater mechanical strength and can possibly be investigated further for use in specific clinical applications where higher graft strength is a prerequisite.

7.7 Acknowledgements

The authors acknowledge financial support from RSBO, Quebec Government MDEIE Catalonia-Quebec grant.

7.8 Experimental

7.8.1 Method and materials

7.8.1.1 Synthesis

Monetite grafts were prepared by conversion of preset brushite cement discs. Brushite was prepared with a mixture of β -TCP (Merck) and commercially available MCPM (ABCR, GmbH & Co.KG) using a ratio of 1.2 to 1 respectively. The cements were produced at P/L mixing ratio of 3. The powders were hand ground with a pestle and mortar and cement pastes prepared by mixing the powder with appropriate amount of distilled water on a glass slab for 20 s. Once all of the powder was combined with the liquid, the cement paste was kneaded for a further 30 s. The manipulated cement slurry was cast into polyvinylsiloxane mould forming hardened cement discs having a diameter of ~9.5 mm and 4 mm thick. The center of the mould had a 1.5 mm thick needle to produce space for the screw to fix the discs during experiments. The discs were allowed to set for 24 h at $37^{\circ}\text{C} \pm 1^{\circ}\text{C}$ in a vacuum desiccator to form hard brushite. At the end of the incubation period, the samples were removed from the mould and weighed until constant mass was reached.

Monetite grafts were prepared next by conversion of set brushite cement discs utilizing two different methods: wet heat and dry heat conversion. Wet heat transformation was performed with the brushite cylinders being autoclaved at sterilizing conditions (121°C , 100% humidity and 15 psi, for 30 min). For dry heat conversion, the brushite discs were heated at 250°C for 30 minutes under vacuum (80 mTorr).

7.8.1.2 Characterisation of the prepared discs

The phase purity of prepared brushite and the monetite grafts was confirmed using X-ray diffraction (XRD). XRD data was collected (Bruker Discover D8 diffractometer) with Ni filtered $\text{CuK}\alpha$ radiation ($\lambda = 1.54\text{\AA}$) with a two dimensional VANTEC area detector at 40 kV and 40 mA. A step size of 0.02° was used to

measure from 10 to 40° 2 θ over 3 frames with a count time of 300 s per frame. The phase composition was checked by means of the International Centre for Diffraction Data reference pattern for monetite (PDF Ref. 09-0080), JCPDS 2010 database. Microstructural morphology of the prepared monetite grafts was examined with a scanning electron microscope (Hitachi S-4700 FE-SEM; Tokyo, Japan) operating at an accelerating voltage of 20 kV using a back-scattered electron (BSE) detector. Elemental composition (Ca/P ratio) of the bioceramics was assessed with energy dispersive X-ray (EDX) analysis using Oxford detector with a scanning electron microscope (Hitachi S-4700 FE-SEM; Tokyo, Japan) and INCA software (Oxford Instruments, Abingdon, UK). The true density of the disc grafts was determined using a helium pycnometer (Accupyc 1330, Micromeritics). The volume of each sample was measured 10 times following 10 purges of the measurement chamber with helium. The relative porosity (bulk porosity) of the cements was calculated from apparent and true density measurements. The specific surface area (SSA) of cements was determined by using the Brunauer–Emmett–Teller (BET) method with helium adsorption–desorption (Tristar3000, Micromeritics). Macroporosity of the prepared grafts was calculated by using μ -CT (SkyScan 1172; SkyScan; Kontich, Belgium) set at a resolution of 6.0 μ m and 0.5 mm Al filter. μ -CT was also employed to scan the prepared monetite grafts to generate 3D models of the onlay grafts before implantation. The compressive strength of the prepared monetite discs was measured before implantation. The geometrical measurements were made in triplicate and the samples were mounted on the testing machine (5544, Instron) so that the long axes of the discs were perpendicular to the lower anvil. A compressive force was then applied to the upper surface of the cylinders at a constant crosshead displacement rate of 1 mm/min until failure occurred. The applied load was measured using a 100 N load cell (5544, Instron). Mean compressive strength was determined from the average of 5 measurements.

7.8.1.3 Surgical procedure

After obtaining approval from McGill University Health Care Center Ethical Committee, the study was performed on six male New Zealand rabbits (4-6 months) weighing 3-4 kg each. Briefly, calvarial bone was exposed through a skin incision approximately 4 cm in length over the linea media. A pair of tweezers were used to lift the skin before the periosteum was also incised in the same place. A periosteal elevator was used for separating the periosteum from the bone surface and two holes (1.4 mm diameter) were drilled in the parietal bone using a trephine bur on a slow-speed electric handpiece. The drill holes were made on each side of the median sagittal suture without crossing it. The bioceramic disc grafts were stabilized by utilizing stainless steel screws (1.5 mm screw diameter and 5 mm screw length) on either side of the midline. The wound was next closed with 3-0 running subcuticular monocryl sutures. Post implantation, computed tomography (CT) was performed at day 0 and 4, 8 and 12 weeks using Fidex imaging system (Animage, LLC, Pleasanton, CA, U.S.A) with a voltage of 110 kv and a current of 0.080 μ a. The total protocol period was 12 weeks after which the animals were sacrificed. Post mortem, bone blocks containing the stabilized bioceramic discs were retrieved from the animal's calvaria and processed for further characterisation and analysis.

7.8.1.4 Histomorphometric analysis

Once the implant sites were retrieved, blocks of bone with grafts were fixed in 4% formaldehyde for 1 day before being dehydrated in ascending concentrations of ethanol and infiltrated with polymethyl methacrylate histological resin (Technovit[®] 9100, Heraeus Kulzer, Wehrheim, Germany). After the resin was polymerized the samples were sectioned into histological slides with a diamond saw (SP1600, Leica Microsystems GmbH, Wetzlar, Germany) and dyed with basic fuchsin and methylene blue for histological analysis. A series of three slides (~20 μ m each), cutting through the centre of the discs, were prepared for each sample.

Histomorphometric analysis of the implanted area from the images of histological coronal sections crossing the centre of grafts was performed using a Zeiss microscope Axio Imager.M2 (Zeiss® Gottingen, Germany) with a digital AxioCam IC camera (Zeiss® Gottingen, Germany) and the image software GIMP2 (v2.10). Bone growing within the onlay grafts, as well as the area occupied by the remaining unresorbed graft material was identified and measured. This was used to calculate the percentage bone volume, bone height gained, and remaining material within the onlay. In each image section, the augmented bone area was divided into 16 smaller squares (1mm x 1mm) using 4 column x 4 row computer generated grid which was adjusted to cover entire onlay in the image. Localized histomorphometrical analysis was performed for each square [13, 21]. The amount of graft resorption was measured by subtracting the area of remaining monetite in histological sections from the original cross-sectional area of each onlay disc including microporosity.

In order to evaluate the gain in bone height in the onlay grafts during implantation, vertical bone height was measured by calculating the distance between original calvarial surface and the maximum bone height gained. The maximum bone height in each square was measured and a map was created indicating bone height for the entire mediolateral axis of the grafts.

7.8.1.5 Scanning electron microscopy and micro-computed tomography

Electron microscopy was used to examine the microstructural progression upon onlay grafting with a scanning electron microscope (Hitachi S-4700 FE-SEM; Tokyo, Japan) operating at an accelerating voltage of 20 kV using a back-scattered electron (BSE) detector. The resin embedded sections were sputter coated with gold–palladium alloy prior to electron beam analysis at high vacuum. μ -CT (SkyScan 1172; SkyScan; Kontich, Belgium) set at a resolution of 6.0 μ m and 0.5 mm Al filter was employed to scan the retrieved implant sites to construct 3D models of the onlay grafts.

7.8.1.6 Statistical analysis

Statistical analysis was performed using IBM® SPSS® (v. 19, IBM Corp.; New York; USA) statistical software. Mann-Whitney test was used to evaluate head-to-head differences between the implanted onlay grafts. Statistical significance was set at a value of $p < 0.05$.

7.9 Tables & Figures

7.9.1: Characterisation of prepared monetite disc grafts.

Bioceramic graft type	Physico-chemical characteristics						
	Density (g/cm ³)	SSA (m ² /g)	Ca/P	Total relative porosity (%) ^a	Macroporosity (%) ^b		Microporosity (%) ^b
					Open	Closed	Total
Monetite AC	2.88 ± 0.04	1.59 ± 0.07	1.16 ± 0.12	55.94 ± 2.04	4.32 ± 0.57	7.48 ± 0.21	11.8 ± 1.64
Monetite DH	2.87 ± 0.05	20.15 ± 1.08	1.17 ± 0.11	45.58 ± 3.26	2.06 ± 0.73	4.85 ± 0.44	6.91 ± 1.70
							38.67 ± 2.82
							7.62 ± 1.82
							14.3 ± 2.40

Values are presented as mean ± standard deviation (*n*=5).

AC-autoclaved and DH-dry heat

Total porosity, macroporosity and microporosity calculated as percentages from total volume of graft material.

^a Calculated from density measurements.

^b Calculated from μ -CT measurements and all pores larger than 1 μ m in diameter were considered macropores.

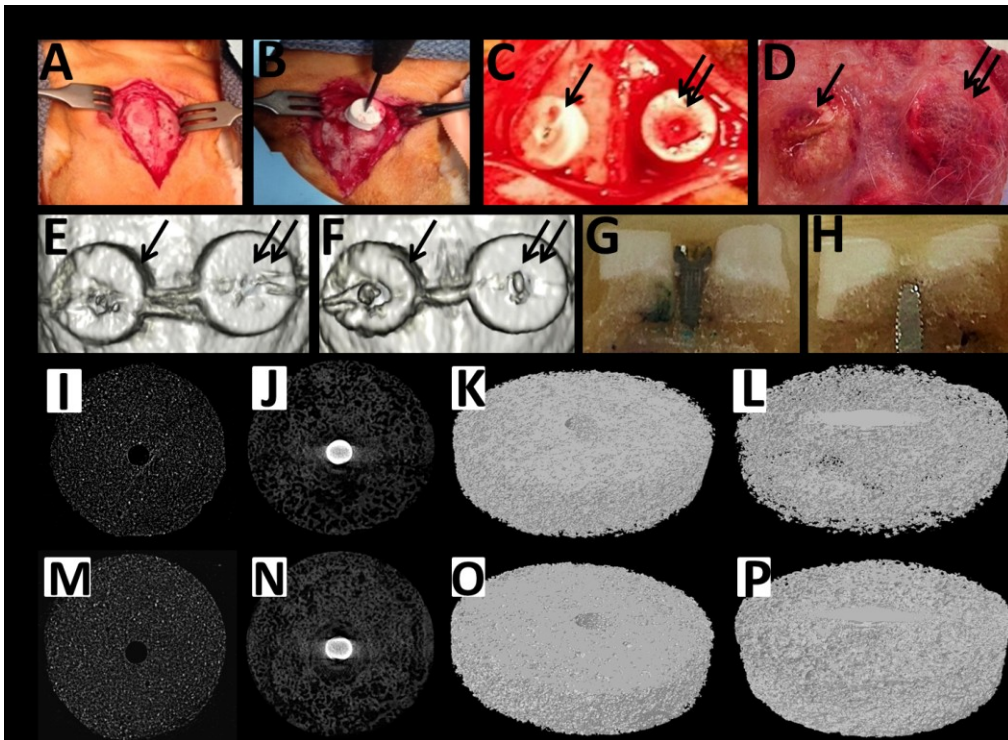


Figure 7.9.1: (A) Retraction of tissues after incision, (B) Disc onlay graft being fixed onto the calvaria, (C) Screw stabilized monetite grafts, (D) Appearance of retrieved grafts after 12 weeks of onlay grafting, (E) Computed tomographic 3D image of grafts immediately after implantation, (F) Computed tomographic 3D image of grafts after 12 weeks of implantation, (G) Resin embedded bone blocks with autoclaved monetite graft after sectioning, (H) Resin embedded bone blocks with dry heat monetite graft after sectioning, (I) μ -CT slice of autoclaved monetite graft before implantation, (J) μ -CT slice of autoclaved monetite graft after 12 weeks of implantation, (K) 3D-modelling of autoclaved monetite graft before implantation, (L) 3D-modelling of autoclaved monetite graft after 12 weeks of implantation, (M) μ -CT slice of dry heat monetite graft before implantation, (N) μ -CT slice of dry heat monetite graft after 12 weeks of implantation, (O) 3D-modelling of dry heat monetite graft before implantation, and (P) 3D-modelling of dry heat monetite graft after 12 weeks of implantation. (Single arrow represents autoclaved monetite grafts and double arrows represent dry heat monetite grafts in the images).

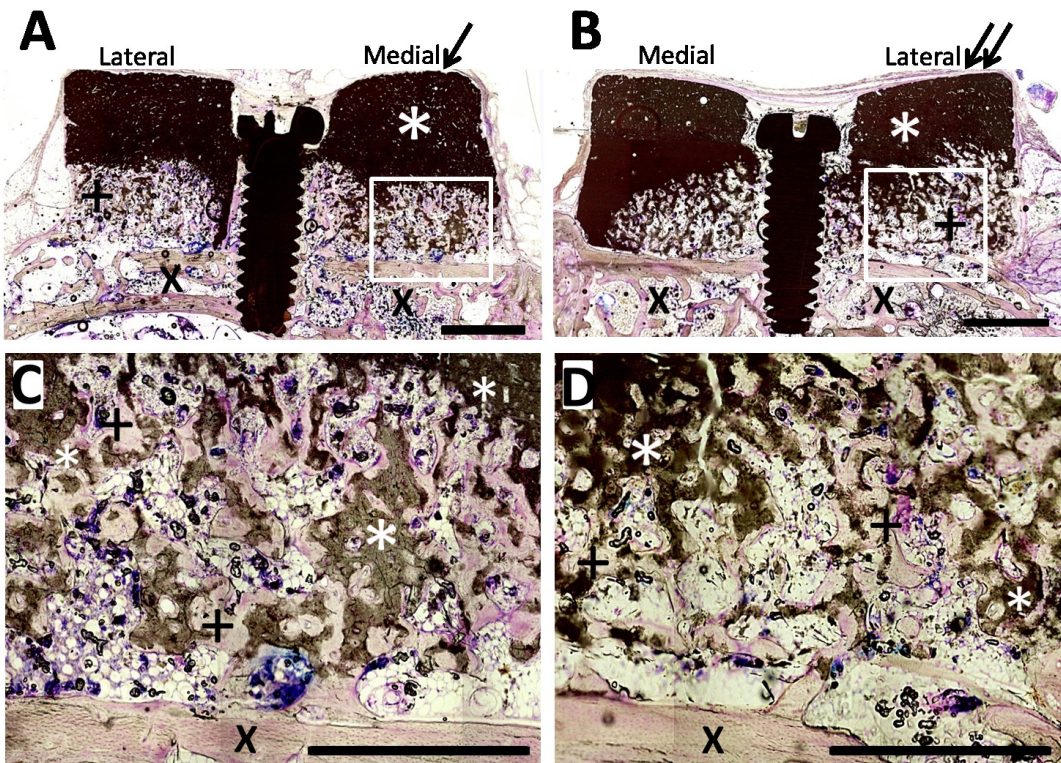


Figure 7.9.2: Histological micrographs of a coronal section from the bone explant sites stained with H&E of: **(A)** autoclaved monetite onlay graft (1 arrow) after 12 weeks, **(B)** Dry heat monetite onlay graft (2 arrows) after 12 weeks, **(C)** Higher magnification image of the area marked in image A, **(D)** Higher magnification image of the area marked in image B. The sections show remaining monetite block material (*), bone augmented free of unresorbed graft material (+), and the original bone calvarium (X). (Scale bars in images A & B represents 2 mm and in images C & D represents 0.5 mm).

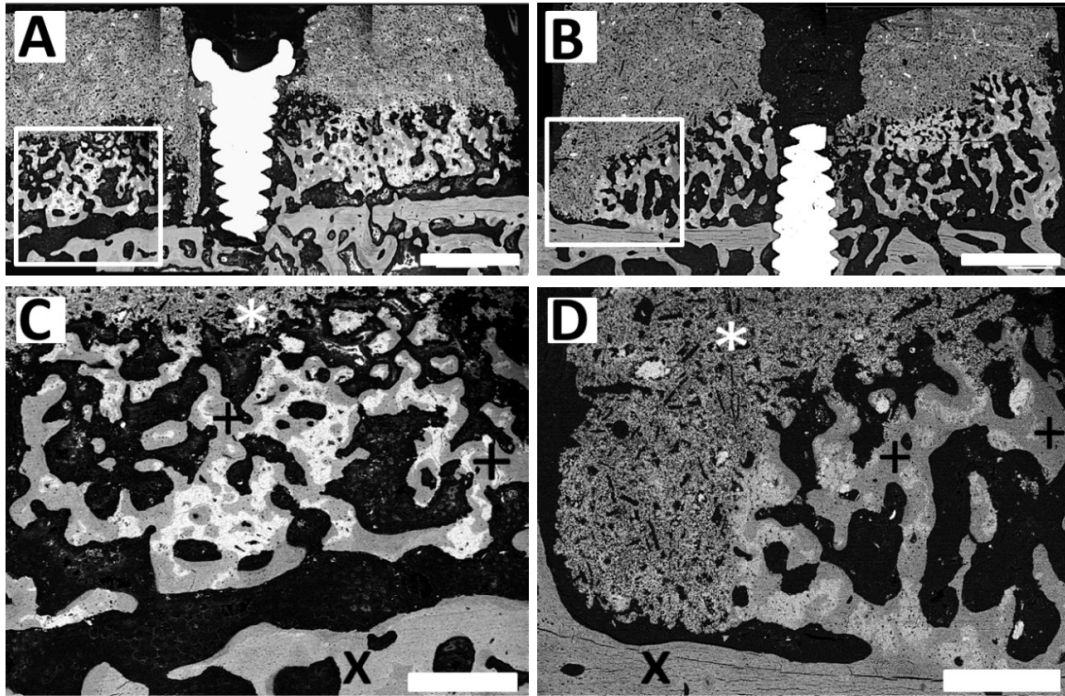


Figure 7.9.3: BSE-SEM images of: **(A)** autoclaved monetite graft after 12 weeks, **(B)** dry heat monetite graft after 12 weeks, **(C)** higher magnification image of the area marked in image A, **(D)** higher magnification image of the area marked in image B. The images show remaining monetite graft material (*), bone augmented (+), and the original bone calvarium (X). (Scale bars in the images A & B represents 2 mm and in images C & D represents 0.5 mm).

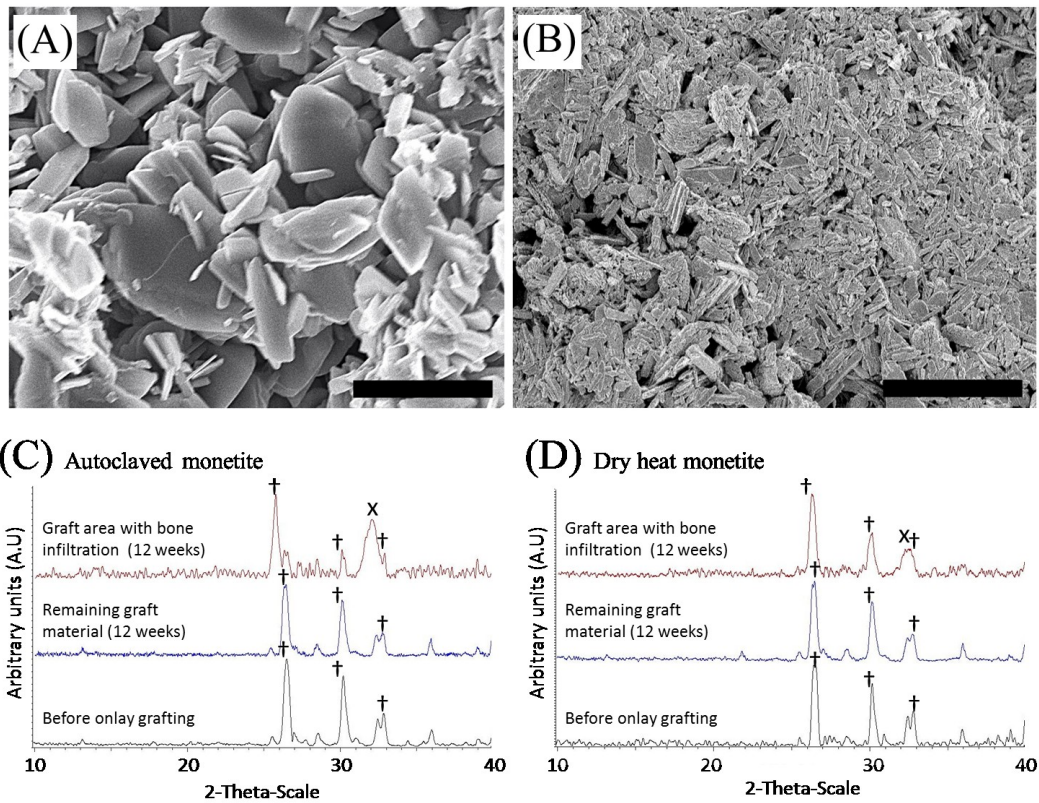


Figure 7.9.4: BSE-SEM images of disc grafts prepared: **(A)** autoclaved monetite, and **(B)** dry heat monetite. (Scale bars in the images represent 0.5 μm). X-ray diffraction patterns obtained before and after implantation from: **(C)** autoclaved monetite grafts, and **(D)** dry heat monetite grafts. [†) represents monetite and (x) represents HA peaks].

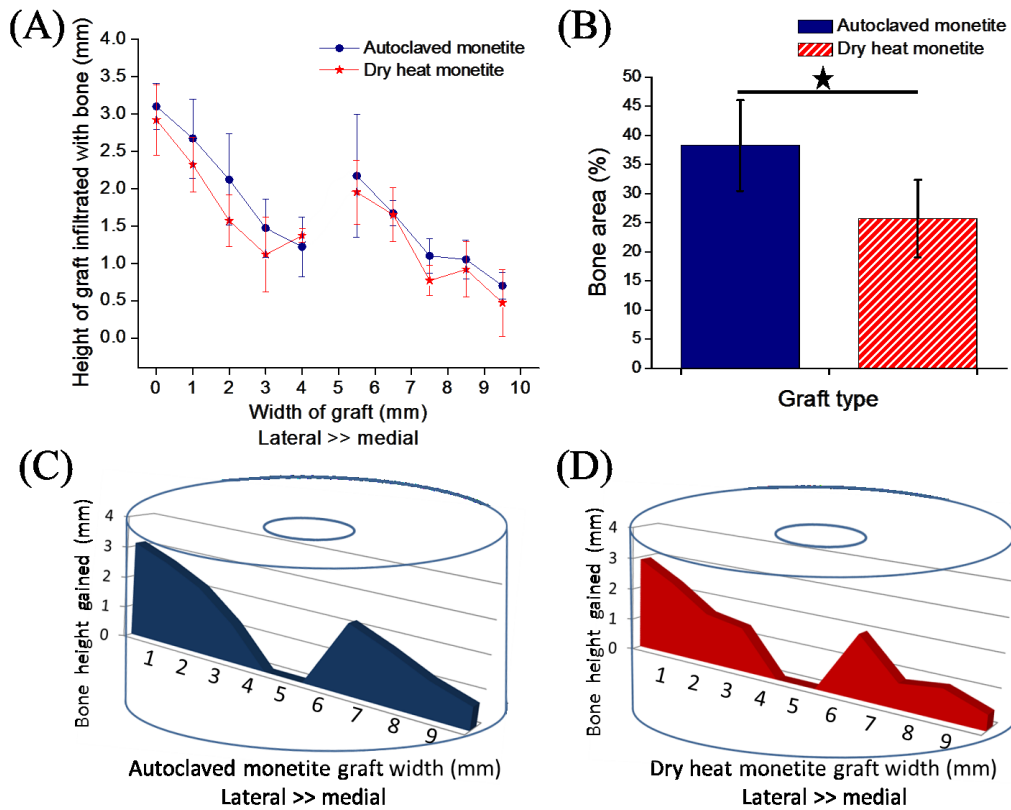


Figure 7.9.5: (A) Relative bone height gained along the mediolateral axis of the grafts. The measurements represent percentage of bone height (mean plus standard deviation) gained between the original calvarial surface and the superior surface of the monetite grafts. (B) The percentage of bone tissue within the grafts' augmented area. (C) Mapping of average bone height augmented with autoclaved monetite grafts. (D) Mapping of average bone height augmented with dry heat monetite grafts.

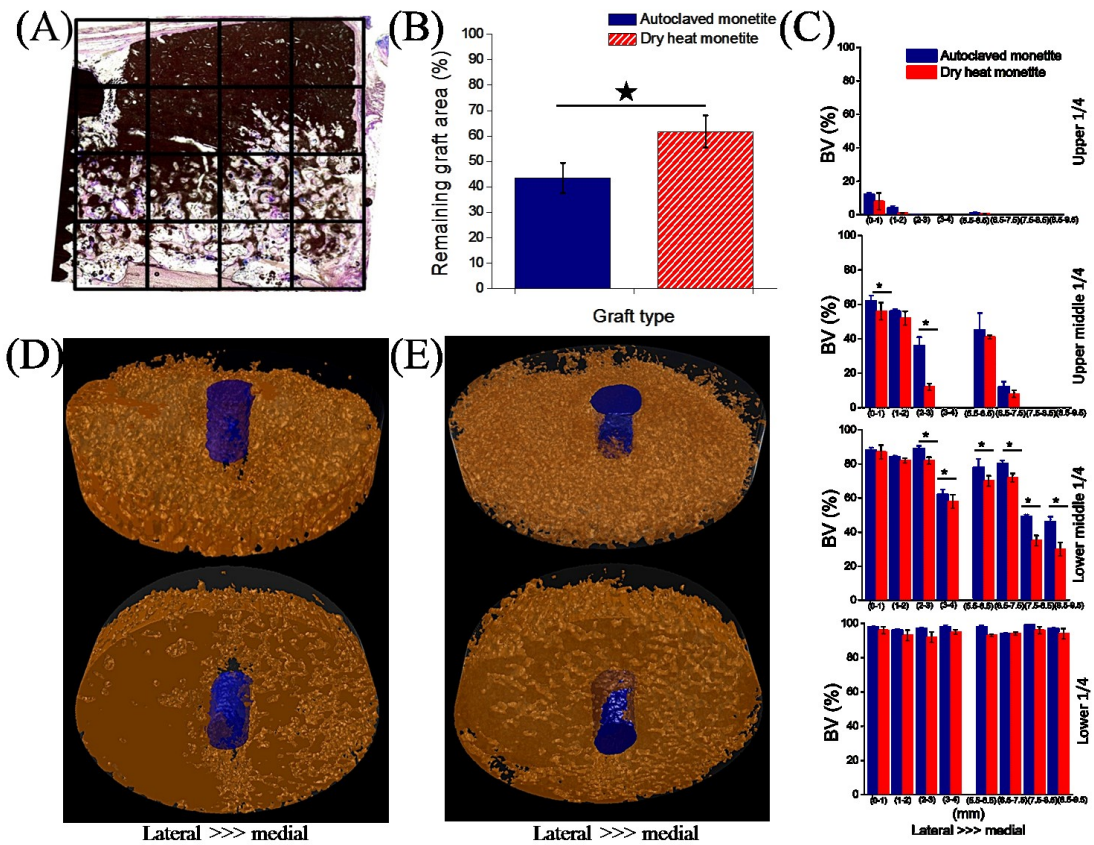


Figure 7.9.6: (A) Graft and bone block histological section divided into 16 smaller areas (1x1mm each), using a 4x4 grid for histomorphological measurements. (B) The percentage of remaining graft area after 12 weeks of onlay grafting. (C) Histomorphological measurements showing percentage of bone volume present in the areas delimited by the grids. (D) 3D-model of autoclaved monetite onlay graft from above (top image) and surface in contact with calvarial bone (bottom image) constructed after 12 weeks of implantation. Lateral area shows more bone augmented than the medial area. (E) 3D-model of dry heat monetite onlay graft from above (top image) and surface in contact with calvarial bone (bottom image) constructed after 12 weeks of implantation. The lateral most area shows more bone than the medial area, but less in comparison to the autoclaved monetite graft.

7.10 Supplementary figures

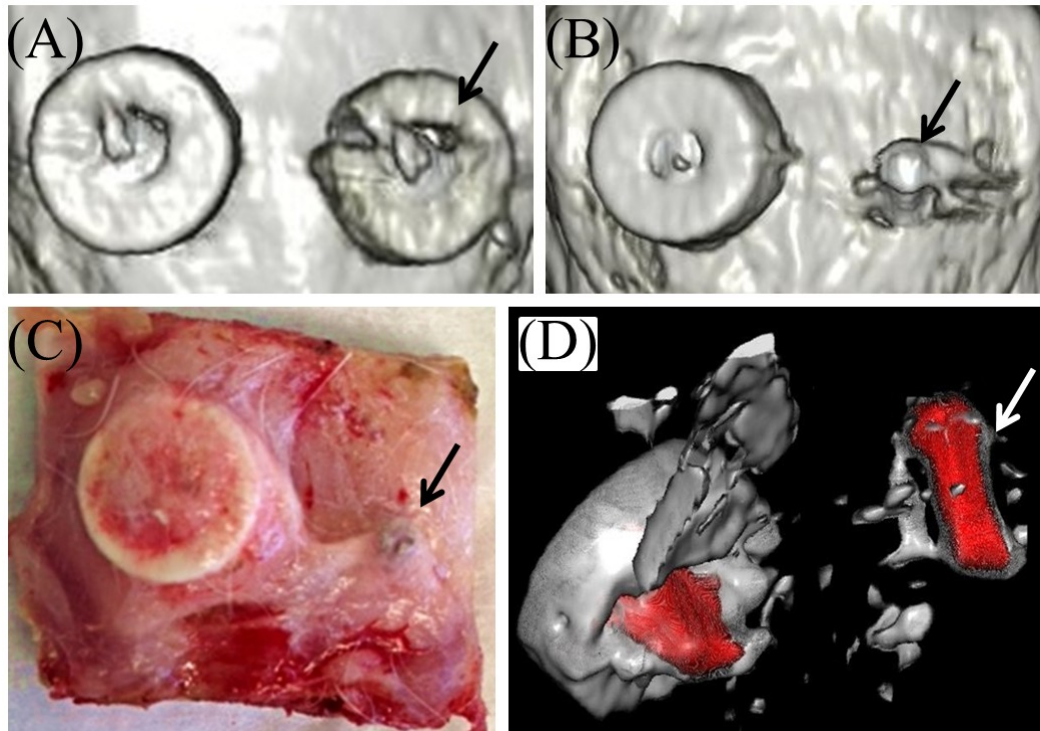


Figure 7.10.1: (A) 3D image of grafts immediately after implantation. (B) 3D image of grafts after 4 weeks of implantation. (C) Appearance of retrieved grafts after 12 weeks of onlay grafting. (D) 3D image obtained by removing the calvarial surface to visualize the graft and screw from underneath after 4 weeks of implantation. (Single arrows in the images represent autoclaved monetite grafts prepared with a P/L ratio of 1).

Chapter 8: Development of alkali ions substituted-silica reinforced calcium phosphate cement, set with phytic acid.

8.1 Preface

Previous chapters have discussed and conclusively demonstrated the superior *in vivo* performance of monetite grafts in comparison with brushite grafts. These results are attributed to the phase conversion of brushite grafts to the slowly resorbing insoluble apatite. This phase conversion was not observed for wet heat and dry heat converted monetite grafts. However, it was noted that the autoclaving process used to convert brushite to monetite affected mechanical properties adversely. Conversely, the dry heating conversion process resulted in production of monetite grafts with mechanical properties comparable with their original brushite precursors. The results from the preceding studies in this thesis led to the experiments presented in this chapter. This chapter reports the development of alkali ions substituted calcium phosphate cements that were reinforced with silica to potentially improve the mechanical properties. The cements were set by utilising phytic acid (a strong chelating agent) with varying concentrations. The objective and focus of the experiments was to prepare calcium phosphate cements that would have improved mechanical properties and not convert to insoluble HA resulting in continued dissolution upon *in vitro* ageing in PBS.

Development of alkali ions substituted-silica reinforced calcium phosphate cement, set with phytic acid.

Zeeshan Sheikh¹, Martha Geffers², Jake Barralet^{1,3}, Uwe Gbureck²

¹Faculty of Dentistry, McGill University, Montreal, Quebec, Canada

²Department for Functional Materials in Medicine and Dentistry, Julius-Maximilians-Universität-Würzburg, Germany

³Division of Orthopaedics, Department of Surgery, Faculty of Medicine, McGill University, Montreal, Quebec, Canada

8.2 Abstract

Research in the past few decades has focused towards exploring suitable alternatives to autologous bone grafting. Among the other available bone substitutes, inorganic calcium phosphates are commonly used. Sodium and/or potassium phosphate can be added in the calcium phosphate cements to improve their biodegradability. $\text{Ca}_2\text{KNa}(\text{PO}_4)_2$ is a calcium alkali orthophosphate that stimulates osteoblast growth and shows excellent biocompatibility both *in vitro* and *in vivo*. Most commonly, alkali ion substituted calcium phosphate cement reactants are prepared via sintering or molten processing routes. These cements traditionally are mechanically weak and convert to slowly resorbing apatite. We report the development and assessment of the physico-chemical properties of alkali ions substituted calcium phosphate cements reinforced with the silica and set using phytic acid after *in vitro* ageing in PBS. The concentration of phytic acid used to set cements was found to have an inverse effect on mechanical properties. Cements set with lower concentration of phytic acid had higher compressive strengths in comparison to the higher concentration acid cements. All cements set with different concentrations of phytic acid showed no phase conversion to apatite upon *in vitro* ageing. This indicated their potential to

be evaluated further for orthopaedic and dental bone repair and regeneration applications as fully resorbable bone graft substitutes.

8.3 Introduction

Bone grafts are frequently used as substitutes for diseased, damaged or missing bone tissue. This is imperative to prevent fibrous tissue ingrowth into the defect and to maintain mechanical function. The most commonly used graft materials for orthopaedic and dental applications are the autologous bone grafts which are considered to be the gold standard (1, 83). Although they have higher biological acceptability (7, 412), they have disadvantages such as donor site morbidity, the need for a second surgery, increased cost due to hospitalization and limited amounts that can be procured (412). Research in the past few decades has focused towards exploring suitable alternatives for the said purpose (9-11). Among the other available bone substitutes, inorganic calcium phosphates are commonly used (16, 116, 145, 150). Cements made from calcium phosphates known as calcium phosphate cements are non-toxic and do not induce cell lysis in the surrounding tissues after being implanted (222). The calcium phosphate cements undergo a process of dissolution and precipitation leading to a strong material-bone interface (366, 413-415). Due to their relatively fast setting time and ease of manipulation, these materials are a good option as bone substitutes (145, 150, 416).

Sodium and/or potassium phosphate can be added in the calcium phosphate cements to improve their biodegradability (417), and cell cultures have shown that materials like $\text{Ca}_2\text{KNa}(\text{PO}_4)_2$ which is a calcium alkali orthophosphate stimulates osteoblast growth (418). In addition, these cements show excellent biocompatibility both *in vitro* and *in vivo* (419), so $\text{Ca}_2\text{KNa}(\text{PO}_4)_2$ is one of the promising materials that can be used as bone filler to heal bone defects. However, calcium alkali orthophosphates remains underrated as materials for bone repair and augmentation applications. The literature shows research on development of alkali ion substituted calcium phosphate cements via sintering or molten methods but only few cements prepared from acids (417, 420). These cements prepared by sintering or molten methods are mechanically weak and convert to apatite upon implantation limiting the success of orthopaedic and

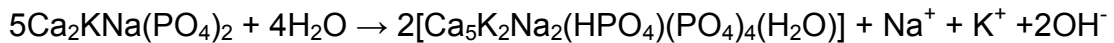
dental procedures due to the extremely low resorption (rate and extent) associated with the less soluble HA (145).

We report the development of a calcium phosphate cement which is reinforced with the addition of silica (SiO_2) and set using inositol phosphate ($\text{C}_6\text{H}_6(\text{OPO}_3\text{H}_2)_6$; IP6), also known as phytic acid which is a chelating agent (419, 421-423). Phytic acid is found in rice, corn, wheat, and soybean (424), and has strong chelating capability towards calcium ions due to its 6 phosphate groups, in comparison with other chelating compounds such as ethylenediaminetetraacetic acid (EDTA), which have only 3 phosphate groups (425). The newly developed cement was created by mixing $\text{Ca}_2\text{KNa}(\text{PO}_4)_2$ + SiO_2 powders that were set by the chelate bonding of phytic acid at different concentrations. In this study we have evaluated the physico-chemical effects of alkali ion substitution and addition of silica to calcium phosphate cements set with phytic acid with different concentrations after ageing in PBS solutions.

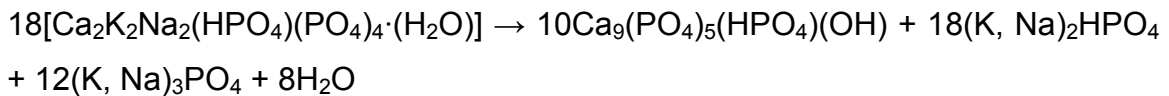
8.4 Results and discussion

The preparation of the $\text{Ca}_2\text{KNa}(\text{PO}_4)_2$ cements reinforced with silica was carried out with relative ease. However, it was noted that the cements set with higher concentrations of phytic acid (40% and 50%) were clumpy and had a relatively shorter working time in comparison to the 20% and 30% concentration phytic acid set cements. Setting of cements such as $\text{Ca}_2\text{KNa}(\text{PO}_4)_2$ using H_2O is thought to take place via the following two steps (426):

[1] The formation of an alkali ion containing nano-apatite which results in the quick hardening of cement paste:



[2] The conversion of this substituted apatite to calcium deficient HA:



Apatitic calcium phosphate cements are used very commonly as bone substitute biomaterials in orthopaedic, craniofacial and maxillofacial surgery because of their excellent biocompatibility in soft and hard tissue contact (427-429). However, the setting of cements as HA is undesired due to the slow or negligible resorption upon implantation (15). By utilising phytic acid to set $\text{Ca}_2\text{KNa}(\text{PO}_4)_2$ powders, we prepared cements that did not set as HA (**Figure 8.9.6**).

8.4.1 Compressive strength

Before the $\text{Ca}_2\text{KNa}(\text{PO}_4)_2 + 6\% \text{SiO}_2$ cements were set using different concentrations of phytic acid (**Table 8.9.1**), the powders alone and with 3% and 6% silica added to them were set using 40% phytic acid. This was performed in order to determine whether addition of 3% or 6% would affect mechanical properties of the set cements. It was observed that the $\text{Ca}_2\text{KNa}(\text{PO}_4)_2$ powders

without the addition of silica, set with 40% phytic acid having a compressive strength of 2.54 ± 0.33 MPa ($n=6$). The $\text{Ca}_2\text{KNa}(\text{PO}_4)_2$ powders with 3% and 6% silica added to them had compressive strengths after setting with 40% phytic acid of 2.51 ± 0.59 and 7.72 ± 0.22 MPa respectively ($n=6$). Based on these results it was decided to use $\text{Ca}_2\text{KNa}(\text{PO}_4)_2$ powders reinforced with 6% silica.

After cements were set using 20, 30, 40 and 50% concentration phytic acid, compressive strengths were measured before and after *in vitro* ageing in PBS (**Table 8.9.1 and Figure 8.9.2**). The cements set with 20% phytic acid had the highest recorded compressive strengths (22.01 ± 5.33) which reduced as the concentration of phytic acid was increased (**Table 8.9.1**). Cements set with higher concentrations of phytic acid (30, 40 and 50%) had 2, 3 and 5 times less compressive strengths noted respectively than the 20% phytic acid cements (**Table 8.9.1**). Upon ageing in PBS for 1 week the compressive strength of the $\text{Ca}_2\text{KNa}(\text{PO}_4)_2$ cements set with 20% phytic acid reduced to 17 ± 3.1 MPa and after 4 weeks it reduced to ~50% of the original strength observed (**Figure 8.9.2**). The higher concentration phytic acid set cements after 4 weeks of ageing had a significantly greater decrease in compressive strength (**Figure 8.9.2**).

8.4.2 Porosity

The concentration of phytic acid used to set cements had an effect on total porosity present (**Table 8.9.1**). Cements set with 20% phytic acid had ~35% initial porosity which increased to ~38% after 7 days and to ~52% after 4 weeks in PBS. The 30% phytic acid cements had an initial porosity of ~44% which went up to ~60% after 4 weeks in PBS. Similarly, the 40 and 50% phytic acid set cements had starting porosities of ~53 and 61% which increased to ~68 and 72% respectively after 4 weeks of ageing *in vitro* (**Figure 8.9.3**).

8.4.3 In vitro dissolution and mass loss

The mechanical properties and porosity of cements had a direct effect upon the mass loss observed after ageing in PBS. As would be expected, the higher compressive strength and lower porosity cements (set with 20% phytic acid) lost the least amount of mass after 4 weeks in PBS ~29% (**Figure 8.9.4**). The 30, 40 and 50% phytic acid set samples lost ~45, 55 and 62% mass respectively after 4 weeks of ageing *in vitro* (**Figure 8.9.4**). The mass loss observed for these cements set by phytic acid was more when compared with that of the dicalcium phosphate cements aged in PBS for similar time period (**Chapter 5**). The high energy ball milling of the $\text{Ca}_2\text{KNa}(\text{PO}_4)_2$ powders was probably responsible for the increase in solubility of these materials as also shown by Gbureck *et al.* (420). The dissolution of $\text{Ca}_2\text{KNa}(\text{PO}_4)_2$ has the effect of being antimicrobial due to the cations present in the biomaterial that are released (430, 431). Ca^{2+} , Na^{2+} and K^+ are released from the surface of these cements which result in elevated osmotic pressure locally influencing the viability of micro-organisms in the immediate environment (430-433). However, further *in vitro* and *in vivo* experiments are required to assess the antimicrobial properties of these cements.

8.4.4 Scanning electron microscopic imaging

The SEM images revealed the changes in microstructural appearance of cements upon ageing. The cements set with higher concentrations of phytic acid had a more porous appearance than the ones set with lower concentration acid (**Figures 8.9.5 a, b, c and d**). Upon ageing for 7 days and 28 days, the 20 and 30% phytic acid cements showed cracks in their structure (**Figures 8.9.5 e, f, I and j**). The 40 and 50% phytic acid cements got progressively more porous upon ageing and disintegrated (**Figures 8.9.5 g, h, k and l**).

8.4.5 X-Ray diffraction

X-ray diffraction data revealed the phase composition of set cements before and after ageing (**Figure 8.9.6**). All cements prepared showed peaks representing

[Ca₂KNa(PO₄)₂ (●)] (420, 434) and [SiO₂ (▼)] (435, 436) and it was observed that phytic acid concentration inversely affected peak intensity (**Figures 8.9.6 a, b, c and d**). The amorphous broad peak (at 10-15 2 θ) observed prior to ageing and after 7 days in PBS disappeared after 28 days in PBS (**Figures 8.9.6 a, b, c and d**). During preparation, the high energy ball milling of the Ca₂KNa(PO₄)₂ in ethanol for 24 hours probably resulted in the mechanically induced phase transformation from crystalline to amorphous state. Upon ageing for 7 and 28 days in PBS, no phase transformation was observed for any cement group. The non-conversion of phytic acid set Ca₂KNa(PO₄)₂ cements reinforced with silica is encouraging and these biomaterials can potentially be used as bone substitutes. However, further studies are required to prove that similar results can be achieved *in vivo*.

8.4.6 Density and specific surface area

The initial density of the Ca₂KNa(PO₄)₂+6%SiO₂ cements set with phytic acid was in the range of 2.14 to 2.20 g/cm³. The density slightly increased with the higher concentration of phytic acid used to set the cements (**Table 8.9.1**). Upon ageing for 4 weeks, the density for all cements increased significantly from the initial values recorded ($p < 0.01$). However it was interesting to note that the lower concentration of phytic acid set cements had a much greater increase in density upon ageing (**Figure 8.9.7**). The initial SSA of the prepared cements was low (~2 to 5 m²/g). The lower phytic acid concentration cements had higher SSA in comparison with the higher concentration prepared samples (**Table 8.9.1**). After ageing in PBS it was observed that the highest increase in SSA was recorded for the 50% phytic acid cements (from ~2 to ~56 m²/g) (**Figure 8.9.8**). The SSA increased significantly from the initial recorded values for all other cements after 4 weeks in PBS as well (**Figure 8.9.8**).

8.5 Conclusion

In conclusion, the alkali ion substituted calcium phosphate cements reinforced with silica were prepared with the aim of improving solubility of the cements. The concentration of phytic acid used to set the cements was found to have an inverse effect on mechanical properties. The lower concentration (20%) phytic acid set cements samples had higher compressive strength in comparison to the brushite cements discussed earlier (**Chapter 5**). All cements set with different concentrations of phytic acid showed no phase conversion to apatite upon *in vitro* ageing. The results obtained indicate their potential to be evaluated further for orthopaedic and dental bone repair and regeneration applications.

8.6 Acknowledgements

The authors acknowledge financial support from GPS, Graduate Research Mobility Award (McGill University) and FMZ-Department for Functional Materials in Medicine and Dentistry, Dr. Uwe Gbureck group. Julius-Maximilians-Universität-Würzburg, Germany.

8.8 Experimental

8.8.1 Method and materials

8.8.1.1 Synthesis

$\text{Ca}_2\text{KNa}(\text{PO}_4)_2 + 6\% \text{SiO}_2$ was prepared by sintering CaHPO_4 , Na_2CO_3 , K_2CO_3 and SiO_2 in a molar ratio of 4:0.63:0.63:0.79 for 24 h at 1050 °C. The sintered cakes were crushed and sieved with 355 μm pore size-mesh followed by ball milling with ethanol in a planetary ball mill for 24 h at 250 rpm. Finally the cement powder was vacuum dried at 60 °C. In order to investigate the effect of concentration of the chelating agent cements were produced by mixing the $\text{Ca}_2\text{KNa}(\text{PO}_4)_2 + 6\% \text{SiO}_2$ powders with phytic acid having 20, 30, 40 and 50% concentration respectively, using a powder of liquid ratio of 2. The cement pastes were prepared on a glass slab for 20 s. To mix the cement paste, powder mixture was divided into four equal portions and added to liquid phase a quarter at a time and mixed using a non-corrodible spatula for a period of 10 s. Once all of the powder was combined with the liquid, the cement paste was kneaded for a further 30 s. The manipulated cement slurry was cast into silicone moulds forming hardened cement blocks (~6 x 12 mm), and cement discs (~15 mm diameter, 2mm thickness). The samples were allowed to set for 24 h at 37°C \pm 1°C in a water bath for 24 hours. At the end of the incubation period, the samples were removed from the mould, dried and weighed until constant weight was reached. Five different batches of ten samples each (for each phytic acid concentration) were produced to obtain a total of fifty blocks respectively. Even though the sample homogeneity was very high (either within a batch or between batches), the sample were randomized before testing.

8.8.1.2 Characterisation

The phase purity was confirmed for the alkali substituted calcium phosphate cement samples set by phytic acid by using X-ray diffraction (XRD). XRD data was collected (Siemens D5005 X-ray diffractometer) with Ni filtered $\text{CuK}\alpha$ radiation ($\lambda = 1.54\text{\AA}$) with 2 dimensional area detector at 40 kV and 40 mA.

A step size of 0.02° was used to measure from 10 to 40° over a count time of 2 s per degree. The phase composition was compared and confirmed with the International Centre for Diffraction Data reference JCPDS 2010 database. The compressive strength (wet) of the prepared cement blocks was measured before and after *in vitro* ageing in PBS solutions. Before testing, geometrical measurements of the samples were made in triplicate and their weight noted. Samples were mounted on the testing machine (Zwick/ Roell Z010) so that the long axes of the cement cylinders were perpendicular to the lower anvil. A compressive force was then applied to the upper surface of the cement samples at a constant crosshead displacement rate of 1 mm/min until failure occurred. The applied load was measured using a 2 kN load cell (Zuick/Roell Z010). Mean strength was determined from the average of 6 measurements. After testing in compression, cement fragments were retrieved, weighed and dried in a vacuum desiccator at a temperature of 37°C . The cement fragments were then ground to powder using a pestle and mortar. The true density of the powders was determined using a helium pycnometer (Accupyc 1330, Micromeritics). The volume of each sample was measured 10 times following 10 purges of the measurement chamber with helium. The relative porosity (bulk porosity) of the cements was calculated from apparent and true density measurements. The specific surface area (SSA) of cements was determined by using the Brunauer–Emmett–Teller (BET) method with helium adsorption–desorption (Tristar3000, Micromeritics). Bioceramic microstructure was observed using scanning electron microscopy imaging (Hitachi S-4700 FE-SEM; Tokyo, Japan), at an accelerating voltage of 2 kV.

8.8.1.3 *In vitro* ageing

After initial characterisation was completed, the samples were stored at $37 \pm 1^\circ\text{C}$ and $\sim 100\%$ relative humidity for 24 h. The cement discs prepared were immersed in PBS solutions ($n=5$). The samples were aged at a liquid to cement volume ratio (LCVR) of 60 as used by Grover et al. (228) for 28 days at $37 \pm 1^\circ\text{C}$. Dynamic ageing protocols were achieved by refreshing the liquid every 24 h

throughout the experiment to remove any dissolution products. To quantify the amount of mass loss over time, the samples were weighed daily. The sample weight loss was measured according to:

$$\Delta W = (W_1 - W_2)/W_1$$

(Weight before in vitro incubation was measured as W_1 , weight after incubation washed by distilled water and dried until constant was measured as W_2).

After a time period of 7 and 28 days, all the samples were removed from the solutions and tested in compression and characterised for changes in phase structure, SSA, density and porosity.

8.8.1.4 Statistical analysis

Statistical analysis was performed using IBM® SPSS® (v. 19, IBM Corp.; New York; USA) statistical software. Mann-Whitney test was used to evaluate head-to-head differences between the aged cement blocks. Statistical significance was set at a value of $p < 0.05$.

8.9 Tables & Figures

Table 8.9.1 Characterisation of cements produced by setting with different concentrations of phytic acid.

Concentration of phytic acid used to set the cements	Total relative porosity (%)	SSA (m ² /g)	Density (g/cm ³)	Compressive Strength (MPa)
20 %	35.26 ± 1.41	5.08 ± 0.07	2.14 ± 0.04	22.01 ± 5.33
30 %	43.84 ± 1.81	4.51 ± 0.08	2.18 ± 0.05	8.45 ± 1.60
40 %	53.30 ± 1.32	3.93 ± 0.41	2.19 ± 0.04	7.86 ± 0.18
50 %	60.98 ± 1.03	2.18 ± 0.40	2.20 ± 0.06	4.03 ± 1.04

Values are presented as mean ± standard deviation ($n=5$).

SSA- specific surface area



Figure 8.9.1: Photograph of cement blocks prepared for *in vitro* experiments.

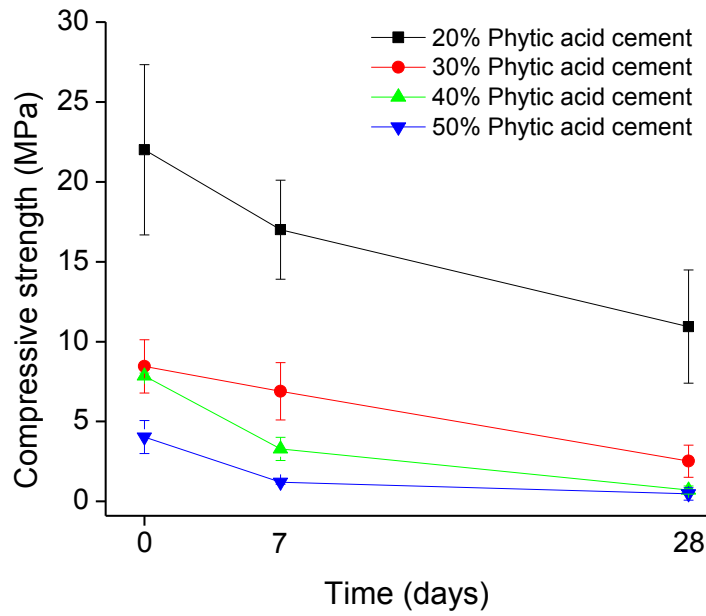


Figure 8.9.2: Effect of *in vitro* ageing time on the mechanical properties of cement blocks.

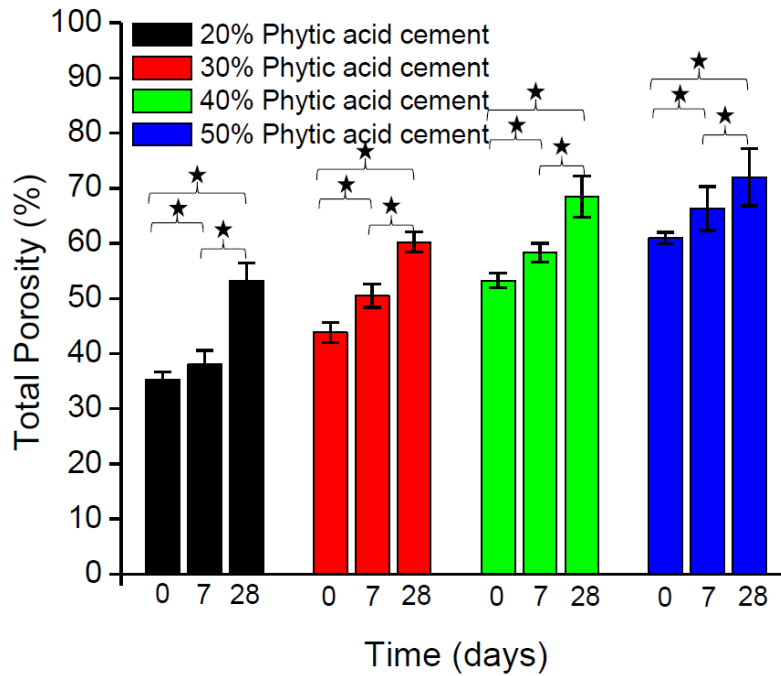


Figure 8.9.3: Effect of *in vitro* ageing time on total porosity of cement blocks set with 20, 30, 40 and 50% concentrated phytic acid.

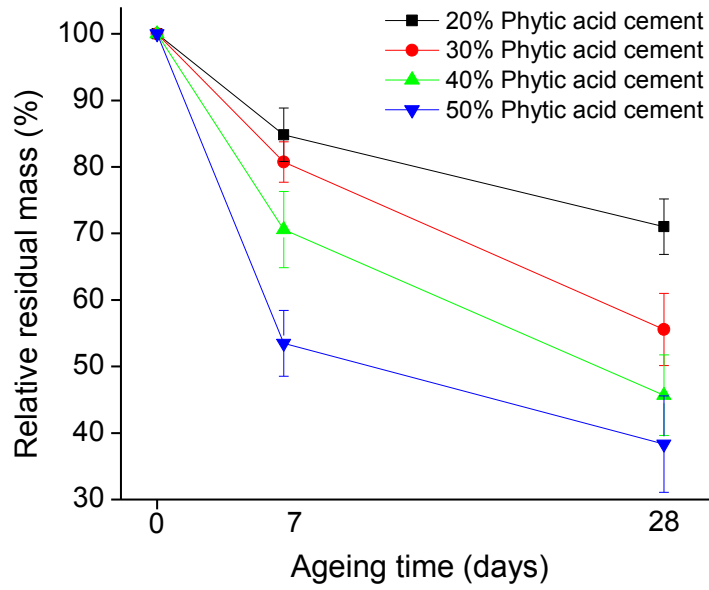


Figure 8.9.4: Effect of phytic acid concentration on resorption of cements *in vitro*.

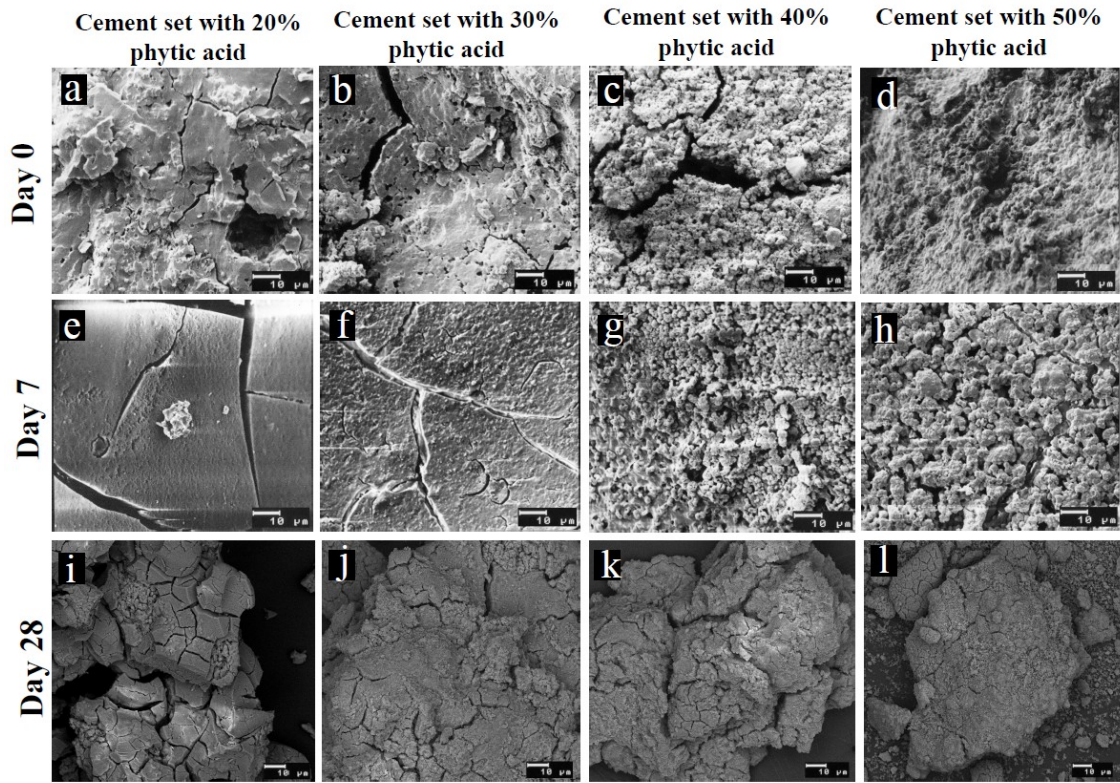


Figure 8.9.5: SEM images of surface of cements set with varying concentrations of phytic acid respectively after *in vitro* ageing at day 0 (**a, b, c, d**), day 7 (**e, f, g, h**) and day 60 (**i, j, k, h**) (Scale bars represent 10 μm).

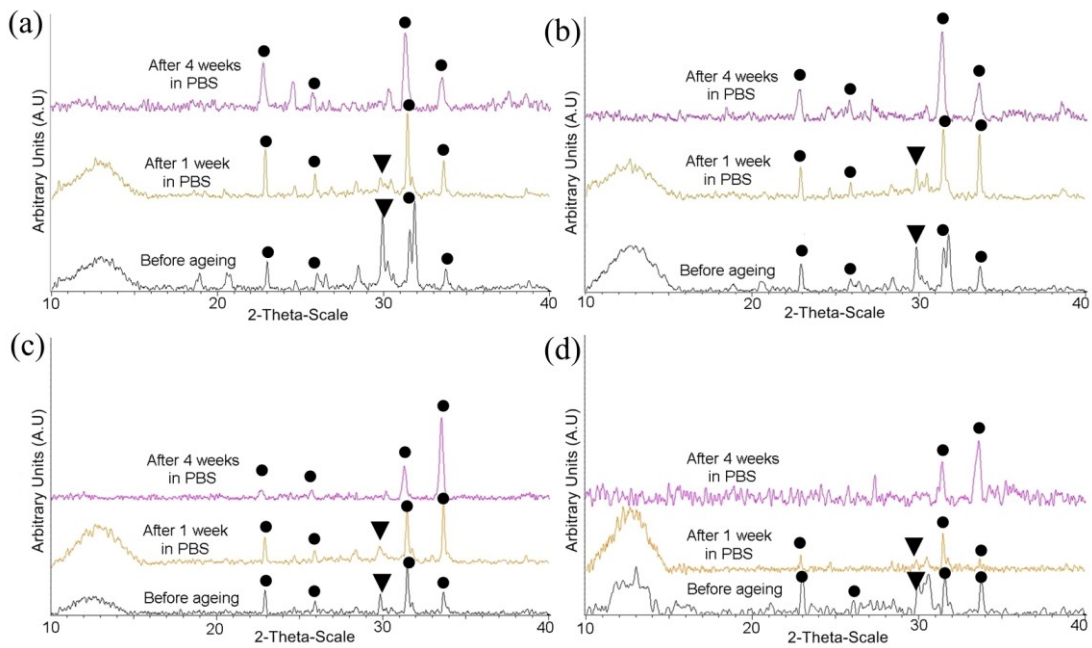


Figure 8.9.6: X-ray diffraction patterns showing phase composition before and after ageing of:

a. Cement set with 20% phytic acid.

b. Cement set with 30% phytic acid.

c. Cement set with 40% phytic acid.

d. Cement set with 50% phytic acid.

None of the cements showed any phase conversion to apatite.

(●) represents $\text{Ca}_2\text{KNa}(\text{PO}_4)_2$, and (▼) represents SiO_2 peaks.

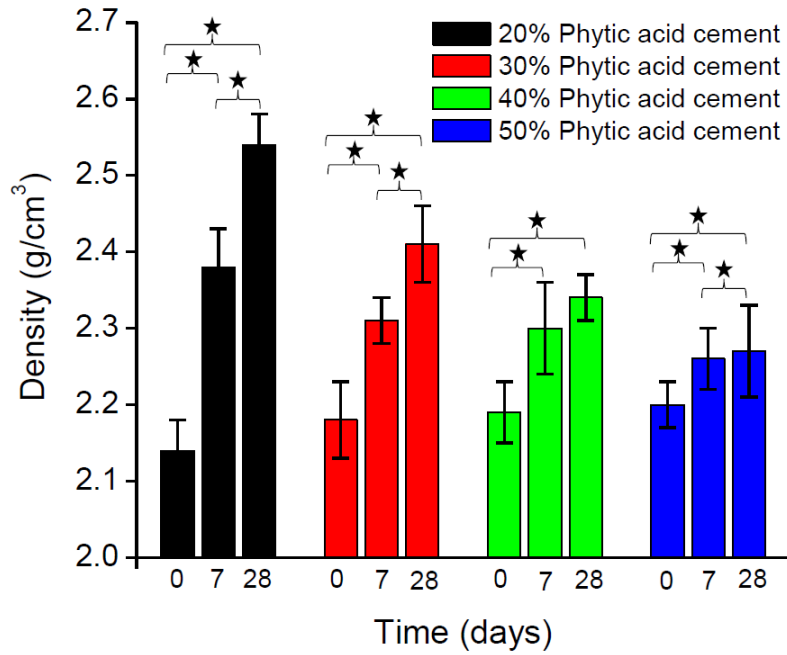


Figure 8.9.7: Effect of *in vitro* ageing on density of cement blocks set with 20, 30, 40 and 50% concentrated phytic acid.

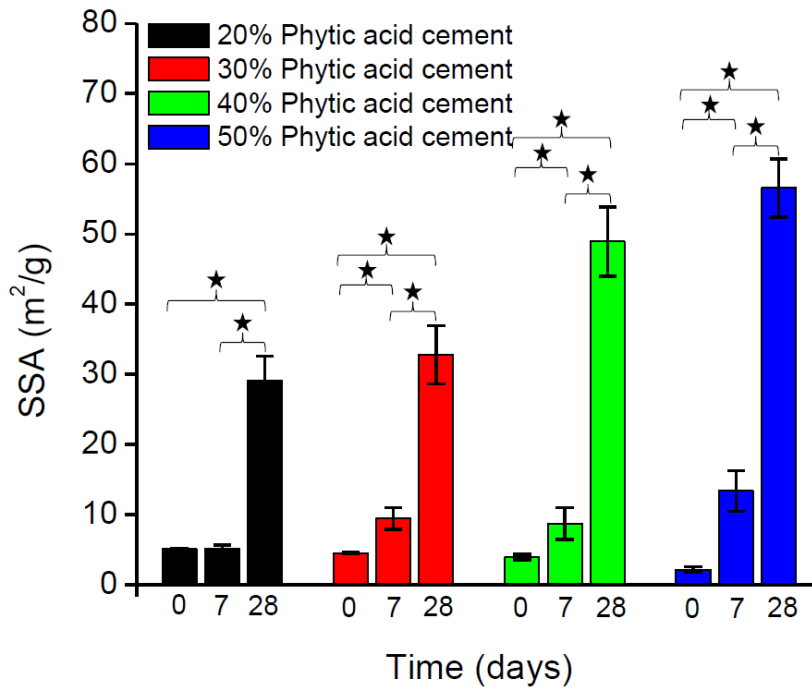


Figure 8.9.8: Effect of *in vitro* ageing on specific surface area of cement blocks set with 20, 30, 40 and 50% concentrated phytic acid.

Chapter 9: Final discussion and conclusions

Autoclaving and dry heating pre-set brushite bioceramics resulted in transformation to monetite-based biomaterials with higher porosity, density and specific surface area than their original brushite precursors. It was observed that the dry heat monetite grafts demonstrated much higher surface area and had mechanical properties that were comparable with brushite grafts. Whereas, autoclaved monetite grafts had significantly reduced mechanical properties. Alkali ionic substitution of calcium phosphate cements and their setting with a strong chelating agent resulted in biomaterials that upon *in vitro* ageing resorbed consistently without any phase transformation to insoluble apatite.

The *in vitro* ageing study revealed that serum inhibited both the dissolution of brushite and formation of HA in brushite cement. Monetite cements produced by autoclaving and dry heating methods did not demonstrate any phase conversion when aged in PBS or serum. While surface area did not play a significant role, fragmentation of cements seemed to be the main factor which dictated mass loss in high porosity grafts. For cements having lower porosity, solubility played a more crucial role towards mass loss during *in vitro* ageing and subcutaneous *in vivo* resorption. When the prepared bioceramics were implanted in rabbit femurs, both types of monetite grafts demonstrated more resorption and greater bone formation than brushite grafts. The brushite grafts underwent phase conversion to form insoluble HA. Conversely, no phase conversion was observed in both types of monetites. The autoclaved monetites upon implantation generated greater amounts of new bone than the dry heat monetite grafts.

The onlay grafting experiments revealed that both types of monetite grafts achieved similar levels of vertical bone augmentation (as high as 3.2 mm). However, total resorption and bone volume percentage of the area augmented with autoclaved monetite grafts were significantly greater than their dry heat counterparts. The dry heat converted monetite grafts had greater mechanical

strength and could potentially be used in applications where higher graft strength is a prerequisite.

The alkali ion substituted calcium phosphate cements reinforced with silica appeared to have improved the solubility and the mechanical properties depending on the concentration of phytic acid used to set the materials. The concentration of phytic acid used to set cements had an inverse effect on mechanical properties. Lower concentration phytic acid set cements samples had higher compressive strengths in comparison to the brushite cements prepared in the first study. All cements set with different concentrations of phytic acid showed no phase conversion to apatite upon *in vitro* ageing. This indicates their potential to be utilised for orthopaedic and dental bone repair and regeneration applications.

It appears that it is not only the material composition that dictates graft behavior *in vivo* and *in vitro*, but is a combination of various physical and chemical characteristics. The differences in the physical and chemical characteristics of graft materials have a profound effect on the *in vivo* bone response and graft resorption. Graft cement resorption from implant site is a complex phenomenon and dependent on a variety of physiologic processes other than simple dissolution. The results obtained from the studies presented in this Ph.D thesis provides a better understanding of the graft degradation, resorption and bone formation processes allowing graft preparation in future with higher clinical efficacy.

Chapter 10: Bibliography

- 1. Gross RH. The use of bone grafts and bone graft substitutes in pediatric orthopaedics: an overview. Journal of pediatric orthopedics. 2012;32(1):100-5.**
- 2. Muschler GF, Negami S, Hyodo A, Gaisser D, Easley K, Kambic H. Evaluation of collagen ceramic composite graft materials in a spinal fusion model. Clin Orthop Relat R. 1996(328):250-60.**
- 3. Lewandrowski KU, Gresser JD, Wise DL, Trantolo DJ. Bioresorbable bone graft substitutes of different osteoconductivities: a histologic evaluation of osteointegration of poly(propylene glycol-co-fumaric acid)-based cement implants in rats. Biomaterials. 2000;21(8):757-64.**
- 4. Arrington ED, Smith WJ, Chambers HG, Bucknell AL, Davino NA. Complications of iliac crest bone graft harvesting. Clin Orthop Relat Res. 1996(329):300-9.**
- 5. Scarano A, Degidi M, Iezzi G, Pecora G, Piattelli M, Orsini G, et al. Maxillary sinus augmentation with different biomaterials: a comparative histologic and histomorphometric study in man. Implant dentistry. 2006;15(2):197-207.**
- 6. Chung CH, Wang SJ, Chang YC, Wu SS. Reconstruction of the coronoid process with iliac crest bone graft in complex fracture-dislocation of elbow. Archives of orthopaedic and trauma surgery. 2007;127(1):33-7.**
- 7. LeGeros RZ. Properties of osteoconductive biomaterials: calcium phosphates. Clin Orthop Relat Res. 2002(395):81-98.**

8. Moses O, Nemcovsky CE, Langer Y, Tal H. Severely resorbed mandible treated with iliac crest autogenous bone graft and dental implants: 17-year follow-up. *The International journal of oral & maxillofacial implants*. 2007;22(6):1017-21.
9. Sarkar MR, Wachter N, Patka P, Kinzl L. First histological observations on the incorporation of a novel calcium phosphate bone substitute material in human cancellous bone. *J Biomed Mater Res*. 2001;58(3):329-34.
10. Damien CJ, Parsons JR. Bone graft and bone graft substitutes: a review of current technology and applications. *Journal of applied biomaterials : an official journal of the Society for Biomaterials*. 1991;2(3):187-208. Epub 1991/10/01.
11. Van der Stok J, Van Lieshout EM, El-Massoudi Y, Van Kralingen GH, Patka P. Bone substitutes in the Netherlands - a systematic literature review. *Acta Biomater*. 2011;7(2):739-50.
12. Bauer TW, Muschler GF. Bone graft materials. An overview of the basic science. *Clin Orthop Relat Res*. 2000(371):10-27. Epub 2000/02/29.
13. Tamimi F, Torres J, Lopez-Cabarcos E, Bassett DC, Habibovic P, Luceron E, et al. Minimally invasive maxillofacial vertical bone augmentation using brushite based cements. *Biomaterials*. 2009;30(2):208-16.
14. Tamimi F, Torres J, Kathan C, Baca R, Clemente C, Blanco L, et al. Bone regeneration in rabbit calvaria with novel monetite granules. *Journal of Biomedical Materials Research Part A*. 2008;87A(4):980-5.
15. Tamimi F, Torres J, Bassett D, Barralet J, Cabarcos EL. Resorption of monetite granules in alveolar bone defects in human patients. *Biomaterials*. 2010;31(10):2762-9.

16. Tamimi F, Sheikh Z, Barralet J. Dicalcium phosphate cements: brushite and monetite. *Acta Biomater.* 2012;8(2):474-87.
17. Tamimi F, Torres J, Al-Abedalla K, Lopez-Cabarcos E, Alkhraisat MH, Bassett DC, et al. Osseointegration of dental implants in 3D-printed synthetic onlay grafts customized according to bone metabolic activity in recipient site. *Biomaterials.* 2014. Epub 2014/04/15.
18. Tamimi F, Le Nihouannen D, Eimar H, Sheikh Z, Komarova S, Barralet J. The effect of autoclaving on the physical and biological properties of dicalcium phosphate dihydrate bioceramics: brushite vs. monetite. *Acta Biomater.* 2012;8(8):3161-9.
19. Syftestad GT, Urist MR. Bone aging. *Clin Orthop Relat Res.* 1982(162):288-97.
20. Glimcher MJ. Bone: nature of the calcium phosphate crystals and cellular, structural, and physical chemical mechanisms in their formation. *Reviews in Mineralogy and Geochemistry.* 2006;64(1):223-82.
21. Taichman RS. Blood and bone: two tissues whose fates are intertwined to create the hematopoietic stem-cell niche. *Blood.* 2005;105(7):2631-9.
22. Urist MR, DeLange RJ, Finerman GA. Bone cell differentiation and growth factors. *Science.* 1983;220(4598):680-6.
23. Cypher TJ, Grossman JP. Biological principles of bone graft healing. *The Journal of foot and ankle surgery : official publication of the American College of Foot and Ankle Surgeons.* 1996;35(5):413-7.

24. Turner CH. Three rules for bone adaptation to mechanical stimuli. *Bone*. 1998;23(5):399-407.
25. Logan CY, Nusse R. The Wnt signaling pathway in development and disease. *Annu Rev Cell Dev Bi*. 2004;20:781-810.
26. Mackie EJ. Osteoblasts: novel roles in orchestration of skeletal architecture. *Int J Biochem Cell B*. 2003;35(9):1301-5.
27. Harada S, Rodan GA. Control of osteoblast function and regulation of bone mass. *Nature*. 2003;423(6937):349-55.
28. Einhorn TA. Clinically applied models of bone regeneration in tissue engineering research. *Clin Orthop Relat Res*. 1999(367 Suppl):S59-67. Epub 1999/11/05.
29. Manolagas SC. Birth and death of bone cells: Basic regulatory mechanisms and implications for the pathogenesis and treatment of osteoporosis. *J Aging Phys Activ*. 2000;8(3):248-.
30. Boyle WJ, Simonet WS, Lacey DL. Osteoclast differentiation and activation. *Nature*. 2003;423(6937):337-42.
31. Schmitz JP, Hollinger JO. The critical size defect as an experimental model for craniomandibulofacial nonunions. *Clin Orthop Relat Res*. 1986(205):299-308. Epub 1986/04/01.
32. Hollinger JO, Kleinschmidt JC. The critical size defect as an experimental model to test bone repair materials. *The Journal of craniofacial surgery*. 1990;1(1):60-8. Epub 1990/01/01.

33. Cowin SC. Bone poroelasticity. *J Biomech.* 1999;32(3):217-38.
34. Bellino FL, Wise PM. Nonhuman primate models of menopause workshop. *Biology of reproduction.* 2003;68(1):10-8. Epub 2002/12/21.
35. Marie PJ. Fibroblast growth factor signaling controlling osteoblast differentiation. *Gene.* 2003;316:23-32.
36. Salmon R, Duncan W. Determination of the critical size for non-healing defects in the mandibular bone of sheep. Part 1: A pilot study. *Journal of the New Zealand Society of Periodontology.* 1997(81):6-15. Epub 1997/01/01.
37. Toombs JP, Wallace LJ, Bjorling DE, Rowland GN. Evaluation of Key's hypothesis in the feline tibia: an experimental model for augmented bone healing studies. *American journal of veterinary research.* 1985;46(2):513-8. Epub 1985/02/01.
38. Kusumoto K, Bessho K, Fujimura K, Akioka J, Okubo Y, Ogawa Y, et al. The effect of blood supply in muscle and an elevated muscle flap on endogenous tissue-engineered bone by rhBMP-2 in the rat. *Annals of plastic surgery.* 2000;45(4):408-14. Epub 2000/10/19.
39. Kostenuik PJ, Halloran BP, Morey-Holton ER, Bikle DD. Skeletal unloading inhibits the in vitro proliferation and differentiation of rat osteoprogenitor cells. *The American journal of physiology.* 1997;273(6 Pt 1):E1133-9. Epub 1998/01/22.
40. Whyte MP. Hypophosphatasia and the Role of Alkaline-Phosphatase in Skeletal Mineralization. *Endocr Rev.* 1994;15(4):439-61.
41. Wolff D, Goldberg VM, Stevenson S. Histomorphometric analysis of the repair of a segmental diaphyseal defect with ceramic and titanium fibermetal

implants: effects of bone marrow. *Journal of orthopaedic research : official publication of the Orthopaedic Research Society*. 1994;12(3):439-46. Epub 1994/05/01.

42. Einhorn TA, Lane JM, Burstein AH, Kopman CR, Vigorita VJ. The healing of segmental bone defects induced by demineralized bone matrix. A radiographic and biomechanical study. *J Bone Joint Surg Am*. 1984;66(2):274-9. Epub 1984/02/01.

43. Mills LA, Simpson AH. In vivo models of bone repair. *J Bone Joint Surg Br*. 2012;94(7):865-74. Epub 2012/06/27.

44. Ohura K, Bohner M, Hardouin P, Lemaitre J, Pasquier G, Flautre B. Resorption of, and bone formation from, new beta-tricalcium phosphate-monocalcium phosphate cements: An in vivo study. *Journal of Biomedical Materials Research*. 1996;30(2):193-200.

45. Arsenault AL, Ottensmeyer FP. Visualization of early intramembranous ossification by electron microscopic and spectroscopic imaging. *The Journal of cell biology*. 1984;98(3):911-21.

46. Ely LW. The formation of bone. *Annals of surgery*. 1919;69(3):225.

47. Mackey MS, Stevens ML, Ebert DC, Tressler DL, Combs KS, Lowry CK, et al. The ferret as a small animal model with BMU-based remodeling for skeletal research. *Bone*. 1995;17(4 Suppl):191S-6S. Epub 1995/10/01.

48. Thompson Z, Miclau T, Hu D, Helms JA. A model for intramembranous ossification during fracture healing. *Journal of orthopaedic research*. 2002;20(5):1091-8.

49. Xian CJ, Zhou FH, McCarty RC, Foster BK. Intramembranous ossification mechanism for bone bridge formation at the growth plate cartilage injury site. *Journal of orthopaedic research*. 2004;22(2):417-26.
50. Rengachary SS. Bone morphogenetic proteins: basic concepts. *Neurosurgical focus*. 2002;13(6):1-6.
51. McLean FC, Bloom W. Calcification and ossification. Calcification in normal growing bone. *The Anatomical Record*. 1940;78(3):333-59.
52. Clarke B. Normal Bone Anatomy and Physiology. *Clin J Am Soc Nephro*. 2008;3:S131-S9.
53. Jerome CP, Peterson PE. Nonhuman primate models in skeletal research. *Bone*. 2001;29(1):1-6. Epub 2001/07/27.
54. Manolagas SC. Birth and death of bone cells: Basic regulatory mechanisms and implications for the pathogenesis and treatment of osteoporosis. *Endocr Rev*. 2000;21(2):115-37.
55. Doblare M, Garcia JM, Gomez MJ. Modelling bone tissue fracture and healing: a review. *Eng Fract Mech*. 2004;71(13-14):1809-40.
56. Aerssens J, Boonen S, Lowet G, Dequeker J. Interspecies differences in bone composition, density, and quality: potential implications for in vivo bone research. *Endocrinology*. 1998;139(2):663-70. Epub 1998/02/04.
57. Lammens J, Liu Z, Aerssens J, Dequeker J, Fabry G. Distraction bone healing versus osteotomy healing: a comparative biochemical analysis. *J Bone Miner Res*. 1998;13(2):279-86. Epub 1998/03/12.

58. Kenney EB, Lekovic V, Sa Ferreira JC, Han T, Dimitrijevic B, Carranza FA, Jr. Bone formation within porous hydroxylapatite implants in human periodontal defects. *J Periodontol.* 1986;57(2):76-83.
59. Chumlea W, Malina R, Rarick G, Seefeldt V. Growth of short bones of the hand in children with Down's syndrome. *Journal of Intellectual Disability Research.* 1979;23(2):137-50.
60. Dow E, Semwal S, editors. A framework for modeling the human muscle and bone shapes. *Proceedings of the Third International Conference on CAD and Computer Graphics;* 1993.
61. Wang X, Mabrey JD, Agrawal CM. An interspecies comparison of bone fracture properties. *Bio-medical materials and engineering.* 1998;8(1):1-9. Epub 1998/08/26.
62. Holstein JH, Garcia P, Histing T, Kristen A, Scheuer C, Menger MD, et al. Advances in the establishment of defined mouse models for the study of fracture healing and bone regeneration. *Journal of orthopaedic trauma.* 2009;23(5 Suppl):S31-8. Epub 2009/04/29.
63. Raisz LG. Physiology and pathophysiology of bone remodeling. *Clin Chem.* 1999;45(8):1353-8.
64. Frost HM, Straatsma C. Bone remodelling dynamics. *Plastic and reconstructive surgery.* 1964;33(2):196.
65. Fraher LJ. Biochemical Markers of Bone Turnover. *Clin Biochem.* 1993;26(6):431-2.
66. Parfitt AM. Targeted and nontargeted bone remodeling: relationship to basic multicellular unit origination and progression. *Bone.* 2002;30(1):5-7.

67. **Canalis E, Mccarthy TL, Centrella M. The Role of Growth-Factors in Skeletal Remodeling. Endocrin Metab Clin. 1989;18(4):903-18.**
68. **Burr DB. Targeted and nontargeted remodeling. Bone. 2002;30(1):2-4.**
69. **Grynpas MD, Holmyard DP, Pritzker KPH. Bone Mineralization and Histomorphometry in Biopsies of Osteoporotic Patients Treated with Fluoride. Cell Mater. 1994;4(3):287-97.**
70. **Turner CH, Roeder RK, Wiczorek A, Foroud T, Liu G, Peacock M. Variability in skeletal mass, structure, and biomechanical properties among inbred strains of rats. J Bone Miner Res. 2001;16(8):1532-9. Epub 2001/08/14.**
71. **Ferguson C, Alpern E, Miclau T, Helms JA. Does adult fracture repair recapitulate embryonic skeletal formation? Mechanisms of development. 1999;87(1):57-66.**
72. **Badrinath K. Bone fracture repair apparatus and method. Google Patents; 1993.**
73. **Burr DB, Martin RB, Schaffler MB, Radin EL. Bone remodeling in response to in vivo fatigue microdamage. J Biomech. 1985;18(3):189-200.**
74. **Newman E, Turner AS, Wark JD. The potential of sheep for the study of osteopenia: current status and comparison with other animal models. Bone. 1995;16(4 Suppl):277S-84S. Epub 1995/04/01.**
75. **Tsakamoto T, Pape HC. Animal models for trauma research: what are the options? Shock. 2009;31(1):3-10. Epub 2008/07/19.**

76. Trueta J. The Role of the Vessels in Osteogenesis. *J Bone Joint Surg Br.* 1963;45(2):402-18.
77. Glowacki J. Angiogenesis in fracture repair. *Clin Orthop Relat R.* 1998;355:S82-S9.
78. Gosain AK, Song L, Riordan P, Amarante MT, Nagy PG, Wilson CR, et al. A 1-year study of osteoinduction in hydroxyapatite-derived biomaterials in an adult sheep model: part I. Plastic and reconstructive surgery. 2002;109(2):619-30. Epub 2002/01/31.
79. Habibovic P, Gbureck U, Doillon CJ, Bassett DC, van Blitterswijk CA, Barralet JE. Osteoconduction and osteoinduction of low-temperature 3D printed bioceramic implants. *Biomaterials.* 2008;29(7):944-53. Epub 2007/12/07.
80. Denissen H, Martinetti R, van Lingen A, van den Hooff A. Normal osteoconduction and repair in and around submerged highly bisphosphonate-complexed hydroxyapatite implants in rat tibiae. *J Periodontol.* 2000;71(2):272-8.
81. Garrett S, Bogle G. Periodontal regeneration with bone grafts. *Current opinion in periodontology.* 1994:168-77.
82. Frayssinet P, Gineste L, Rouquet N. Osteointegration of different kinds of calcium phosphate biomaterials: Ceramics and hydraulic cements. *Morphologie.* 1998;82(256):3-7.
83. Goldberg VM, Stevenson S. Natural history of autografts and allografts. *Clin Orthop Relat Res.* 1987(225):7-16.
84. Goldberg VM. Natural history of autografts and allografts. *Bone implant grafting: Springer; 1992. p. 9-12.*

85. Younger EM, Chapman MW. Morbidity at bone graft donor sites. *Journal of orthopaedic trauma*. 1989;3(3):192-5.
86. Dodd CA, Fergusson CM, Freedman L, Houghton GR, Thomas D. Allograft versus autograft bone in scoliosis surgery. *J Bone Joint Surg Br*. 1988;70(3):431-4.
87. Summers BN, Eisenstein SM. Donor site pain from the ilium. A complication of lumbar spine fusion. *J Bone Joint Surg Br*. 1989;71(4):677-80.
88. Sandhu HS, Grewal HS, Parvataneni H. Bone grafting for spinal fusion. *The Orthopedic clinics of North America*. 1999;30(4):685-98.
89. Hauser CJ. Preclinical models of traumatic, hemorrhagic shock. *Shock*. 2005;24 Suppl 1:24-32. Epub 2005/12/24.
90. Heslop BF, Zeiss IM, Nisbet NW. Studies on transference of bone. I. A comparison of autologous and homologous bone implants with reference to osteocyte survival, osteogenesis and host reaction. *British journal of experimental pathology*. 1960;41:269-87.
91. Enneking WF, Burchardt H, Puhl JJ, Piotrowski G. Physical and biological aspects of repair in dog cortical-bone transplants. *J Bone Joint Surg Am*. 1975;57(2):237-52.
92. Duncan RL, Turner CH. Mechanotransduction and the functional response of bone to mechanical strain. *Calcified tissue international*. 1995;57(5):344-58.
93. Oxlund H, Andersen NB, Ortoft G, Orskov H, Andreassen TT. Growth hormone and mild exercise in combination markedly enhance cortical bone formation and strength in old rats. *Endocrinology*. 1998;139(4):1899-904.

94. Shetty V, Han TJ. Alloplastic materials in reconstructive periodontal surgery. *Dental clinics of North America*. 1991;35(3):521-30.
95. Centers for Disease C, Prevention. Septic arthritis following anterior cruciate ligament reconstruction using tendon allografts--Florida and Louisiana, 2000. *MMWR Morbidity and mortality weekly report*. 2001;50(48):1081-3.
96. Tomford WW. Transmission of disease through transplantation of musculoskeletal allografts. *J Bone Joint Surg Am*. 1995;77(11):1742-54.
97. Centers for Disease C, Prevention. Update: allograft-associated bacterial infections--United States, 2002. *MMWR Morbidity and mortality weekly report*. 2002;51(10):207-10.
98. Bolander ME, Balian G. The use of demineralized bone matrix in the repair of segmental defects. Augmentation with extracted matrix proteins and a comparison with autologous grafts. *J Bone Joint Surg Am*. 1986;68(8):1264-74.
99. Boyce T, Edwards J, Scarborough N. Allograft bone. The influence of processing on safety and performance. *The Orthopedic clinics of North America*. 1999;30(4):571-81.
100. Friedlaender GE, Strong DM, Sell KW. Studies on the antigenicity of bone. I. Freeze-dried and deep-frozen bone allografts in rabbits. *J Bone Joint Surg Am*. 1976;58(6):854-8.
101. Luepke PG, Mellonig JT, Brunsvold MA. A clinical evaluation of a bioresorbable barrier with and without decalcified freeze-dried bone allograft in the treatment of molar furcations. *Journal of Clinical Periodontology*. 1997;24(6):440-6.

102. Guillemin MR, Mellonig JT, Brunsvold MA. Healing in Periodontal Defects Treated by Decalcified Freeze-Dried Bone Allografts in Combination with Eptfe Membranes .1. Clinical and Scanning Electron-Microscope Analysis. *Journal of Clinical Periodontology*. 1993;20(7):528-36.
103. Mellonig JT. Freeze-dried bone allografts in periodontal reconstructive surgery. *Dental clinics of North America*. 1991;35(3):505-20.
104. Quattlebaum JB, Mellonig JT, Hensel NF. Antigenicity of freeze-dried cortical bone allograft in human periodontal osseous defects. *J Periodontol*. 1988;59(6):394-7.
105. Turner DW, Mellonig JT. Antigenicity of freeze-dried bone allograft in periodontal osseous defects. *Journal of periodontal research*. 1981;16(1):89-99.
106. Mellonig JT, Bowers GM, Bailey RC. Comparison of bone graft materials. Part I. New bone formation with autografts and allografts determined by Strontium-85. *J Periodontol*. 1981;52(6):291-6.
107. Russell J, Scarborough N, Chesmel K. Re: Ability of commercial demineralized freeze-dried bone allograft to induce new bone formation (1996;67:918-26). *J Periodontol*. 1997;68(8):804-6.
108. Urist MR, Chang JJ, Lietze A, Huo YK, Brownell AG, DeLange RJ. Preparation and bioassay of bone morphogenetic protein and polypeptide fragments. *Methods in enzymology*. 1987;146:294-312.
109. Mellonig JT, Valderrama P, Cochran DL. Clinical and histologic evaluation of calcium-phosphate bone cement in interproximal osseous defects in humans: a report in four patients. *The International journal of periodontics & restorative dentistry*. 2010;30(2):121-7.

110. Mellonig JT, Bowers GM, Cotton WR. Comparison of bone graft materials. Part II. New bone formation with autografts and allografts: a histological evaluation. *J Periodontol.* 1981;52(6):297-302.
111. Quintero G, Mellonig JT, Gambill VM, Pelleu GB, Jr. A six-month clinical evaluation of decalcified freeze-dried bone allografts in periodontal osseous defects. *J Periodontol.* 1982;53(12):726-30.
112. Bowers GM, Schallhorn RG, Mellonig JT. Histologic evaluation of new attachment in human intrabony defects. A literature review. *J Periodontol.* 1982;53(8):509-14.
113. Dodson SA, Bernard GW, Kenney EB, Carranza FA. In vitro comparison of aged and young osteogenic and hemopoietic bone marrow stem cells and their derivative colonies. *J Periodontol.* 1996;67(3):184-96.
114. Scarano A, Piattelli A, Perrotti V, Manzon L, Iezzi G. Maxillary sinus augmentation in humans using cortical porcine bone: a histological and histomorphometrical evaluation after 4 and 6 months. *Clinical implant dentistry and related research.* 2011;13(1):13-8.
115. Ramirez-Fernandez MP, Calvo-Guirado JL, Delgado-Ruiz RA, Mate-Sanchez del Val JE, Gomez-Moreno G, Guardia J. Experimental model of bone response to xenografts of bovine origin (Endobon): a radiological and histomorphometric study. *Clinical oral implants research.* 2011;22(7):727-34.
116. Jarcho M. Calcium phosphate ceramics as hard tissue prosthetics. *Clin Orthop Relat Res.* 1981(157):259-78.

117. Melcher AH, Dent HD. The use of heterogenous anorganic bone as an implant material in oral procedures. Oral surgery, oral medicine, and oral pathology. 1962;15:996-1000.
118. Emmings FG. Chemically modified osseous material for the restoration of bone defects. J Periodontol. 1974;45(5):385-90.
119. Wenz B, Oesch B, Horst M. Analysis of the risk of transmitting bovine spongiform encephalopathy through bone grafts derived from bovine bone. Biomaterials. 2001;22(12):1599-606.
120. Sogal A, Tofe AJ. Risk assessment of bovine spongiform encephalopathy transmission through bone graft material derived from bovine bone used for dental applications. J Periodontol. 1999;70(9):1053-63.
121. Boyne PJ. Bone induction and the use of HTR polymer as a vehicle for osseous inductor materials. Compendium. 1988(10):S337-41.
122. Guillemin G, Patat JL, Fournie J, Chetail M. The use of coral as a bone graft substitute. J Biomed Mater Res. 1987;21(5):557-67.
123. Yukna RA. Clinical evaluation of coralline calcium carbonate as a bone replacement graft material in human periodontal osseous defects. J Periodontol. 1994;65(2):177-85.
124. Piattelli A, Podda G, Scarano A. Clinical and histological results in alveolar ridge enlargement using coralline calcium carbonate. Biomaterials. 1997;18(8):623-7.

125. Mora F, Ouhayoun JP. Clinical evaluation of natural coral and porous hydroxyapatite implants in periodontal bone lesions: results of a 1-year follow-up. *J Clin Periodontol.* 1995;22(11):877-84.
126. Kim CK, Choi EJ, Cho KS, Chai JK, Wikesjo UM. Periodontal repair in intrabony defects treated with a calcium carbonate implant and guided tissue regeneration. *J Periodontol.* 1996;67(12):1301-6.
127. Gao TJ, Tuominen TK, Lindholm TS, Kommonen B, Lindholm TC. Morphological and biomechanical difference in healing in segmental tibial defects implanted with Biocoral or tricalcium phosphate cylinders. *Biomaterials.* 1997;18(3):219-23.
128. Yung M. Literature review of alloplastic materials in ossiculoplasty. *The Journal of Laryngology & Otology.* 2003;117(06):431-6.
129. Eppley BL, Pietrzak WS, Blanton MW. Allograft and alloplastic bone substitutes: a review of science and technology for the craniomaxillofacial surgeon. *Journal of Craniofacial Surgery.* 2005;16(6):981-9.
130. Tencer AF, Woodard PL, Swenson J, Brown KL. Mechanical and bone ingrowth properties of a polymer-coated, porous, synthetic, coralline hydroxyapatite bone-graft material. *Annals of the New York Academy of Sciences.* 1988;523:157-72. Epub 1988/01/01.
131. Tayton E, Fahmy S, Purcell M, Aarvold A, Smith JO, Kalra S, et al. An analysis of polymer type and chain length for use as a biological composite graft extender in impaction bone grafting: a mechanical and biocompatibility study. *Journal of biomedical materials research Part A.* 2012;100(12):3211-9. Epub 2012/06/19.

132. Sokolsky-Papkov M, Agashi K, Olaye A, Shakesheff K, Domb AJ. Polymer carriers for drug delivery in tissue engineering. *Advanced drug delivery reviews*. 2007;59(4-5):187-206.
133. Yukna RA. HTR polymer grafts in human periodontal osseous defects. I. 6-month clinical results. *J Periodontol*. 1990;61(10):633-42.
134. Stahl SS, Froum SJ, Tarnow D. Human clinical and histologic responses to the placement of HTR polymer particles in 11 intrabony lesions. *J Periodontol*. 1990;61(5):269-74.
135. Yukna RA, Greer RO, Jr. Human gingival tissue response to HTR polymer. *J Biomed Mater Res*. 1992;26(4):517-27.
136. Murray VK. Clinical applications of HTR polymer in periodontal surgery. *Compendium*. 1988(10):S342-7.
137. Buck BE, Malinin TI, Brown MD. Bone transplantation and human immunodeficiency virus. An estimate of risk of acquired immunodeficiency syndrome (AIDS). *Clin Orthop Relat Res*. 1989(240):129-36.
138. Zhao S, Li Y, Li D. Synthesis of CaO-SiO₂-P₂O₅ mesoporous bioactive glasses with high P₂O₅ content by evaporation induced self assembly process. *J Mater Sci Mater Med*. 2011;22(2):201-8. Epub 2010/12/21.
139. Vallet-Regi M, Izquierdo-Barba I, Salinas AJ. Influence of P₂O₅ on crystallinity of apatite formed in vitro on surface of bioactive glasses. *J Biomed Mater Res*. 1999;46(4):560-5. Epub 1999/07/09.
140. Hench LL, Wilson J. Surface-active biomaterials. *Science*. 1984;226(4675):630-6.

141. Thompson ID, Hench LL. Mechanical properties of bioactive glasses, glass-ceramics and composites. *Proceedings of the Institution of Mechanical Engineers Part H, Journal of engineering in medicine*. 1998;212(2):127-36. Epub 1998/06/05.
142. el-Ghannam A, Ducheyne P, Shapiro IM. Formation of surface reaction products on bioactive glass and their effects on the expression of the osteoblastic phenotype and the deposition of mineralized extracellular matrix. *Biomaterials*. 1997;18(4):295-303.
143. Hamadouche M, Nizard RS, Meunier A, Blanchat C, Sedel L. [Osteoconductive properties of bioactive glasses in a bulk form and as a coating on alumina]. *Revue de chirurgie orthopedique et reparatrice de l'appareil moteur*. 2000;86(2):162-72. Epub 2000/05/11. Evaluation du caractere osteoconducteur de verres bioactifs sous forme massive et en revetement sur de l'alumine.
144. Chan HL, Wang HL. Using bioactive glasses for the treatment of periodontal intrabony defects may result in modest probing depth reduction and clinical attachment level gain compared to open flap debridement. *The journal of evidence-based dental practice*. 2012;12(4):209-11. Epub 2012/11/28.
145. Bohner M. Calcium orthophosphates in medicine: from ceramics to calcium phosphate cements. *Injury*. 2000;31:37-47.
146. Hollinger JO, Brekke J, Gruskin E, Lee D. Role of bone substitutes. *Clin Orthop Relat Res*. 1996(324):55-65.
147. Oh S, Oh N, Appleford M, Ong JL. Bioceramics for Tissue Engineering Applications-A Review. *American Journal of Biochemistry & Biotechnology*. 2006;2(2).

148. Hing K. Bioceramic bone graft substitutes: influence of porosity and chemistry. *Int J Appl Ceram Technol.* 2005;2:184-99.
149. Heimann RB. Materials science of crystalline bioceramics: a review of basic properties and applications. *CMU Journal.* 2002;1(1):23-46.
150. Dorozhkin SV. Calcium orthophosphate cements for biomedical application. *Journal of Materials Science.* 2008;43(9):3028-57.
151. Lemaitre J, Mirtchi AA, Mortier A. Calcium phosphate cements for medical use: state of the art and perspectives of development. *Silicates Industriels.* 1987;10:141-6.
152. Lemaitre J, Munting E, Mirtchi AA. Setting, hardening and resorption of calcium phosphate hydraulic cements. *Rev Stomatol Chir Maxillofac.* 1992;93(3):163-5.
153. Han B, Ma PW, Zhang LL, Yin YJ, Yao KD, Zhang FJ, et al. beta-TCP/MCPM-based premixed calcium phosphate cements. *Acta Biomaterialia.* 2009;5(8):3165-77.
154. Oh KS, Kim SR. Effect of the composition in beta-TCP-MCPM bone cement containing dense beta-TCP granules. *Bioceramics* 17. 2005;284-286:141-4.
155. Pina S, Torres PMC, Ferreira JMF. Injectability of brushite-forming Mg-substituted and Sr-substituted alpha-TCP bone cements. *Journal of Materials Science-Materials in Medicine.* 2010;21(2):431-8.
156. Strub JR, Gaberthuel TW, Firestone AR. Comparison of tricalcium phosphate and frozen allogenic bone implants in man. *J Periodontol.* 1979;50(12):624-9.

157. Flautre B, Maynou C, Lemaitre J, Van Landuyt P, Hardouin P. Bone colonization of beta-TCP granules incorporated in brushite cements. *Journal of Biomedical Materials Research*. 2002;63(4):413-7.
158. Tamimi FM, Torres J, Tresguerres I, Clemente C, Lopez-Cabarcos E, Blanco LJ. Bone augmentation in rabbit calvariae: comparative study between Bio-Oss (R) and a novel beta-TCP/DCPD granulate. *Journal of Clinical Periodontology*. 2006;33(12):922-8.
159. Klein CP, Driessen AA, de Groot K, van den Hooff A. Biodegradation behavior of various calcium phosphate materials in bone tissue. *J Biomed Mater Res*. 1983;17(5):769-84.
160. Meffert RM, Thomas JR, Hamilton KM, Brownstein CN. Hydroxylapatite as an alloplastic graft in the treatment of human periodontal osseous defects. *J Periodontol*. 1985;56(2):63-73.
161. Rabalais ML, Jr., Yukna RA, Mayer ET. Evaluation of durapatite ceramic as an alloplastic implant in periodontal osseous defects. I. Initial six-month results. *J Periodontol*. 1981;52(11):680-9.
162. Wagner JR. Clinical and histological case study using resorbable hydroxylapatite for the repair of osseous defects prior to endosseous implant surgery. *The Journal of oral implantology*. 1989;15(3):186-92.
163. Ricci JL, Blumenthal NC, Spivak JM, Alexander H. Evaluation of a low-temperature calcium phosphate particulate implant material: physical-chemical properties and in vivo bone response. *Journal of oral and maxillofacial surgery : official journal of the American Association of Oral and Maxillofacial Surgeons*. 1992;50(9):969-78.

164. Mirtchi AA, Lemaitre J, Munting E. Calcium-phosphate-cements - Action of setting regulators on the properties of the beta-tricalcium phosphate monocalcium phosphate cements. *Biomaterials*. 1989;10(9):634-8.
165. Mirtchi AA, Lemaitre J, Munting E. Calcium-phosphate-cements- Study of the beta-tricalcium phosphate dicalcium phosphate calcite cements *Biomaterials*. 1990;11(2):83-8.
166. Tamimi F, Sheikh Z, Barralet J. Dicalcium phosphate cements: Brushite and monetite. *Acta Biomaterialia*. 2012;8(2):474-87.
167. Bohner M, Merkle HP, Lemaitre J. In vitro aging of a calcium phosphate cement. *Journal of Materials Science: Materials in Medicine*. 2000;11(3):155-62.
168. Pina S, Torres PM, Goetz-Neunhoeffler F, Neubauer J, Ferreira JMF. Newly developed Sr-substituted alpha-TCP bone cements. *Acta Biomaterialia*. 2010;6(3):928-35.
169. Bohner M, Merkle HP, Landuyt PV, Trophard G, Lemaitre J. Effect of several additives and their admixtures on the physico-chemical properties of a calcium phosphate cement. *Journal of Materials Science-Materials in Medicine*. 1999;11(2):111-6.
170. Nurit J, Margerit J, Terol A, Boudeville P. pH-metric study of the setting reaction of monocalcium phosphate monohydrate/calcium oxide-based cements. *Journal of Materials Science-Materials in Medicine*. 2002;13(11):1007-14.
171. Desai TR, Bhaduri SB, Tas AC. A self-setting, monetite (CaHPO₄) cement for skeletal repair. *Advances in Bioceramics and Biocomposites II*. 2007;27(6):61-9.

172. Lilley KJ, Gbureck U, Wright AJ, Farrar DF, Barralet JE. Cement from nanocrystalline hydroxyapatite: Effect of calcium phosphate ratio. *Journal of Materials Science-Materials in Medicine*. 2005;16(12):1185-90.
173. Barralet JE, Lilley KJ, Grover LM, Farrar DF, Ansell C, Gbureck U. Cements from nanocrystalline hydroxyapatite. *Journal of Materials Science-Materials in Medicine*. 2004;15(4):407-11.
174. Martin RI, Brown PW. Phase equilibria among acid calcium phosphates. *Journal of the American Ceramic Society*. 1997;80(5):1263-6.
175. Lilley KJ, Gbureck U, Knowles JC, Farrar DF, Barralet JE. Cement from magnesium substituted hydroxyapatite. *Journal of Materials Science-Materials in Medicine*. 2005;16(5):455-60.
176. Marino FT, Torres J, Hamdan M, Rodriguez CR, Cabarcos EL. Advantages of using glycolic acid as a retardant in a brushite forming cement. *Journal of Biomedical Materials Research Part B-Applied Biomaterials*. 2007;83B:571-9.
177. Frayssinet P, Gineste L, Conte P, Fages J, Rouquet N. Short-term implantation effects of a DCPD-based calcium phosphate cement. *Biomaterials*. 1998;19(11-12):971-7.
178. Bohner M, Lemaitre J, Ring TA. Effects of sulfate, pyrophosphate, and citrate ions on the physicochemical properties of cements made of beta-tricalcium phosphate-phosphoric acid-water mixtures. *Journal of the American Ceramic Society*. 1996;79(6):1427-34.
179. Van Landuyt P, Lowe C, Lemaitre J. Optimization of setting time and mechanical strength of beta-TCP/MCPM cements. *Bioceramics, Vol 10*. 1997:477-80.

180. Grover LM, Gbureck U, Young AM, Wright AJ, Barralet JE. Temperature dependent setting kinetics and mechanical properties of beta-TCP-pyrophosphoric acid bone cement. *Journal of Materials Chemistry*. 2005;15(46):4955-62.
181. Moseley JP, Carroll ME, McCanless JD, inventors; Wright Medical Technology Inc, assignee. Particulate composition used for bone graft substitute cement for, e.g. treating bone defect, comprises alpha-calcium sulfate hemihydrate powder, and calcium phosphate powders combination that forms brushite in presence of aqueous solution patent US2010249794-A1. 2010.
182. Barralet JE, Grover LM, Gbureck U. Ionic modification of calcium phosphate cement viscosity. Part II: hypodermic injection and strength improvement of brushite cement. *Biomaterials*. 2004;25(11):2197-203.
183. Alkhraisat MH, Marino FT, Retama JR, Jerez LB, Lopez-Cabarcos E. Beta-tricalcium phosphate release from brushite cement surface. *Journal of Biomedical Materials Research Part A*. 2008;84A(3):710-7.
184. Giocondi JL, El-Dasher BS, Nancollas GH, Orme CA. Molecular mechanisms of crystallization impacting calcium phosphate cements. *Philosophical Transactions of the Royal Society a-Mathematical Physical and Engineering Sciences*. 2010;368(1917):1937-61.
185. Tamimi F, Kumarasami B, Doillon C, Gbureck U, Le Nihouannen D, Cabarcos EL, et al. Brushite-collagen composites for bone regeneration. *Acta Biomaterialia*. 2008;4(5):1315-21.
186. Guo F, Li B. Effects of collagen on the properties of TTCP/MCPM bone cement. *Sheng Wu Yi Xue Gong Cheng Xue Za Zhi*. 2010;27(2):328-31.

187. Gbureck U, Vorndran E, Muller FA, Barralet JE. Low temperature direct 3D printed bioceramics and biocomposites as drug release matrices. *Journal of Controlled Release*. 2007;122:173-80.
188. Gorst NJS, Perrie Y, Gbureck U, Hutton AL, Hofmann MP, Grover LM, et al. Effects of fibre reinforcement on the mechanical properties of brushite cement. *Acta Biomaterialia*. 2006;2(1):95-102.
189. Young AM, Ho SM, Abou Neel EA, Ahmed I, Barralet JE, Knowles JC, et al. Chemical characterization of a degradable polymeric bone adhesive containing hydrolysable fillers and interpretation of anomalous mechanical properties. *Acta Biomaterialia*. 2009;5(6):2072-83.
190. Alkhraisat MH, Rueda C, Jerez LB, Marino FT, Torres J, Gbureck U, et al. Effect of silica gel on the cohesion, properties and biological performance of brushite cement. *Acta Biomaterialia*. 2010;6(1):257-65.
191. Flautre B, Lemaitre J, Maynou C, Van Landuyt P, Hardouin P. Influence of polymeric additives on the biological properties of brushite cements: an experimental study in rabbit. *Journal of Biomedical Materials Research Part A*. 2003;66A(2):214-23.
192. Chauhan S, Hofmann MP, Shelton RM. Effect of protein addition on the setting behaviour of a calcium phosphate cement. *Bioceramics* 18, Pts 1 and 2. 2006;309-311:841-4.
193. Alkhraisat MH, Rueda C, Marino FT, Torres J, Jerez LB, Gbureck U, et al. The effect of hyaluronic acid on brushite cement cohesion. *Acta Biomater*. 2009;5(8):3150-6.

194. Bohner M, Matter S, inventors; Mathys Stiftung H C Robert; Stratec Medical Ag; Synthes Gmbh; Stiftung Mathys Stratec Medical Ag H C R, assignee. Hydraulic calcium phosphate cement for teeth and bone repair patent WO200141824-A; EP1235599-A; WO200141824-A1; AU200013721-A; BR9917570-A; EP1235599-A1; KR2002064926-A; CN1378464-A; JP2003516190-W; EP1235599-B1; DE69909850-E; AU766371-B; US6733582-B1; MX2002004591-A1; MX239978-B; CA2391947-C; ZA200202800-A; ES2204198-T3; CN101347635-A. 2001.

195. Alkhraisat MH, Marino FT, Rodriguez CR, Jerez LB, Cabarcos EL. Combined effect of strontium and pyrophosphate on the properties of brushite cements. *Acta Biomaterialia*. 2008;4(3):664-70.

196. Huan ZG, Chang J. Novel. bioactive composite bone cements based on the beta-tricalcium phosphate-monocalcium phosphate monohydrate composite cement system. *Acta Biomaterialia*. 2009;5(4):1253-64.

197. Pina S, Vieira SI, Rego P, Torres PMC, Silva O, Silva E, et al. Biological responses of brushite-forming Zn- and ZnSr-substituted beta-tricalcium phosphate bone cements. *European Cells & Materials*. 2010;20:162-77.

198. Alkhraisat MH, Moseke C, Blanco L, Barralet JE, Lopez-Carbacos E, Gbureck U. Strontium modified biocements with zero order release kinetics. *Biomaterials*. 2008;29(35):4691-7.

199. Klammert U, Reuther T, Blank M, Reske I, Barralet JE, Grover LM, et al. Phase composition, mechanical performance and in vitro biocompatibility of hydraulic setting calcium magnesium phosphate cement. *Acta Biomaterialia*. 2010;6(4):1529-35.

200. Pina S, Olhero SM, Gheduzzi S, Miles AW, Ferreira JMF. Influence of setting liquid composition and liquid-to-powder ratio on properties of a Mg-substituted calcium phosphate cement. *Acta Biomaterialia*. 2009;5(4):1233-40.
201. Bohner M, vanLanduyt P, Merkle HP, Lemaitre J. Composition effects on the pH of a hydraulic calcium phosphate cement. *Journal of Materials Science-Materials in Medicine*. 1997;8(11):675-81.
202. Bohner M, Gbureck U. Thermal reactions of brushite cements. *Journal of Biomedical Materials Research Part B-Applied Biomaterials*. 2008;84B(2):375-85.
203. Tamimi-Marino F, Mastio J, Rueda C, Blanco L, Lopez-Cabarcos E. Increase of the final setting time of brushite cements by using chondroitin 4-sulfate and silica gel. *Journal of Materials Science-Materials in Medicine*. 2007;18(6):1195-201.
204. Bohner M, Lemaitre J, VanLanduyt P, Zambelli PY, Merkle HP, Gander B. Gentamicin-loaded hydraulic calcium phosphate bone cement as antibiotic delivery system. *Journal of Pharmaceutical Sciences*. 1997;86(5):565-72.
205. Bohner M, Theiss F, Apelt D, Hirsiger W, Houriet R, Rizzoli G, et al. Compositional changes of a dicalcium phosphate dihydrate cement after implantation in sheep. *Biomaterials*. 2003;24(20):3463-74.
206. Pina S, Vieira SI, Torres PMC, Goetz-Neunhoeffler F, Neubauer J, Silva O, et al. In Vitro performance assessment of new brushite-forming Zn- and ZnSr-substituted beta-TCP bone cements. *Journal of Biomedical Materials Research Part B-Applied Biomaterials*. 2010;94B(2):414-20.

207. Gbureck U, Hozel T, Klammert U, Wurzler K, Muller FA, Barralet JE. Resorbable dicalcium phosphate bone substitutes prepared by 3D powder printing. *Advanced Functional Materials*. 2007;17(18):3940-5.
208. Alshaaer M, Cuypers H, Rahier H, Wastiels J. Production of monetite-based Inorganic Phosphate Cement (M-IPC) using hydrothermal post curing (HTPC). *Cement and Concrete Research*. 2011;41(1):30-7.
209. Jokic B, Mitric M, Radmilovic V, Drmanic S, Petrovic R, Janackovic D. Synthesis and characterization of monetite and hydroxyapatite whiskers obtained by a hydrothermal method. *Ceramics International*. 2011;37(1):167-73.
210. Eshtiagh-Hosseini H, Houssaindokht MR, Chahkandhi M, Youssefi A. Preparation of anhydrous dicalcium phosphate, DCPA, through sol-gel process, identification and phase transformation evaluation. *Journal of Non-Crystalline Solids*. 2008;354(32):3854-7.
211. Hofmann MP, Young AM, Gbureck U, Nazhat SN, Barralet JE. FTIR-monitoring of a fast setting brushite bone cement: effect of intermediate phases. *Journal of Materials Chemistry*. 2006;16(31):3199-206.
212. Galea LG, Bohner M, Lemaitre J, Kohler T, Muller R. Bone substitute: Transforming beta-tricalcium phosphate porous scaffolds into monetite. *Biomaterials*. 2008;29(24-25):3400-7.
213. Gbureck U, Dembski S, Thull R, Barralet JE. Factors influencing calcium phosphate cement shelf-life. *Biomaterials*. 2005;26(17):3691-7.
214. Haghbin-Nazarpak M, Moztarzadeh F, Solati-Hashjin M, Mirhabibi AR, Tahriri M. Preparation, characterization and gentamycin sulfate release

investigation of biphasic injectable calcium phosphate bone cement. *Ceramics-Silikaty*. 2010;54(4):334-40.

215. Mosselmans G, Biesemans M, Willem R, Wastiels J, Leermakers M, Rahier H, et al. Thermal hardening and structure of a phosphorus containing cementitious model material. *Journal of Thermal Analysis and Calorimetry*. 2007;88(3):723-9.

216. Hofmann MP, Mohammed AR, Perrie Y, Gbureck U, Barralet JE. High-strength resorbable brushite bone cement with controlled drug-releasing capabilities. *Acta Biomaterialia*. 2009;5(1):43-9.

217. Pioletti DP, Takei H, Lin T, Van Landuyt P, Ma QJ, Kwon SY, et al. The effects of calcium phosphate cement particles on osteoblast functions. *Biomaterials*. 2000;21(11):1103-14.

218. Charriere E, Terrazzoni S, Pittet C, Mordasini P, Dutoit M, Lemaitre J, et al. Mechanical characterization of brushite and hydroxyapatite cements. *Biomaterials*. 2001;22(21):2937-45.

219. Grover LM, Hofmann MP, Gbureck U, Kumarasami B, Barralet JE. Frozen delivery of brushite calcium phosphate cements. *Acta Biomaterialia*. 2008;4(6):1916-23.

220. Apelt D, Theiss F, El-Warrak AO, Zlinszky K, Bettschart-Wolfisberger R, Bohner M, et al. In vivo behavior of three different injectable hydraulic calcium phosphate cements. *Biomaterials*. 2004;25(7-8):1439-51.

221. Oberle A, Theiss F, Bohner M, Muller J, Kastner SB, Frei C, et al. Investigation about the clinical use of brushite-and hydroxylapatite-cement in sheep. *Schweizer Archiv Fur Tierheilkunde*. 2005;147(11):482-90.

222. Theiss F, Apelt D, Brand BA, Kutter A, Zlinszky K, Bohner M, et al. Biocompatibility and resorption of a brushite calcium phosphate cement. *Biomaterials*. 2005;26(21):4383-94.
223. Kuemmerle JM, Oberle A, Oechslin C, Bohner M, Frei C, Boecken I, et al. Assessment of the suitability of a new brushite calcium phosphate cement for cranioplasty - an experimental study in sheep. *Journal of Cranio-Maxillofacial Surgery*. 2005;33(1):37-44.
224. Grossardt C, Ewald A, Grover LM, Barralet JE, Gbureck U. Passive and Active In Vitro Resorption of Calcium and Magnesium Phosphate Cements by Osteoclastic Cells. *Tissue Engineering Part A*. 2010;16(12):3687-95.
225. Constantz BR, Barr BM, Ison IC, Fulmer MT, Baker J, McKinney L, et al. Histological, chemical, and crystallographic analysis of four calcium phosphate cements in different rabbit osseous sites. *J Biomed Mater Res*. 1998;43(4):451-61.
226. Xia ZD, Grover LM, Huang YZ, Adamopoulos LE, Gbureck U, Triffitt JT, et al. In vitro biodegradation of three brushite calcium phosphate cements by a macrophage cell-line. *Biomaterials*. 2006;27(26):4557-65.
227. Ikenaga M, Hardouin P, Lemaitre J, Andrianjatovo H, Flautre B. Biomechanical characterization of a biodegradable calcium phosphate hydraulic cement: a comparison with porous biphasic calcium phosphate ceramics. *J Biomed Mater Res*. 1998;40(1):139-44.
228. Grover LM, Knowles JC, Fleming GJP, Barralet JE. In vitro ageing of brushite calcium phosphate cement. *Biomaterials*. 2003;24(23):4133-41.
229. Grover LM, Gbureck U, Wright AJ, Tremayne M, Barralet JE. Biologically mediated resorption of brushite cement in vitro. *Biomaterials*. 2006;27(10):2178-85.

230. Jiang WG, Chu XB, Wang B, Pan HH, Xu XR, Tang RK. Biomimetically Triggered Inorganic Crystal Transformation by Biomolecules: A New Understanding of Biomineralization. *Journal of Physical Chemistry B*. 2009;113(31):10838-44.
231. Tamimi F, Torres J, Gbureck U, Lopez-Cabarcos E, Bassett DC, Alkhraisat MH, et al. Craniofacial vertical bone augmentation: A comparison between 3D printed monolithic monetite blocks and autologous onlay grafts in the rabbit. *Biomaterials*. 2009;30(31):6318-26.
232. Flautre B, Delecourt C, Blary MC, Van Landuyt P, Lemaitre J, Hardouin P. Volume effect on biological properties of a calcium phosphate hydraulic cement: Experimental study in sheep. *Bone*. 1999;25(2):35S-9S.
233. Munting E, Mirtchi AA, Lemaitre J. Bone repair of defects filled with phosphoclastic hydraulic cement- an in vitro study. *Journal of Materials Science-Materials in Medicine*. 1993;4(3):337-44.
234. Lu JX, About I, Stephan G, Van Landuyt P, Dejou J, Fiocchi M, et al. Histological and biomechanical studies of two bone colonizable cements in rabbits. *Bone*. 1999;25(2):41S-5S.
235. Marinno FT, Torres J, Tresguerres I, Jerez LB, Cabarcos EL. Vertical bone augmentation with granulated brushite cement set in glycolic acid. *Journal of Biomedical Materials Research Part A*. 2007;81A(1):93-102.
236. Habibovic P, Gbureck U, Doillon CJ, Bassett DC, van Blitterswijk CA, Barralet JE. Osteoconduction and osteoinduction of low-temperature 3D printed bioceramic implants. *Biomaterials*. 2008;29(7):944-53.

237. Klammert U, Reuther T, Jahn C, Kraski B, Kubler AC, Gbureck U. Cytocompatibility of brushite and monetite cell culture scaffolds made by three-dimensional powder printing. *Acta Biomaterialia*. 2009;5(2):727-34.
238. Penel G, Leroy N, Van Landuyt P, Flautre B, Hardouin P, Lemaitre J, et al. Raman microspectrometry studies of brushite cement: In vivo evolution in a sheep model. *Bone*. 1999;25(2):81S-4S.
239. De la Riva B, Sanchez E, Hernandez A, Reyes R, Tamimi F, Lopez-Cabarcos E, et al. Local controlled release of VEGF and PDGF from a combined brushite-chitosan system enhances bone regeneration. *Journal of Controlled Release*. 2010;143(1):45-52.
240. Schneider G, Blehschmidt K, Linde D, Litschko P, Korbs T, Beletes E. Bone regeneration with glass ceramic implants and calcium phosphate cements in a rabbit cranial defect model. *J Mater Sci Mater Med*. 2010;21(10):2853-9.
241. Bohner M, Matter S. Effect of bioglass granules on the physico-chemical properties of brushite cements. *Bioceramics*. 2000;192-1:809-12.
242. Le Nihouannen D, Hacking SA, Gbureck U, Komarova SV, Barralet JE. The use of RANKL-coated brushite cement to stimulate bone remodelling. *Biomaterials*. 2008;29(22):3253-9.
243. Ryf C, Goldhahn S, Radziejowski M, Blauth M, Hanson B. A New Injectable Brushite Cement: First Results in Distal Radius and Proximal Tibia Fractures. *European Journal of Trauma and Emergency Surgery*. 2009;35(4):389-96.
244. Heini PF, Berlemann U, Kaufmann M, Lippuner K, Fankhauser C, van Landuyt P. Augmentation of mechanical properties in osteoporotic vertebral bones -

a biomechanical investigation of vertebroplasty efficacy with different bone cements. European Spine Journal. 2001;10(2):164-71.

245. Van Landuyt P, Peter B, Beluze L, Lemaitre J. Reinforcement of osteosynthesis screws with brushite cement. Bone. 1999;25(2):95S-8S.

246. Paxton JZ, Donnelly K, Keatch RP, Baar K, Grover LM. Factors Affecting the Longevity and Strength in an In Vitro Model of the Bone-Ligament Interface. Annals of Biomedical Engineering. 2010;38(6):2155-66.

247. Mehrban N, Paxton JZ, Bowen J, Bolarinwa A, Vorndran E, Gbureck U, et al. Comparing physicochemical properties of printed and hand cast biocements designed for ligament replacement. Advances in Applied Ceramics. 2011;110(3):162-7.

248. Wen CY, Qin L, Lee KM, Chan KM. The Use of Brushite Calcium Phosphate Cement for Enhancement of Bone-Tendon Integration in an Anterior Cruciate Ligament Reconstruction Rabbit Model. Journal of Biomedical Materials Research Part B-Applied Biomaterials. 2009;89B(2):466-74.

249. Paxton JZ, Grover LM, Baar K. Engineering an In Vitro Model of a Functional Ligament from Bone to Bone. Tissue Engineering Part A. 2010;16(11):3515-25.

250. Gehrke SA FG. Buccal dehiscence and sinus lift cases - Predictable bone augmentation with synthetic bone material. implants. 2010;11(1):4.

251. Ji C, Ahn JG. Clinical Experience of the Brushite Calcium Phosphate Cement for the Repair and Augmentation of Surgically Induced Cranial Defects Following the Pterional Craniotomy. Journal of Korean Neurosurgical Society. 2010;47(3):180-4.

252. Klammert U, Gbureck U, Vorndran E, Rodiger J, Meyer-Marcotty P, Kubler AC. 3D powder printed calcium phosphate implants for reconstruction of cranial and maxillofacial defects. *Journal of Cranio-Maxillofacial Surgery*. 2010;38(8):565-70.
253. Tamimi F, Torres J, Bettini R, Ruggera F, Rueda C, Lopez-Ponce M, et al. Doxycycline sustained release from brushite cements for the treatment of periodontal diseases. *Journal of Biomedical Materials Research Part A*. 2008;85A(3):707-14.
254. Alkhraisat MH, Rueda C, Cabrejos-Azama J, Lucas-Aparicio J, Marino FT, Garcia-Denche JT, et al. Loading and release of doxycycline hyclate from strontium-substituted calcium phosphate cement. *Acta Biomaterialia*. 2010;6(4):1522-8.
255. Young AM, Ng PYJ, Gbureck U, Nazhat SN, Barralet JE, Hofmann MP. Characterization of chlorhexidine-releasing, fast-setting, brushite bone cements. *Acta Biomaterialia*. 2008;4(4):1081-8.
256. Barralet J, Gbureck U, Habibovic P, Vorndran E, Gerard C, Doillon CJ. Angiogenesis in calcium phosphate scaffolds by inorganic copper ion release. *Tissue engineering Part A*. 2009;15(7):1601-9. Epub 2009/02/03.
257. Vorndran E, Ewald A, Muller FA, Zorn K, Kufner A, Gbureck U. Formation and properties of magnesium-ammonium-phosphate hexahydrate biocements in the Ca-Mg-PO₄ system. *Journal of Materials Science-Materials in Medicine*. 2011;22(3):429-36.
258. Lopez MSP, Lopez-Ruiz B. A Sensitive Glucose Biosensor Based on Brushite, a Biocompatible Cement. *Electroanalysis*. 2011;23(1):280-6.

259. Sanchez-Paniagua Lopez M, Tamimi F, Lopez-Cabarcos E, Lopez-Ruiz B. Highly sensitive amperometric biosensor based on a biocompatible calcium phosphate cement. *Biosens Bioelectron.* 2009;24(8):2574-9.
260. Neyt JG, Buckwalter JA, Carroll NC. Use of animal models in musculoskeletal research. *The Iowa orthopaedic journal.* 1998;18:118-23. Epub 1998/11/10.
261. Gilsanz V, Roe TF, Gibbens DT, Schulz EE, Carlson ME, Gonzalez O, et al. Effect of sex steroids on peak bone density of growing rabbits. *The American journal of physiology.* 1988;255(4 Pt 1):E416-21. Epub 1988/10/01.
262. Wang XD, Masilamani NS, Mabrey JD, Alder ME, Agrawal CM. Changes in the fracture toughness of bone may not be reflected in its mineral density, porosity, and tensile properties. *Bone.* 1998;23(1):67-72. Epub 1998/07/14.
263. Cunin G, Boissonnet H, Petite H, Blanchat C, Guillemin G. Experimental vertebroplasty using osteoconductive granular material. *Spine.* 2000;25(9):1070-6. Epub 2000/05/02.
264. Martiniakova M, Omelka R, Chrenek P, Ryban L, Parkanyi V, Grosskopf B, et al. Changes of femoral bone tissue microstructure in transgenic rabbits. *Folia biologica.* 2005;51(5):140-4. Epub 2005/11/16.
265. Lowell S, Shields JE. Powder surface area and porosity: Springer; 1991.
266. Pierotti R, Rouquerol J. Reporting physisorption data for gas/solid systems with special reference to the determination of surface area and porosity. *Pure Appl Chem.* 1985;57(4):603-19.

267. Gilkey RW, Lagus PL, Turner PL. Gas comparison pycnometer. Google Patents; 1978.
268. Viana M, Jouannin P, Pontier C, Chulia D. About pycnometric density measurements. *Talanta*. 2002;57(3):583-93.
269. Tamari S. Optimum design of the constant-volume gas pycnometer for determining the volume of solid particles. *Measurement Science and Technology*. 2004;15(3):549.
270. Abell A, Willis K, Lange D. Mercury intrusion porosimetry and image analysis of cement-based materials. *Journal of Colloid and Interface Science*. 1999;211(1):39-44.
271. Webb PA, Orr C. Analytical methods in fine particle technology: Micromeritics Instrument Corp; 1997.
272. Good RJ, Mikhail RS. The contact angle in mercury intrusion porosimetry. *Powder Technology*. 1981;29(1):53-62.
273. Webb P, DeSousa T. Mercury intrusion porosimetry. *Ceramic Industry*. 2010;160(6):29-32.
274. Wenzel A, Gröndahl H. Direct digital radiography in the dental office. *International dental journal*. 1995;45(1):27-34.
275. Goodman LR, Foley WD, Wilson CR, Rimm A, Lawson T. Digital and conventional chest images: observer performance with Film Digital Radiography System. *Radiology*. 1986;158(1):27-33.

276. Lehmann L, Alvarez R, Macovski A, Brody W, Pelc N, Riederer S, et al. Generalized image combinations in dual KVP digital radiography. *Medical physics*. 1981;8(5):659-67.
277. Yaffe M, Rowlands J. X-ray detectors for digital radiography. *Physics in Medicine and Biology*. 1997;42(1):1.
278. Chotas HG, Dobbins JT, Ravin CE. Principles of digital radiography with large-area, electronically readable detectors: a review of the basics. *Radiology*. 1999;210(3):595-9.
279. Rhodes J, Ford T, Lynch J, Liepins P, Curtis R. Micro - computed tomography: a new tool for experimental endodontology. *International Endodontic Journal*. 1999;32(3):165-70.
280. Gauthier O, Müller R, von Stechow D, Lamy B, Weiss P, Bouler J-M, et al. In vivo bone regeneration with injectable calcium phosphate biomaterial: a three-dimensional micro-computed tomographic, biomechanical and SEM study. *Biomaterials*. 2005;26(27):5444-53.
281. Ritman EL. Micro-computed tomography-current status and developments. *Annu Rev Biomed Eng*. 2004;6:185-208.
282. Brooks RA, Di Chiro G. Theory of Image Reconstruction in Computed Tomography 1. *Radiology*. 1975;117(3):561-72.
283. Pearce A, Richards R, Milz S, Schneider E, Pearce S. Animal models for implant biomaterial research in bone: a review. *Eur Cell Mater*. 2007;13(1):1-10.

284. Pearce AI, Richards RG, Milz S, Schneider E, Pearce SG. Animal models for implant biomaterial research in bone: a review. *Eur Cell Mater.* 2007;13:1-10. Epub 2007/03/06.
285. Martini L, Fini M, Giavaresi G, Giardino R. Sheep model in orthopedic research: a literature review. *Comparative medicine.* 2001;51(4):292-9. Epub 2002/04/02.
286. Kuhn JL, Goldstein SA, Ciarelli MJ, Matthews LS. The limitations of canine trabecular bone as a model for human: a biomechanical study. *J Biomech.* 1989;22(2):95-107. Epub 1989/01/01.
287. Kruyt MC, van Gaalen SM, Oner FC, Verbout AJ, de Bruijn JD, Dhert WJ. Bone tissue engineering and spinal fusion: the potential of hybrid constructs by combining osteoprogenitor cells and scaffolds. *Biomaterials.* 2004;25(9):1463-73. Epub 2003/12/31.
288. Kruyt MC, de Bruijn JD, Yuan H, van Blitterswijk CA, Verbout AJ, Oner FC, et al. Optimization of bone tissue engineering in goats: a peroperative seeding method using cryopreserved cells and localized bone formation in calcium phosphate scaffolds. *Transplantation.* 2004;77(3):359-65. Epub 2004/02/18.
289. Bosch C, Melsen B, Vargervik K. Importance of the critical-size bone defect in testing bone-regenerating materials. *The Journal of craniofacial surgery.* 1998;9(4):310-6. Epub 1998/10/22.
290. Viljanen VV, Lindholm TC, Gao TJ, Lindholm TS. Low dosage of native allogeneic bone morphogenetic protein in repair of sheep calvarial defects. *International journal of oral and maxillofacial surgery.* 1997;26(5):389-93. Epub 1997/11/05.

291. Viljanen VV, Lindholm TS. Comparison of native xenogeneic and allogeneic bone morphogenetic proteins in the sheep skull defect assay model. *Ann Chir Gynaecol.* 1997;86(3):255-9. Epub 1997/01/01.
292. Schmitz JP, Schwartz Z, Hollinger JO, Boyan BD. Characterization of rat calvarial nonunion defects. *Acta anatomica.* 1990;138(3):185-92. Epub 1990/01/01.
293. Indovina A, Jr., Block MS. Comparison of 3 bone substitutes in canine extraction sites. *Journal of oral and maxillofacial surgery : official journal of the American Association of Oral and Maxillofacial Surgeons.* 2002;60(1):53-8. Epub 2002/01/05.
294. Buser D, Hoffmann B, Bernard JP, Lussi A, Mettler D, Schenk RK. Evaluation of filling materials in membrane--protected bone defects. A comparative histomorphometric study in the mandible of miniature pigs. *Clinical oral implants research.* 1998;9(3):137-50. Epub 1999/10/26.
295. Schliephake H, Knebel JW, Aufderheide M, Tauscher M. Use of cultivated osteoprogenitor cells to increase bone formation in segmental mandibular defects: an experimental pilot study in sheep. *International journal of oral and maxillofacial surgery.* 2001;30(6):531-7. Epub 2002/02/07.
296. Hanson LJ, Donovan MG, Hellstein JW, Dickerson NC. Experimental evaluation of expanded polytetrafluoroethylene for reconstruction of orbital floor defects. *Journal of oral and maxillofacial surgery : official journal of the American Association of Oral and Maxillofacial Surgeons.* 1994;52(10):1050-5; discussion 6-7. Epub 1994/10/01.
297. Klug CN, Millesi-Schobel GA, Millesi W, Watzinger F, Ewers R. Preprosthetic vertical distraction osteogenesis of the mandible using an L-shaped osteotomy and titanium membranes for guided bone regeneration. *Journal of oral*

and maxillofacial surgery : official journal of the American Association of Oral and Maxillofacial Surgeons. 2001;59(11):1302-8; discussion 9-10. Epub 2001/11/01.

298. Enislidis G, Fock N, Millesi-Schobel G, Klug C, Wittwer G, Yerit K, et al. Analysis of complications following alveolar distraction osteogenesis and implant placement in the partially edentulous mandible. Oral surgery, oral medicine, oral pathology, oral radiology, and endodontics. 2005;100(1):25-30. Epub 2005/06/15.

299. Iizuka T, Hallermann W, Seto I, Smolka W, Smolka K, Bosshardt DD. Bi-directional distraction osteogenesis of the alveolar bone using an extraosseous device. Clinical oral implants research. 2005;16(6):700-7. Epub 2005/11/26.

300. Chiapasco M, Romeo E, Casentini P, Rimondini L. Alveolar distraction osteogenesis vs. vertical guided bone regeneration for the correction of vertically deficient edentulous ridges: a 1-3-year prospective study on humans. Clinical oral implants research. 2004;15(1):82-95. Epub 2004/01/21.

301. Kunkel M, Wahlmann U, Reichert TE, Wegener J, Wagner W. Reconstruction of mandibular defects following tumor ablation by vertical distraction osteogenesis using intraosseous distraction devices. Clinical oral implants research. 2005;16(1):89-97. Epub 2005/01/12.

302. Rocchietta I, Fontana F, Simion M. Clinical outcomes of vertical bone augmentation to enable dental implant placement: a systematic review. J Clin Periodontol. 2008;35(8 Suppl):203-15. Epub 2008/09/09.

303. Simion M, Jovanovic SA, Trisi P, Scarano A, Piattelli A. Vertical ridge augmentation around dental implants using a membrane technique and autogenous bone or allografts in humans. The International journal of periodontics & restorative dentistry. 1998;18(1):8-23. Epub 1998/04/29.

304. Parma-Benfenati S, Tinti C, Albrektsson T, Johansson C. Histologic evaluation of guided vertical ridge augmentation around implants in humans. *The International journal of periodontics & restorative dentistry*. 1999;19(5):424-37. Epub 2000/03/10.
305. Canullo L, Trisi P, Simion M. Vertical ridge augmentation around implants using e-PTFE titanium-reinforced membrane and deproteinized bovine bone mineral (bio-oss): A case report. *The International journal of periodontics & restorative dentistry*. 2006;26(4):355-61. Epub 2006/08/31.
306. Barone A, Covani U. Maxillary alveolar ridge reconstruction with nonvascularized autogenous block bone: clinical results. *Journal of oral and maxillofacial surgery : official journal of the American Association of Oral and Maxillofacial Surgeons*. 2007;65(10):2039-46. Epub 2007/09/22.
307. Cordaro L, Amade DS, Cordaro M. Clinical results of alveolar ridge augmentation with mandibular block bone grafts in partially edentulous patients prior to implant placement. *Clinical oral implants research*. 2002;13(1):103-11. Epub 2002/05/15.
308. Bahat O, Fontanessi RV. Implant placement in three-dimensional grafts in the anterior jaw. *The International journal of periodontics & restorative dentistry*. 2001;21(4):357-65. Epub 2001/08/25.
309. Chiapasco M, Zaniboni M, Rimondini L. Autogenous onlay bone grafts vs. alveolar distraction osteogenesis for the correction of vertically deficient edentulous ridges: a 2-4-year prospective study on humans. *Clinical oral implants research*. 2007;18(4):432-40. Epub 2007/05/16.
310. Schleier P, Wolf C, Siebert H, Shafer D, Freilich M, Berndt A, et al. Treatment options in distraction osteogenesis therapy using a new bidirectional

distractor system. *The International journal of oral & maxillofacial implants.* 2007;22(3):408-16. Epub 2007/07/12.

311. Turker N, Basa S, Vural G. Evaluation of osseous regeneration in alveolar distraction osteogenesis with histological and radiological aspects. *Journal of oral and maxillofacial surgery : official journal of the American Association of Oral and Maxillofacial Surgeons.* 2007;65(4):608-14. Epub 2007/03/21.

312. McCarthy JG, Schreiber J, Karp N, Thorne CH, Grayson BH. Lengthening the human mandible by gradual distraction. *Plastic and reconstructive surgery.* 1992;89(1):1-8; discussion 9-10. Epub 1992/01/01.

313. Isaksson S, Alberius P. Maxillary alveolar ridge augmentation with onlay bone-grafts and immediate endosseous implants. *Journal of cranio-maxillo-facial surgery : official publication of the European Association for Cranio-Maxillo-Facial Surgery.* 1992;20(1):2-7. Epub 1992/01/01.

314. Tamimi F, Torres J, Gbureck U, Lopez-Cabarcos E, Bassett DC, Alkhraisat MH, et al. Craniofacial vertical bone augmentation: a comparison between 3D printed monolithic monetite blocks and autologous onlay grafts in the rabbit. *Biomaterials.* 2009;30(31):6318-26. Epub 2009/08/22.

315. Torres J, Tamimi F, Alkhraisat MH, Prados-Frutos JC, Rastikerdar E, Gbureck U, et al. Vertical bone augmentation with 3D-synthetic monetite blocks in the rabbit calvaria. *J Clin Periodontol.* 2011;38(12):1147-53. Epub 2011/11/19.

316. Jung UW, Lee JS, Lee G, Lee IK, Hwang JW, Kim MS, et al. Role of collagen membrane in lateral onlay grafting with bovine hydroxyapatite incorporated with collagen matrix in dogs. *Journal of periodontal & implant science.* 2013;43(2):64-71. Epub 2013/05/17.

317. Cho BC, Seo MS, Baik BS. Distraction osteogenesis after membranous bone onlay grafting in a dog model. *Journal of oral and maxillofacial surgery : official journal of the American Association of Oral and Maxillofacial Surgeons.* 2001;59(9):1025-33. Epub 2001/08/30.
318. Frame JW. A convenient animal model for testing bone substitute materials. *J Oral Surg.* 1980;38(3):176-80. Epub 1980/03/01.
319. Prolo DJ, Pedrotti PW, Burres KP, Oklund S. Superior osteogenesis in transplanted allogeneic canine skull following chemical sterilization. *Clin Orthop Relat Res.* 1982(168):230-42. Epub 1982/08/01.
320. Hjorting-Hansen E, Andreasen JO. Incomplete bone healing of experimental cavities in dog mandibles. *The British journal of oral surgery.* 1971;9(1):33-40. Epub 1971/07/01.
321. Leake DL, Rappoport M. Mandibular reconstruction: bone induction in an alloplastic tray. *Surgery.* 1972;72(2):332-6. Epub 1972/08/01.
322. Lindholm TC, Lindholm TS, Marttinen A, Urist MR. Bovine bone morphogenetic protein (bBMP/NCP)-induced repair of skull trephine defects in pigs. *Clin Orthop Relat Res.* 1994(301):263-70. Epub 1994/04/01.
323. Lecllet H, Pasquier G. [Percutaneous injection of bone biomaterials]. *Rev Rhum Ed Fr.* 1993;60(4):299-304. Epub 1993/04/01. Les biomateriaux osseux injectables a usage percutane. GRIBOI (Groupe de Recherche Interdisciplinaire sur les Biomateriaux Osseux Injectables).
324. Frankenburg EP, Goldstein SA, Bauer TW, Harris SA, Poser RD. Biomechanical and histological evaluation of a calcium phosphate cement. *J Bone Joint Surg Am.* 1998;80(8):1112-24. Epub 1998/09/08.

325. Key J. The effect of local calcium depot on osteogenesis and healing of fractures. *J Bone Joint Surg Am.* 1934;16-!:176-84.
326. Cong Z, Jianxin W, Huaizhi F, Bing L, Xingdong Z. Repairing segmental bone defects with living porous ceramic cylinders: an experimental study in dog femora. *J Biomed Mater Res.* 2001;55(1):28-32. Epub 2001/06/28.
327. Bruder SP, Kraus KH, Goldberg VM, Kadiyala S. The effect of implants loaded with autologous mesenchymal stem cells on the healing of canine segmental bone defects. *J Bone Joint Surg Am.* 1998;80(7):985-96. Epub 1998/08/11.
328. Johnson KD, August A, Sciadini MF, Smith C. Evaluation of ground cortical autograft as a bone graft material in a new canine bilateral segmental long bone defect model. *Journal of orthopaedic trauma.* 1996;10(1):28-36. Epub 1996/01/01.
329. Johnson EE, Urist MR, Schmalzried TP, Chotivichit A, Huang HK, Finerman GA. Autogeneic cancellous bone grafts in extensive segmental ulnar defects in dogs. Effects of xenogeneic bovine bone morphogenetic protein without and with interposition of soft tissues and interruption of blood supply. *Clin Orthop Relat Res.* 1989(243):254-65. Epub 1989/06/01.
330. Cook SD, Wolfe MW, Salkeld SL, Rueger DC. Effect of recombinant human osteogenic protein-1 on healing of segmental defects in non-human primates. *J Bone Joint Surg Am.* 1995;77(5):734-50. Epub 1995/05/01.
331. Andersson GB, Gaechter A, Galante JO, Rostoker W. Segmental replacement of long bones in baboons using a fiber titanium implant. *J Bone Joint Surg Am.* 1978;60(1):31-40. Epub 1978/01/01.
332. Andersson GB, Lereim P, Galante JO, Rostoker W. Segmental replacement of the femur in baboons with fiber metal implants and autologous bone grafts of

different particle size. *Acta orthopaedica Scandinavica*. 1982;53(3):349-54. Epub 1982/06/01.

333. Raisz LG. The osteoporosis revolution. *Ann Intern Med*. 1997;126(6):458-62.

334. Schneider GB, Key LL, Popoff SN. Osteopetrosis: Therapeutic strategies. *Endocrinologist*. 1998;8(6):409-17.

335. Khan SN, Lane JM. Spinal fusion surgery: animal models for tissue-engineered bone constructs. *Biomaterials*. 2004;25(9):1475-85. Epub 2003/12/31.

336. Baramki HG, Steffen T, Lander P, Chang M, Marchesi D. The efficacy of interconnected porous hydroxyapatite in achieving posterolateral lumbar fusion in sheep. *Spine*. 2000;25(9):1053-60. Epub 2000/05/02.

337. Sandhu HS, Turner S, Kabo JM, Kanim LE, Liu D, Nourparvar A, et al. Distractive properties of a threaded interbody fusion device. An in vivo model. *Spine*. 1996;21(10):1201-10. Epub 1996/05/15.

338. Cunningham BW, Kanayama M, Parker LM, Weis JC, Seftor JC, Fedder IL, et al. Osteogenic protein versus autologous interbody arthrodesis in the sheep thoracic spine. A comparative endoscopic study using the Bagby and Kuslich interbody fusion device. *Spine*. 1999;24(6):509-18. Epub 1999/04/02.

339. Zdeblick TA, Ghanayem AJ, Rapoff AJ, Swain C, Bassett T, Cooke ME, et al. Cervical interbody fusion cages. An animal model with and without bone morphogenetic protein. *Spine*. 1998;23(7):758-65; discussion 66. Epub 1998/05/01.

340. Sandhu HS, Kanim LE, Kabo JM, Toth JM, Zeegan EN, Liu D, et al. Evaluation of rhBMP-2 with an OPLA carrier in a canine posterolateral (transverse process) spinal fusion model. *Spine*. 1995;20(24):2669-82. Epub 1995/12/15.

341. Pintar FA, Maiman DJ, Hollowell JP, Yoganandan N, Droese KW, Reinartz JM, et al. Fusion rate and biomechanical stiffness of hydroxylapatite versus autogenous bone grafts for anterior discectomy. An in vivo animal study. *Spine*. 1994;19(22):2524-8. Epub 1994/11/15.
342. Sidhu KS, Prochnow TD, Schmitt P, Fischgrund J, Weisbrode S, Herkowitz HN. Anterior cervical interbody fusion with rhBMP-2 and tantalum in a goat model. *The spine journal : official journal of the North American Spine Society*. 2001;1(5):331-40. Epub 2003/11/01.
343. Frenkel SR, Moskovich R, Spivak J, Zhang ZH, Prewett AB. Demineralized bone matrix. Enhancement of spinal fusion. *Spine*. 1993;18(12):1634-9. Epub 1993/09/15.
344. Cook SD, Dalton JE, Tan EH, Tejeiro WV, Young MJ, Whitecloud TS, 3rd. In vivo evaluation of anterior cervical fusions with hydroxylapatite graft material. *Spine*. 1994;19(16):1856-66. Epub 1994/08/15.
345. Wang T, Dang G, Guo Z, Yang M. Evaluation of autologous bone marrow mesenchymal stem cell-calcium phosphate ceramic composite for lumbar fusion in rhesus monkey interbody fusion model. *Tissue engineering*. 2005;11(7-8):1159-67. Epub 2005/09/08.
346. Alden TD, Pittman DD, Beres EJ, Hankins GR, Kallmes DF, Wisotsky BM, et al. Percutaneous spinal fusion using bone morphogenetic protein-2 gene therapy. *Journal of neurosurgery*. 1999;90(1 Suppl):109-14. Epub 1999/07/21.
347. Boden SD. Biology of lumbar spine fusion and use of bone graft substitutes: present, future, and next generation. *Tissue engineering*. 2000;6(4):383-99. Epub 2000/09/19.

348. Rubino F, Deutsch H, Pamoukian V, Zhu JF, King WA, Gagner M. Minimally invasive spine surgery: an animal model for endoscopic approach to the anterior cervical and upper thoracic spine. *Journal of laparoendoscopic & advanced surgical techniques Part A*. 2000;10(6):309-13. Epub 2001/01/02.
349. de Boer J, van Blitterswijk C, Lowik C. Bioluminescent imaging: emerging technology for non-invasive imaging of bone tissue engineering. *Biomaterials*. 2006;27(9):1851-8. Epub 2005/10/26.
350. Boden SD, Martin GJ, Jr., Horton WC, Truss TL, Sandhu HS. Laparoscopic anterior spinal arthrodesis with rhBMP-2 in a titanium interbody threaded cage. *Journal of spinal disorders*. 1998;11(2):95-101. Epub 1998/05/20.
351. Hecht BP, Fischgrund JS, Herkowitz HN, Penman L, Toth JM, Shirkhoda A. The use of recombinant human bone morphogenetic protein 2 (rhBMP-2) to promote spinal fusion in a nonhuman primate anterior interbody fusion model. *Spine*. 1999;24(7):629-36. Epub 1999/04/21.
352. Mirtchi AA, Lemaitre J, Munting E. Calcium-phosphate cements - effect of flourides on the setting and hardening of beta-tricalcium phosphate dicalcium phosphate calcite cements. *Biomaterials*. 1991;12(5):505-10.
353. Penel G, Leroy G, Leroy N, Behin P, Langlois JM, Libersa JC, et al. Raman spectrometry applied to calcified tissue and calcium-phosphorus biomaterials. *Bull Group Int Rech Sci Stomatol Odontol*. 2000;42(2-3):55-63.
354. Lu J DM, Dejoui J, Koubi G, Hardouin P, Lemaitre J, Proust JP. The biodegradation mechanism of calcium phosphate biomaterials in bone. *J Biomed Mater Res*. 2002;63:408-12.

355. Kumar M DH, Riley C. . Electrodeposition of brushite coatings and their transformation to hydroxyapatite in aqueous solutions. *J biomed Mater Res.* 1999;45:302-10.
356. Xie J RC, Chittur K. Effect of albumin on brushite transformation to hydroxyapatite. *J biomed Mater Res.* 2001;57:357-65.
357. Constantz BR, Barr BM, Ison IC, Fulmer MT, Baker J, McKinney LA, et al. Histological, chemical, and crystallographic analysis of four calcium phosphate cements in different rabbit osseous sites. *Journal of Biomedical Materials Research.* 1998;43(4):451-61.
358. Maria SM, Prukner C, Sheikh Z, Mueller F, Barralet JE, Komarova SV. Reproducible quantification of osteoclastic activity: Characterization of a biomimetic calcium phosphate assay. *J Biomed Mater Res B Appl Biomater.* 2013.
359. Steinberg D KA, Kohavi D, Sela MN. Adsorption of human salivary proteins to titanium powder. *Biomaterials.* 1995;16:1339-43.
360. Bohner M, Baumgart F. Theoretical model to determine the effects of geometrical factors on the resorption of calcium phosphate bone substitutes. *Biomaterials.* 2004;25(17):3569-82. Epub 2004/03/17.
361. Ishikawa K TS, Chow LC, Suzuki K. Reaction of calcium phosphates with different amounts of tetracalcium phosphate and dicalcium phosphate anhydrous. . *J Biomed Mater Res B Appl Biomater.* 1999;46:504-10.
362. Ishikawa K AK. Estimation of ideal mechanical strength and critical porosity of calcium phosphate cement. . *J biomed Mater Res.* 1995;29:1537-43.

363. Mirtchi AA, Lemaitre J, Terao N. Calcium phosphate cements: study of the beta-tricalcium phosphate-monocalcium phosphate system. . *Biomaterials*. 1989;10(7):475-80.
364. Schildhauer TA, Gekle CJ, Muhr G. [Biomaterials in the skeletal system]. *Der Chirurg; Zeitschrift für alle Gebiete der operativen Medizin*. 1999;70(8):888-96. Epub 1999/08/25. Neue Biomaterialien am Skelettsystem.
365. Kurz LT, Garfin SR, Booth RE, Jr. Harvesting autogenous iliac bone grafts. A review of complications and techniques. *Spine*. 1989;14(12):1324-31. Epub 1989/12/01.
366. Gerngross H, Burri C, Kinzl L, Merk J, Müller GW. Complications at removal sites of autologous cancellous bone transplants. *Aktuelle Traumatologie*. 1982;12(3):146-52. Epub 1982/06/01. Komplikationen an den Entnahmestellen autologer Spongiosatransplantate.
367. LeGeros RZ. Biodegradation and bioresorption of calcium phosphate ceramics. *Clinical materials*. 1993;14(1):65-88. Epub 1992/12/09.
368. Nilsson M, Fernandez E, Sarda S, Lidgren L, Planell JA. Characterization of a novel calcium phosphate/sulphate bone cement. *J Biomed Mater Res*. 2002;61(4):600-7. Epub 2002/07/13.
369. Aberg J, Brisby H, Henriksson HB, Lindahl A, Thomsen P, Engqvist H. Premixed Acidic Calcium Phosphate Cement: Characterization of Strength and Microstructure. *Journal of Biomedical Materials Research Part B-Applied Biomaterials*. 2010;93B(2):436-41.

370. Hamdan Alkhraisat M, Moseke C, Blanco L, Barralet JE, Lopez-Carbacos E, Gbureck U. Strontium modified bioceramics with zero order release kinetics. *Biomaterials*. 2008;29(35):4691-7.
371. Tas AC, Bhaduri SB. Chemical processing of $\text{CaHPO}_4 \cdot 2\text{H}_2\text{O}$: Its conversion to hydroxyapatite. *Journal of the American Ceramic Society*. 2004;87(12):2195-200.
372. Cama G, Barberis F, Botter R, Cirillo P, Capurro M, Quarto R, et al. Preparation and properties of macroporous brushite bone cements. *Acta Biomaterialia*. 2009;5(6):2161-8.
373. Yin YJ, Ye F, Cai S, Yao KD, Cui JF, Song XF. Gelatin manipulation of latent macropores formation in brushite cement. *Journal of Materials Science-Materials in Medicine*. 2003;14(3):255-61.
374. LeGeros RZ DG, Orly I et al. Substrate surface dissolution and interfacial biological mineralisation. In: JED D, editor. *Bone biomaterial interface*. Toronto: University of Toronto Press; 1991. p. 76-88.
375. Chang YL, Stanford CM, Keller JC. Calcium and phosphate supplementation promotes bone cell mineralization: implications for hydroxyapatite (HA)-enhanced bone formation. *J Biomed Mater Res*. 2000;52(2):270-8. Epub 2000/08/22.
376. Levin L. Dealing with dental implant failures. *Refuat Hapeh Vehashinayim*. 2010;27(3):6-12, 60. Epub 2011/04/13.
377. Tolman DE, Keller EE. Endosseous implant placement immediately following dental extraction and alveoloplasty: preliminary report with 6-year

follow-up. *The International journal of oral & maxillofacial implants*. 1991;6(1):24-8. Epub 1991/01/01.

378. Tolman DE. Advanced residual ridge resorption: surgical management. *The International journal of prosthodontics*. 1993;6(2):118-25. Epub 1993/03/01.

379. Tonetti MS, Hammerle CH. Advances in bone augmentation to enable dental implant placement: Consensus Report of the Sixth European Workshop on Periodontology. *J Clin Periodontol*. 2008;35(8 Suppl):168-72. Epub 2008/09/09.

380. Chiapasco M, Consolo U, Bianchi A, Ronchi P. Alveolar distraction osteogenesis for the correction of vertically deficient edentulous ridges: a multicenter prospective study on humans. *The International journal of oral & maxillofacial implants*. 2004;19(3):399-407. Epub 2004/06/25.

381. Raghoobar GM, Liem RS, Vissink A. Vertical distraction of the severely resorbed edentulous mandible: a clinical, histological and electron microscopic study of 10 treated cases. *Clinical oral implants research*. 2002;13(5):558-65. Epub 2002/11/28.

382. Jensen OT, Cockrell R, Kuhike L, Reed C. Anterior maxillary alveolar distraction osteogenesis: a prospective 5-year clinical study. *The International journal of oral & maxillofacial implants*. 2002;17(1):52-68. Epub 2002/02/23.

383. Rachmiel A, Srouji S, Peled M. Alveolar ridge augmentation by distraction osteogenesis. *International journal of oral and maxillofacial surgery*. 2001;30(6):510-7. Epub 2002/02/07.

384. McAllister BS. Histologic and radiographic evidence of vertical ridge augmentation utilizing distraction osteogenesis: 10 consecutively placed distractors. *J Periodontol*. 2001;72(12):1767-79. Epub 2002/01/29.

385. Simion M, Fontana F, Rasperini G, Maiorana C. Vertical ridge augmentation by expanded-polytetrafluoroethylene membrane and a combination of intraoral autogenous bone graft and deproteinized anorganic bovine bone (Bio Oss). *Clinical oral implants research*. 2007;18(5):620-9. Epub 2007/09/20.
386. Tinti C, Parma-Benfenati S. Vertical ridge augmentation: surgical protocol and retrospective evaluation of 48 consecutively inserted implants. *The International journal of periodontics & restorative dentistry*. 1998;18(5):434-43. Epub 1999/03/27.
387. Tinti C, Parma-Benfenati S, Manfrini F. Spacemaking metal structures for nonresorbable membranes in guided bone regeneration around implants. Two case reports. *The International journal of periodontics & restorative dentistry*. 1997;17(1):53-61. Epub 1997/02/01.
388. Piattelli M, Scarano A, Piattelli A. Vertical ridge augmentation using a resorbable membrane: a case report. *J Periodontol*. 1996;67(2):158-61. Epub 1996/02/01.
389. Simion M, Trisi P, Piattelli A. Vertical ridge augmentation using a membrane technique associated with osseointegrated implants. *The International journal of periodontics & restorative dentistry*. 1994;14(6):496-511. Epub 1994/12/01.
390. Tinti C, Parma-Benfenati S, Polizzi G. Vertical ridge augmentation: what is the limit? *The International journal of periodontics & restorative dentistry*. 1996;16(3):220-9. Epub 1996/06/01.
391. Torres J, Tamimi F, Alkhraisat MH, Manchon A, Linares R, Prados-Frutos JC, et al. Platelet-rich plasma may prevent titanium-mesh exposure in alveolar

ridge augmentation with anorganic bovine bone. *J Clin Periodontol.* 2010;37(10):943-51. Epub 2010/08/28.

392. Hill NM, Horne JG, Devane PA. Donor site morbidity in the iliac crest bone graft. *The Australian and New Zealand journal of surgery.* 1999;69(10):726-8. Epub 1999/10/20.

393. Felice P, Pellegrino G, Checchi L, Pistilli R, Esposito M. Vertical augmentation with interpositional blocks of anorganic bovine bone vs. 7-mm-long implants in posterior mandibles: 1-year results of a randomized clinical trial. *Clinical oral implants research.* 2010;21(12):1394-403. Epub 2010/08/04.

394. Araujo MG, Sonohara M, Hayacibara R, Cardaropoli G, Lindhe J. Lateral ridge augmentation by the use of grafts comprised of autologous bone or a biomaterial. An experiment in the dog. *J Clin Periodontol.* 2002;29(12):1122-31. Epub 2002/12/21.

395. Felice P, Pistilli R, Lizio G, Pellegrino G, Nisii A, Marchetti C. Inlay versus onlay iliac bone grafting in atrophic posterior mandible: a prospective controlled clinical trial for the comparison of two techniques. *Clinical implant dentistry and related research.* 2009;11 Suppl 1:e69-82. Epub 2009/08/18.

396. Rothamel D, Schwarz F, Herten M, Ferrari D, Mischkowski RA, Sager M, et al. Vertical ridge augmentation using xenogenous bone blocks: a histomorphometric study in dogs. *The International journal of oral & maxillofacial implants.* 2009;24(2):243-50. Epub 2009/06/06.

397. De Santis R AL, Nicolais L. Mechanical properties of tooth structures. R B, editor. New york: US: Springer; 2002.

398. Bays RA. The influence of systemic bone disease on bone resorption following mandibular augmentation. Oral surgery, oral medicine, and oral pathology. 1983;55(3):223-31. Epub 1983/03/01.
399. Felice P, Marchetti C, Iezzi G, Piattelli A, Worthington H, Pellegrino G, et al. Vertical ridge augmentation of the atrophic posterior mandible with interpositional bloc grafts: bone from the iliac crest vs. bovine anorganic bone. Clinical and histological results up to one year after loading from a randomized-controlled clinical trial. Clinical oral implants research. 2009;20(12):1386-93. Epub 2009/08/18.
400. Felice P, Checchi V, Pistilli R, Scarano A, Pellegrino G, Esposito M. Bone augmentation versus 5-mm dental implants in posterior atrophic jaws. Four-month post-loading results from a randomised controlled clinical trial. European journal of oral implantology. 2009;2(4):267-81. Epub 2009/01/01.
401. Felice P, Cannizzaro G, Checchi V, Marchetti C, Pellegrino G, Censi P, et al. Vertical bone augmentation versus 7-mm-long implants in posterior atrophic mandibles. Results of a randomised controlled clinical trial of up to 4 months after loading. European journal of oral implantology. 2009;2(1):7-20. Epub 2010/05/15.
402. Stellingsma C, Vissink A, Meijer HJ, Kuiper C, Raghoobar GM. Implantology and the severely resorbed edentulous mandible. Critical reviews in oral biology and medicine : an official publication of the American Association of Oral Biologists. 2004;15(4):240-8. Epub 2004/07/31.
403. Slotte C, Lundgren D, Sennerby L. Bone morphology and vascularization of untreated and guided bone augmentation-treated rabbit calvaria: evaluation of an augmentation model. Clinical oral implants research. 2005;16(2):228-35. Epub 2005/03/22.

404. Cutting CB, McCarthy JG, Berenstein A. Blood supply of the upper craniofacial skeleton: the search for composite calvarial bone flaps. *Plastic and reconstructive surgery*. 1984;74(5):603-10. Epub 1984/11/01.
405. Tamura K, Sato S, Kishida M, Asano S, Murai M, Ito K. The use of porous beta-tricalcium phosphate blocks with platelet-rich plasma as an onlay bone graft biomaterial. *J Periodontol*. 2007;78(2):315-21. Epub 2007/02/06.
406. Gosain AK, Gosain SA, Sweeney WM, Song LS, Amarante MT. Regulation of osteogenesis and survival within bone grafts to the calvaria: the effect of the dura versus the pericranium. *Plastic and reconstructive surgery*. 2011;128(1):85-94. Epub 2011/03/15.
407. Hallman M, Sennerby L, Lundgren S. A clinical and histologic evaluation of implant integration in the posterior maxilla after sinus floor augmentation with autogenous bone, bovine hydroxyapatite, or a 20:80 mixture. *The International journal of oral & maxillofacial implants*. 2002;17(5):635-43. Epub 2002/10/17.
408. Hallman M, Hedin M, Sennerby L, Lundgren S. A prospective 1-year clinical and radiographic study of implants placed after maxillary sinus floor augmentation with bovine hydroxyapatite and autogenous bone. *Journal of oral and maxillofacial surgery : official journal of the American Association of Oral and Maxillofacial Surgeons*. 2002;60(3):277-84; discussion 85-6. Epub 2002/03/12.
409. Carmagnola D, Adriaens P, Berglundh T. Healing of human extraction sockets filled with Bio-Oss. *Clinical oral implants research*. 2003;14(2):137-43. Epub 2003/03/27.
410. Berglundh T, Lindhe J. Healing around implants placed in bone defects treated with Bio-Oss. An experimental study in the dog. *Clinical oral implants research*. 1997;8(2):117-24. Epub 1997/04/01.

411. Artzi Z, Tal H, Dayan D. Porous bovine bone mineral in healing of human extraction sockets. Part 1: histomorphometric evaluations at 9 months. *J Periodontol.* 2000;71(6):1015-23. Epub 2000/07/29.
412. Goulet JA, Senunas LE, DeSilva GL, Greenfield ML. Autogenous iliac crest bone graft. Complications and functional assessment. *Clin Orthop Relat Res.* 1997(339):76-81. Epub 1997/06/01.
413. LeGeros RZ, Daculsi, G. In vivo transformation of biphasic calcium phosphate ceramics: Ultrstructural and physicochemical characterizations. . *Handbook of Bioactive Ceramics.* Boca Raton, FL, USA: CRC Press; 1992. p. 17–28.
414. LeGeros RZ, LeGeros. *Bone Substitute Materials and Their Properties.* Stuttgart/New York, Germany/USA: Georg Thieme Verlag; 1997. p. 12–8.
415. de Bruijn JD, Klein CP, de Groot K, van Blitterswijk CA. The ultrastructure of the bone-hydroxyapatite interface in vitro. *J Biomed Mater Res.* 1992;26(10):1365-82. Epub 1992/10/01.
416. Ginebra MP, Traykova T, Planell JA. Calcium phosphate cements: competitive drug carriers for the musculoskeletal system? *Biomaterials.* 2006;27(10):2171-7. Epub 2005/12/08.
417. Berger G, Gildenhaar R, Ploska U. Rapid resorbable, glassy crystalline materials on the basis of calcium alkali orthophosphates. *Biomaterials.* 1995;16(16):1241-8. Epub 1995/11/01.
418. Knabe C, Ostapowicz W, Radlanski RJ, Gildenhaar R, Berger G, Fitzner R, et al. In vitro investigation of novel calcium phosphates using osteogenic cultures. *J Mater Sci Mater Med.* 1998;9(6):337-45. Epub 2004/09/07.

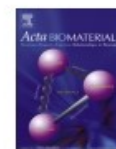
419. Konishi T, Horiguchi Y, Mizumoto M, Honda M, Oribe K, Morisue H, et al. Novel chelate-setting calcium-phosphate cements fabricated with wet-synthesized hydroxyapatite powder. *J Mater Sci Mater Med.* 2013;24(3):611-21. Epub 2012/12/12.
420. Gbureck U, Thull R, Barralet JE. Alkali ion substituted calcium phosphate cement formation from mechanically activated reactants. *J Mater Sci Mater Med.* 2005;16(5):423-7. Epub 2005/05/06.
421. M. Aizawa YH, and I. Okada. Development of novel cement processing using hydroxyapatite particles modified with inositol phosphate. *Archives of BioCeramics Research.* 2003;3:134–8.
422. T. Konishi ZZ, M. Mizumoto, M. Honda, and M. Aizawa. Fabrication of chelate-setting cement from hydroxyapatite powder prepared by simultaneously grinding and surface-modifying with sodium inositol hexaphosphate and their material properties. *Journal of the Ceramic Society of Japan.* 2012;120:1-7.
423. Y.Horiguchi AY, K.Oribe, and M. Aizawa. Fabrication of chelate-setting hydroxyapatite cements from four kinds of commercially-available powder with various shape and crystallinity and their mechanical property. *Nippon Seramikkusu Kyokai Gakujutsu Ronbunshi.* 2008;116(1349):50-5.
424. Dao TH. Polyvalent cation effects on myo-inositol hexakis dihydrogenphosphate enzymatic dephosphorylation in dairy wastewater. *Journal of environmental quality.* 2003;32(2):694-701. Epub 2003/04/24.
425. Chow LC HS, Takagi S, Parry E. Diametral tensile strength and compressive strength of a calcium phosphate cement: effect of applied pressure. *J Biomed Mater Res Appl Biomater* 2000;53:511-7.

426. Driessens FC, Boltong MG, de Maeyer EA, Wenz R, Nies B, Planell JA. The Ca/P range of nanoapatitic calcium phosphate cements. *Biomaterials*. 2002;23(19):4011-7. Epub 2002/08/07.
427. Kveton JF, Friedman CD, Costantino PD. Indications for hydroxyapatite cement reconstruction in lateral skull base surgery. *The American journal of otology*. 1995;16(4):465-9. Epub 1995/07/01.
428. Kveton JF, Friedman CD, Piepmeier JM, Costantino PD. Reconstruction of suboccipital craniectomy defects with hydroxyapatite cement: a preliminary report. *The Laryngoscope*. 1995;105(2):156-9. Epub 1995/02/01.
429. Kamerer DB, Hirsch BE, Snyderman CH, Costantino P, Friedman CD. Hydroxyapatite cement: a new method for achieving watertight closure in transtemporal surgery. *The American journal of otology*. 1994;15(1):47-9. Epub 1994/01/01.
430. Herzlieb W, Kohler KM, Ewald A, Hofmann N, Gbureck U. Antimicrobial and physicochemical properties of experimental light curing composites with alkali-substituted calcium phosphate fillers. *Dental materials : official publication of the Academy of Dental Materials*. 2012;28(6):597-603. Epub 2012/03/01.
431. Staehle HJ, Pioch T, Hoppe W. The alkalizing properties of calcium hydroxide compounds. *Endodontics & dental traumatology*. 1989;5(3):147-52. Epub 1989/06/01.
432. Stoor P, Soderling E, Salonen JI. Antibacterial effects of a bioactive glass paste on oral microorganisms. *Acta odontologica Scandinavica*. 1998;56(3):161-5. Epub 1998/08/04.

433. Gbureck U, Knappe O, Grover LM, Barralet JE. Antimicrobial potency of alkali ion substituted calcium phosphate cements. *Biomaterials*. 2005;26(34):6880-6. Epub 2005/07/12.
434. Jinlong N, Zhenxi Z, Dazong J, Shenghong Y, Guanglai M, Keguang W. Preparation, structure and solubility of $\text{Ca}_2\text{KNa}(\text{PO}_4)_2$. *Journal of Materials Science*. 2001;36(15):3805-8.
435. Fritz SE, Martin SM, Frisbie CD, Ward MD, Toney MF. Structural characterization of a pentacene monolayer on an amorphous SiO_2 substrate with grazing incidence X-ray diffraction. *Journal of the American Chemical Society*. 2004;126(13):4084-5.
436. Enzo S, Fagherazzi G, Benedetti A, Polizzi S. A profile-fitting procedure for analysis of broadened X-ray diffraction peaks. I. Methodology. *Journal of Applied Crystallography*. 1988;21(5):536-42.

Chapter 11: Additional co-authored articles published by the candidate during Ph.D studies

Included in this section is the collection of the first pages of research and review articles written and published by the candidate as co-author during the Ph.D studies not included in the main text of the thesis. In each of these articles the candidate contributed a significant amount of technical and scientific content and was involved in the preparation of the text.



Review

Dicalcium phosphate cements: Brushite and monetite

Faleh Tamimi*, Zeeshan Sheikh, Jake Barralet

Faculty of Dentistry, McGill University, Montreal, Quebec, Canada

ARTICLE INFO

Article history:

Received 29 May 2011

Received in revised form 3 August 2011

Accepted 6 August 2011

Available online 12 August 2011

Keywords:

Brushite

Monetite

Dicalcium phosphate

Cement

Mechanical properties

ABSTRACT

Dicalcium phosphate cements were developed two decades ago and ever since there has been a substantial growth in research into improving their properties in order to satisfy the requirements needed for several clinical applications. The present paper presents an overview of the rapidly expanding research field of the two main dicalcium phosphate bioceramics: brushite and monetite. This review begins with a summary of all the different formulae developed to prepare dicalcium phosphate cements, and their setting reaction, in order to set the scene for the key cement physical and chemical properties, such as compressive and tensile strength, cohesion, injectability and shelf-life. We address the issue of brushite conversion into either monetite or apatite. Moreover, we discuss the *in vivo* behavior of the cements, including their ability to promote bone formation, biodegradation and potential clinical applications in drug delivery, orthopedics, craniofacial surgery, cancer therapy and biosensors.

© 2011 Acta Materialia Inc. Published by Elsevier Ltd. All rights reserved.

1. Introduction

Brushite cements were discovered by Mirtchi and Lemaître in 1989. These materials were prepared by mixing water with a powder consisting of an acidic calcium phosphate (monocalcium phosphate monohydrate) and a basic calcium phosphate (β -tricalcium phosphate). The result of this mixture was a moldable paste that eventually solidified in an exothermic reaction forming a hard material that was composed mainly of dicalcium phosphate dihydrate, also known by the mineral name “brushite” [1].

Subsequent studies showed that brushite cement is biocompatible and it has a unique advantage over the other calcium phosphate cement system (hydroxyapatite cement), which is its ability to be resorbed under physiological conditions. However, the original formula of brushite cement resulted in a material that was difficult to handle, set too fast (~ 30 s) and had low mechanical properties (~ 1 MPa diametral strength) [2,3].

During the past two decades many studies have been aimed at improving the properties of brushite cement systems. In the current study we discuss all the developments that have been introduced in brushite cements to improve their setting time, mechanical properties, biocompatibility, bioactivity and bioresorption. Moreover, we also present the most relevant biomedical applications of this material.

2. Cement composition

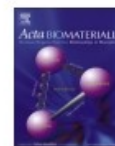
The main constituents of dicalcium phosphate (DCP) cements are an alkaline calcium source, an acidic phosphate source and water, as well as other additives to prolong the cement setting time, increase its mechanical properties and improve its handling. In Table 1 we present the different compositions that have been evaluated in the literature [1,4–50].

2.1. Alkaline calcium source

The alkaline calcium source in DCP cements can be very basic, such as calcium oxide [49] and calcium hydroxide [50]. These two components have the main advantage of being easy to manufacture and inexpensive. On the other hand, brushite has a calcium to phosphate ratio of 1, therefore calcium phosphate compounds with higher calcium to phosphate ratios can be used as alkaline calcium source in brushite cements. For instance, tetracalcium phosphate (TTCP) has a calcium to phosphate ratio of 2, which is ideal for DCP cements. However, its preparation is highly energy demanding, and its use in DCP cements has been very limited [44]. Hydroxyapatite (HAp) has a calcium to phosphate ratio of 1.67, and its ions can be easily substituted [51]. Therefore, introducing HA into a brushite cement setting system allows modulation of the cement setting reaction through ionic substitution [19,46]. Nano-crystalline HAp (nHAp) has also been used to prepare DCP cements [44].

The most common basic calcium source in brushite cements is tricalcium phosphate (TCP) (calcium to phosphate ratio 1.5). This

* Corresponding author. Tel.: +1 5143987203.
E-mail address: faleh.tamimimarino@mcgill.ca (F. Tamimi).



The effect of autoclaving on the physical and biological properties of dicalcium phosphate dihydrate bioceramics: Brushite vs. monetite

Faleh Tamimi^{a,*}, Damien Le Nihouannen^b, Hazem Eimar^a, Zeeshan Sheikh^a, Svetlana Komarova^a, Jake Barralet^a

^a Faculty of Dentistry, McGill University, Montreal, Quebec, Canada

^b UFR Sciences de la Vie, University of Bordeaux Segalen, Bordeaux, France

ARTICLE INFO

Article history:

Received 17 January 2012

Received in revised form 11 April 2012

Accepted 13 April 2012

Available online 20 April 2012

Keywords:

Brushite

Monetite

Dicalcium phosphate

Gene expression

Bone regeneration

ABSTRACT

Dicalcium phosphate dihydrate (brushite) is an osteoconductive biomaterial with great potential as a bioresorbable cement for bone regeneration. Preset brushite cement can be dehydrated into dicalcium phosphate anhydrous (monetite) bioceramics by autoclaving. This heat treatment results in changes in the physical characteristics of the material, improving in vivo bioresorption. This property is a great advantage in bone regeneration; however, it is not known how autoclaving brushite preset cement might improve its capacity to regenerate bone. This study was designed to compare brushite bioceramics with monetite bioceramics in terms of physical characteristics in vitro, and in vivo performance upon bone implantation. In this study we observed that monetite bioceramics prepared by autoclaving preset brushite cements had higher porosity, interconnected porosity and specific surface area than their brushite precursors. In vitro cell culture experiments revealed that bone marrow cells expressed higher levels of osteogenic genes *Runx2*, *Opn*, and *Alp* when the cells were cultured on monetite ceramics rather than on brushite ones. In vivo experiments revealed that monetite bioceramics resorbed faster than brushite ones and were more infiltrated with newly formed bone. In summary, autoclaving preset brushite cements results in a material with improved properties for bone regeneration procedures.

© 2012 Acta Materialia Inc. Published by Elsevier Ltd. All rights reserved.

1. Introduction

Calcium phosphate biomaterials are of special interest in bone regeneration due to their similar composition to bone. Dicalcium phosphate dihydrate, mineral name brushite, is a calcium phosphate biomaterial that can be prepared in the form of hydraulic cements with a wide range of applications [1]. Besides their ability to regenerate bone, brushite biomaterials can resorb in vivo faster than most calcium phosphates, enabling the replacement of the bioceramic by newly regenerated tissues. However, in vivo studies have shown that even though brushite is initially resorbable after implantation, the bioceramic tends to react with the surrounding medium, forming insoluble hydroxyapatite [1,2]. This reaction results in a severe reduction in the resorption rate of the biomaterial, limiting its clinical applications.

Monetite is the anhydrous form of brushite, and it is also a useful biomaterial for bone regeneration. Monetite bioceramics can be prepared by modifying the precipitation conditions of brushite cements [2]. For instance, setting brushite cements in excessively low pH conditions, in water-deficient environments, or in the presence

of metallic ions would disrupt brushite crystals favouring monetite formation [2–5]. Another method of preparing monetite bioceramics is by thermal dehydration of already set brushite cements [6]:



Thermal dehydration of brushite bioceramics can cause shrinkage of the material and damage its mechanical properties. However, by maintaining high pressure and humidity during the dehydration process, overall shrinkage can be prevented [7]. Sterilizing pre-set brushite cements by autoclaving provides the adequate temperature, pressure and humidity conditions that result in their dehydration into monetite without altering the overall macroscopic geometry of the material. Monetite bioceramics prepared by this method have been shown to stimulate vertical bone augmentation, and regeneration of bone defects in animals as well as in human patients [6,8,9], and can achieve higher volumes of bone regeneration than hydroxyapatite-based biomaterials [6,10].

Monetite bioceramics prepared by autoclaving of brushite preset cements have inferior mechanical strength to that of their brushite precursor, and similar levels of cytotoxicity [11]. However, monetite bioceramics prepared by this method release ions at a slower rate than their brushite precursors, do not form insoluble hydroxyapatite in vivo [6,10], and upon subcutaneous

* Corresponding author. Tel.: +1 514 3987203x09654; fax: +1 514 3988900.

E-mail address: faleh.tamimimarino@mcgill.ca (F. Tamimi).

Reproducible quantification of osteoclastic activity: Characterization of a biomimetic calcium phosphate assay

Salwa M. Maria,^{1,2} Christiane Prukner,³ Zeeshan Sheikh,¹ Frank Mueller,³ Jake. E. Barralet,¹ Svetlana V. Komarova^{1,2}

¹Faculty of Dentistry, McGill University, Montreal, Quebec, Canada

²Shriners Hospital for Children-Canada, Montreal, Quebec, Canada

³Institute of Materials Science and Technology, Friedrich Schiller University, Jena, Germany

Received 12 March 2013; revised 31 July 2013; accepted 13 October 2013

Published online 00 Month 2013 in Wiley Online Library (wileyonlinelibrary.com). DOI: 10.1002/jbm.b.33071

Abstract: Osteoclasts are responsible for bone and joint destruction in rheumatoid arthritis, periodontitis, and osteoporosis. Animal tusk slice assays are standard for evaluating the effect of therapeutics on these cells. However, in addition to batch-to-batch variability inherent to animal tusks, their use is clearly not sustainable. Our objective was to develop and characterize a biomimetic calcium phosphate assay based on the use of phase pure hydroxyapatite coated as a thin film on the surface of culture plates, to facilitate the reproducible quantification of osteoclast resorptive activity. Osteoclasts were formed from RAW 264.7 mouse monocyte cell line using a pro-resorptive cytokine RANKL (50 ng/mL). No change in substrate appearance was noted after culture with media without cells, or undifferentiated monocytes.

Only in the presence of osteoclasts localized areas of calcium phosphate dissolution were observed. The total area resorbed positively correlated with the osteoclast numbers ($R^2 = 0.99$). The resorbed area was significantly increased by the addition of RANKL, and decreased after application of known inhibitors of osteoclast resorptive activity, calcitonin (10 μ M), or alendronate (100 μ M). Thus, calcium phosphate coated substrates allow reliable monitoring of osteoclast resorptive activity and offer an alternative to animal tusk slice assays. © 2013 Wiley Periodicals, Inc. *J Biomed Mater Res Part B: Appl Biomater* 00B: 000–000, 2013.

Key Words: osteoclast, resorption, biomimetic substrate, hydroxyapatite, quantification

How to cite this article: Maria SM, Prukner C, Sheikh Z, Mueller F, Barralet JE, Komarova SV. 2013. Reproducible quantification of osteoclastic activity: Characterization of a biomimetic calcium phosphate assay. *J Biomed Mater Res Part B* 2013;00B:000–000.

INTRODUCTION

Osteoclasts are bone cells responsible for the resorption of the mineralized tissues. The abnormally increased osteoclast resorptive activity contributes to development of osteoporosis,¹ rheumatoid arthritis,^{2–5} periodontitis,⁶ and cancer metastasis to bone.⁷ Therefore, it is important to develop reliable methods to examine the alteration of osteoclast function in different diseases and to assess the effects of potential drug treatments on this important therapeutic target.

The widely accepted technique to study osteoclastic resorption is *in vitro* pit formation assay, which is generally performed on bone and dentine slices.^{8–10} However, cortical bovine bone, commonly used as a resorbable substrate, exhibits haversian canals that complicate identification and measurement of resorption pits,¹¹ and large animal dentin, which does not have this problem, relies on obtaining tusks from extinct or protected animals, such as mammoth,^{12,13} elephant,¹⁴ whale,¹⁵ or walrus.¹⁶ Furthermore, these materials are not suitably transparent to allow easy visualization of resorbing osteoclasts.

Alternative osteoclast resorption assays either measure chemical species released into the medium from an acid soluble substrate or seek to mimic bone or dentine in the form of either a mineral coating or an organic-inorganic hybrid as reviewed recently.¹⁷ Calcium phosphate cements have been used previously as synthetic biomimetic materials for studies of osteoclast function.^{18,19} Multiple solution compositions have been used to deposit calcium phosphate minerals onto titanium or tissue culture plastic, resulting variously in deposition of hydroxyapatite, β -tricalcium phosphate, carbonated apatite, tetracalcium phosphate, α -tricalcium phosphate, dicalcium phosphate dihydrate, and octacalcium phosphate²⁰; and osteoclasts were shown to adhere to, differentiate, and resorb these different calcium phosphate matrices.^{21–24} However, in a few studies where detailed analyses of the regulation of osteoclastic resorption were performed,^{18,19} non-osteoclast specific substrate degradation was also noted, diminishing the potential value of these systems for resorption assays.

Patntirapong et al.,²⁵ reported the formation of crystalline calcium phosphate substrate to determine the role of

Correspondence to: S. V. Komarova (e-mail: Svetlana.komarova@mcgill.ca)

Matrix metalloproteinases and their pathological upregulation in multiple sclerosis: an overview

Mohammad A. Javaid · Mohamed-Nur Abdallah ·
Ahad S. Ahmed · Zeeshan Sheikh

Received: 20 May 2013 / Accepted: 24 July 2013 / Published online: 4 September 2013
© Belgian Neurological Society 2013

Abstract Matrix metalloproteinases (MMPs) are a family of extracellular proteases associated with extracellular matrix remodeling. They are involved in many physiological and reparative processes. MMPs can break down all extracellular constituents; therefore, their expression is very tightly regulated and their abnormal activity or over production has been linked to many diseases including multiple sclerosis (MS) which is a leading cause of non-traumatic disability in young adults in North America. Recently many studies, both in animals and humans, have been conducted to better elucidate the underlying causes, mechanisms and pathophysiology of MS. In this review, we discuss the potential role of pathological upregulation

of MMPs in MS and future challenges which if properly addressed might help in development of potential cure for this disease.

Keywords Matrix metalloproteinases · Extracellular matrix · Multiple sclerosis · Experimental autoimmune encephalomyelitis

Introduction

Extracellular matrix (ECM) proteases are critical regulators for normal cell function [1]. One such family of ECM proteases, matrix metalloproteinases (MMPs) have been characteristically associated with ECM remodeling including tissue morphogenesis, wound healing, angiogenesis, neuronal growth, cell differentiation, migration, regulation of growth factors and apoptosis [2]. These proteolytic enzymes are thought to be mediators of ECM degradation [3, 4]. Other than ECM, growth factors, receptors and adhesion molecules are also known substrates for MMPs [3]. Because of these activities MMPs can also regulate cell survival, proliferation and inflammation [4]. Other physiological and reparative processes involving MMPs include synaptic remodeling, long-term potentiation, Nogo signaling, regulation of neural stem biology and remyelination [4].

Twenty-six members of the MMP family have been identified (summarized in Table 1 [5, 6]) and these enzymes together can break down all constituents of ECM [7]. Due to their inherent proteolytic potential, MMPs production is very tightly regulated and their abnormal activity or over expression along with altered MMPs:TIMPs (tissue inhibitors of metalloproteinases) ratio has been linked to several diseases and many

M. A. Javaid · M.-N. Abdallah (✉) · Z. Sheikh
Division of Biomedical Sciences, Faculty of Dentistry,
McGill University, 3640 University Street, Montreal,
QC H3A 0C7, Canada
e-mail: mohamed.nur.abdallah@gmail.com

M. A. Javaid
e-mail: mohammad.javaid2@mail.mcgill.ca

M.-N. Abdallah
Division of Restorative Dentistry, Faculty of Dentistry, McGill
University, 3640 University Street, Montreal, QC H3A 0C7,
Canada

A. S. Ahmed
Department of Dentistry, Jewish General Hospital/McGill
University, 3755 Cote Ste Catherine, Suite H416.2, Montreal,
QC H3T 1E2, Canada

Z. Sheikh
Department of Material Sciences and Preclinical Dentistry,
Altamash Institute of Dental Medicine, Karachi, Pakistan

Z. Sheikh
Department of Oral Anatomy, Altamash Institute of Dental
Medicine, Karachi, Pakistan